Investigation of Hydrothermal Characteristics of Nanofluids and Turbulators in Double Tube Heat Exchangers

By

Ebrahim Tavousi

Submitted in partial fulfilment of the requirements for the degree of

Doctor of Philosophy

Supervised by

Dr. Noel Perera

Dr. Md Mostafizur Rahman

Prof. Reaz Hasan

Dr. Dominic Flynn

College of Engineering

Faculty of Computing, Engineering and the Built Environment

Birmingham City University

2024

ABSTRACT

The growing demand for energy efficiency underscores the vital importance of heat exchangers in a wide range of industries, from power generation to HVAC systems. With growing demands for improved efficiency and reduced operational costs, there has been significant research into thermal management technologies. Double tube heat exchangers (DTHEs), due to their simplicity and effectiveness, are widely used in industrial applications. This research aims to enhance the performance of DTHEs by integrating innovative turbulator designs and advanced nanofluids, contributing to the development of more energy-efficient thermal systems.

Turbulators disrupt fluid flow, enhancing heat transfer by breaking up the boundary layer on heat transfer surfaces. This study examines various turbulator shapes—rectangular, triangular, oval, and trapezoidal—in both transverse and helical configurations. Additionally, it explores the effects of different nanofluids, such as CuO, ZnO, Fe_3O_4, Diamond, Ag, TiO_2, Al_2O_3, SiC, and SiO_2, on heat transfer. Using volume fractions from 0 to 0.1, the nanofluids are selected for their ability to enhance thermal conductivity and convective heat transfer. The research employs the finite volume method and advanced computational tools, including ANSYS Fluent, to model and analyze these effects.

The results indicate that SiO_2 nanofluids provide the highest improvement in heat transfer efficiency, with an 18.4% enhancement compared to the base fluid. Among turbulator configurations, helical designs, particularly triangular ones, offer the best performance in terms of Nusselt number, pressure drop, and overall heat transfer efficiency. The study also highlights that adjusting the geometrical parameters of turbulators, such as rib height, can significantly impact heat transfer, with transverse turbulators showing up to a 471% increase. The substantial improvements observed in this study affirm the potential of these technologies to improve thermal systems design, offering significant advantages over traditional methods and contributing to sustainability and cost-effectiveness in thermal management.

KEYWORDS

Double tube heat exchanger, Passive method, Heat transfer, Fluid flow, Turbulator, Nanofluid.

TABLE OF CONTENTS

LIST OF FIGURES

LIST OF TABLES

NOMENCLATURE

Symbols

C_p	Heat capacity, J/kg K
D	Tube diameter, m
d	Diameter, m
$\dot{E}_D$	Exergy destruction
e_r	Relative error
f	Friction factor
h	Height of rib, m, Convective heat transfer coefficient, W/m^2 K
k	Thermal conductivity, W/m K and turbulent kinetic energy, m^2s^{-2}
L	Tube length, m
Nu	Nusselt number
P	Pressure, Pa
Pr	Prandtl number
R	Radius of the tube, m
Re	Reynolds number
R^2	Coefficient of determination
s	Distance between ribs, m
t	Thickness of inner tube, m
T	Temperature, K
V	Velocity, m/s
w	Width of rib, m
$Y_{num,i}$	Numerical value
$Y_{pre,i}$	Predicted value

Subscripts

Ave	Average
b	Base fluid, Bulk
c	Cold
e	Ambient
h	Hot, Hydraulic

i	Inner, Inlet
in	Inlet
max	Maximum
min	Minimum
nf	Nanofluid
o	Outer, Outlet, Plain
out	Outlet
p	Solid nanoparticles

Greek letters

ε	Target parameter
φ	Nanoparticle volume fraction
μ	Dynamic viscosity, N s/m^2
ρ	Density, kg/m^3

Abbreviations

CFD	Computational fluid dynamics
DTHE	Double tube heat exchanger
FVM	Finite volume method
HPC	High performance computing
HVAC	Heating, ventilation, and air conditioning
PEC	Performance evaluation criteria
PTFE	Poly tetra fluoro ethylene
RMSE	Root mean squared error

.

STATEMENT OF ORIGINAL AUTHORSHIP

The work contained in this thesis has not been previously submitted to meet requirements for an award at this or any other higher education institution. To the best of my knowledge and belief, the thesis contains no material previously published or written by another person except where due reference is made.

Signature: ______Ebrahim Tavousi___________________

Date: ________30-07-2024_________________

ACKNOWLEDGEMENTS

I extend my profound gratitude to all those who supported and guided me through the journey of my PhD. This thesis would not have been possible without their collective encouragement and insights, which have been invaluable to my academic and personal growth.

First and foremost, I wish to express my deepest appreciation to my primary supervisor, Dr. Noel Perera, whose expertise and understanding were instrumental in shaping the research direction of this thesis. Dr. Perera's steadfast support and meticulous attention to detail have been a constant source of motivation throughout my study. His willingness to give his time so generously has been very much appreciated.

I am equally grateful to my other supervisors, Dr. Md Mostafizur Rahman, Professor Reaz Hasan, and Dr. Dominic Flynn, for their invaluable mentorship and support. Dr. Rahman's profound knowledge and insights in the field have significantly enriched my work, pushing me to refine my ideas and research methodologies. Professor Hasan has been a pillar of wisdom and encouragement, offering both critical academic guidance and moral support throughout my PhD journey. Dr. Flynn's practical advice and hands-on approach were immensely helpful, particularly in navigating the complex technical challenges of my research.

A special word of thanks goes to Dr. Roger Tait for his expert advice and guidance on the use of the High Performance Computing (Cluster 3) resource. His assistance was crucial in facilitating the computational aspect of my research, allowing me to execute complex simulations and data analysis. I am also grateful to the Faculty of Computing, Engineering and the Built Environment at Birmingham City University for providing the High Performance Computing resources that were essential for my research.

On a personal note, I must express my heartfelt gratitude to my wife, Melika, for her endless patience, understanding, and love. Melika's unwavering support and sacrifice during the ups and downs of this academic pursuit have been the bedrock of my endurance and success. Her belief in my capabilities has been a constant source of encouragement that pushed me to persevere even during the most challenging times.

I also wish to thank my parents, brothers, and sisters for their love, prayers, and constant encouragement. Their unyielding support in every aspect of my life has not only paved the way for this academic achievement but has also kept me grounded and focused on my goals. Their

sacrifices have not gone unnoticed, and I am eternally grateful for everything they have done for me.

In conclusion, the journey to completing this PhD has been a transformative experience, enriched by the contributions and support of many. Each of you played a pivotal role in this journey, and for that, I am eternally appreciative. Thank you for investing your time, effort, and faith in me and my work. This thesis stands as a testament to the collective effort and spirit of collaboration that has surrounded me these past years.

Chapter 1: Introduction

The development and improvement of heat exchangers represent a pivotal area of research in the field of engineering, underscored by the critical role these devices play in a myriad of industrial, automotive, and energy systems. Heat exchangers facilitate the transfer of heat between two or more fluids, making them indispensable in processes requiring heating, cooling, or thermal management. The efficiency and effectiveness of heat exchangers directly impact energy consumption, operational costs, and environmental sustainability, highlighting the importance of advancing heat exchanger technology. This study focuses on double tube heat exchangers (DTHEs), one of the most common types of heat exchangers. DTHEs are widely used due to their simplicity and effectiveness in transferring heat between fluids. By investigating and improving DTHE performance, this research aims to contribute to the development of more efficient and cost-effective thermal systems, which are critical for reducing energy consumption and enhancing environmental sustainability.

Turbulators, introduced into the flow path of a heat exchanger, serve to disrupt the laminar flow and promote turbulence. This increased turbulence enhances the heat transfer coefficient by improving the mixing of the fluid, thereby allowing for more efficient thermal energy exchange between the fluid and the tube walls. The strategic placement and design of turbulators can significantly augment the overall efficiency of heat exchangers by optimizing the flow patterns and heat transfer characteristics within them [1-3]. In recent years, the introduction of nanofluids has emerged as a revolutionary approach to enhance the thermal performance of heat exchangers. Nanofluids, which are engineered colloidal suspensions of nanoparticles in a base fluid, exhibit significantly enhanced thermal properties compared to traditional heat transfer fluids. The dispersion of nanoparticles, such as metals, metal oxides, or carbon nanotubes, within a base fluid like water, ethylene glycol, or oil, results in improved thermal conductivity, heat transfer coefficients, and reduced thermal resistance [4, 5].

Integrating the use of nanofluids with the implementation of turbulators in heat exchangers represents a synergistic approach to thermal management. This combination leverages the distinct advantages of each method: the enhancement of heat transfer through turbulence induction and the intrinsic thermal property improvements offered by nanofluids. Studies have shown that the application of nanofluids and turbulator insertions in heat exchangers can lead to remarkable increases in heat transfer efficiency, surpassing the performance achievable by either technique alone. This synergy not only facilitates the development of more compact and efficient heat exchangers but also opens new avenues for energy-efficient design and operation in thermal systems [6, 7]. However, the implementation of turbulators and nanofluids also introduces challenges, including the potential for increased pressure drop and concerns regarding nanoparticle stability and dispersion within the base fluid. Addressing these issues requires a comprehensive understanding of fluid dynamics, heat transfer, and nanomaterial science, underscoring the interdisciplinary nature of this research area [5, 8].

Figure 1.1 illustrates the yearly number of publications in the areas of nanofluids and heat exchangers (Data is collected from the Scopus website). The increasing trend observed over the last decade highlights the growing significance and interest in these fields among researchers.

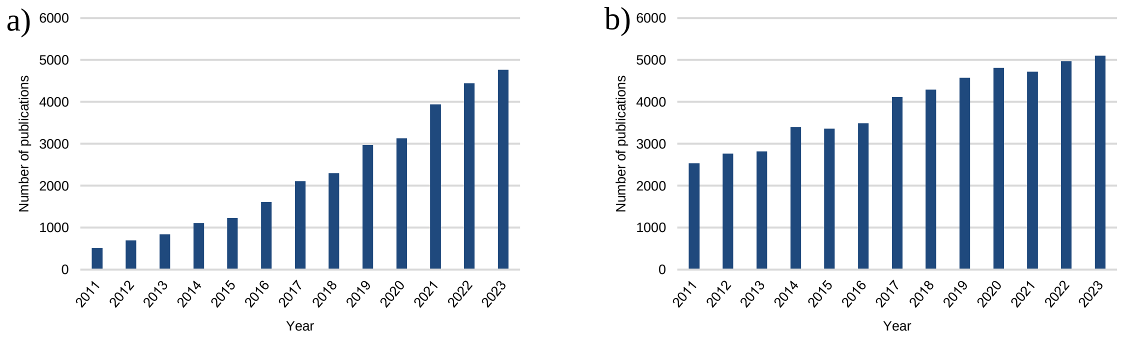

Figure 1.1: Trend in the number of publications over time for a) nanofluids and b) heat exchangers.

1.1 Problem statement

Enhancing heat transfer and fluid flow characteristics in double tube heat exchangers (DTHEs) is a critical challenge in thermal engineering, necessitating innovative solutions to boost efficiency and performance. This research addresses this challenge using passive method, specifically the combination of turbulator insertion and nanofluid techniques. The study examines the effects of various turbulator designs, including transverse and helical configurations (rectangular, triangular, oval, and trapezoidal), in conjunction with different nanofluids (CuO, ZnO, Fe_3O_4, Diamond, Ag, TiO_2, Al_2O_3, SiC, and SiO_2 with volume fractions from 0 to 0.1), on the hydrothermal performance of a DTHE. This range was chosen because it is more applicable in real-world scenarios, and higher concentrations increase the risk of friction and clogging in the system. Inserting turbulators enhances mixing and induces secondary flows, which reduces the thermal boundary layer and increases the heat transfer rate within a DTHE. Additionally, incorporating nanoparticles into the base fluid improves the thermophysical properties of the working fluid, thereby enhancing the overall performance of the DTHE. By combining turbulator insertion with nanofluids, it is expected to achieve maximum enhancement in the heat transfer rate of the DTHE.

1.2 Aim of the research

In light of aforementioned considerations, this Ph.D. thesis endeavours to explore the combined effects of turbulator insertion and nanofluid application within a double tube heat exchanger. By investigating these dual enhancement strategies, the thesis aims to contribute to improving performance of a double tube heat exchanger design and operation, paving the way for more energy-efficient and sustainable thermal systems.

1.3 Novelty and originality of the research

The research introduces the following novel contributions.

- A robust and comprehensive numerical methodology to evaluate the heat transfer and fluid flow characteristics of nanofluids and turbulators insertion in a double tube heat exchanger.
- Investigate the impact of introducing novel turbulators (transverse and helical types) combined with nanofluids (CuO, ZnO, Fe_3O_4, Diamond, Ag, TiO_2, Al_2O_3, SiC, and SiO_2 with volume fractions from 0 to 0.1) on enhancing the performance of a double tube heat exchanger.
- Examine how the geometric parameters of turbulator insertion-specifically the spacing, height, and width of the turbulators-affect the performance of a double tube heat exchanger.

1.4 Research objectives

The specific objectives of this research are outlined below.

1. To conduct a comprehensive and critical literature review to identify the most effective techniques for enhancing heat transfer, focusing on the performance improvements

achieved through various turbulator designs and nanofluid applications in double tube heat exchangers.

2. To validate numerical simulations with existing experimental results, such as average Nusselt number and friction factor, using computational fluid dynamics (CFD) software, ensuring that the simulations accurately reflect real-world performance.
3. To perform numerical simulations using a single-phase flow model for various nanofluids with different nanoparticle volume fractions, considering both counter-flow and parallel-flow configurations, as well as a novel transverse turbulator insertion design for a double tube heat exchanger.
4. To numerically assess the impact of geometrical parameters of turbulators, such as the height and shape, in combination with nanofluids, on the thermal performance of a double tube heat exchanger, identifying the parameters that lead to the highest heat transfer enhancement.
5. To simulate innovative helical turbulator configurations and compare their performance against traditional transverse and other conventional turbulator designs in double tube heat exchangers, providing insights into the most effective design strategies for heat transfer enhancement.
6. To summarize and draw conclusions from the simulations, offering recommendations for the optimal design and selection of turbulators and nanofluids in double tube heat exchangers to maximize energy efficiency and heat transfer performance.

1.5 Thesis Outline

Chapter 1 introduces heat exchangers, emphasizing their significance, and provides an overview of turbulators and nanofluids. It outlines the research's goals, novelty, and objectives. Additionally, the structure of the thesis is detailed in this chapter.

Chapter 2 presents an exhaustive review of the literature on methods for enhancing heat transfer in heat exchangers, with a particular emphasis on the passive method. It encompasses information on the four main techniques: turbulator insertion, extended surface area (fins), geometry change, and nanofluids. Subsequently, the chapter delves into each method, elucidating an investigation on the heat transfer rate and friction factor and presenting a statistical analysis of the results derived from other published works on the passive method.

Chapter 3 outlines the research methodology employed in this study. This chapter comprehensively discusses the models implemented in the numerical analysis, along with the assumptions made. It methodically details the procedural steps of the research, including grid independence tests and validations. The chapter also describes the domain and geometry of the double-tube heat exchangers. Furthermore, it elaborates on the designs of turbulators and nanofluids utilised in this research, providing detailed explanations of each.

Chapter 4 provides the fundamental equations employed in the research. It comprehensively explicates all the equations utilised, including the continuity, momentum, and energy equations which are pivotal for solving the problem domain through Computational Fluid Dynamics (CFD) software. Furthermore, the chapter delves into the equations governing the density, heat capacity, thermal conductivity, and viscosity of nanofluids, providing detailed discussions on each.

Chapter 5 presents the results and discussion of the research, wherein the outcomes of numerical simulations are detailed. The heat transfer and fluid flow characteristics resulting from the insertion of turbulators and the use of nanofluids in a double tube heat exchanger are explained comprehensively. Key parameters such as the Nusselt number, friction factor, and performance evaluation criteria are presented to facilitate a thorough evaluation of the heat exchanger's performance. Additionally, this chapter includes a comparative study aimed at evaluating the performance of new turbulator designs relative to traditional turbulator insertions in double tube heat exchangers.

Chapter 6 concludes the research and offers recommendations for future work. This chapter discusses the key findings of the research and outlines potential areas for future research endeavours.

This research also included efforts in experimental work. By reviewing literature and standards, possible designs of a DTHE were investigated to find the best option based on low cost and reliable leak prevention. After finalizing the designs, the required materials for the test rig were carefully identified. A price list of materials and equipment was submitted to the university for purchasing. Details about the experimental work are provided in Appendix A.

1.6 Publications

Six publications resulting from this PhD study have been published in high-quality Q1 journals. The full texts of these publications are provided in Appendix C. The list of all publications are as follows.

1. Tavousi, E., Perera, N., Flynn, D. and Hasan, R., 2023. Heat transfer and fluid flow characteristics of the passive method in double tube heat exchangers: a critical review. International Journal of Thermofluids, 17, p.100282.
2. Tavousi, E., Perera, N., Flynn, D. and Hasan, R., 2023. Numerical investigation of laminar heat transfer and fluid flow characteristics of Al_2O_3 nanofluid in a double tube heat exchanger. International Journal of Numerical Methods for Heat & Fluid Flow, 33(12), pp.3994-4014.
3. Tavousi, E., Perera, N., Flynn, D. and Hasan, R., 2023. Numerical Investigation of Heat Transfer and Fluid Flow Characteristics of Al_2O_3 Nanofluid in A Double Tube Heat Exchanger With Turbulator Insertion. Proceedings of the 9th World Congress on Mechanical, Chemical, and Material Engineering (MCM'23) Brunel University, London, United Kingdom –August 06-08, 2023, Paper No. HTFF 218.
4. Tavousi, E., Perera, N., Flynn, D., Hasan, R. and Rahman, M., 2024. Effect of novel turbulators on the hydrothermal performance of counterflow double tube heat exchanger using nanofluids. International Journal of Heat and Fluid Flow, 107, p.109427.
5. Tavousi, E., Perera, N., Rahman, M., Hasan, R., and Flynn, D., Effects of Various Nanofluids on the Performance of a Double Tube Heat Exchanger, 17th International Conference on Knowledge Science, Engineering and Management (KSEM 2024).
6. Tavousi, E., Perera, N., Rahman, M., Hasan, R., and Flynn, D., Enhancement of Heat Transfer and Hydrodynamic Performance in a Double Tube Heat Exchanger Using Transverse and Helical Turbulators with Nanofluid, International Journal of Heat and Mass Transfer. (In the process of submission)

Chapter 2: Literature Review

This chapter provides a comprehensive review of the literature on heat exchangers, focusing specifically on DTHEs. It begins by defining heat exchangers, detailing their applications, and classifying them. The chapter then extensively discusses the methods for enhancing heat transfer in DTHEs and presents the key findings from published research on each method. The conditions and findings of each pervious published research are summarised in detailed tables. The chapter concludes with a novel statistical analysis of the heat transfer rate and friction factor for each technique, providing a comparative analysis of the different techniques.

2.1 Introduction

A heat exchanger is a device used to transfer thermal energy between two or more fluids, separated by solid material. The applications of heat exchangers are extensive in industries where they are used to crystallize, concentrate, distil, fractionate, pasteurize, sterilize and control a process fluid. Some common heat exchangers are cooling towers, air preheaters, evaporators, condensers, automobile radiators, and shell and tube exchangers. Heat exchangers are classified in many ways, for example, according to the transfer process, the number of fluids, surface compactness, construction, flow arrangements, and heat transfer mechanisms. One of the standard classifications is based on the construction of heat exchangers (Figure 2.1). These classifications are divided into four subcategories: tubular, plate-type, extended surface, and regenerative. The tubular section is divided into four subcategories: double-pipe, shell and tube, spiral tube, and pipe coil [9, 10].

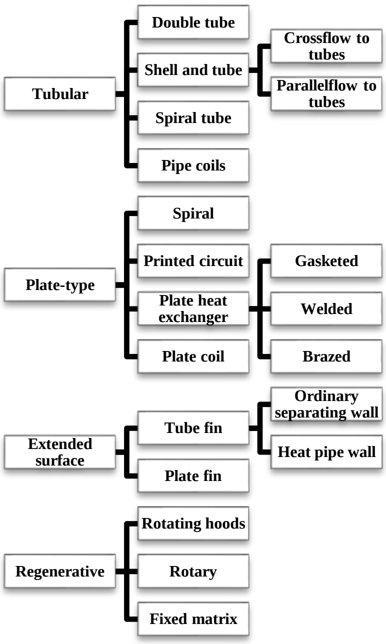

Figure 2.1: Classification of heat exchangers according to construction.

One of the common heat exchangers is the double tube heat exchanger (DTHE). These are used widely in industries and engineering applications such as refrigeration, air-conditioning, power plant, solar water heater and the process industry [11]. The main advantages of DTHEs are working with high pressure and temperature of working fluids, simple maintenance, modular construction, cost-effectiveness, and its simplicity (consisting of two concentric tubes) [12]. The purpose of using DTHEs is to transfer heat between the cold and hot regions (Figure 2.2). The flow directions of hot and cold fluids in DTHEs can either be parallel or counter. It is crucial and challenging for researchers to find ways and solutions to increase the DTHE's heat transfer rate and efficiency. In this regard, extensive research was carried out experimentally and numerically related to DTHEs to enhance heat transfer and improve fluid characteristics.

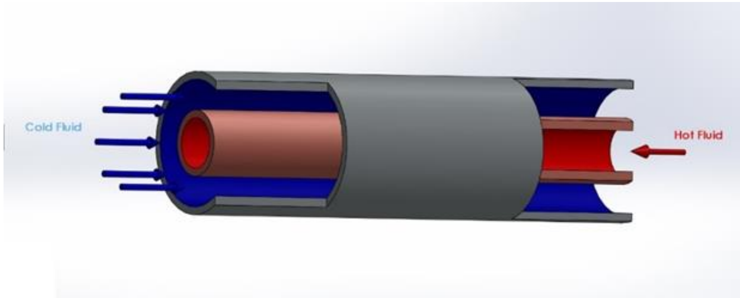

Figure 2.2: Counterflow double tube heat exchanger.

One of the earliest publications related to DTHEs dates back to 1928 [13]. The research into DTHEs expanded rapidly after 1928 and was divided into different categories. Some scholars focused on geometry change and the insertion of elements in inner and outer tubes [14, 15]. Some researchers investigated different shapes of fins, and others investigated different working fluids such as nanofluids [16, 17]. Using external forces such as magnetic field and vibration was the interest of some scholars in the subsequent years[18-20].

2.2 Heat transfer enhancement methods in DTHE

Enhancing the heat transfer rate in DTHEs is divided into three main methods: active, passive, and compound. In the active method, some external forces and energy are used to improve the heat transfer rate in the heat exchangers. For example, establishing a magnetic field for flow disturbance, using flow or surface vibration, rotating tubes and reciprocating plungers, pulsation by cams, and mechanical aids [21-25]. This method has limited practical applications because it needs extra equipment and instruments to add energy. The potential of the active method is less than the passive method as it is difficult to exert external energy in most cases [26].

In the passive methods of increasing heat transfer rate, external forces are not used to enhance the heat transfer rate in DTHEs. Some examples of passive methods to create turbulence in the flow field by inserting fins, coiled wires, swirl flow inducement, and wall roughness. In general, the passive method is preferred compared to the active method because, in this method, there is no need for external forces and its cost-effectiveness [27, 28].

Using two or more methods of the passive and active method together to increase the heat transfer rate and performance of heat exchangers is known as the compound method [29-33]. Using various enhancement methods together increases the heat transfer coefficient in heat exchangers because of interactions among the methods compared to just using one method. This compound method takes advantage of both the external forces and induces turbulence in the flow to increase the heat transfer rate [34].

2.2.1 Passive method

In the passive method, there are no external forces and energy for increasing the heat transfer. Researchers find the passive method widely attractive because of the cost-effective manufacturing, no external forces, simple to set up, and low maintenance requirements. It should be mentioned that the detrimental effect of the passive methods is the increased pumping power due to the increased friction factor. Generally, passive methods are proposed to attain a high heat transfer rate with the smallest energy input for pumping fluids [12, 35]. Therefore, many studies have been conducted experimentally and numerically focused on this method to increase heat transfer. Some of the main techniques are turbulator insertion, extended surface area (fins), geometry changes, and using nanofluids.

Passive methods are divided into insertion elements as turbulator insertion, using different shapes of fins as extended surface area and modification in tubes and tube's wall (different roughness) as geometry change, and using nanofluids. With the passive method, the key factors that decrease the thermal boundary layer are the creation of secondary flow, disturbance, turbulence, and increasing the surface area.

- ✓ Turbulator insertion

Turbulator insertions are used to induce disturbance and perturbation in the flow. This is achieved by inserting the coiled wire, twisted tape, or louvered strip.

- ✓ Extended surface area (fins)

Fins are used to increase surface area, creating secondary flow and turbulence in the flow.

- ✓ Geometry change

Changing tubes cross-section, different shapes of tube walls, and roughness increases the heat transfer by creating turbulence and increasing the surface area. Some examples are corrugated tubes, helical tubes, and different cross-sections of tubes.

- ✓ Nanofluids

Nanofluids are used to increase heat capacity, the thermal conductivity of the base fluid, fluctuations and turbulence in the fluid flow.

- ✓ Combination of different techniques

The key factors of different techniques interact with each other in this method to increase the heat transfer rate.

2.3 Impact of different passive techniques on the heat transfer and fluid flow characteristics of DTHE

One of the critical mechanisms to increase heat transfer between tube wall and fluid flow is reducing the thickness of the thermal boundary layer. The thickness of the thermal boundary layer is affected by the condition of the fluid flow, which is smaller in the turbulent flow. Therefore, the heat transfer in the turbulent flow is faster than laminar flow because the eddies convey the thermal energy quickly in the turbulent flow and the thickness of the thermal boundary layer is smaller in the turbulent flow [35, 36]. This section discusses the impact of different passive methods on the heat transfer and fluid flow properties in a DTHE.

2.3.1 Turbulator insertion

Inserting turbulators is simple, easy, cost-effective, and produces a good performance in heat exchangers. Turbulator insertion increases heat transfer by mixing fluid and creating turbulence in the flow. In this way, the thermal boundary decreases, and the convective heat transfer improves [26]. There are different turbulators insertion to enhance the heat transfer in DTHEs, such as coiled wire, twisted tape, and louvered strip [37-45]. These elements are generally used in the inner tube since there is a greater heat transfer improvement [46].

There are many publications [47-51] on the effects of twisted tape, coiled wire, and louvered strip elements on the heat transfer and fluid flow properties in a DTHE. Turbulator insertion makes flows swirl and changes fluid velocity near the wall because of various vorticity distributions in the vortex core of the tube. The swirl flow induces a tangential velocity component that enhances flow mixing between the tube core and near-wall region. Although the heat transfer increased with swirl flow, the pressure drag and shear stress in the tube also increased because of the coiled wire, twisted tape, and louvered strip [52].

Naphon [14] experimentally studied typical twisted tape configuration with different pitches in a double tube heat exchanger. The working fluids were hot water for the inner tube and cold water for the outer tube. They found that inserting twisted tape increases the heat transfer coefficient and pressure drop compared to a simple double tube heat exchanger. The overall heat transfer coefficient increased by 254% and decreased by increasing the Reynolds number.

Naphon [53] experimentally studied the heat transfer characteristics and pressure drop of a DTHE with coil wire insert (Figure 2.3). Cold and hot water were used as a working fluid in the outer and inner sides. The results showed that heat transfer enhancement decreases by increasing Reynolds number, and wire coil insertion significantly increases the heat transfer rate in the laminar flow region.

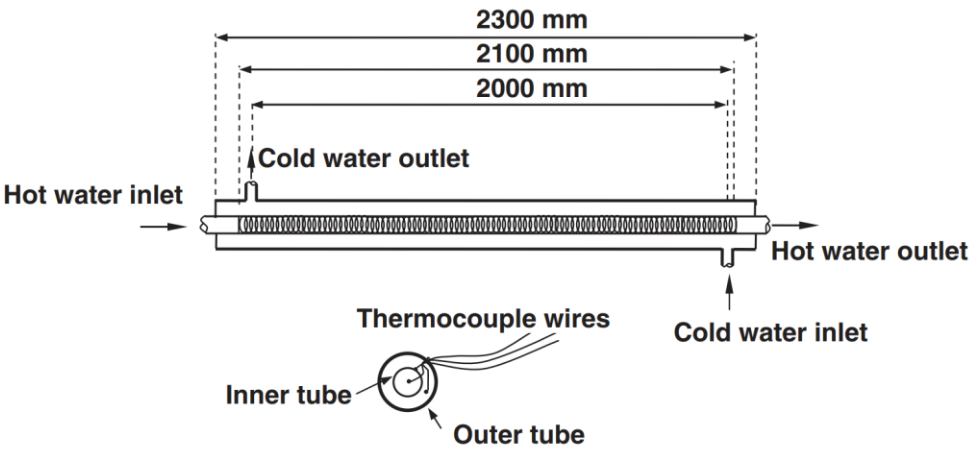

Figure 2.3: A schematic diagram of the test section [53].

The heat transfer rate in a DTHE can be increased by inserting louvered strips. Eiamsa-ard, et al. [54] experimentally investigated the louvered strips with forward, backwards, and different inclined angles (θ=15°, 25° and 30°) configuration in a DTHE (Figure 2.4). It was reported that the louvered strips increased the average Nusselt number and friction loss up to 284% and 413%, respectively, compared to a conventional DTHE.

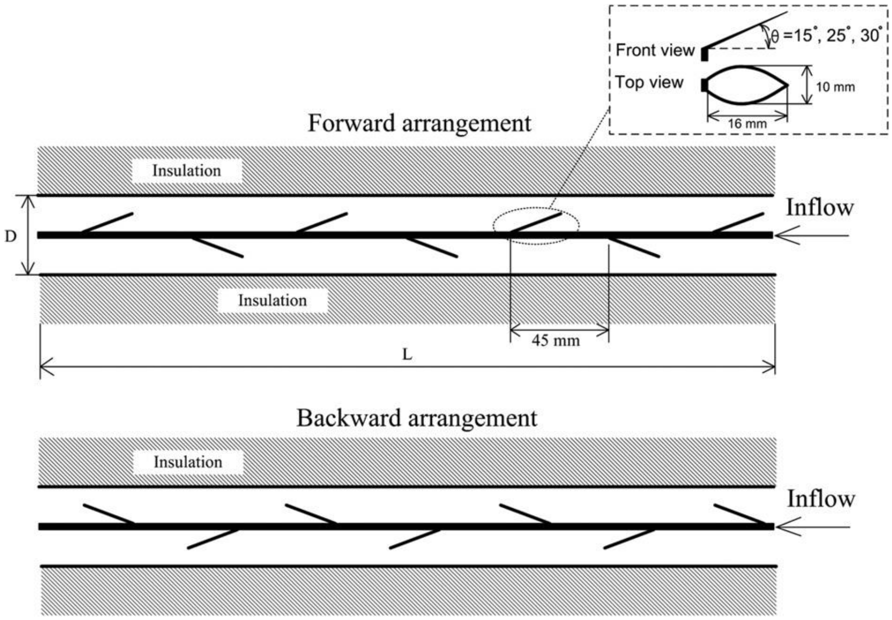

Figure 2.4: Louvered strips with forward and backward arrangements [54].

Zhang, et al. [55] conducted an experiment to study the heat transfer and fluid flow characteristics of a DTHE fitted with a stationary and self-rotating twisted tape (Figure 2.5). The experiment was conducted under turbulence flow and for different twist ratios. It was observed that the self-rotating twisted tape increased the heat transfer more than the stationary twisted tape. The thermal performance factor, pressure drop, and Nusselt number also increased with decreasing twist ratios.

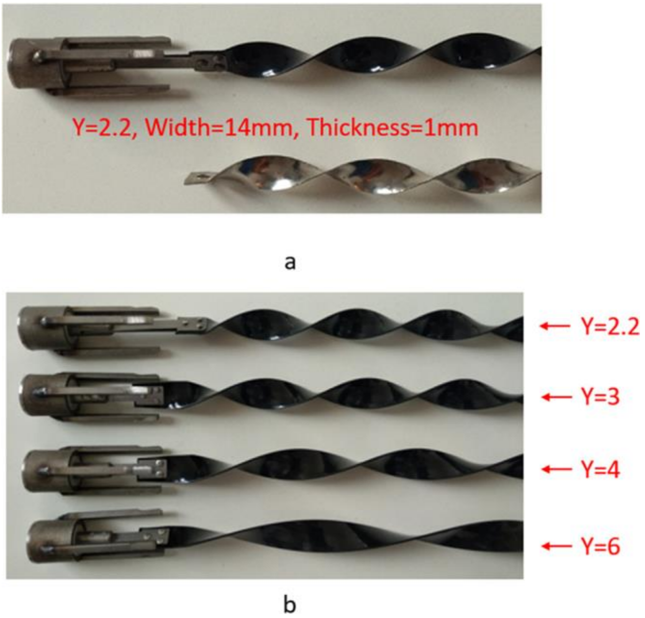

Figure 2.5: a) Self-rotating twisted tapes and stationary twisted tape with the same geometry; b) Pictorial view of self-rotating twisted tapes with different twist ratios [55].

Other types of turbulators insertion, such as propellers and swirl generators, are used to increase the heat transfer rate. Since the increase of pressure drop of such turbulators is high compared to the increase in heat transfer rate, they are not commonly used. Yildiz, et al. [36] showed that using propellers as turbulators increases, the pressure drop up to 1000% with an increase of 250% in the heat transfer rate. Using swirl generators with holes in the entrance increased the Nusselt number and friction factor by 130% and 190%, respectively [56]. Aridi, et al. [57] presented a numerical investigation on the performance of heat transfer enhancement using a trapezoidal vortex generator in a DTHE. They wanted to compare the effect of the turbulator in three cases. These are the turbulator in the inner tube (case 1), in the outer side of the inner tube (case 2), and in the inner side of the outer tube (case 3). The results showed that the turbulator is effective in all cases, and the greatest improvement was 97% for case 1, 92% for case 2, and 56% for case 3. Table 2.1 summarises the information on different turbulators insertions and their effects in comparison to a conventional DTHE.

Table 2.1: Summary of information on different turbulators insertion compared to a conventional DTHE.

Author	Configuration	Conditions	Findings
Akpinar [58]	Helical wire 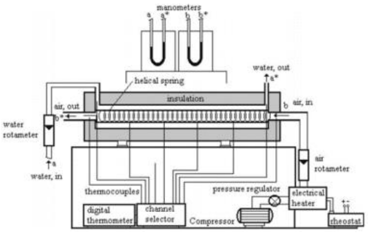	Experimental Re: 6500-13000 Inner: hot air Outer: cold water Parallel and Counter flow	✓Increase of Nusselt number: 164% ✓Increase of friction factor: 174%
Naphon [14]	Twisted tape 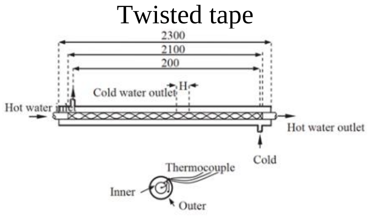	Experimental Re: 7000-23000 Inner: hot water, temperature: 40-45 °C Outer: cold water, temperature: 15-20 °C Counter flow	✓Increase of heat transfer rate coefficient: up to 253% ✓The overall heat transfer coefficient decreases by increasing the Reynolds number.
Eiamsa-ard, et al. [54]	Louvered strip 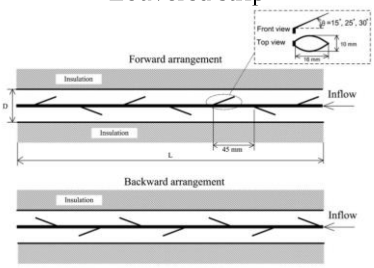	Experimental Re: 6000-42000 Inner: hot water, temperature: 25°C Outer: cold water, temperature: 25°C Counter flow	✓Increase of average Nusselt number: 284% ✓Increase of friction factor: 413%
Yadav [59]	Half-length twisted tape inserted in U-bend [60] 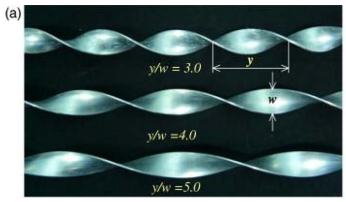	Experimental Inner: hot oil Outer: cold water, temperature: 25°C Counter flow	✓Increase of heat transfer: 40% ✓Thermal performance of smooth tube is better than half-length twisted tape by 30% ✓Thermal performance of plain heat exchanger is better than half-length twisted tape by 30 to 50%
Shashank and Taji [61]	Coil wire with different materials (copper, aluminum, and stainless steel) [49] 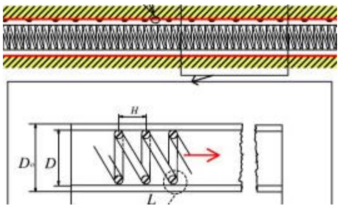	Experimental Re: 4000-13000 Inner: hot water Outer: cold water Counter flow	✓The increase of heat transfer for copper, aluminum, and stainless steel: 58, 41, and 31% ✓The increase of friction factor for aluminum, stainless steel and copper: 570, 490, and 440% ✓The friction factor increases with decreasing coil wire pitch
Sheikholeslami, et al. [62]	Agitator	Experimental Re: 6000-12000	✓Inserting the agitator in the inner tube increases the heat transfer rate

Author	Configuration	Conditions	Findings
	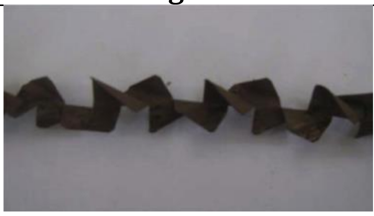	Inner: hot water, temperature: 70, 80, 90°C Outer: cold air Counter flow	✓Enhancement of heat transfer decreases with increase of Reynolds number
Moya-Rico, et al. [63]	Twisted tape 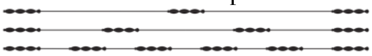	Experimental Re: 6000–12000 Inner: hot sugar-water mix, temperature: 57, 46, 32, and 17°C Outer: cold propylene glycol, temperature: constant inlet 8°C Counter flow	✓Increase of heat transfer: up to 80% ✓Increase of pressure drop: up to 50% ✓Nusselt number and friction factor is higher in the shorter spacer
Slaiman and Znad [64]	Wire coil [65] 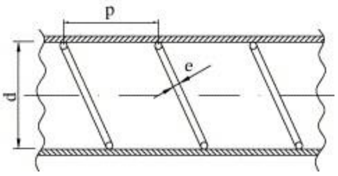	Experimental Re: 5000-40000 Inner: hot water, temperature: 60 and 70 Outer: cold water Counter flow	✓Increase of heat transfer: up to 143% ✓Increase of pressure drop: up to 375% ✓Maximum Nusselt number enhancement occurred at Re: 5000 ✓Heat transfer enhancement is more effective at low values of Reynolds number than high values
Padmanabhan, et al. [66]	Helical wire insertion 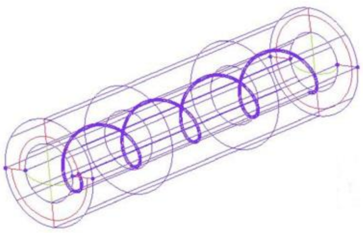	Numerical Inner: cold water, temperature: inlet 28°C Outer: hot water, temperature: inlet 90°C Counter flow	✓Increase of heat transfer coefficient: up to 63.91% ✓The wall thermal transmission and heat flux increase by reducing the pitch gap
Ibrahim [52]	Helical screw-tape 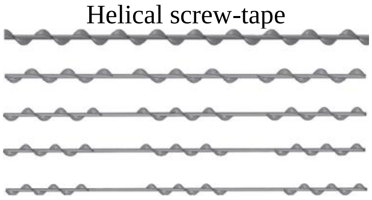	Experimental Re: 570-1310 Inner: cold water Outer: hot water Counter flow	✓Increase of Nusselt number: 115% ✓Increase of friction factor: 60% ✓The Nusselt number increase increases with the increase of Reynolds number and with the decrease in spacer length twist ratio
Pourahmad and Pesteei [67]	Wavy strip	Experimental Re: 3000-13500 Inner: hot water, temperature: 54°C Outer: cold water Counter flow	✓Increase of effectiveness: up to 71% ✓Increase of friction factor: up to 600% ✓The effectiveness increases with the increase of Reynolds number and increases with the decrease of the wavy strip angle

Author	Configuration	Conditions	Findings
	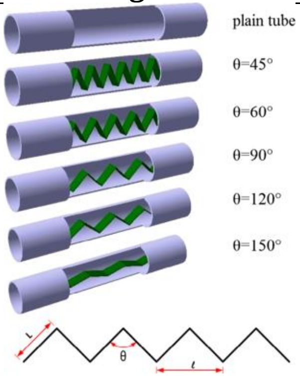		✓The effectiveness and Number of Transfer Units (NTU) have a maximum value at the angle of 45°
Murugesan, et al. [68]	With and without V-cut twisted tape 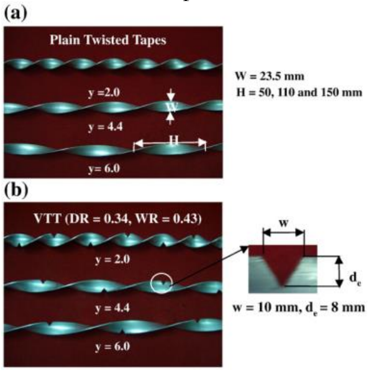	Experimental Re: 2000-12000 Inner: hot water, temperature: 54°C Outer: cold water, temperature: 30°C Counter flow	✓Increase of Nusselt number with and without cut: 150% and 100% ✓Increase of friction factor with and without cut: 470% and 280% ✓The V-cut twisted tape offered a higher heat transfer rate, friction factor and thermal performance factor compared to the plain twisted tape
Wijayanta, et al. [69]	Square-cut Twisted Tape 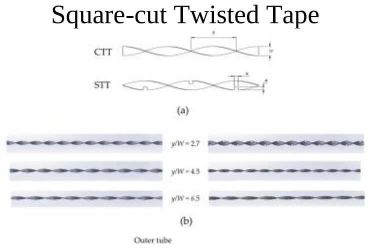	Numerical Re: 8000-18000 Inner: hot water Outer: cold Counter flow	✓Increase of Nusselt number with and without cut: 80.7% and 74.4% ✓Increase of friction factor with and without cut: 230% and 200% ✓The decrease of the pitch ratio leads to the increase of efficiency, Nusselt number and friction factor

2.3.2 Extended surface area (fin)

Another way to increase the heat transfer rate in DTHEs is to use fins and enlarge the surface area of the fins [70-87]. This technique can help fluids with naturally low heat transfer coefficients, such as gases and high-viscosity liquids, by placing them on the fin side. Designing DTHEs by fins is very cost-effective because they are cheaper than prime tube surfaces. When fins are used in the fluid side, which has a lower heat transfer coefficient, it decreases the thermal resistance and the heat transfer capacity increases due to the bigger heat transfer surface area [88, 89]. The geometry and type of the fins are two critical factors for improving the hydrothermal properties in DTHEs. These two elements establish secondary flow in DTHEs, reducing hydraulic diameter, increased surface area, vortices, and intensifying turbulence induced by the vortex generators [90-92].

In the helical fin designs, by decreasing the helical pitch, pressure drop increased sharply at a high Reynolds number; conversely, the efficiency of the heat transfer enhancement is low at the large helical pitch. So, using helical fins to enhance heat transfer is suitable for applications at low Reynolds numbers [93]. Zhang, et al. [90] installed helical fins and vortex generators on the surface of the outer tube of a DTHE shown in Figure 2.6 and concluded that heat transfer and pressure drop increased up to 46% and 146%, respectively, compared to the conventional tube.

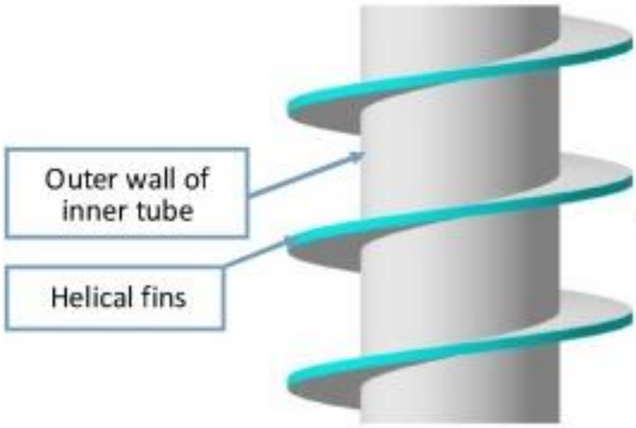

Figure 2.6: Inner tubes with helical fins and vortex generators on its outer wall [94].

El Maakoul, et al. [95] numerically studied the heat transfer and fluid flow characteristics and performance of an air-water DTHE with helical and longitudinal fins (Figure 2.7). The results showed that helical fins have a better heat transfer rate, about 3-24% higher than longitudinal fins. It was also reported that the heat transfer rate and friction factor increased when decreasing the helical space. In another publication, El Maakoul, et al. [96] numerically compared a DTHE with conventional longitudinal fins and split longitudinal fins (Figure 2.8). The results showed that split longitudinal fins increase heat transfer 31%-48% more than conventional longitudinal fins.

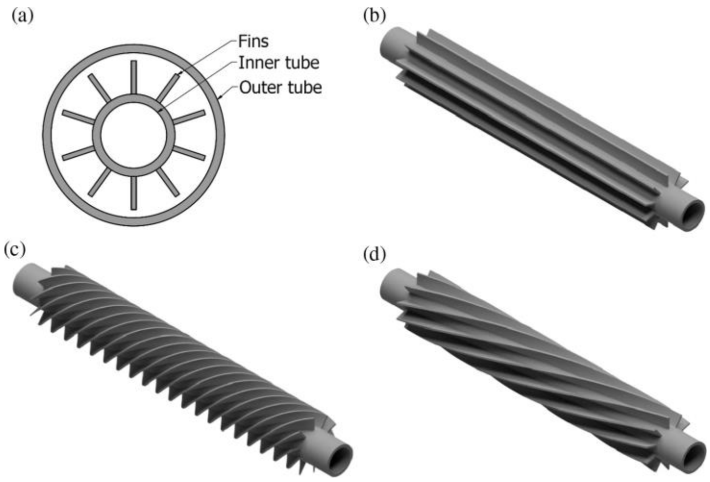

Figure 2.7: Models of double pipe heat exchangers with longitudinal fins and helical fins with a) and b) longitudinal, c) and d) helical [95].

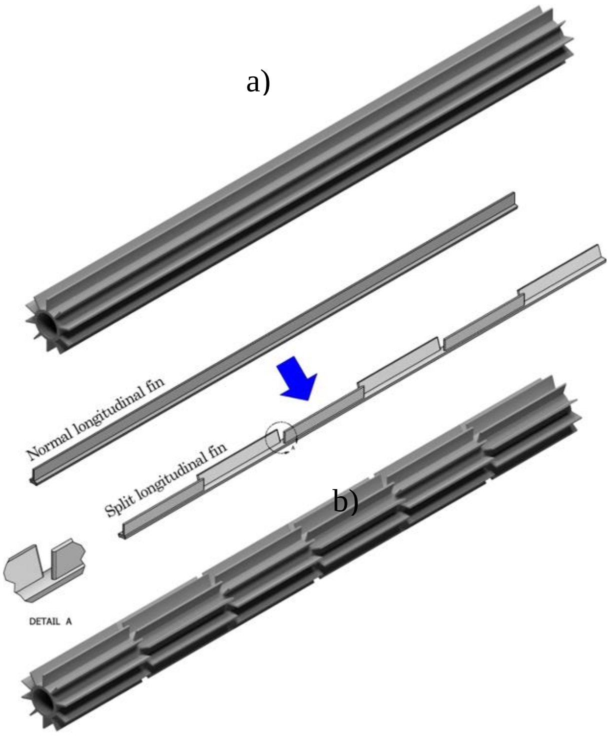

Figure 2.8: Schematic of DTHEs with a) normal longitudinal fins and b) split longitudinal fins [96].

Majidi, et al. [97] experimentally worked on the air heat transfer in a helical fin DTHE and presented an equation for increasing the overall heat transfer coefficient due to the fin. The results showed that the presence of the annulus fin increases the overall heat transfer coefficient. Syed, et al. [98] introduced the tip thickness in fins design as a new parameter by significant impacts on the heat transfer and flow properties in DTHEs (Figure 2.9). The tip thickness was controlled by the ratio of tip to base angles as a parameter with values varying from 0 to 1 corresponding to the fin shapes varying from the triangular to the rectangular cross-section. Variation in fin-tip thickness appears to significantly influence the primary flow variable, the velocity field, displacing the high-velocity region and changing the velocity gradients at the wetted perimeter. Table 2.2 summarises information on different extended surface areas and their effects in comparison to a conventional DTHE.

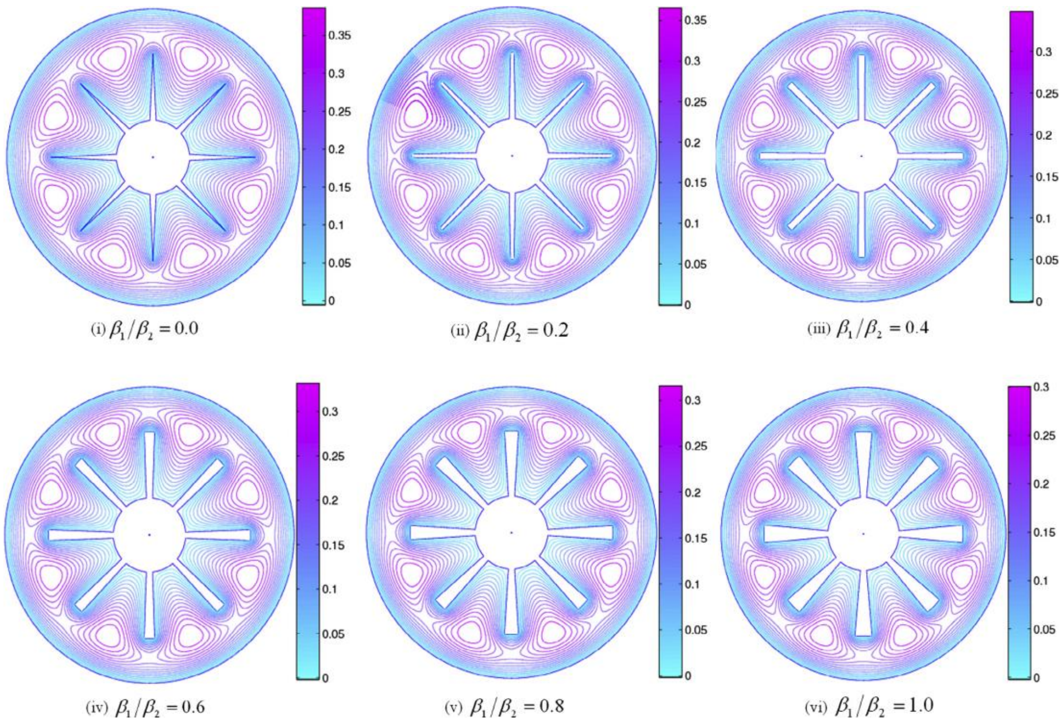

Figure 2.9: Different fin-tip thickness [98].

Table 2.2: Summary of information on different extended surface compared to a conventional DTHE.

Author	Configuration	Conditions	Findings
Braga and Saboya [16]	Longitudinal rectangular fins 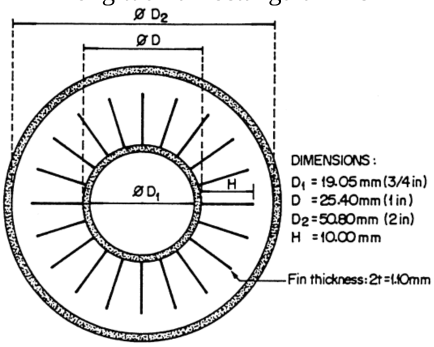 	Experimental and numerical Re: 10000-50000 Inner: hot water, temperature: 98°C Outer: cold air, temperature: 10-25°C Parallel flow	✓The fin or the region efficiency are known functions of the Reynolds number of the airflow and thermal conductivity of the fin material
Zhang, et al. [90]	Helical fins and vortex generators [94] 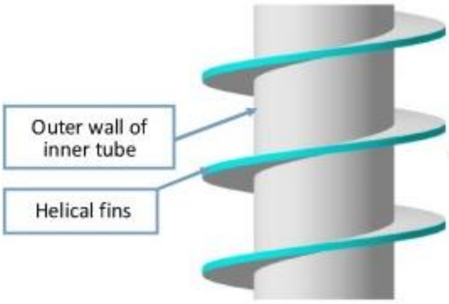 	Experimental Re: 6627-13387 Inner: steam, temperature: 100°C Outer: cold air, temperature: 24–28°C Counter flow	✓Increase of heat transfer: up to 46% ✓Increase of pressure drop: up to 146% ✓Heat exchanger with helical fins and vortex generators have better performance than heat exchangers only with helical fins at shorter pitch ratio
Zohir, et al. [99]	Coil wire around outer surface of inner tube [100] 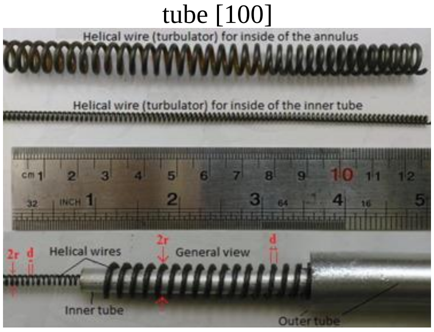 	Experimental Re: 4000-14000 Inner: hot water, temperature: 65°C Outer: cold water, temperature: 25°C Parallel and counter flow	✓Increase of heat transfer: 450% for counterflow and 400% for parallel flow ✓The Nusselt number increases with Reynolds number and pitch ratio
Sheikholeslami, et al. [101]	Typical and perforated circular-ring 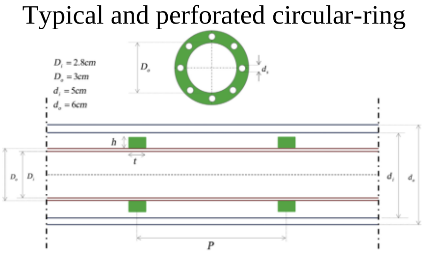	Experimental Re: 6000–12000 Inner: hot water Outer: cold air, temperature: 28°C Counter flow	✓Increase of Nusselt number with and without holes: 48% and 56% ✓Increase of friction factor with and without holes: 310% and 650% ✓Nusselt number and friction factor decrease by increasing the pitch ratio and

Author	Configuration	Conditions	Findings
			number of perforated hole
Sheikholeslami, et al. [102]	Typical and perforated discontinuous helical 	Experimental Re: 6000-12000 Inner: hot water Outer: cold air, temperature: 28°C Counter flow	✓Increase of Nusselt number with and without holes: 62% and 76% ✓Increase of friction factor with and without holes: 46% and 610% ✓Nusselt number and friction factor decrease with the increase of pitch ratio and perforated hole
Karanth and Murthy [103]	Rectangular, triangular and concave parabolic fin [95] 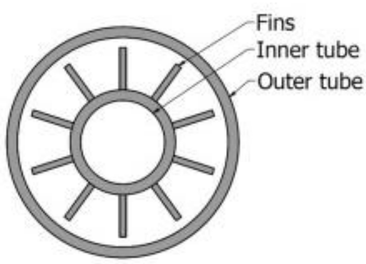	Numerical Re: 3000-20000 Inner: hot water, temperature: 59°C Outer: cold water, temperature: 30°C Parallel flow	✓Increase of heat transfer: 128% ✓Increase of pressure drop: 368% ✓Rectangular fin has the highest heat transfer rate and pressure drop compared to triangular and concave parabolic fin
El Maakoul, et al. [104]	Continuous helical baffle 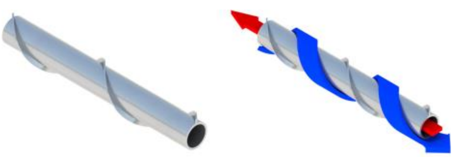	Numerical Re: 6000-72000 Inner: hot water, temperature: 36-40°C Outer: cold water, temperature: 8-17°C Counter flow	✓Increase of heat transfer: 45% ✓Increase of pressure drop: 21 times ✓The highest thermo-hydraulic performance is achieved when helical baffles are used in laminar flow regime
Sreedhard and Varghese [105]	Longitudinal fin patterns [95] 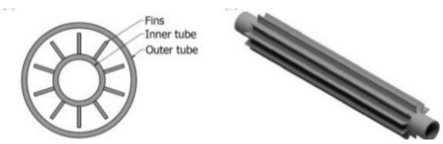	Numerical Re: 2230 Inner: hot water, temperature: 97°C Outer: cold water, temperature:27°C Counter flow	✓Increase of heat transfer: 60.5% ✓Maximum heat transfer and overall heat transfer coefficient is found when using four external fins
Zhang, et al. [106]	Helically petal-shaped fin 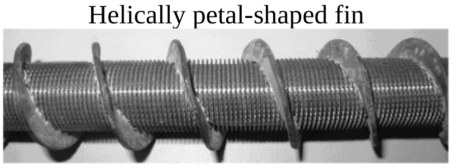	Experimental Re: 12000-18000 Inner: cold water Outer: hot water Counter flow	✓Increase of heat transfer: 233% ✓Increase of pressure drop: 111% ✓The increase in heat transfer is

Author	Configuration	Conditions	Findings
			significantly greater than that of the increase in pressure drop at constant Reynolds number
Salem, et al. [107]	Helical tape 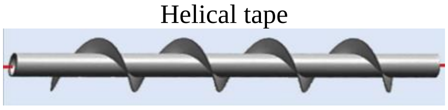	Experimental Re: 2050-26700 Inner: hot water, temperature: 50°C Outer: cold water, temperature: 15, 20, 25°C Counter flow	✓Increase of Nusselt number: 164.4% ✓Increase of friction factor: 113.1% ✓The annulus average Nusselt number and friction factor increased an increase in the height ratio, and decrease in the pitch ratio
Yadav and Sahu [108]	Helical surface disc 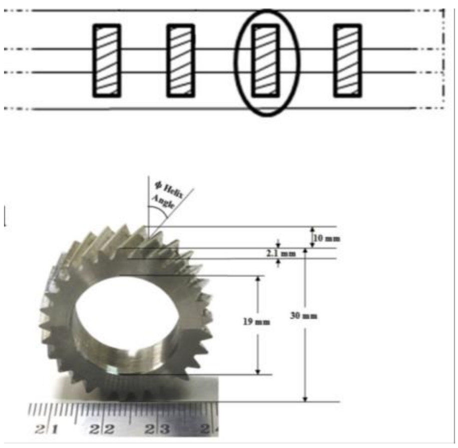	Experimental Re: 3500-10500 Inner: hot water, temperature: 75°C Outer: cold air Counter flow	✓Increase of Nusselt number: 290% ✓Increase of friction factor: 990% ✓The Nusselt number increased with the increase in Reynolds number and helix angle. It decreased with an increase in the diameter ratio ✓The friction factor increases with the increase in the helix angle and decreases with the increase in the diameter ratio and Reynolds number
Sheikholeslami and Ganji [109]	Perforated turbulator 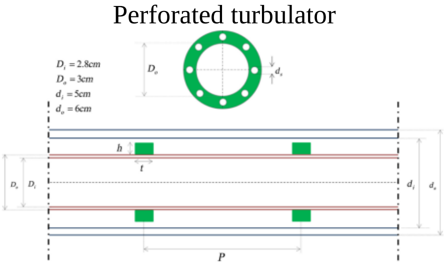	Experimental Re: 6000-12000 Inner: hot water Outer: cold air Counter flow	✓Increase of Nusselt number: 112.5% ✓Increase of friction factor: 760% ✓Thermal performance enhances with augment of open area ratio

Author	Configuration	Conditions	Findings
			✓Temperature gradient reduces with augment of the pitch ratio
Shaji [110]	Twisted Tape 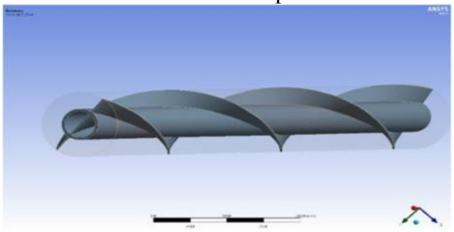	Numerical Re: 4717-14591 Inner: hot water, temperature: 80°C Outer: cold water, temperature:27°C Counter flow	✓Increase of Nusselt number: 43% ✓Increase of friction factor: 177% ✓Secondary flows induced by the twisted tape, enhanced cross stream mixing of the fluids, increase in the effective flow length
Yassin, et al. [111]	Straight fin 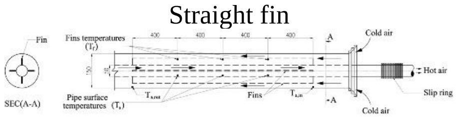	Experimental Re: 30000-90000 Inner: hot air Outer: cold air Counter flow	✓Increase of Nusselt number: 118% ✓The Nusselt number is proportional to the axial Re, Ta, fin heights and number of fins
Ravikumar and Raj [112]	Different profiles of fin 	Numerical Mass flow: 0.01-0.07 kg/s Inner: hot water Outer: cold water Counter flow	✓Increase of heat transfer: 220% ✓Increase of pressure drop: 10%
Sivalakshmi, et al. [113]	Helical fin 	Experimental Mass flow: 0.01-0.05 kg/s Inner: hot water, temperature: 80°C Outer: cold air, temperature: 30°C Counter flow	✓Increase of heat transfer: 38.46% ✓utilising of helical fin in water–air exchanger in annulus side could improve the heat transfer rate

2.3.3 Geometry change

This technique is usually used to modify the inner and outer tubes to increase the DTHEs heat transfer rate [114-124]. Corrugated tubes, helical and spiral tubes, and different cross-sections of tubes are examples of this technique that can be used widely in various industries' waste heat recovery systems [125]. This technique increases the heat transfer rate by increasing fluid mixing in the boundary layer, turbulence level of the fluid flow, and heat transfer surface area [126-128]. There are many publications that use different geometries in DTHEs to improve the heat transfer rate compared to conventional DTHEs, for example, inner curved-pipe [129], oval pipe[130, 131], coaxial annular tube with wall deformations[132], different conical tubes[133], inner sinusoidal tube[134], and inner corrugated tube[128].

Dizaji, et al. [127] performed an experiment to compare inner and outer corrugated tubes in a DTHE. It was shown that using both inner and outer corrugated tubes increased the Nusselt number and friction factor from 23-117% and 200-254%, respectively. With the inner tube being corrugated, the Nusselt number and friction factor increased from 10-52% and 150-190%, respectively. Also, Zambaux, et al. [132] numerically confirmed that the wall deformation on both inner and outer tubes increased the performance evaluation criteria up to 43% compared with only deformation on the outer or inner tube (Figure 2.10).

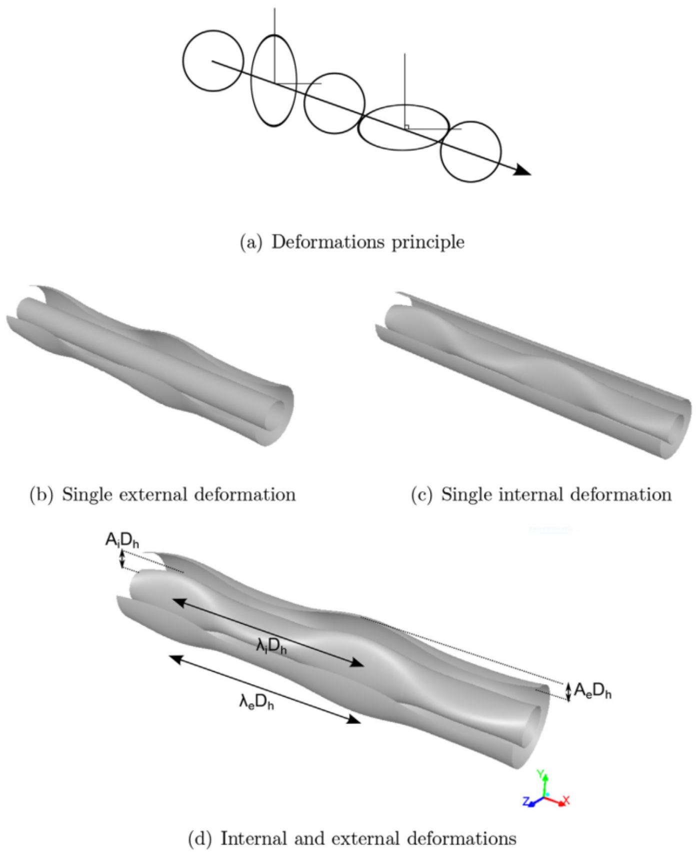

Figure 2.10: Different inner and outer tube deformation [132].

Webb [135] showed that if the rib pitch decreased less than required for reattachment of the boundary layer, the heat transfer coefficient decreased. So, the maximum amount occurs at the reattachment point. Bhadouriya, et al. [136] developed experimental and numerical investigation on hydrothermal properties in a DTHE with the inner twisted square duct and outer circular pipe (Figure 2.11). It was reported that with this configuration of DTHE, the heat transfer enhancement is suitable for laminar flow rather than turbulent flow. Table 2.3 summarises information on different geometry changes and their effects in comparison to a conventional DTHE.

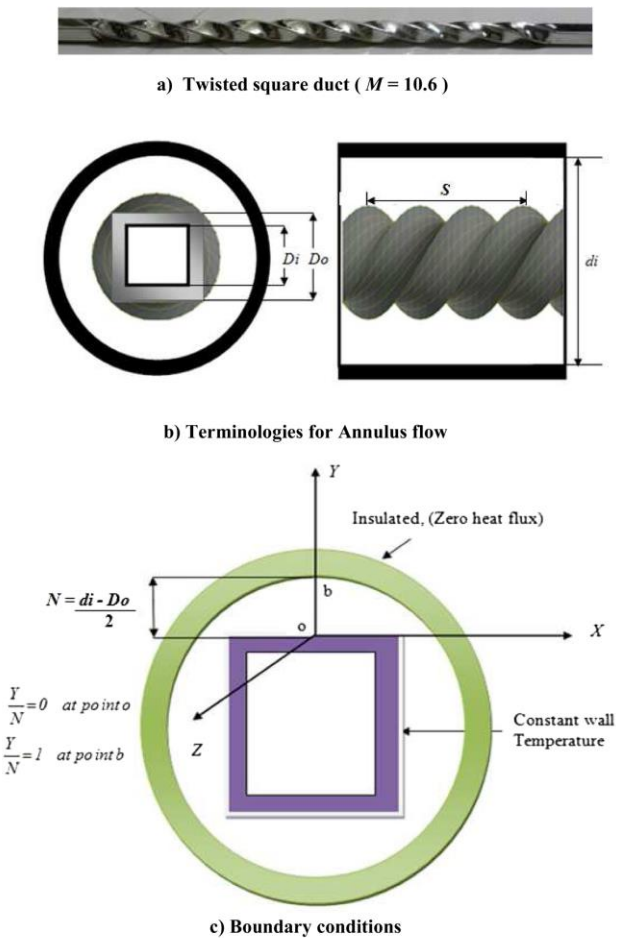

Figure 2.11: Details of twisted square duct and outer circular pipe [136].

Table 2.3: Summary of information on different extended surface compared to a conventional DTHE.

Author	Configuration	Conditions	Findings
Córcoles, et al. [15]	Spirally corrugated tube 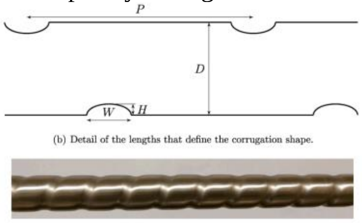	Experimental and numerical Re: 25000-50000 Inner: cold water, temperature: 22.1°C Outer: hot water, temperature: 60°C Counter flow	✓Increase of average heat transfer rate: up to 23% ✓Increase of pressure drop: 315 and 27% for inner and outer tube respectively ✓With decreasing helical pitch and increasing corrugation height the heat transfer and pressure drop increased
Luo and Song [137]	Counter-twisted oval tubes 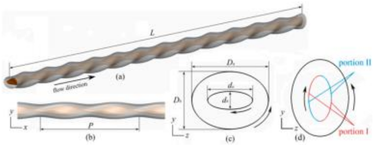	Numerical Re: 1000–15000 Inner: wall temperature constant at 300°C Outer: inlet temperature 20°C Counter flow	✓Increase of Nusselt number: up to 157% ✓Increase of friction factor: up to 118% ✓The intensity of the vortices increases with the decrease of aspect ratio and twist ratio
Hashemian, et al. [133]	Conical tube form 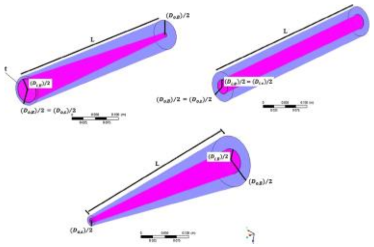	Numerical Re: 12202-48808 Inner: hot water, temperature: 52°C Outer: cold water, temperature: 25°C Counter and parallel flow	✓Increase of Nusselt number: 63% ✓Increase of friction factor: 700% ✓The Nusselt number is highest in both inner and outer conical tubes
Dizaji, et al. [138]	Corrugated shell and tube 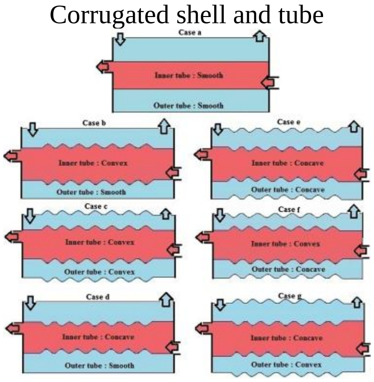	Experimental Re: 3500-18000 Inner: hot water, temperature: 50°C Outer: cold water, temperature: 22°C Counter flow	✓Increase of NTU: 34 to 60% ✓Exergy loss: 17 to 81% ✓Maximum NTU is obtained for heat exchanger made of corrugated shell and corrugated tube
Han, et al. [128]	Inner corrugated tube 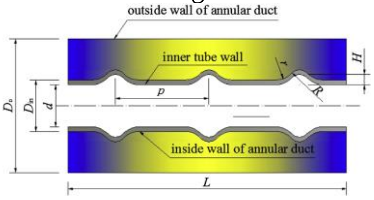	Numerical Re: 26250-65625 Inner: constant wall temperature: 427°C Outer: steam, temperature: 290°C	✓Increase of Nusselt number: 81% ✓Increase of friction factor: 500% ✓The decrease of corrugation height and Reynolds number increase the overall heat transfer coefficient
Dizaji, et al. [127]	Convex and concave corrugated tube	Experimental Re: 3500-18000 Inner: hot water, temperature: 40°C	✓Increase of Nusselt number: 117% ✓Increase of friction factor: 254%

Author	Configuration	Conditions	Findings
	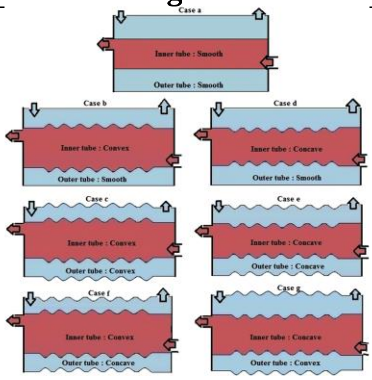	Outer: cold water, temperature: 8°C Counter flow	✓Maximum effectiveness is obtained for the heat exchanger with a concave corrugated outer and convex corrugated inner tube.
Wang, et al. [139]	Outward helically corrugated tube 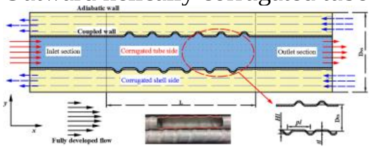	Numerical Re: 4300-18800 Inner: Helium, temperature: 390°C Outer: Helium, temperature: 300°C Counter flow	✓Increase of heat transfer: 28% ✓The heat transfer performance linearly decreased with the increase in the shell diameter, but the pressure drop sharply decreased when the shell diameter equals 38 mm
Pethkool, et al. [140]	Helical corrugated tube 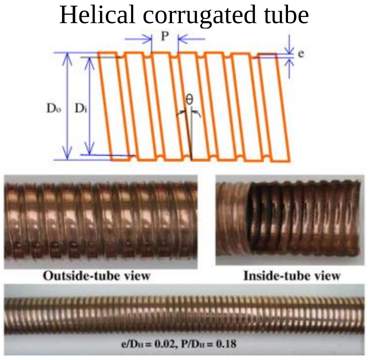	Experimental Re: 5500-60000 Inner: hot water, temperature: 70°C Outer: cold water, temperature: 28°C Counter flow	✓Increase of heat transfer rate: 232% ✓Increase of friction factor: 115% ✓The Nusselt number, friction factor and thermal performance factor increased when increasing the pitch ratio and the rib-height ratio
Laohalertdecha and Wongwises [141]	Corrugated tube 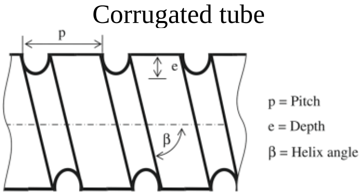	Experimental Re:8000-27000 Inner: R-134a, temperature: 40, 45 and 50°C Outer: Cold water Counter flow	✓Increase of heat transfer rate: 50% ✓Increase of friction factor: 70% ✓The average heat transfer coefficient and pressure drop increased when increasing the mass flux as well as average quality
Webb, et al. [142]	Helical-rib roughness [143] 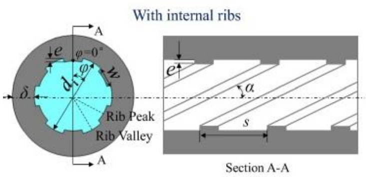	Experimental Re: 20000-80000 Inner: water Outer: R-12	✓Increase of heat transfer coefficient: 133% ✓Increase of friction factor: 120% ✓The area increase and fluid mixing in the interfin region caused by flow separation and reattachment are two key factors, which affect the enhancement heat transfer rate

Author	Configuration	Conditions	Findings
Han, et al. [144]	Outward convex corrugated tube 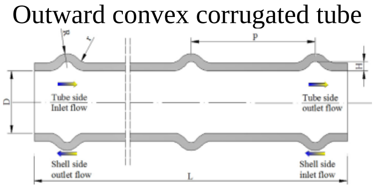 	Numerical Re: 45938-26250 Inner: Helium, temperature: 330°C Outer: constant wall temperature: 327°C	✓Increase of Nusselt number: 63.6% ✓Increase of friction factor: 380% ✓The most significant factor in Nu is Re, which intensively relates to the thickness of the thermal boundary layer and turbulent intensity. ✓The most significant effect factor on heat transfer and friction factor is the ratio of corrugation height to tub diameter
Wongwises and Polsongkram [145]	Helically coiled tube 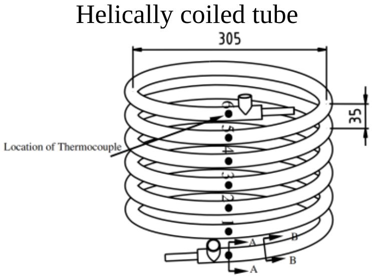 	Experimental Mass flux: 400 and 800 $kg/m^2.s$ Inner: HFC-134a, temperature: 40 and 50°C Outer: water Counter flow	✓Increase of heat transfer coefficient; 33 to 53% ✓Increase of pressure drop: 29 to 46% ✓The average heat transfer coefficient increases when increasing average vapor quality and mass flux and decreases with increasing saturation temperature ✓The frictional pressure drop of the condensation process increases with increasing average vapor quality and mass flux and decreases with increasing saturation temperature of condensation
Kumar, et al. [146]	Helically coiled tube 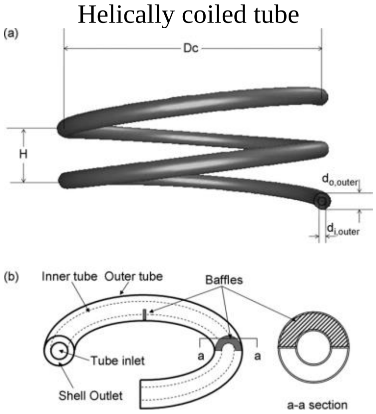 	Numerical Re: 5000-70000 Inner: air Outer: water Counter and parallel flow	✓Increase of Nusselt number: 70% ✓Increase of friction factor: 435% ✓With the increase in operating pressure in the inner tube the overall heat transfer coefficient increases
Yang and Chiang [129]	Curved pipe 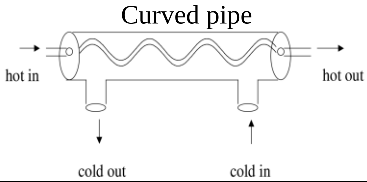 	Experimental Re: 1000-20000 Inner: hot water Outer: cold water Counter flow	✓Increase of heat transfer rate: 100% ✓Increase of friction factor: 40%

Author	Configuration	Conditions	Findings
Chen and Dung [130]	Vertical oval cross section pipe 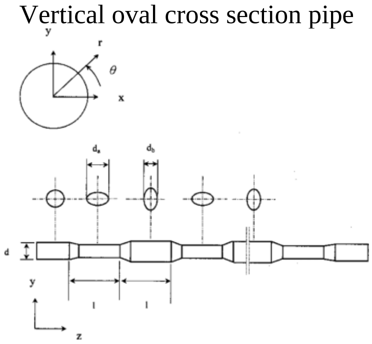	Numerical Re: 100-2000 Inner: hot water Outer: cold water Counter and parallel flow	✓A higher Dean number results in a higher heat transfer rate ✓Increase of heat transfer rate: 37% ✓The magnitude of the overall heat transfer coefficient decreases as the total length increases, however, the heat transfer enhancement coefficient behaves oppositely, as this quantity increases while the tube is elongated
Zambaux, et al. [132]	Wall deformation 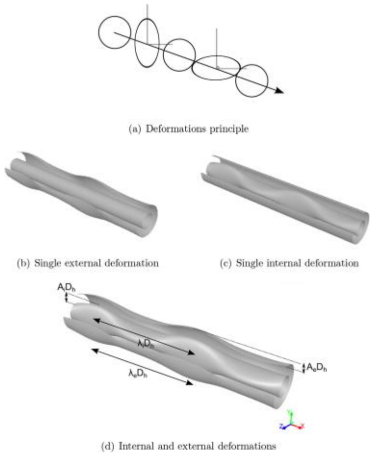	Numerical Inner: constant wall temperature 26°C Outer: mixture of glycol and water, temperature: 48°C	✓Increase of heat transfer rate: 43%
Shao, et al. [147]	Helically coiled tube [145] 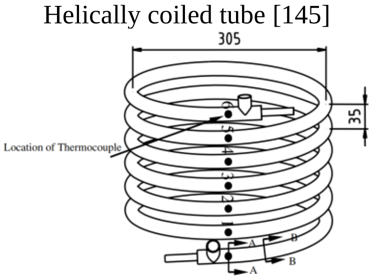	Experimental Mass flux: 100-400 $kg/m^2.s$ Inner: R-134a, temperature: 35, 40 and 45°C Outer: water Counter flow	✓Increase of heat transfer coefficient: 4 to 13.8% ✓The average heat transfer coefficients for both the straight and helical sections increase with the mass flux of R-134a and the vapor quality as well
Moawed, et al. [134]	Sinusoidal inner pipe 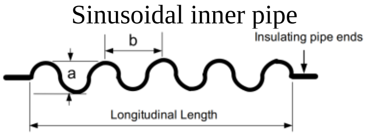	Experimental Re: 8800-28000 Inner: cold water Outer: hot water Counter flow	✓Increase of Nusselt number: 18 to 93% ✓Increase of friction factor: 69 to 130%
Luo, et al. [131]	Twisted oval tube 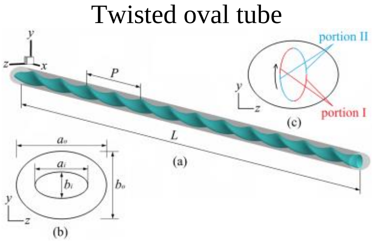	Numerical Re: 1000-15000 Inner: constant wall temperature 90°C Outer: air, temperature: 20°C	✓Increase of Nusselt number: 116% ✓Increase of friction factor: 46% ✓The thermal performance enhancement is more significant in the laminar regime

2.3.4 Nanofluids

Nanofluid is defined as a fluid in which nanometer-sized particles are suspended [148, 149]. Nanofluids, including suspended nanoparticles in liquids, increase the base fluids' thermal convective and conductive heat transfer performance [150]. The classification of nanofluids is various; however, they are generally classified based on nanoparticles or base fluids. The two categories of nanofluids based on nanoparticles are metallic or non-metallic nanofluids [151-153]. The suspension of metallic nanoparticles makes the metallic-based nanofluids that it can be as metal or metal oxides such as Al, Cu, Zn, CuO, ZnO [154-158]. On the other side, the non-metallic-based nanofluids are made by suspension of non-metallic nanoparticles such as SiO_2, carbon-based nanoparticles, nanofibers, graphene, graphene oxide, and nanotubes [159-163]. When more than one type of nanoparticle is used, non-metallic or metallic nanoparticles, the nanofluids are classified as hybrid nanofluids. [164-166]. According to the base fluid, nanofluids are classified as water-based, aqueous-based, or non-aqueous–based. Nanoparticles can be dispersed in different base fluids such as oils or ethylene glycol [161, 167-169]. Figure 2.12 shows one of the most common classifications of nanofluids.

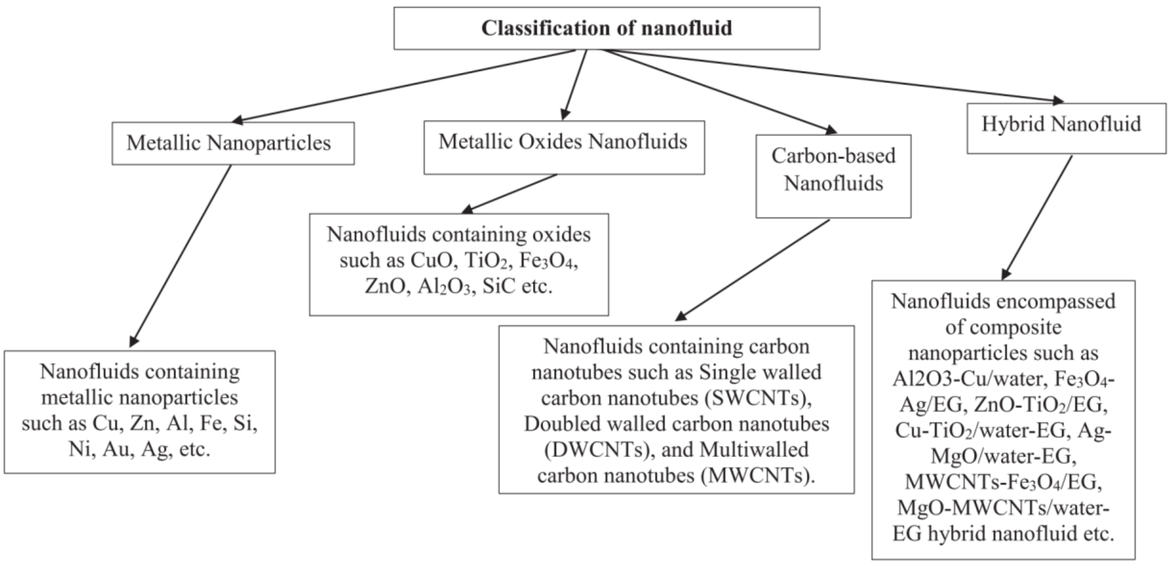

Figure 2.12: Classification of nanofluid [170].

Nanofluids enhance the heat transfer rate by increasing the surface area of nanoparticles, heat capacity, effective and apparent thermal conductivity, interactions and collisions among particles, fluctuations and turbulence of the fluid [171, 172].

Using nanofluids in DTHEs instead of pure water or other liquids can enhance the performance of the system. So, this area of research has caught the attention of many researchers [37, 38, 173-184]. Generally, researchers investigate nanofluids as a working fluid in DTHEs. For example, some researchers investigated different nanoparticles such as aluminum oxide, copper oxide, titanium dioxide to determine their effect on the heat transfer rate in a heat exchanger [185-187]. Table 2.4 summarises information on using different nanofluids and their effects in comparison to pure water in a conventional DTHE.

Table 2.4: Summary of information on using different nanofluids in comparison to pure water in a conventional DTHE.

Author	Conditions	Findings
Chun, et al. [17]	Experimental Re: 100-450 Nanofluid: Al_2O_3, base fluid: water and transformer oil, concentration: 0.25% and 0.5% Inner: cold nanofluid and water Outer: hot water and nanofluid Parallel and counter flow	✓Increase of the heat transfer coefficient: up to 25% ✓The surface properties of nanoparticles, particle loading, and particle shape are key factors for enhancing the heat transfer properties of nanofluids
Zamzamian, et al. [188]	Experimental Re: turbulent flow Nanofluid: Al_2O_3 and CuO, base fluid: ethylene glycol, mean diameter 20 nm, concentration: Al_2O_3: 0.1, 0.5, and 1%, CuO: 0.1, 0.3, 0.5, 0.7, and 1% Inner: hot nanofluid, temperature: 45, 60, and 75°C Outer: cold water	✓Increase of the heat transfer coefficient: up to 37.2% ✓the convective heat transfer coefficient of nanofluid increases with increasing volume fraction and temperature of nanofluid ✓The theoretical and experimental results are same in lower temperatures
Darzi, et al. [189]	Experimental Re: 5000-20000 Nanofluid: Al_2O_3, base fluid: water, mean diameter 20 nm, concentration: 0.25, 0.5, 0.75, and 1% Inner: cold nanofluid, temperature: 27-55°C Outer: hot water	✓Increase of Nusselt number: 19% ✓Increase of friction factor: 15% ✓By increasing the volume fraction of nanofluid, the heat transfer and pressure drop increase ✓Adding nanoparticles has better results at high Reynolds number
Aghayari, et al. [190]	Experimental Re: 15000–28000 Nanofluid: Al_2O_3, mean diameter 20 nm, base fluid: water, concentration: 0.1, 0.2, and 0.3% Inner: hot nanofluid, temperature: 40 and 50°C Outer: cold water Counter flow	✓The increase of heat transfer: 12% ✓The nanofluid with suspended nanoparticles increases the thermal conductivity of the Mixture and a large energy exchange process resulting from the chaotic movement of nanoparticles
Sarafraz and Hormozi [191]	Experimental Re: 1000-11000 Nanofluid: green tea leaves and silver nitrate, mean diameter 40-50 nm, base fluid: 50% water and 50% ethylene	✓Increase of heat transfer coefficient: up to 67% ✓Increase of friction factor: 11.3% ✓Pressure drop and friction factor increases by increasing volume fraction

Author	Conditions	Findings
	glycol, concentration: 0.1, 0.5 and 1%, temperature: 25-80°C Inner: hot nanofluid Outer: cold water Counter flow	
El-Maghlany, et al. [185]	Experimental Re: 2500-5000 Nanofluid: Cu, mean diameter: 63-100 nm, base fluid: water, concentration: 1, 1.5, 2, 2.5, and 3% Inner: hot water Outer: cold nanofluid Counter flow	✓Increase of NTU and effectiveness: 23.4% and 16.5% ✓Increase of pressure drop: 36%
Han, et al. [186]	Experimental Re: 20000-60000 Vertical DTHE Nanofluid: Al_2O_3, base fluid: water, concentration: 0.25 and 0.5% Inner: cold nanofluid, temperature: 40 and 50°C Outer: superheat steam Counter flow	✓Increase of Nusselt number: up to 24.5% at 50°C ✓The heat transfer increases with the increase in volume fraction and temperature of nanoparticles
Mohamed, et al. [192]	Numerical Re: 2473– 4947 Nanofluid: Al_2O_3, Cu, base fluid: water, concentration: 1, 2, and 3% Inner: hot water, temperature: 60°C Outer: cold nanofluid, temperature: constant 28°C Counter flow	✓Increase of average heat transfer rate: up to 13% and 7.6% for Cu and Al_2O_3 ✓Increase of NTU: up to 18.8% and 10.72% for Cu and Al_2O_3 ✓Increase of effectiveness: up to 13.06 and 7.56% for Cu and Al_2O_3 ✓Increase of pressure drop: up to 37.26 and 27.1% for Cu and Al_2O_3 ✓By increasing inlet temperature heat transfer of nanofluids increases which shows nanofluids dependency on temperature
Zheng, et al. [193]	Experimental Re: 4500-14500 Nanofluid (mean diameter): Al_2O_3 (20 nm), CuO (40 nm), Fe_3O_4 (20 nm), ZnO (30 nm), SiC (40 nm), and SiO_2 (30 nm), base fluid: water, concentration: 0.5, 1, 1.5, and 2.0% Inner: cold nanofluid, temperature: 25°C Outer: hot water, temperature: 60°C Counter flow	✓Increase of Nusselt number (concentration): Al_2O_3: 12.2% (2%), CuO: 44.3% (1%), Fe_3O_4: 53.5% (1.5%), ZnO: 43% (1.5%), SiC: 68.4% (1.5%), SiO_2: 6.6% (0.5%) ✓Increase of friction factor (concentration): Al_2O_3: 53.4% (2%), CuO: 45.5% (2%), Fe_3O_4: 73.1% (2%), ZnO: 73.5% (2%), SiC: 77.6% (2%), SiO_2: 46.4% (2%)
Esfe, et al. [178]	Experimental Re: 4000-31000 Nanofluid: COOH-functionalized double-walled carbon nanotubes, base fluid: water, concentration: 0.01 to 0.4% Inner: cold nanofluid Outer: hot water Temperature: 300-340 K Counter flow	✓Increase of heat transfer coefficient: 32% ✓Increase of pressure drop: 20% ✓Nanofluid concentration of the maximum heat transfer coefficient and pressure drop: 0.4%
Duangthongsuk and Wongwises [194]	Experimental Re: 3000-18000 Nanofluid: TiO_2, mean diameter: 21 nm, base fluid: water, concentration: 0.2 to 2% Inner: cold nanofluid, temperature: 15, 20, 25 °C	✓Increase of heat transfer coefficient: 26% ✓Increase of pressure drop: 28% ✓The pressure drop of nanofluids increases with increasing Reynolds number and there is a small increase

Author	Conditions	Findings
	Outer: hot water, temperature: 35, 45 °C Counter flow	with increasing particle volume concentrations
Arani and Amani [179]	Experimental Re: 8000-51000 Nanofluid: TiO_2, mean diameter: 30 nm, base fluid: water, concentration: 0.002 to 0.02 Inner: cold nanofluid Outer: hot water, temperature: 60 °C Counter flow	✓Increase of heat transfer coefficient: 72% ✓Increase of pressure drop: 54% ✓The use of nanofluid with the higher concentration provides considerably higher Nusselt number and thermal performance for all Reynolds numbers examined
Esfe, et al. [180]	Experimental Re: 3200-19000 Nanofluid: MgO, mean diameter: 40 nm, base fluid: water, concentration: 0.0625 to 1% Inner: cold nanofluid, temperature: 24.7 to 60 °C Outer: hot water Counter flow	✓Increase of heat transfer coefficient: 35.93% ✓Increase of pressure drop: 16% ✓The maximum thermal conductivity is belonged to maximum nanofluid concentration
Khalifa and Banwan [181]	Experimental Re: 3000-6000 Nanofluid: Al_2O_3, mean diameter: 10 nm, base fluid: water, concentration: 0.25 to 1% Inner: cold nanofluid, temperature: 20 to 35 °C Outer: hot water, temperature: 50 °C Counter flow	✓Increase of heat transfer coefficient: 22.8% ✓Increase of Nusselt number: 20% ✓The heat transfer coefficient and Nusselt number are increased by increasing Reynolds number and particles volume fraction
Madhesh and Kalaiselvam [195]	Experimental Re: 300-700 Nanofluid: Ag, mean diameter: 10-65 nm, base fluid: ethylene glycol, concentration: 0.1 to 2% Inner: hot nanofluid, temperature: 60 °C Outer: cold water, temperature: 40 °C Counter flow	✓Increase of heat transfer coefficient: 54.3% ✓Increase of pressure drop: 23.7% ✓At a lower volume concentration, the mean free path available for particles moving between the inner fluids layers could benefit in transferring the heat effectively
Khedkar, et al. [182]	Experimental Re: 500-4000 Nanofluid: TiO_2, mean diameter: 20 nm, base fluid: water, concentration: 2 and 3% Inner: cold nanofluid Outer: hot water, temperature: 55-75 °C Counter flow	✓Increase of heat transfer coefficient: 33% ✓For the same range of Reynold's number, addition of nanoparticles to the base fluid enhances the heat-transfer performance and results in the higher heat transfer coefficient than that of the base fluid

2.3.5 Combination of different techniques

To enhance the thermal performance of DTHEs, it is possible to use two or three techniques together [196, 197]. In this way, the key factors that increase the heat transfer rates reinforce each other and improve the performance of the heat exchanger. For example, a combination of turbulator insertion with geometry change [198], nanofluids with turbulator insertion and geometry change makes a good improvement in the thermal performance of

DTHEs [187, 199]. Some researchers use these techniques in a single pipe with the appropriate boundary condition that matches to the DTHEs to investigate its performance [200-217].

2.3.5.1 Combination of turbulator insertion and geometry change

Mashoofi, et al. [46] experimentally studied the thermal-frictional behaviour of helically coiled a DTHE, which contains the turbulator (Figure 2.13). Hot water and cold air were used as working fluids in the outer and inner tubes with inlet temperatures of 50°C and 25°C, respectively. The results showed that using a turbulator in the outer tube increased the airside Nusselt number by around 8-32%. However, the employment of the turbulator in the inner side increased the Nusselt number of the inner side by around 52-81%. The friction factor increased about 519% when compared to a conventional DTHE without a turbulator.

Mokkapati and Lin [198] numerically studied the combination of turbulator insertion and geometry change in a DTHE (Figure 2.14). Hot water was employed in the inner corrugated tube with twisted tape insertion at 510°C and cold water on the outer side at 90.55°C. It showed that corrugated tubes with twisted tape insert increased the heat transfer rate by about 235.3% and 67.26% compared with a straight tube and corrugated tube without twisted tape insertion, respectively.

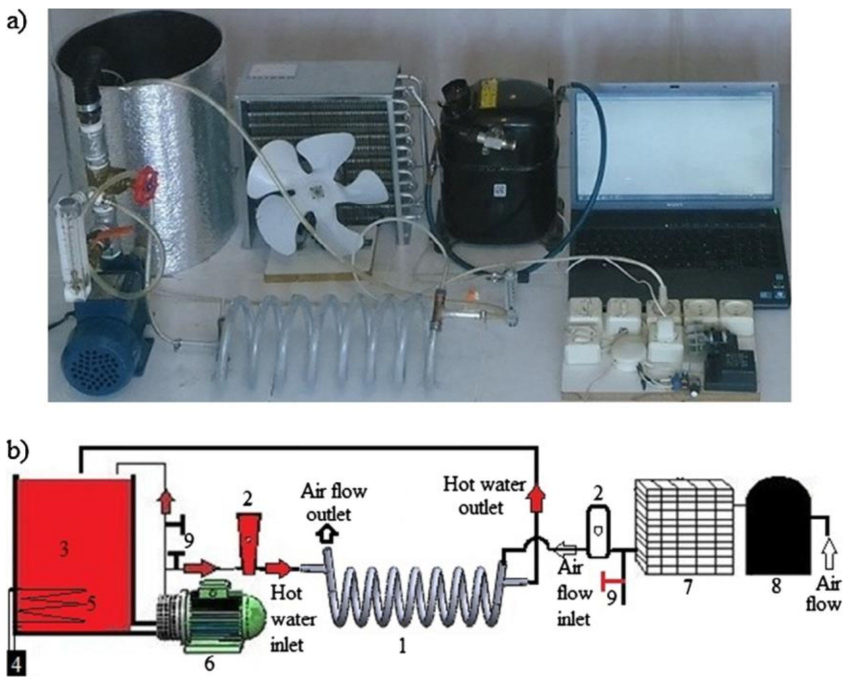

Figure 2.13: a) Experimental setup and b) a schematic illustration of the test set-up: 1. test section, 2. Rotameter, 3. warm water tank, 4. dimmer and thermostat, 5. heater, 6. water pump, 7. condenser, 8. compressor, 9.valves [46].

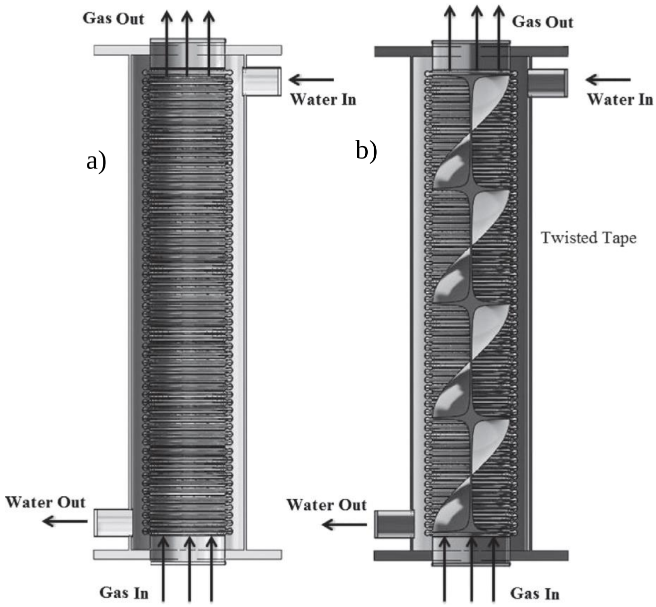

Figure 2.14: Cross sectioned view of a) ACT heat exchanger and b) ACT heat exchanger with twisted tape [198].

2.3.5.2 Combination of nanofluids and turbulator insertion

Chandra Sekhara Reddy and Vasudeva Rao [218] conducted experiments on TiO_2 nanofluid with the base fluid of 60% water and 40% ethylene glycol in the range of Reynolds number from 4000 to 15000 (Figure 2.15). Nanofluid with the mean diameter of nanoparticles 21 nm and hot water flowed in the inner and outer tube as working fluids, respectively. This study aimed to indicate the effects of nanofluid with and without helical coil insertion. The results showed that heat transfer coefficient enhancement due to nanofluid with and without helical insertion was 17.71% and 10.73%, respectively. However, the friction factor increased by16.58% due to nanofluid and helical coil insertion. Table 2.5 summarises information on the combination of different nanofluids and turbulator insertion and their effects in comparison to pure water and a conventional DTHE.

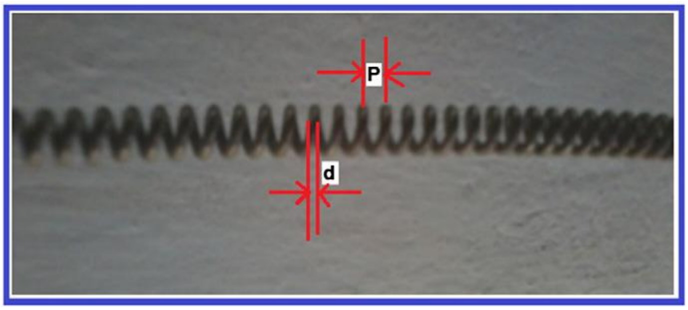

Figure 2.15: Photograph of wire coil inserts [218].

Table 2.5: Summary of information on the combination of different nanofluids and turbulator insertion and their effects compared to pure water and a conventional DTHE.

Author	Conditions	Findings
Maddah, et al. [199]	Experimental Twisted tape Re: 5000-21000 Nanofluid: Al_2O_3, mean diameter 20-22 nm, base fluid: water, concentration: 0.2, 0.5, and 0.9% Inner: hot nanofluid, temperature: constant inlet 40°C Outer: cold water, temperature: constant inlet 25°C Counter flow	✓Increase of heat transfer rate: up to 300% ✓Increase of friction factor: up to 180%
Chandra Sekhara Reddy and Vasudeva Rao [218]	Experimental Helical coil Re: 4000-15000 Nanofluid: TiO_2, mean diameter 21 nm, base fluid: 60% water and 40% ethylene glycol, concentration: 0.004, 0.012, and 0.02% Inner: cold nanofluid Outer: hot water Counter flow	✓Increase of heat transfer due to nanofluid: up to 10.73% ✓Increase of heat transfer due to nanofluid and helical coil: up to 17.71% ✓Increase of friction factor due to nanofluid and helical coil: up to 16.58%
Prasad, et al. [219]	Experimental Trapezoidal-cut twisted tape Re: 3000-30000 Nanofluid: Al_2O_3, mean diameter less than 50 nm, base fluid: water, concentration: 0.01 and 0.03% Inner: cold nanofluid Outer: hot water, temperature: 70°C Counter flow	✓Increase of Nusselt number: 34.24% ✓Increase of friction factor: 29% ✓The average Nusselt number increase by increasing Reynolds number
Karimi, et al. [220]	Numerical Twisted tape Re: 250-2250 and 3000-9000 Nanofluid: Al_2O_3, base fluid: water, mean diameter 20 nm, concentration: 1, 2, and 3% Inner: cold nanofluid, temperature: 26°C Outer: superheat steam, temperature: 37°C Counter flow	✓Increase of the Nusselt number due to twisted tape: 22% ✓Increase of heat transfer due to twisted tape and nanoparticles: up to 30% ✓Increase of the pressure drop due to twisted tape and nanoparticles: up to 40% ✓The use of twisted tapes at high Reynolds numbers is more economical compared to low Reynolds numbers.
Gnanavel, et al. [221]	Numerical Spiral Spring insertion Re: 1000-10000 Nanofluid: TiO_2, BeO, ZnO, and CuO, base fluid: water Inner: hot nanofluid Outer: cold water	✓Increase of Nusselt number: TiO_2: 117.39%, BeO: 63.09%, ZnO: 56.63%, and CuO: 47.62% ✓Increase of friction factor: CuO: 312%, ZnO: 304.89%, BeO: 288%, TiO_2: 275.55% ✓The thermal performance factor tends to decrease with the rise of Reynolds number, for most of the cases
Karuppasamy, et al. [222]	Numerical Cone shape insertion Re: 2000-10000	✓Increase of Nusselt number: Al_2O_3: 65%, CuO: 56% ✓Increase of friction factor: Al_2O_3: 50%, CuO: 47%

Author	Conditions	Findings
	Nanofluid: Al_2O_3 and CuO, mean diameter 100 nm, base fluid: water, concentration: 1%	✓Aluminum oxide nano fluid gives the higher heat transfer rate than the copper Oxide nano fluid because of the nano layer and thermophysical properties of liquid and nanosolid particles
Singh and Sarkar [166]	Experimental Tapered wire coil Re: 9000-40000 Nanofluid: Al_2O_3 + MgO (50/50 volume ratio), mean diameter less than 50 nm for Al_2O_3 and 90 nm for MgO, base fluid: water, concentration: 0.1% Inner: hot nanofluid, temperature: 50, 60, and 70°C Outer: cold water, temperature: constant at 30°C Counter flow	✓Increase of the Nusselt number: up to 84% ✓Increase of the friction factor: up to 68% ✓Nusselt number increases with increase in temperature from 50 to 70 °C ✓The entropy generation of nanofluid is lower than the base fluid in all cases
Singh and Sarkar [223]	Experimental V-cut twisted tape Re: 8000-40000 Nanofluid: Al_2O_3, PCM, and Al_2O_3+PCM, mean diameter 50 nm, base fluid: water, concentration: 0.01 and 0.1% Inner: cold nanofluid, temperature: 30°C Outer: hot water, temperature: constant at 60°C Counter flow	✓Increase of heat transfer coefficient due to the nanofluid: up to 25.6% ✓Increase of pressure drop due to the nanofluid: up to 16.05% ✓Increase of heat transfer coefficient due to the nanofluid and V-cut twisted tape: up to 47.62% ✓Increase of pressure drop due to the nanofluid and V-cut twisted tape: up to 63.69%
Singh and Sarkar [224]	Experimental Conical wire coil insertion Re: 9000-45000 Nanofluid: Al_2O_3, CNT, hybrid (Al_2O_3+CNT), mean diameter: 10-100 nm, base fluid: water, concentration: 0.01% Inner: cold nanofluid, temperature: 30°C Outer: hot water, temperature: 60°C Counter flow	✓Increase of Nusselt number (hybrid nanofluid): up to 171, 152, and 139% for diverging, converging-diverging and converging wire coil insertion ✓Increase of friction factor (hybrid nanofluid): up to 106, 92, and 72% for diverging, converging-diverging and converging wire coil insertion ✓The hybrid nanofluid has better heat transfer than Al_2O_3 and CNT ✓CNT nanofluid has better heat transfer than Al_2O_3
Mohammed, et al. [11]	Numerical Louvered strip insert Re: 10000-50000 Nanofluid: Al_2O_3, CuO, SiO_2 and ZnO, mean diameter 20-50 nm, base fluid: water, concentration: 1-4% Inner: nanofluid Outer: constant heat flux	✓Increase of heat transfer: 367-411% for backward louvered strip arrangement and 350-400% for forward louvered strip arrangement ✓Increase of friction factor: 900% ✓SiO_2 nanofluid has the highest Nusselt number value, followed by Al_2O_3, ZnO, and CuO ✓The Nusselt number increases with decreasing the nanoparticle diameter and it increases slightly with increasing the volume fraction of nanoparticles
Sundar, et al. [173]	Experimental Wire coil insert Re: 16000-30000 Nanofluid: Fe_3O_4, base fluid: water, concentration: 0.005-0.06% Inner: hot nanofluid, temperature: 60°C	✓Increase of Nusselt number: 32.03% ✓Increase of friction factor: 16.2% ✓The heat transfer of nanofluids increases with increasing particle concentration, Reynolds number and

Author	Conditions	Findings
	Outer: cold water, temperature: 29°C Counter flow	decreasing pitch ratio of the wire coil inserts
Akyürek, et al. [37]	Experimental Wire coil insert Re: 4000-20000 Nanofluid: Al_2O_3, mean diameter less than 100 nm, base fluid: water, concentration: 0.4-1.6% Inner: cold nanofluid Outer: hot water, temperature: 70°C Counter flow	✓Increase of Nusselt number: 271.92% ✓Increase of friction factor: 500% ✓The Nusselt number increase as the pitch of the turbulators placed in the heat exchanger decreases
Khoshvaght-Aliabadi, et al. [225]	Experimental Perforated-tape, jagged-tape, twisted-tape, helical-screw, vortex-generator, offset-strip Flow rate: 2-5 l/min Nanofluid: Cu, mean diameter 40 nm, base fluid: water, concentration: 0.1 and 0.3% Inner: cold nanofluid, temperature: 30°C Outer: steam Counter flow	✓Increase of Nusselt number: 293% ✓Increase of pressure drop: 509% ✓The vortex-generator gets the highest effect and perforated-tape gets the lowest effect
Prasad, et al. [226]	Experimental Helical tape insert Re: 3000-30000 Nanofluid: Al_2O_3, mean diameter less than 50 nm, base fluid: water, concentration: 0.01 and 0.03% Inner: cold nanofluid Outer: hot water Counter flow	✓Increase of Nusselt number: 32.91% ✓Increase of friction factor: 38% ✓The pressure drop in the inner tube increases with an increase in nanoparticle volume concentration and aspect ratio of the insert
Khoshvaght-Aliabadi, et al. [227]	Experimental Vortex-generator insert Re: 5200-12200 Nanofluid: Cu, base fluid: water, concentration: 0.2% Inner: cold nanofluid Outer: hot water Counter flow	✓Increase of Nusselt number: 123.9% ✓Increase of pressure drop: 203.4% ✓The winglets-width ratio, winglets-pitch ratio, and winglets-length ratio have strong effects on the heat transfer and pressure drop
Prasad and Gupta [228]	Experimental Twisted tape insert Re: 3000-30000 Nanofluid: Al_2O_3, mean diameter less than 50 nm, base fluid: water, concentration: 0.01 and 0.03% Inner: cold nanofluid Outer: hot water Counter flow	✓Increase of Nusselt number: 31.28% ✓Increase of friction factor: 23% ✓Significant improvement in the performance parameters of the heat exchanger with a rise in volume concentration of the nanoparticle
Kumar, et al. [177]	Experimental Longitudinal strip insert Re: 15000-30000 Nanofluid: Fe_3O_4, mean diameter 36 nm, base fluid: water, concentration: 0.005, 0.01, 0.03 and 0.06% Inner: hot nanofluid, temperature: 60 °C Outer: cold water, temperature: 29 °C Counter flow	✓Increase of Nusselt number: 41.29% ✓Increase of friction factor: 26.7% ✓Heat transfer increases with increasing values of particle concentration, Reynolds number and with decreasing values of the aspect ratio of the longitudinal strip insert

2.3.5.3 Combination of nanofluids and geometry change

Qi, et al. [187] represented an experimental study to investigate a combination of corrugated tubes and nanofluid in DTHEs based on thermal efficiency assessment (Figure 2.16). TiO_2-H_2O nanofluid and water were used as working fluids in outer and inner tubes, respectively. The results showed that the overall thermal performance was significantly enhanced using nanofluids and corrugated tubes, which was reflected in the increase of the Number of Transfer Units (NTU) and its effectiveness. In the best condition, the NTU was improved by 47.5%. However, for thermal fluid in the shell-side, the NTU and effectiveness decreased firstly and then increased with an increase in the Reynolds number. Table 2.6 summarises information on the combination of different nanofluids and geometry change and their effects in comparison to pure water and a conventional DTHE.

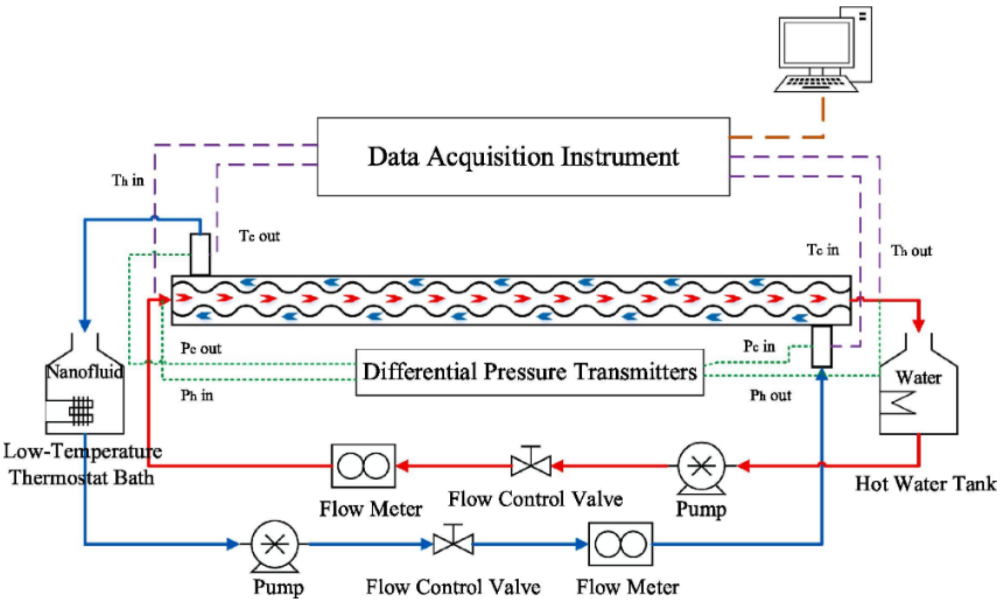

Figure 2.16: Schematic diagram of the experimental system [187].

Table 2.6: Summary of information on the combination of different nanofluids and geometry change, and their effects compared to pure water and a conventional DTHE.

Author	Conditions	Findings
Qi, et al. [187]	Experimental Corrugated tube Re: 3000–12000 Nanofluid: TiO_2, base fluid: water, concentration: 0.1, 0.3 and 0.5% Inner: hot water, temperature: 40°C Outer: cold nanofluid, temperature: 20°C Counter flow	✓Increase of heat transfer: 14.8% at concentration 0.5% ✓Increase of the pressure drop: up to 51.9% ✓The number of transfer unit (NTU) and effectiveness decrease firstly and then increase with the increase of Reynolds number ✓When nanofluid is in the shell-side, the comprehensive performance index is stronger
Khanmohammadi, et al. [229]	Numerical Spiral tube Re: 10000-50000 Nanofluid: TiO_2, mean diameter 25 nm, base fluid: water, concentration: 0.1, 0.2, and 0.3% Inner: cold nanofluid, temperature: 30°C Outer: hot water, temperature: 50°C Counter flow	✓The increase of heat transfer: up to 6% ✓The increase of friction factor: up to 2% ✓The friction factor increases with increase of spiral diameter ✓With increasing the concentration, the temperature increases and the temperature contour became uniform because of turbulence of the boundary layer due to adding nanoparticles
Kumar and Chandrasekar [230]	Experimental Helical coiled tube Re: laminar flow Nanofluid: multiwall carbon nanotube, mean diameter 50-80 nm, base fluid: water, concentration: 0.2, 0.4, and 0.6% Inner: cold nanofluid Outer: hot water Parallel flow	✓Increase of heat transfer: 35% ✓Increase of friction factor: 40%
Huminic and Huminic [231]	Numerical Helical tube Re laminar flow Nanofluid: Cu and TiO_2, mean diameter 24 nm, base fluid: water, concentration: 0.5-3% Inner: hot nanofluid, temperature: 80°C Outer: cold water, temperature: 10°C Counter flow	✓Increase of heat transfer rate: 19% ✓The convective heat transfer coefficients of the nanofluids and water increased with increasing of the mass flow rate and with the Dean number
Wu, et al. [232]	Experimental Helical coiled tube Re: 1000-15000 Nanofluid: Al_2O_3, mean diameter 40 nm, base fluid: water, concentration: 0.20, 0.56, 1.02, 1.50, and 1.88% Inner: hot nanofluid, temperature: 28°C Outer: cold water, temperature: 5.5°C Counter flow	✓Increase of heat transfer: 3.43% ✓The apparent friction factor decreases with Re when Re<6000 and increases with Re when Re>6000 ✓Additional possible effects of nanoparticles, e.g., Brownian motion, thermophoresis and diffusiophoresis, on the convective heat transfer characteristics of the nanofluids are insignificant compared to

Author	Conditions	Findings
Aly [233]	Numerical Coiled tube Re: 5000-30000 Nanofluid: Al_2O_3, mean diameter 40 nm, base fluid: water, concentration: 0.5, 1, 2% Inner: hot nanofluid, temperature: 50°C Outer: cold water, temperature: 20°C Counter flow	the dominant thermophysical properties of the nanofluids ✓Increase of heat transfer coefficient: 30% ✓Increase of pressure drop: 17% ✓The heat transfer coefficient increases by increasing the coil diameter and nanoparticles volume concentration ✓The friction factor increases with the increase in curvature ratio, and pressure drop penalty is negligible when increasing the nanoparticles volume concentration

2.4 Statistical investigation

A statistical investigation was performed on 100 published articles to determine the impact of the different techniques on the heat transfer and friction factor. Twenty data were randomly selected for each technique from 1998 to 2022 to have a logical and equitable comparison among all techniques. The articles were chosen by searching keywords such as "double pipe heat exchanger", "double tube heat exchanger", and "concentric heat exchanger" in google scholar. Figure 2.17 shows the average heat transfer and friction factor augmentation for the combination of nanofluid and turbulator insertion, turbulator insertion, extended surface area, geometry change, and nanofluids in DTHEs.

Reviewing articles in these five categories showed that the combination of nanofluid and turbulator insertion technique had the highest heat transfer enhancement of an average of 131% as compared to the other techniques. This technique employs the beneficial characteristics of turbulator insertion and nanofluids simultaneously. Nanofluids contribute by increasing the surface area of nanoparticles, enhancing heat capacity, and improving both effective and apparent thermal conductivity. The interactions and collisions among nanoparticles further boost thermal properties. Concurrently, turbulator insertions promote effective fluid mixing, generate secondary flows, induce turbulence, create swirl, and alter fluid velocity near the wall.

These phenomena collectively reduce the thermal boundary layer, significantly improving the heat transfer rate in DTHEs. This combined approach leverages the strengths of both nanofluid technology and turbulator design, leading to substantial improvements in the efficiency of heat exchangers. The turbulator insertion technique is rated second with an average of 120% enhancement in the heat transfer rate. It showed the significance of the impact of turbulator insertion on increasing the heat transfer rate in DTHEs. The extended surface area improved the heat transfer by an average of 110% more than the geometry changes and nanofluids technique. Extended surface area by establishing secondary flow, vortices, intensification of turbulence and increasing heat transfer area in the annulus side improves heat transfer rate. In this technique, fins in the outer tube side cause turbulating in the fluid flow. However, the main thermal boundary layer for increasing the heat transfer is on the inner tube side.

In addition, the concentration of fins is on the increment surface area, not turbulating and mixing fluid flow, so this technique has a lower heat transfer enhancement in comparison to turbulator insertion. It can be concluded that creating mixing fluid flow and turbulator is more effective in the inner tube compared to the outer tube. The geometry changes and the use of nanofluids have the lowest heat transfer enhancement by an average of 91% and 35%, respectively. In these techniques, creating turbulence and mixing in the fluid are not as effective as the turbulator insertion and extended surface area. It can be concluded that increasing the convective and conductive heat transfer coefficient of the base fluid are the main reasons for the heat transfer enhancement when using nanofluids. The fluctuation and turbulence of nanoparticles in the flow have a low effect on increasing the heat transfer rate compared to other techniques. Using nanofluids does not significantly improve the heat transfer rate. Hence, incorporating the use of nanofluids with other techniques is recommended.

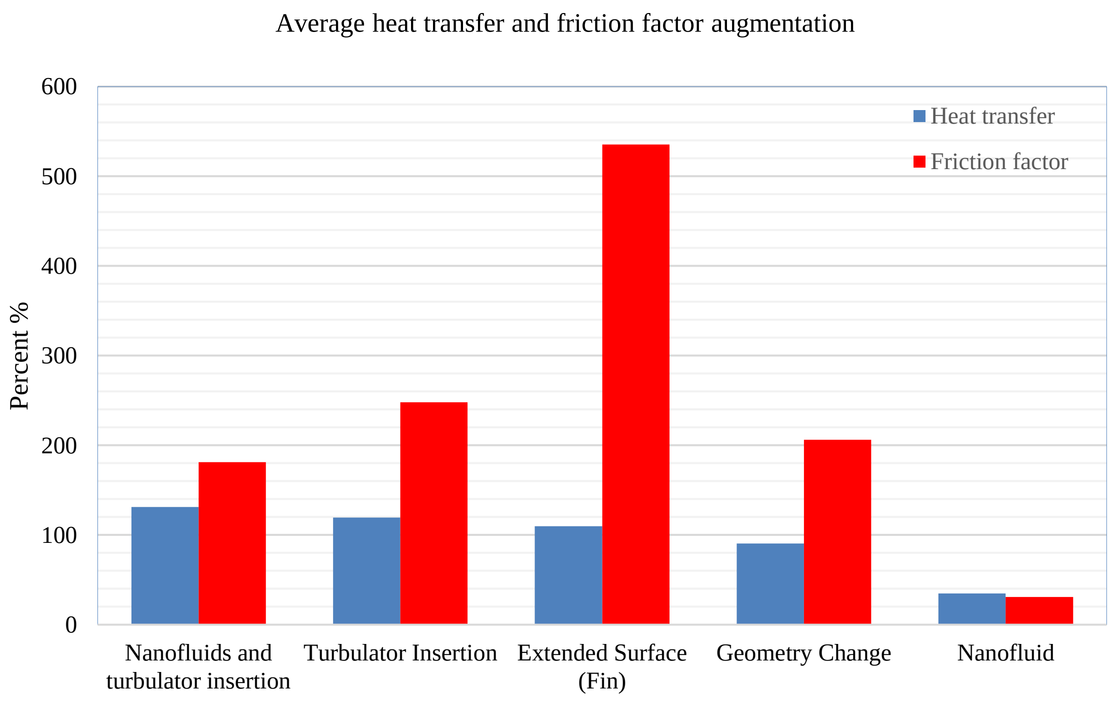

Figure 2.17: Average heat transfer and friction factor augmentation of different techniques.

As shown in Figure 2.17, the extended surface area has the highest increment of friction factor, an average value of 536% than the other techniques This is due to the presence of the fins giving a larger surface area against the flow in comparison to the turbulator insertion, geometry change, and nanofluids techniques. The average friction factor increments of the turbulator insertion, geometry change, and combination of nanofluid and turbulator insertion is about 248%, 206%, and 181%, respectively. In the turbulator insertion technique, an external element in the tube gives a high friction factor. While in the geometry change technique, the increment of friction factor is because of the modification in tubes' wall. Nanofluids have the lowest friction factor by an average of 31% because there is no change or elements hindering the fluid flow. The increase in friction factor is because of an increase in fluid viscosity.

According to the thermal performance factor equation, the thermal performance factor is the ratio of heat transfer enhancement to friction factor increment. It can be concluded that using nanofluid and the combination of nanofluids and turbulator insertion have the best thermal performance factor with the extended surface area the lowest thermal performance factor.

The standard deviation and box and whisker diagram were used to show the dispersion of heat transfer and friction factor augmentation data of each technique (Table 2.7 and Figure 2.18). Among these five techniques, the combination of turbulator insertion and nanofluid technique has the highest heat transfer standard deviation by an average value of approximately 132. From the standard deviation, minimum, maximum and median values, it can be concluded that the potential for the increase of the average heat transfer for this technique is extensive. The extended surface area and turbulator insertion techniques are rated second and third respectively with approximate standard deviation heat transfer averages of 81 and 79. The average heat transfer standard deviation decreases respectively for the extended surface area, turbulator insertion, geometry change and nanofluids. It can be concluded that decreasing the standard deviation is accompanied by a decrease in the potential of increased heat transfer for that technique. Figure 2.18 presents a box and whisker plot illustrating the heat transfer enhancements achieved by different techniques. The standard deviation for friction factor has a high value for all techniques except nanofluid. This means that the range of friction factor increment for these techniques is extensive, especially for the extended surface area. The range of friction factors varies extensively by the occupation of the flow area in the tube in the extended surface area.

Table 2.7: Average enhancement of heat transfer and friction factor and standard deviation of different techniques

Technique	Standard deviation	
	Heat transfer	Friction factor
Nanofluids and turbulator insertion	131.70	244.91
Extended surface (fin)	81.28	581.58
Turbulator insertion	78.80	157.66
Geometry change	54.28	194.71
Nanofluid	18.30	18.21

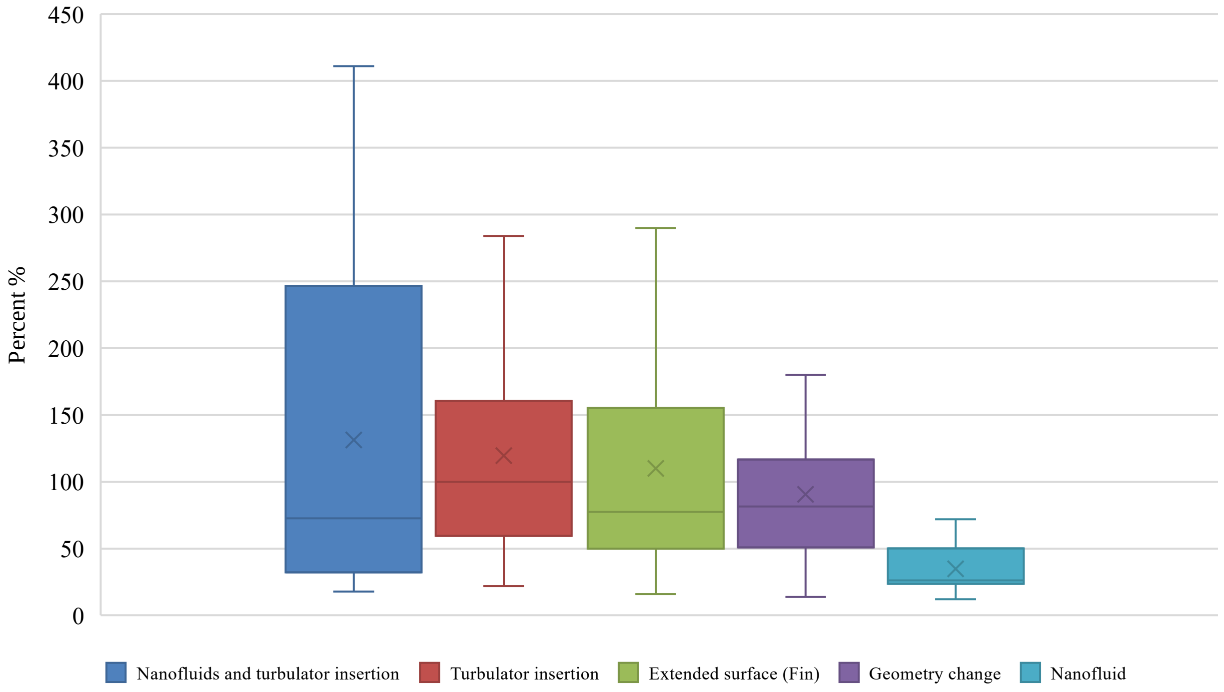

Figure 2.18: Heat transfer enhancement of different techniques (box and whisker plot)

2.5 Conclusion

This literature review has explored various passive methods to enhance heat transfer and friction factors in double tube heat exchangers. These passive techniques include turbulator insertion, extended surface area (fin), geometry changes, and the use of nanofluids. The primary objective of these methods is to improve heat transfer rates by reducing the thermal boundary layer and modifying the thermal properties of the fluids involved. This review has identified key parameters that influence the effectiveness of each technique and quantified their potential to enhance heat transfer rates in DTHEs. The key conclusions are:

- Heat transfer rate generally increases with higher Reynolds numbers across all techniques, but the enhancement effect of coil-wire inserts diminishes as Reynolds numbers rise. Conversely, turbulator insertion demonstrates greater heat transfer improvement at lower Reynolds numbers, where it significantly intensifies perturbations in laminar flow.
- Reducing the pitch of coil, twisted tape, and helical inserts leads to higher heat transfer rates but also increases pressure drops, highlighting the trade-off between thermal performance and pressure loss in these techniques.
- Nanofluids combined with turbulator insertion provide the greatest enhancement in heat transfer, outperforming nanofluids used alone. The synergistic benefits of these two methods result in superior thermal performance.
- The extended surface area (fin) technique exhibits the worst impact on pressure drop and friction factor, making it less efficient in terms of fluid flow compared to other methods, despite its potential for heat transfer enhancement.
- Modifications to both the inner and outer tubes significantly enhance heat transfer and friction factor, with greater improvements compared to modifying only the inner tube. These geometric changes amplify heat transfer but also elevate pressure losses.
- The combination of turbulator insertion and nanofluids has the highest potential for heat transfer enhancement, though it also results in a higher increase in friction factor. For most techniques, the friction factor rises more sharply than the heat transfer rate, indicating a greater potential for flow resistance than for thermal improvement.

This literature review demonstrates that the combination of turbulator insertion and nanofluids has the highest potential for enhancing heat transfer rates. While there is substantial research on other techniques such as geometry changes, extended surface areas, and nanofluids individually, there is a lack of comprehensive studies on the combined approach of turbulator insertion and nanofluids. Additionally, turbulator insertion requires less modification to the DTHE design compared to geometry changes and extended surfaces, as it only involves adding an external object inside the inner tube. This makes turbulator insertion a more practical and advantageous method for improving heat transfer in DTHEs.

Chapter 3: Research Methodology

This chapter of the thesis provides a comprehensive research methodology adopted to investigate the stated problem, emphasizing the intricate design and systematic approach employed. Initially, the problem statement is meticulously defined, laying the foundation for the research, followed by a detailed exposition of the numerical method employed, underscoring the computational fluid dynamics (CFD) simulations that constitute the core of the numerical analysis. Subsequent sections delve into the grid independence test, a critical procedure to ensure the accuracy and reliability of the CFD results by evaluating the effect of grid size on simulation outcomes. Validation of the numerical model is then rigorously conducted by comparing simulation results with existing experimental, theoretical and numerical data, establishing the credibility of the research findings. The chapter further explores the innovative use of nanofluids, examining their potential to enhance thermal performance due to their superior thermal properties. Finally, the insertion of turbulators within the flow field is discussed as a strategic approach to augment heat transfer rates, showcasing the practical implications of these methodologies in improving the performance of DTHEs. Collectively, this chapter sets the stage for a thorough investigation, combining theoretical frameworks with practical applications to address the research objectives.

3.1 Numerical setup

The enhancement of heat transfer and fluid flow characteristics within DTHEs represents a pivotal challenge in the field of thermal engineering, necessitating innovative approaches to improve their efficiency and performance. This research focuses on investigating the impact of various turbulator designs, including both transverse and helical configurations (rectangular, triangular, oval, and trapezoidal shapes), in conjunction with the application of nanofluids (CuO, ZnO, Fe_3O_4, Diamond, Ag, TiO_2, Al_2O_3, SiC, and SiO_2 with volume fractions ranging from 0 to 0.1), on the hydrothermal performance of a DTHE. The study aims to understand how these modifications affect heat transfer rates and fluid flow dynamics within a system where the inner tube is tasked with transporting cold nanofluid, and the outer tube circulates hot water.

To address this problem, a comprehensive numerical simulation approach was employed, utilising the finite volume method (FVM) in ANSYS Fluent to discretise the governing equations for laminar forced convection. The DTHE system under investigation was specifically designed with an inner tube diameter of 0.014 m and an outer tube diameter of 0.08 m, extending a total length of 1.8 meters. Tube sizes were selected as 1/2 and 3 inches, a decision driven by their widespread availability and applicability in practical and industrial settings. The choice of copper as the material for the inner tube, with a thickness of 0.001 m, was based on its superior thermal conductivity. Turbulator inserts with a diameter of 0.002 m were placed within the centre of inner tube, ribs starting 0.01 m from the inlet, to disrupt the flow and enhance heat transfer. The transverse turbulator insertion case was modelled to maintain axisymmetric along the longitudinal axis, simplifying the simulations and saving computational time.

Operating conditions were set with the inner tube carrying cold nanofluids at a constant inlet temperature of 295 K, while the outer tube was charged with pure hot water at a constant inlet temperature of 335 K. These temperatures were selected to align with common industrial practices to provide results that are more applicable to real-world scenarios [54, 234, 235].As some published work concluded that the single-phase approach and constant thermophysical properties of fluids agree with the experimental results, these two approaches were selected for the numerical investigation [236, 237]. This setup explored the thermal interaction between the hot and cold fluids under the influence of inserted turbulators and nanofluid properties. The numerical methodology adopted a coupled approach for velocity-pressure coupling and a second-order upwind scheme for the momentum and energy equations to enhance the precision of the simulations. The convergence criterion for numerical calculations was rigorously set up to 10^{-7} for all variables, ensuring high accuracy in the simulation outcomes.

In the context of computational analysis, the following assumptions are typically imposed to facilitate the modelling process and reduce computational complexity. These assumptions are critical for defining the scope and applicability of the simulation outcomes.

- Steady-State flow: The fluid motion and thermal fields are assumed to remain constant over time, indicating that transient effects are negligible.
- Flow in the entry and fully developed regions: The analysis examines flow at various Reynolds numbers, considering both the entry region and fully developed flow

conditions. At low Reynolds numbers, the boundary layer is primarily developing, while at high Reynolds numbers, fully developed flow conditions are not yet achieved.

- Incompressible flow: The density of the fluid is assumed constant, implying that changes in pressure or temperature have minimal effect on the fluid's density.
- Laminar flow in both inner and outer tubes: The flow within the DTHE's inner and outer tubes is assumed to be laminar, characterized by smooth, orderly motion of fluid particles. This assumption necessitates a Reynolds number below the critical value for transition to turbulence.
- Axisymmetric in the presence of transverse turbulators: The geometric configuration and flow field are assumed to be axisymmetric, particularly in sections with transverse turbulators, simplifying the computational model to a two-dimensional problem.
- 3D simulations for the helical turbulators: The geometry of helical turbulator insertions is designed in a three-dimensional model, and simulations are set up for 3D calculations.
- Constant thermal properties of the fluid: The thermal conductivity, specific heat capacity, and viscosity of the fluid are assumed to remain constant, disregarding any temperature-induced variations.
- Single-phase model of nanofluid: The nanofluid is treated as a single, homogeneous phase, ignoring the discrete phase of the nanoparticles.

3.2 Geometry of DTHE and turbulator insertions

The dimensions of the DTHE, as previously mentioned, include an inner copper tube with a diameter of 0.014 m and a wall thickness of 0.001 m, and an outer tube with a diameter of 0.08 m. Both tubes have a length of 1.8 m. Turbulator insertions are introduced to enhance the heat exchange efficiency by disrupting the flow, thereby reduces the thermal boundary layer close to the wall and enhancing the thermal mixing. These insertions are categorized into transverse and helical types, with shapes including rectangular, triangular, oval, and trapezoidal configurations. The dimensions of the turbulators, specifically, the distances between the ribs (s), the height of the ribs (h), and the width of the ribs (w), are critical parameters that were systematically varied to study their impact on the heat transfer and fluid flow within the DTHE. The diameter of the turbulator insertions is consistently maintained at 0.002 m, with the first rib positioned 0.01 m from the inlet, ensuring a uniform start point for comparing the results of different cases. Figure 3.1 depicts the geometry of the DTHE, both with and without the insertion of transverse turbulators.

For the transverse turbulator, an axisymmetric 2D model was used, and the results showed excellent agreement with the 3D model, confirming the validity of the 2D approach for this configuration. For the simulations of helical turbulator insertion, the same DTHE with the same dimensions was used to ensure comparable results. As with the transverse turbulators, four different shapes of helical turbulators were designed: rectangular, triangular, oval, and trapezoidal. Since the helical turbulator lacks symmetry, the entire DTHE was modeled in 3D for simulations. The helical twist ratio for all cases was set at 1 to 0.04 m, meaning one revolution of the helix is 40 mm. Additionally, the height of the helical turbulators (h) was varied to study its impact on the performance of the DTHE. Figure 3.2 illustrates the configuration of helical turbulator insertions within the inner tube of the DTHE.

Through a comprehensive literature review, it was found that while numerous turbulator designs have been studied, regular shapes such as rectangular, triangular, trapezoidal, and oval have not been investigated in the context of double tube heat exchangers. These regular shapes were selected due to their ease of manufacturing compared to more complex, irregular geometries. This choice makes them highly practical for real-world applications, where manufacturing cost and simplicity are significant considerations. By selecting these shapes, this research not only addresses a gap in the current literature but also provides valuable insights for future research and practical implementations in industrial heat exchangers. The potential for easier fabrication and implementation of these regular geometries enhances the feasibility of transferring the findings from this study to practical heat transfer systems, contributing to both academic knowledge and industrial innovation.

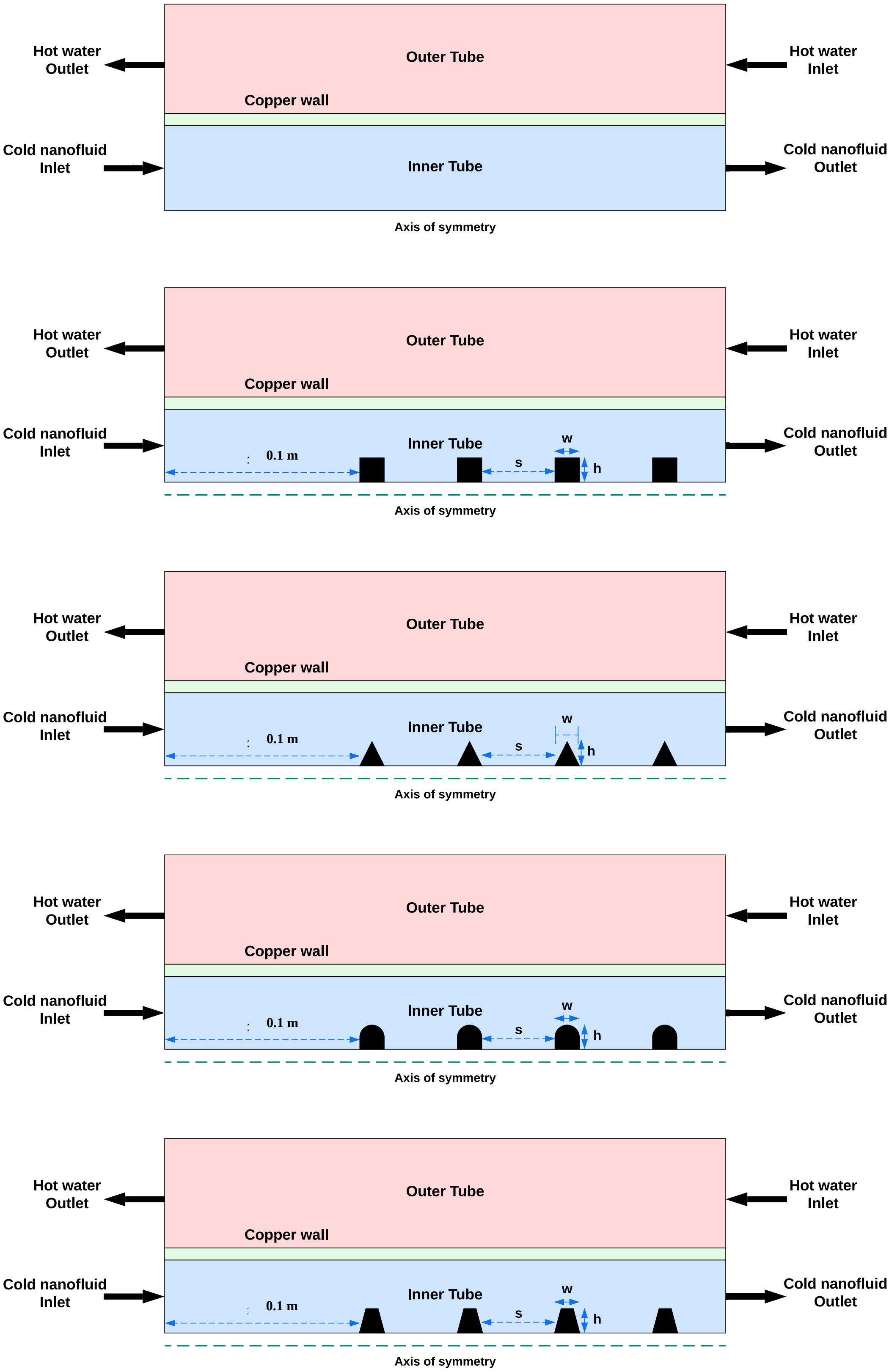

Figure 3.1: Schematic of the analyzed DTHE, both with and without transverse turbulator inserts (not to scale).

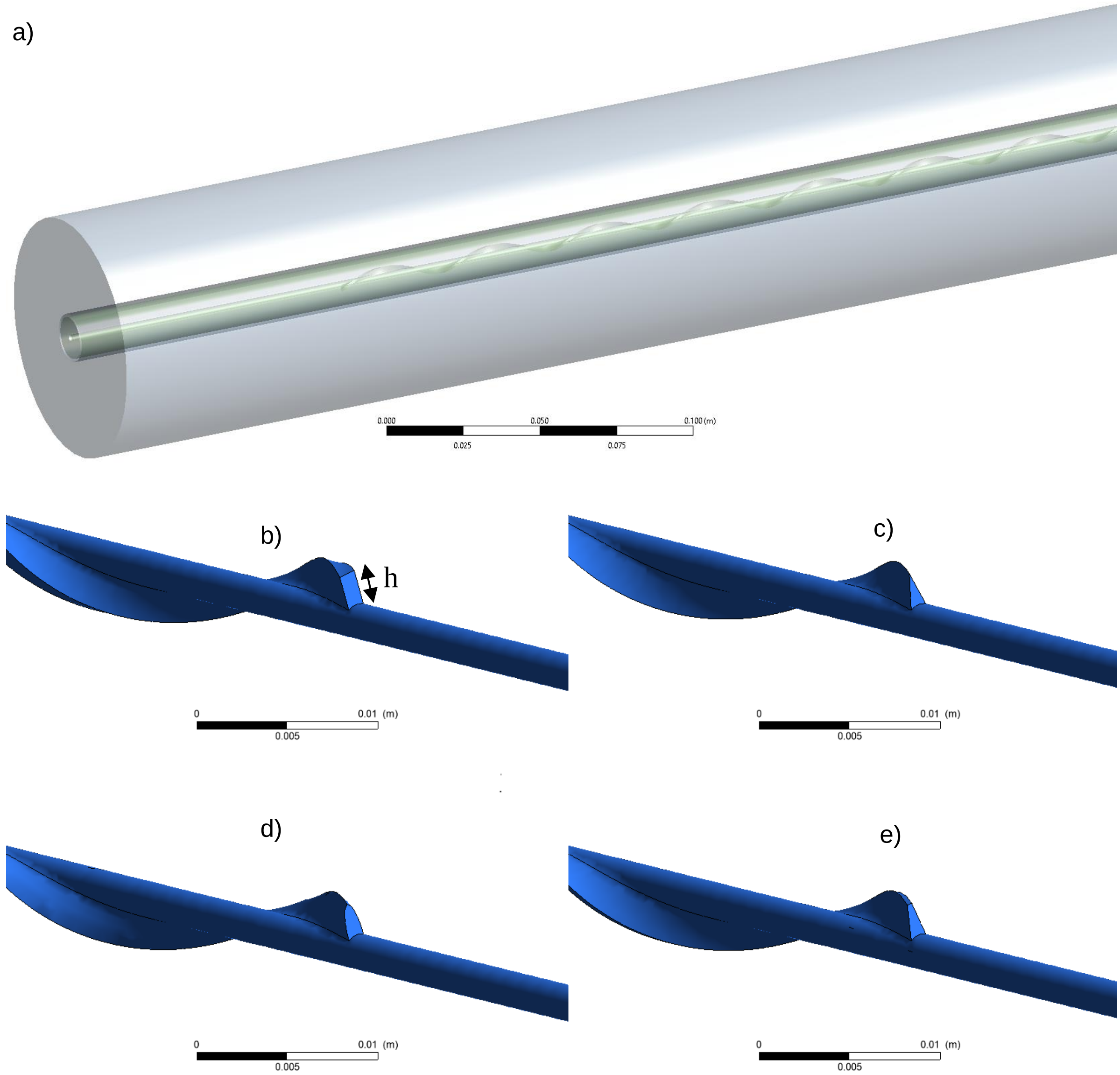

Figure 3.2: Schematic of the analyzed DTHE, a) overall domain and helical turbulators, b) rectangular, c) triangular, d) oval, e) trapezoidal.

The values of the three dimensionless key parameters (S, W, and H), as derived from Equation 25 (Chapter 4: Governing Equations), with the selected dimensions for s, w, and h, are presented in Table 3.1.

Table 3.1: The value of dimensionless key parameters.

s [m]	S	w [m]	W	h [m]	H
0.02	2.86	0.001	0.14	0.001	0.14
0.04	5.71	0.002	0.29	0.002	0.29
0.06	8.57	0.003	0.43	0.003	0.43
0.08	11.43	0.004	0.57	0.004	0.57
0.10	14.29	0.005	0.71	0.005	0.71

3.3 Nanofluids

In the investigation of heat transfer and fluid flow characteristics within DTHEs, nanofluids play a pivotal role due to their enhanced thermal properties. This research utilises nanofluids as the working fluid in the inner tube of the DTHE, where cold nanofluids are employed to facilitate heat transfer from the hot water flowing in the outer tube. The selection of nanofluids includes CuO, ZnO, Fe_3O_4, Diamond, Ag, TiO_2, Al_2O_3, SiC, and SiO_2, which are chosen for their varied and potentially beneficial thermal conductivity and viscosity characteristics. The nanofluids are tested across a spectrum of volume fractions ranging from 0 to 0.1, to meticulously evaluate their impact on the heat exchanger's performance. This approach allows for a comprehensive analysis of how different nanofluids, with their unique thermophysical properties, influence the overall efficiency and performance of heat transfer in DTHEs. Table 3.2 presents the thermal properties of water and the nanoparticles utilised in this study. It is essential to note that these properties correspond to a temperature of 300K. Furthermore, the nanoparticles, assumed spherical in shape, have a diameter of 40 nm.

Table 3.2: Thermophysical properties of water and nanoparticles.

Thermophysical properties	ρ (kg/m³)	C_p (J/kg K)	k (W/m K)	μ (N s/m²)
Water [238]	997	4179	0.613	0.000855
Copper [239]	8978	381	387.6	-
CuO [240]	6500	535.6	20	-
ZnO [241]	5600	495.2	13	-

Thermophysical properties	ρ (kg/m^3)	C_p (J/kg K)	k (W/m K)	μ (N s/m^2)
Fe_3O_4 [242]	5180	670	6	-
Diamond [243]	3510	497.26	1000	-
Ag [244]	10500	235	429	-
TiO_2 [245]	4175	692	8.4	-
Al_2O_3 [11]	3600	765	36	-
SiC [246]	3160	675	490	-
SiO_2 [247]	2200	703	1.2	-

Table 3.3 presents the calculated thermophysical properties of three nanofluids—CuO, Al_2O_3, and SiO_2—at a volume fraction of 0.05, which are predominantly investigated in this study. These properties were evaluated at a temperature of 300 K. The nanoparticles are assumed to be spherical in shape with a diameter of 40 nm, as is typical in many studies. It is important to emphasize that these thermophysical properties, including density, specific heat capacity, thermal conductivity, and dynamic viscosity, play a pivotal role in determining the heat transfer and fluid flow characteristics in nanofluids.

Table 3.3: Thermophysical properties of water-based nanofluids at a volume fraction of 0.05.

Thermophysical properties	ρ (kg/m^3)	C_p (J/kg K)	k (W/m K)	μ (N s/m^2)
CuO	1272.2	3248.2	0.70101	0.00169
Al_2O_3	1127.2	3633.8	0.70477	0.00169
SiO_2	1057.2	3817.3	0.63552	0.00169

3.4 Grid independence test

To ensure the accuracy and reliability of computational simulations, a grid independence test was performed in this study, focusing on both transverse and three-dimensional (3D) helical turbulator insertions. The primary aim of this test was to verify that the numerical results remain stable and unaffected by variations in the computational grid size. Achieving grid independence is essential for validating the simulation outcomes, as it identifies the optimal grid size that balances computational efficiency with precision in the simulation results, thereby optimizing both time and cost. To this end, the mesh configuration was carefully designed to be denser near the walls and around the turbulators. This approach is critical, considering these areas exhibit complex heat transfer and fluid flow behaviour, necessitating increased resolution to accurately capture the phenomena. Figure 3.3 and Figure 3.4 illustrate schematic diagrams of a grid with rectangular rib for a case of transverse turbulators and an oval helical turbulator for a case of helical turbulators, respectively.

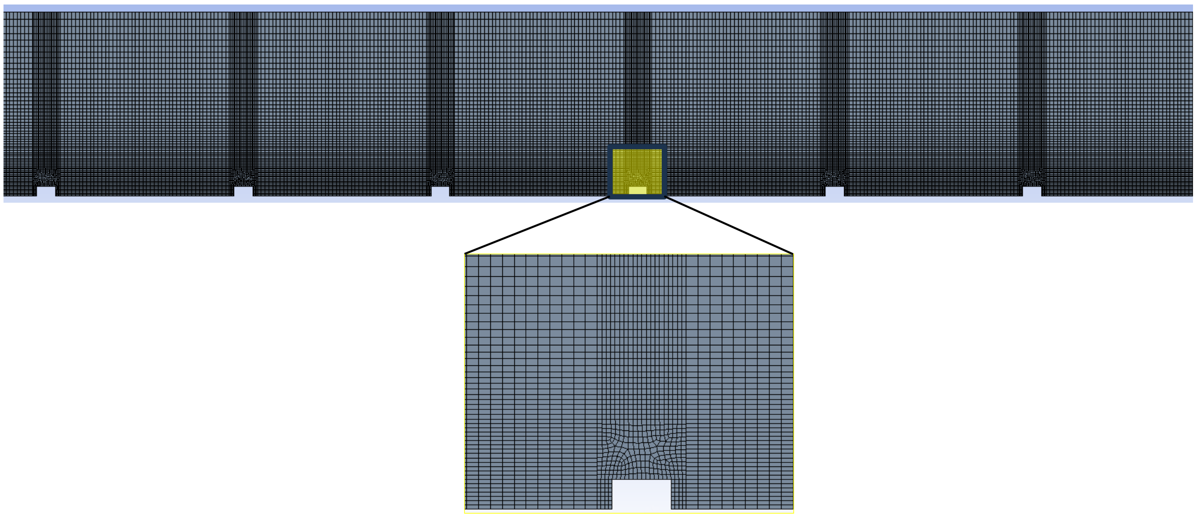

Figure 3.3: Schematic of the overall domain featuring a grid with rectangular ribs.

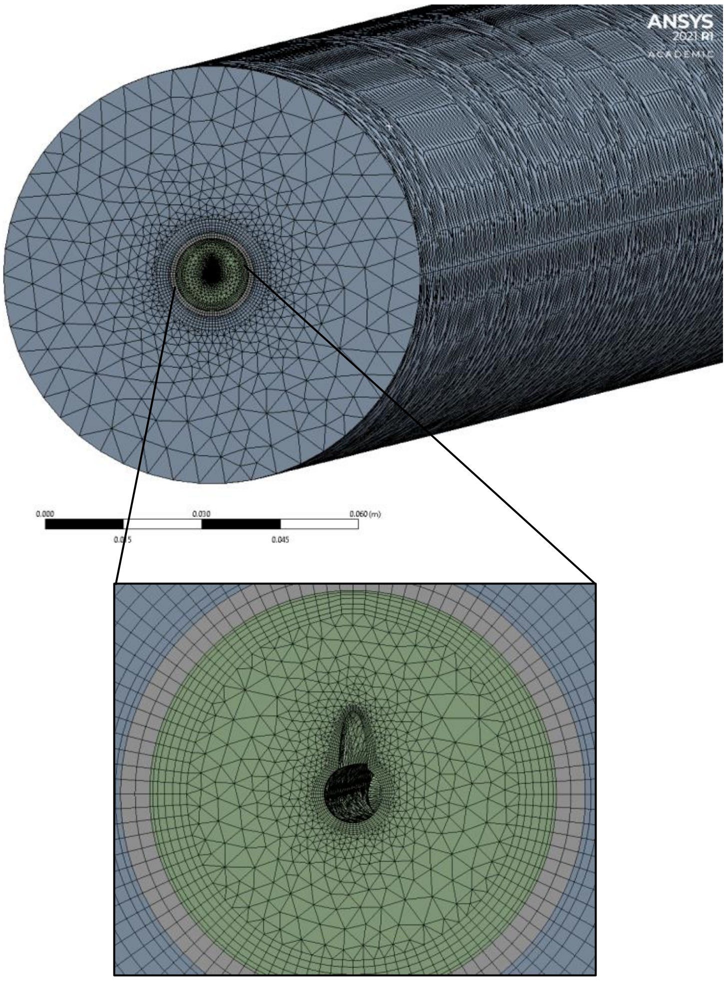

Figure 3.4: Schematic of the overall domain featuring a grid with an oval helical turbulator.

3.5 Validation

The validation section is an essential part of the research methodology for numerical studies, aiming to verify the accuracy and reliability of the results. In this research, the validation was carefully carried out through four distinct comparisons, each confirming the consistency of the simulation outcomes with existing literature. For validation, two key parameters were examined: the Nusselt number, representing heat transfer characteristics, and the friction factor, representing fluid flow characteristics. These parameters were used to compare the present simulation results with those from previously published studies, ensuring the simulations' fidelity to established data.

The first validation compared the derived Nusselt number correlations from experiments with present numerical data for water as the working fluid in a double tube heat exchanger without turbulator insertions. The experimental data from Seider and Tate [248], Shah and

London [249], Gnielinski [250], and Hausen [251] used as reference points for evaluating the accuracy of the present simulations in replicating heat transfer characteristics under laminar flow conditions. Subsequently, the numerical results of the current study were compared with another dataset from Bahmani, et al. [252], which focused on a double tube heat exchanger using a single-phase model to simulate nanofluid flow without turbulator insertions. This comparison evaluated the model's ability to accurately predict heat transfer enhancements when using nanofluids as the working fluid in a DTHE.

An additional validation step involved comparing the results of the present study's single-phase model with the two-phase nanofluid model by Shirvan, et al. [253], and with the experimental data on nanofluid heat transfer in a double tube heat exchanger without turbulator insertions by Heyhat, et al. [254]. This comparison demonstrated the accuracy of the current study and revealed less deviation from experimental results compared to the two-phase model. Lastly, the simulation results were validated against experimental findings from a study conducted by Hong and Bergles [255], which involved the use of turbulator insertion in a double tube heat exchanger. This validation step was critical in affirming the simulation model's efficacy in accurately predicting the thermal performance enhancements attributable to the use of turbulators in double tube heat exchanger designs.

Throughout all validation process, the simulation results demonstrated remarkable agreement with the other published works, thereby underscoring the reliability and accuracy of the numerical models and methodologies employed in this study. This comprehensive validation approach not only strengthens the credibility of the current research findings but also lays a solid groundwork for future investigations into the heat transfer and fluid flow characteristics of nanofluids and turbulator insertions in double tube heat exchangers.

3.6 Hardware and computation time of simulation

One of the significant challenges during this research was the computation time of simulations. The hardware of the system greatly impacts the simulation time and post-processing efficiency. This study involved two types of simulations: 2D axisymmetric simulations for transverse turbulators and 3D models for helical turbulators. The 2D axisymmetric simulations required relatively less computation time. These simulations were performed on a laptop, with specifications provided in Table 3.4, and each simulation took a maximum of three hours. However, the 3D simulations were much more computationally intensive.

A single 3D simulation on the laptop, which involved approximately 7 million cells, took more than 24 hours to complete. To address this issue, the high-performance computing (HPC) provided by Birmingham City University was utilised for the 3D simulations. The specifications of the HPC are also provided in Table 3.4. Using the HPC significantly reduced the computation time for each 3D simulation to about 18 hours. This hardware upgrade not only enhanced the efficiency of the research process but also allowed for more complex simulations to be run within a reasonable timeframe. The use of HPC resources was crucial in managing the extensive computational requirements of the 3D models and ensuring the timely completion of the research.

Table 3.4: Specifications of the laptop and HPC used for simulations.

System	Specification
Laptop	CPU: Processor Intel(R) Core (TM) i5-10210U CPU @ 1.60GHz, 2112 Mhz, 4 Core(s), 8 Logical Processor(s) RAM: Total Physical Memory, 15.8 GB Graphics: NVIDIA GeForce MX330
HPC	CPU compute nodes: [node1-cluster3, node2-cluster3, node3-cluster3, node4-cluster3, node5-cluster3, node6-cluster3] - 72 cores per node! Intel Xeon Gold 6240 2.6G, 18C/36T, 10.4GT/s, 24.75M Cache, Turbo, HT (150W) DDR4-2933, (~180GB RAM) GPU compute nodes: [gpu1-cluster3] - 72 cores per node! Intel Xeon Gold 6240 2.6G, 18C/36T, 10.4GT/s, 24.75M Cache, Turbo, HT (150W) DDR4-2933, (~180GB RAM) NVIDIA(R) Tesla (TM) T4 16GB Passive, Single Slot, Full Height GPU (2 cards per node) - 320 Turing Tensor cores & 2560 Cuda cores per card!

Chapter 4: Governing Equations

This chapter presents the mathematical framework for the study, focusing on the continuity, momentum, and energy equations essential for analyzing fluid flow and heat transfer in double tube heat exchangers. It details the approach for calculating the thermal properties of various nanofluids, providing insights into their impact as working fluids inside the DTHE. Furthermore, it presents essential equations for determining the heat transfer coefficient, Nusselt number, friction factor, and performance evaluation criteria. These elements are pivotal in assessing the efficiency enhancements achieved through the use of turbulator inserts and nanofluids in double tube heat exchangers.

4.1 Fundamental flow equations for laminar flow

This research investigates the heat transfer properties and fluid dynamics of laminar flow in a DTHE. The governing equations for solving flows in the DTHE, including continuity, momentum and energy for laminar flow in steady states, are as follows. These equations provide a comprehensive framework for analysing and predicting the performance of DTHE under steady-state, laminar flow conditions [256].

In the case of steady and incompressible flow, the continuity equation is expressed as follows:

$$\nabla.(\rho V) = 0 \tag{1}$$

For incompressible flow with constant viscosity, the momentum equation can be expressed as follows:

$$\nabla.(\rho V V) = -\nabla P + \nabla.(\mu \nabla V) \tag{2}$$

For incompressible flow where the thermal conductivity remains constant, the energy conservation equation can be expressed as follows:

$$\nabla.(\rho V C_p T) = \nabla.(k \nabla T) \tag{3}$$

Where V, ρ, C_p, and k represent velocity, density, specific heat, and thermal conductivity, respectively.

4.2 Thermophysical properties of nanofluids

Adding nanoparticles to a base fluid changes its thermophysical properties, such as density, specific heat, viscosity, and thermal conductivity. These changes, in turn, affect convective heat transfer in the fluid flow. Different nanoparticles alter these properties to varying degrees, and factors like the concentration of nanoparticles, their purity, shape, and size significantly impact these changes [257]. The present study employed CuO, ZnO, Fe_3O_4, Diamond, Ag, TiO_2, Al_2O_3, SiC, and SiO_2 water-based nanofluids as incompressible working fluids with constant thermophysical properties. The thermophysical properties of these nanofluids need to be calculated and used in simulations to investigate the impact of these different nanofluids on the performance of the DTHE. Four key thermophysical properties, density, specific heat, thermal conductivity, and viscosity, are calculated using empirical and theoretical correlations provided in the literature, as discussed in this section.

4.2.1 Density of nanofluid

Density is a crucial thermophysical property for evaluating the heat transfer performance of nanofluids. Adding even a small amount of nanoparticles to a base fluid changes the nanofluid's density due to the higher density of solid materials compared to liquids. This change in density directly affects the Reynolds number, friction factor, pressure loss, and Nusselt number [257, 258]. Previous studies have shown that the density of nanofluids depends directly on the volume concentration of nanoparticles [259]. Therefore, the density of a nanofluid can be calculated as follows [257, 260-262].

$$\rho_{nf} = (1-\varphi)\rho_b + \varphi\rho_p \tag{4}$$

Where ρ_{nf}, φ, and ρ_p represent density of nanofluid, volume fraction, and density of nanoparticle, respectively.

4.2.2 Specific heat capacity of nanofluid

The specific heat is a crucial property that significantly influences the heat transfer rate of nanofluids. It represents the amount of heat needed to raise the temperature of one gram of nanofluid by one degree Celsius. It directly impacts the thermal characteristics and performance of materials; higher specific heat capacity indicates greater energy storage capability, while lower capacity means less energy retention [257]. Introducing nanoparticles into a fluid generally improves its thermal conductivity, but it can also reduce the specific heat capacity. This reduction can limit its effectiveness as a coolant. Therefore, achieving a balance in the alteration or enhancement of thermophysical properties is essential for optimizing nanofluid applications. Heat transfer fluids with enhanced heat capacity are necessary for efficient and environmentally friendly heat transfer processes. Several mechanisms have been proposed to enhance specific heat capacity, including higher specific surface energy, increased thermal resistance between nanoparticles and surrounding liquid molecules (known as interfacial thermal resistance), and the formation of a semi-solid liquid layer around nanoparticles [259, 263]. The specific heat capacity depends on the volume fraction of nanoparticles and can be calculated as follows [257, 260-262].

$$(C_p)_{nf} = (1-\varphi)(C_p)_b + \varphi(C_p)_p \tag{5}$$

Where C and φ are the specific heat capacity and volume fraction, respectively. The subscripts p, nf, and b denote particles, nanofluid, and base fluid, respectively.

4.2.3 Viscosity of nanofluid

The viscosity refers to a fluid's resistance to motion, which is crucial for understanding heat transfer applications because it affects pressure drop and pumping power [259]. The effective viscosity of nanofluids depends on both the viscosity of the base fluid and the concentration of nanoparticles. Factors such as particle size, temperature, and the type of nanoparticles also influence this effective viscosity. In the flow of nanofluids, striking a balance between enhancing thermal conductivity and managing viscosity is essential. For instance, while a viscous base fluid can enhance thermal conductivity through Brownian motion and micro-convection effects, it can also potentially offset these gains [257]. The viscosity of nanofluids has been extensively studied in past research to develop accurate empirical and theoretical correlations for prediction. This study aims to use the most practical and precise viscosity correlations for calculating nanofluids viscosity. One of the empirical correlations used to predict the viscosity of Al_2O_3 nanofluids was developed by Maïga, et al. [264]. This correlation relates the viscosity of the nanofluid to the volume concentration of Al_2O_3 nanoparticles. The formulation of this correlation is as follows.

$$\mu = \frac{\mu_{nf}}{\mu_b} = 123\varphi^2 + 7.3\varphi + 1 \tag{6}$$

Sharma, et al. [242] presented a viscosity correlation for nanofluids that takes into account the volume concentration of nanoparticles, nanoparticle diameter, and nanofluid temperature. The equation is as follows.

$$\frac{\mu_{nf}}{\mu_b} = \left(1 + \frac{\varphi}{100}\right)^{11.3} \times \left(1 + \frac{T_{nf}}{70}\right)^{-0.038} \times \left(1 + \frac{d_p}{170}\right)^{-0.061} \quad (7)$$

The subscripts p, nf, and b denote particles, nanofluid, and base fluid, respectively.

4.2.4 Thermal conductivity of nanofluid

Thermal conductivity is a transport property defined as the ratio of heat flux to a local temperature gradient. The addition of nanoparticles to a conventional fluid enhances its thermal conductivity. This increase is primarily due to Brownian motion (Figure 4.1), a crucial mechanism influencing the thermal behaviour of nanoparticle-fluid suspensions. Another contributing factor is the formation of an interfacial layer, or nanolayer, where liquid molecules (Figure 4.2) near the solid particle surface create layered structures. These layers act as a thermal bridge between the nanoparticles and the bulk liquid, thereby enhancing thermal conductivity. The relationship between this nanolayer and the thermal properties of solid-liquid suspensions is complex. The molecules in these layers exist in an intermediate state between the bulk liquid and the solid particle. This solid-like nanolayer of liquid molecules can significantly increase thermal conductivity compared to the bulk conventional fluid [259, 265].

To calculate the thermal conductivity of nanofluids, two widely accepted correlations were used: one presented by El Bécaye Maïga, et al. [266], and the other by Vajjha and Das [267]. These correlations are as follows.

$$\frac{k_{nf}}{k_b} = 4.97\varphi^2 + 2.72\varphi + 1 \quad (8)$$

$$\frac{k_{nf}}{k_b} = \left[\frac{k_p + 2k_b - 2(k_b - k_p)\varphi}{k_p + 2k_b + (k_b - k_p)\varphi}\right] \times 5 \times 10^4 \beta\varphi\rho_b C_{p,b} \sqrt{\frac{\kappa T}{\rho_p d_p}} f(T,\varphi) \quad (9)$$

$$\begin{aligned} f(T,\varphi) = {} & (2.8217 \times 10^{-2}\varphi + 3.917 \times 10^{-3})\left(\frac{T}{T_0}\right) \\ & + (-3.0669 \times 10^{-2}\varphi - 3.91123 \times 10^{-3}) \end{aligned} \quad (10)$$

Where β, κ, and T_0 represent fraction of liquid volume traveling with a particle, Boltzmann constant, and reference temperature, respectively. The subscripts p, nf, and b denote particles, nanofluid, and base fluid, respectively.

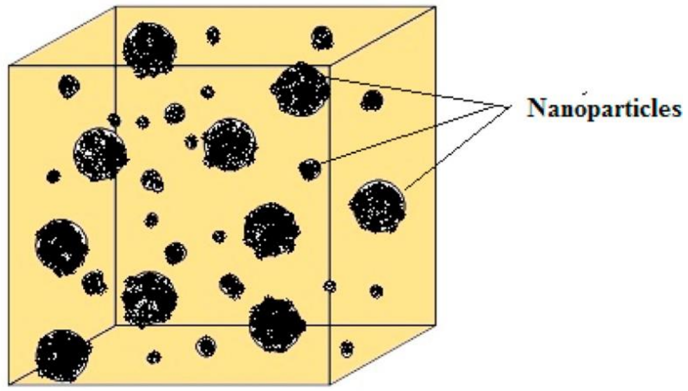

Figure 4.1: Nanofluid domain and Brownian motion of nanoparticles [257].

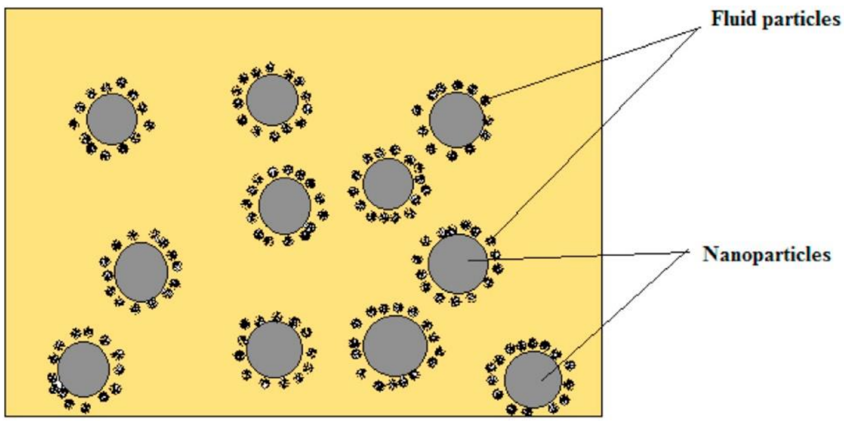

Figure 4.2: Structure of nanofluid featuring nanoparticles, nanolayers, and at bulk liquid the solid/liquid interface [257].

4.3 Exergy analysis

Exergy represents the maximum theoretical work that can be obtained from a system as it reaches equilibrium with its environment through a reversible process. In the context of a DTHE, exergy destruction indicates the amount of potential work lost due to inefficiencies. This measure serves as a clear indicator of energy degradation within the system, highlighting areas where improvements can be made to enhance overall performance and efficiency [56, 268]. Exergy destruction in the heat exchangers can be obtained through following equations [269].

$$\dot{E}_D = T_e \dot{m}_h c_{p,h} \ln\left(\frac{T_{h,o}}{T_{h,i}}\right) + T_e \dot{m}_c c_{p,c} \ln\left(\frac{T_{c,o}}{T_{c,i}}\right) \tag{11}$$

Where $\dot{E}_D$, $\dot{m}_h$, $\dot{m}_c$, $c_{p,h}$, $c_{p,c}$, T_e, $T_{h,o}$, $T_{h,i}$, $T_{c,o}$, and $T_{c,i}$ represent the exergy destruction, mass flow rate of the hot fluid, mass flow rate of the cold fluid, heat capacity of the hot fluid, heat capacity of the cold fluid, ambient temperature (approximately 25 °C), hot fluid outlet temperature, hot fluid inlet temperature, cold fluid outlet temperature, and cold fluid inlet temperature, respectively. Dimensionless exergy destruction for heat exchangers can be obtained from the following equation [56, 270].

$$\text{Dimensionless exergy destruction} = \frac{\dot{E}_D}{T_e(C_{min})} \tag{12}$$

Where C represents the product of mass flow rate and heat capacity, denoting the minimum value between the hot and cold fluids.

4.4 Hydrothermal performance and related parameters

In the computational fluid dynamics simulations of a DTHE, several governing equations play a pivotal role in accurately predicting the system's thermal and flow behaviour. These equations include the heat transfer coefficient, Nusselt number, Reynolds number, friction factor, and performance evaluation criteria. Each of these parameters is essential for a comprehensive understanding of the DTHE's performance under various operating conditions.

The equations below can be used to determine both the local and overall convection heat transfer coefficients, as well as the Nusselt number for nanofluids flowing inside a channel with an inner radius of R_{in} [271, 272].

$$h_{nf} = \frac{-k_{nf}\frac{\partial T}{\partial r}|_{r=R_{in}}}{T_{wall} - T_{b,nf}} \tag{13}$$

$$\overline{h_{nf}} = \frac{1}{L}\int_0^L h_{nf}.\,dx_{|r=R_{in}} \tag{14}$$

$$Nu_{nf} = \frac{h_{nf}(2R_{in})}{k_{in}} \tag{15}$$

$$\overline{Nu_{nf}} = \frac{\overline{h_{nf}}(2R_{in})}{k_{in}} \tag{16}$$

The subscript b denotes a bulk or average value, while L represents the length of the tube.

The Reynolds number, a dimensionless parameter, characterizes the flow regime within the heat exchanger, distinguishing between laminar and turbulent flow. It is a function of the fluid's density, velocity, hydraulic diameter, and viscosity.

$$Re = \frac{\rho V d_h}{\mu} \tag{17}$$

Where ρ, V, d_h and μ are the density, velocity, hydraulic diameter of the tube cross-section, and viscosity, respectively.

The friction factor is crucial for determining the pressure drop across the DTHE. It is dependent on the pressure drop, hydraulic diameter, length, density and velocity of flow. An accurate prediction of the friction factor is essential for evaluating the pumping power requirements and the overall energy efficiency of the DTHE [273].

$$f = \frac{2\Delta P d_h}{L\rho V^2} \tag{18}$$

Where ΔP, L, ρ, and d_h are the pressure drop, length of DTHE, density the hydraulic diameter of the tube cross-section, respectively.

The performance evaluation criteria (thermal efficiency) provide a comprehensive measure of the heat exchanger's effectiveness. The PEC considers both the thermal performance and the friction factor, offering a balanced assessment of the heat exchanger's efficiency. The PEC of DTHE can be obtained from the following equation [274].

$$\text{PEC} = \frac{\left(\frac{Nu}{Nu_0}\right)}{\left(\frac{f}{f_0}\right)^{1/3}} \tag{19}$$

Where the subscribe *o* indicates the base fluid without nanoparticles and turbulator insertion.

To validate the numerical simulations, it is necessary to compare the simulation results with experimental data. In this regard, several empirical correlations for the Nusselt number have been extracted from the literature review. Sieder and Tate [248] presented an empirical correlation for calculating the Nusselt number for both heating and cooling, given by.

$$Nu = 1.86\left(RePr\frac{d}{L}\right)^{0.33} \tag{20}$$

Shah and London [249] provided an empirical correlation for the Nusselt number in laminar flow with pure water as the working fluid, given by.

$$Nu = 1.953\left(RePr\frac{d}{L}\right)^{0.33} \tag{21}$$

Gnielinski [250] derived an empirical correlation for the Nusselt number in laminar flow with pure water as the working fluid, expressed as.

$$Nu = \left[3.66^3 + 1.61^3\left(RePr\frac{d}{L}\right)\right]^{0.33} \tag{22}$$

Hausen [251] presented an empirical correlation for the Nusselt number in laminar flow with pure water as the working fluid, given by.

$$Nu = 3.66 + \frac{0.19\left(RePr\frac{d}{L}\right)^{0.8}}{1 + 0.177\left(RePr\frac{d}{L}\right)^{0.467}} \tag{23}$$

Where *Re* stands for the Reynolds number, *Pr* represents the Prandtl number, *d* is the tube diameter, and *L* denotes the length of DTHE.

The relative error e_r can be calculated as follows.

$$e_r = \frac{|\varepsilon - \hat{\varepsilon}|}{\hat{\varepsilon}} \times 100 \tag{24}$$

In which ε represents the target parameter, and $\hat{\varepsilon}$ represents the corresponding target parameter in the highest mesh element numbers.

The dimensions of the turbulators, specifically, the distances between the ribs (s), the height of the ribs (h), and the width of the ribs (w), are critical parameters that were systematically varied to study their impact on the DTHE. These factors help determine the effect of each dimension on the heat transfer and fluid flow characteristics of the DTHE. To better understand and compare these parameters, the following dimensionless key parameters were defined for s, w, and h.

$$S = \frac{s}{R_i}$$

$$W = \frac{w}{R_i} \tag{25}$$

$$H = \frac{h}{R_i}$$

Where R_i is the radius of the inner tube.

Root mean square error (RMSE) and coefficient of determination (R^2) are used to determine the quality of curve fitting and extracted correlations. The following equations can be used for RMSE and R^2 [275, 276].

$$\text{RMSE} = \left[\frac{1}{N}\sum_{i=1}^{n}(Y_{pre,i} - Y_{num,i})^2\right]^{1/2} \tag{26}$$

$$R^2 = 1 - \frac{\sum_{i=1}^{n}(Y_{num,i} - Y_{pre,i})^2}{\sum_{i=1}^{n}(Y_{num,i})^2} \tag{27}$$

Where the $Y_{pre,i}$ and $Y_{num,i}$ are the predicted and numerical values, respectively.

Chapter 5: Results and Discussion

Chapter 5 presents a detailed analysis and discussion of the results obtained from the numerical simulations conducted to investigate the heat transfer and fluid flow characteristics of nanofluids and various turbulator designs within a double tube heat exchanger. Initially, it addresses the grid independence test results, confirming the computational accuracy and reliability. Subsequently, it compares the results of this study with those in existing literature to validate the simulations' credibility. This chapter explores how different configurations of counter and parallel flow in DTHE, various nanofluid volume fractions, and different types of nanofluids (CuO, ZnO, Fe_3O_4, Diamond, Ag, TiO_2, Al_2O_3, SiC, SiO_2) affect the heat transfer performance of the DTHE. It also explores the influence of distinct transverse and helical turbulator shapes-rectangular, triangular, oval, and trapezoidal-on the performance of DTHE.

5.1 Grid independence test

The impact of varying mesh densities on heat transfer and hydrodynamic parameters was evaluated for both transverse and helical turbulator insertions. This assessment aimed to confirm the adequacy of mesh refinement and ensure independence within the computational simulations. The mesh independence test was evaluated based on three critical parameters: outlet temperature, pressure drop, and the average Nusselt number across the inner tube. Figure 5.1 illustrates that the optimal mesh comprises approximately 107,000 elements, with a maximum discrepancy of less than 2.2% compared to simulations employing the highest mesh density. Furthermore, Figure 5.2 presents the variation in outlet temperature, pressure drop, and Nusselt number for the inner tube equipped with a rectangular helical turbulator. It shows that the deviation in outcomes with the use of 7,000,000 elements, as compared to the case with the highest number of elements, is less than 2%. To optimize computational time and expenses, the simulations utilised mesh sizes of approximately 107,000 for transverse turbulator insertions and about 7,000,000 elements for helical turbulator insertions. It was also concluded that the Nusselt number exhibited greater sensitivity to variations in the number of mesh elements relative to the other considered parameters.

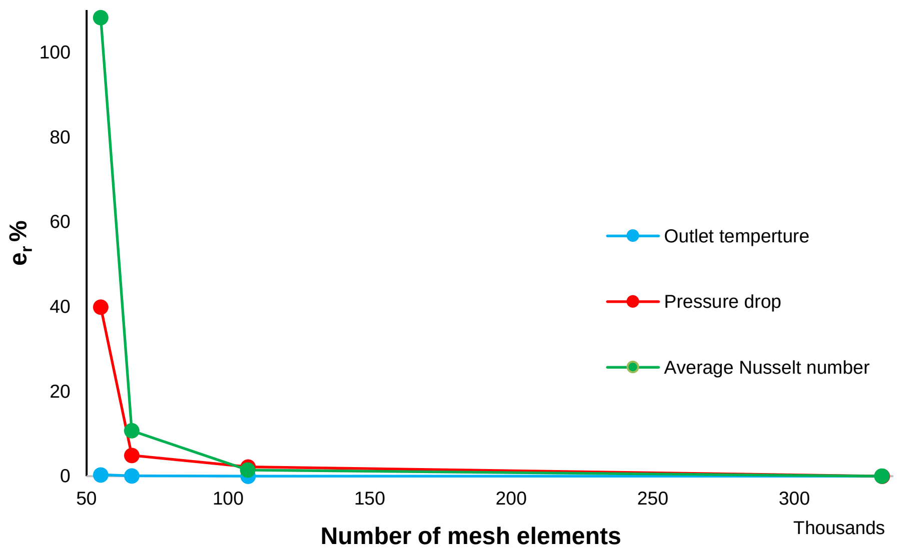

Figure 5.1: Relative error of the selected parameters for different number of mesh elements for rectangular ribs.

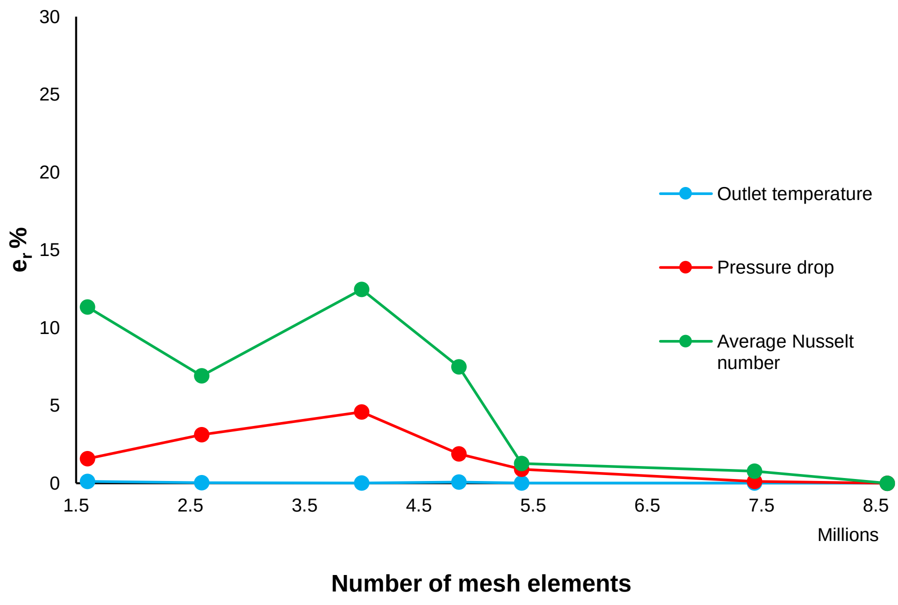

Figure 5.2: Relative error of the selected parameters for different number of mesh elements for rectangular helical turbulator.

5.2 Validation of simulation results

5.2.1 Empirical correlation validation

Figure 5.3 displays the average Nusselt number results against Reynolds number obtained using the empirical correlations presented by Seider and Tate [248] (Equation 20), Shah and London [249] (Equation 21), Gnielinski [250] (Equation 22), and Hausen [251] (Equation 23) for laminar flow with pure water. To validate these correlations, a Python code (Appendix B) was developed to compute the average Nusselt number for each equation and compare them with results from numerical simulations. In this case, the inlet temperatures for the inner and outer tubes were set at 280 K and 350 K, respectively. The Reynolds number for the outer tube was held constant at 800. Also, the length, inner, and outer tube diameter of the DTHE are 1.8 m, 0.014 m, and 0.08 m, respectively. The results of present study revealed a maximum deviation of 5.64% when compared to the findings reported by Seider and Tate [248] results. The friction factor results obtained in this study were compared with the theoretical correlation for laminar flow, as depicted in Figure 5.4. The maximum discrepancy observed between the present study's friction factor and the theoretical value was less than 18.6%.

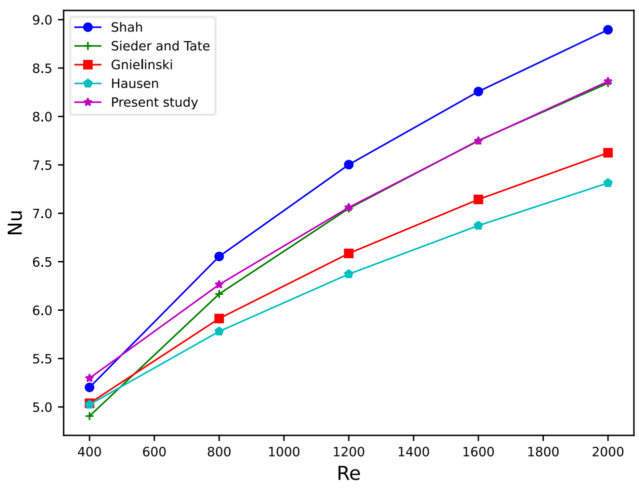

Figure 5.3: Results of the present study vs empirical correlations results for average Nusselt number in counter flow using pure water.

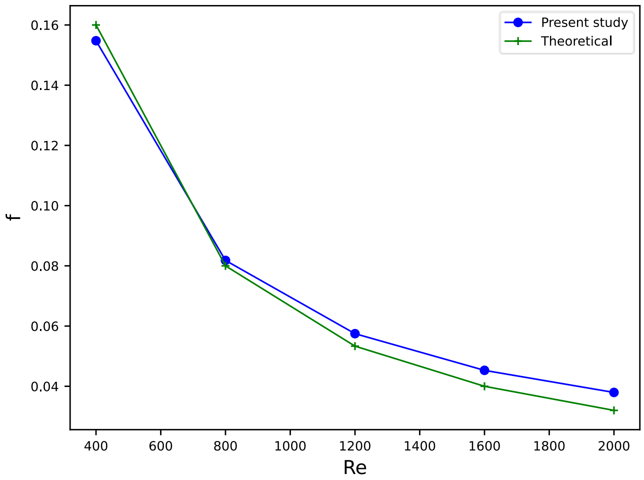

Figure 5.4: Comparison of friction factor results from the present study with the theoretical correlation.

5.2.2 Numerical validation

An additional validation was conducted by comparing the nanofluid simulation results of the present study with those published by Bahmani, et al. [277]. This comparison focused on the average Nusselt number across Reynolds numbers ranging from 100 to 2000 for the inner tube, while maintaining a constant Reynolds number of 500 for the outer tube, along with constant inlet temperatures of 283 K and 353 K, as reported in Bahmani's study. These comparisons are illustrated in Figure 5.5. In this case, the size of the DTHE was characterized by a length of 2 m, an inner tube diameter of 0.026 m, and an outer tube diameter of 0.05 m. The results from the current study demonstrated a deviation of less than 12% compared to those of Bahmani, M.H.

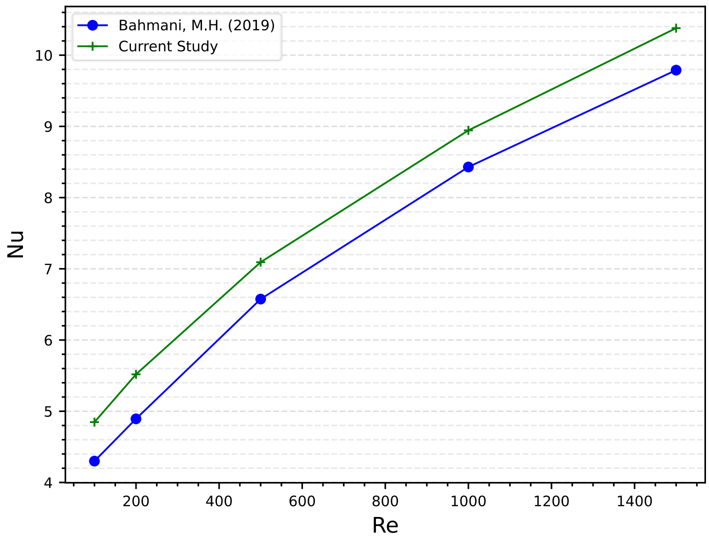

Figure 5.5: Comparison of average Nusselt number results from the present study with numerical findings of Bahmani, M.H. [277], for counterflow configuration.

5.2.3 Experimental validation with nanofluid

Further validation was conducted by comparing the ratio of average Nusselt numbers (nanofluid to pure water) using Al_2O_3 nanofluid and a single-phase model, against numerical results from a two-phase model by Shirvan, et al. [253], and experimental results by Heyhat, et al. [254]. For this validation, the DTHE featured a copper inner tube with a diameter of 0.005 m, a wall thickness of 0.0005 m, and a length of 2 m. The outer tube is immersed in a steam bath to maintain a constant temperature throughout the system, while the inlet temperature of the inner tube is maintained at 333.15 K. Figure 5.6 displays the validation outcomes for the average Nusselt number ratio of nanofluid to pure water across various Reynolds numbers. The results of the current study, utilising a single-phase model, demonstrated a maximum deviation of less than 5.42% compared to the experimental data. Similarly, the two-phase model indicated a deviation of less than 9.83% from the experimental results. Consequently, it can be concluded that the single-phase model aligns more closely with the experimental data.

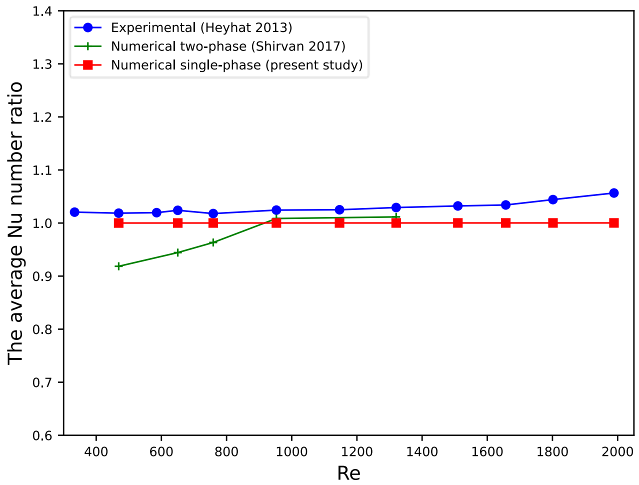

Figure 5.6: Results of present study using single-phase model with numerical two-phase model and experimental results for Al_2O_3 nanofluid at φ=0.01.

5.2.4 Turbulator insertion experimental validation

To enhance the accuracy and reliability of the turbulator insertion simulations, the present study's results were compared with the experimental outcomes of turbulator insertion by Hong and Bergles [255]. In this context, the experimental setup consisted of a tube characterized by a diameter of 0.0102 m, a length of 1.22 m, and a wall thickness of 0.00051 m. The Reynolds number varied between 450 and 1500, under a constant heat flux of 1000 W/m^2 and an inlet temperature of 318.15 K. A twisted tape turbulator, with a thickness of 0.00046 m and a width of 0.0097 m, possessing a twist ratio of 2.45, was inserted inside the tube. Figure 5.7 presents a comparison of the average Nusselt number for numerical and experimental turbulator insertions. The comparison revealed a maximum discrepancy of less than 17.9%, indicating a reasonable agreement with the experimental findings.

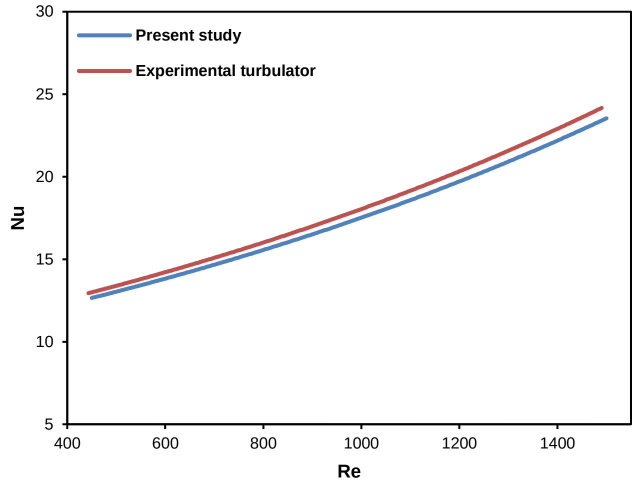

Figure 5.7: Comparison of average Nusselt number results from the present study's simulation with the experimental turbulator insertion.

5.3 Performance of DTHE without turbulator insertion

5.3.1 Parallel and counter flow configuration

Figure 5.8 compares the counter and parallel flow for the average heat transfer coefficient against the Reynolds number for different nanoparticle volume fractions. The results show that counterflow configuration gives a better heat transfer enhancement than parallel flow configuration in all cases. So, the counter flow DTHE is more efficient than parallel flow because it can exchange the maximum amount of heat between cold and hot fluids. The thickness of the boundary layer in counter flow is less than in parallel flow. Also, the counter flow has a better temperature uniformity and smaller outlet temperature difference in comparison with the parallel flow [278, 279]. The outlet temperature difference of counter and parallel flow, at a fixed volume fraction φ=0.05 and various Reynolds numbers, is compared in Figure 5.9.

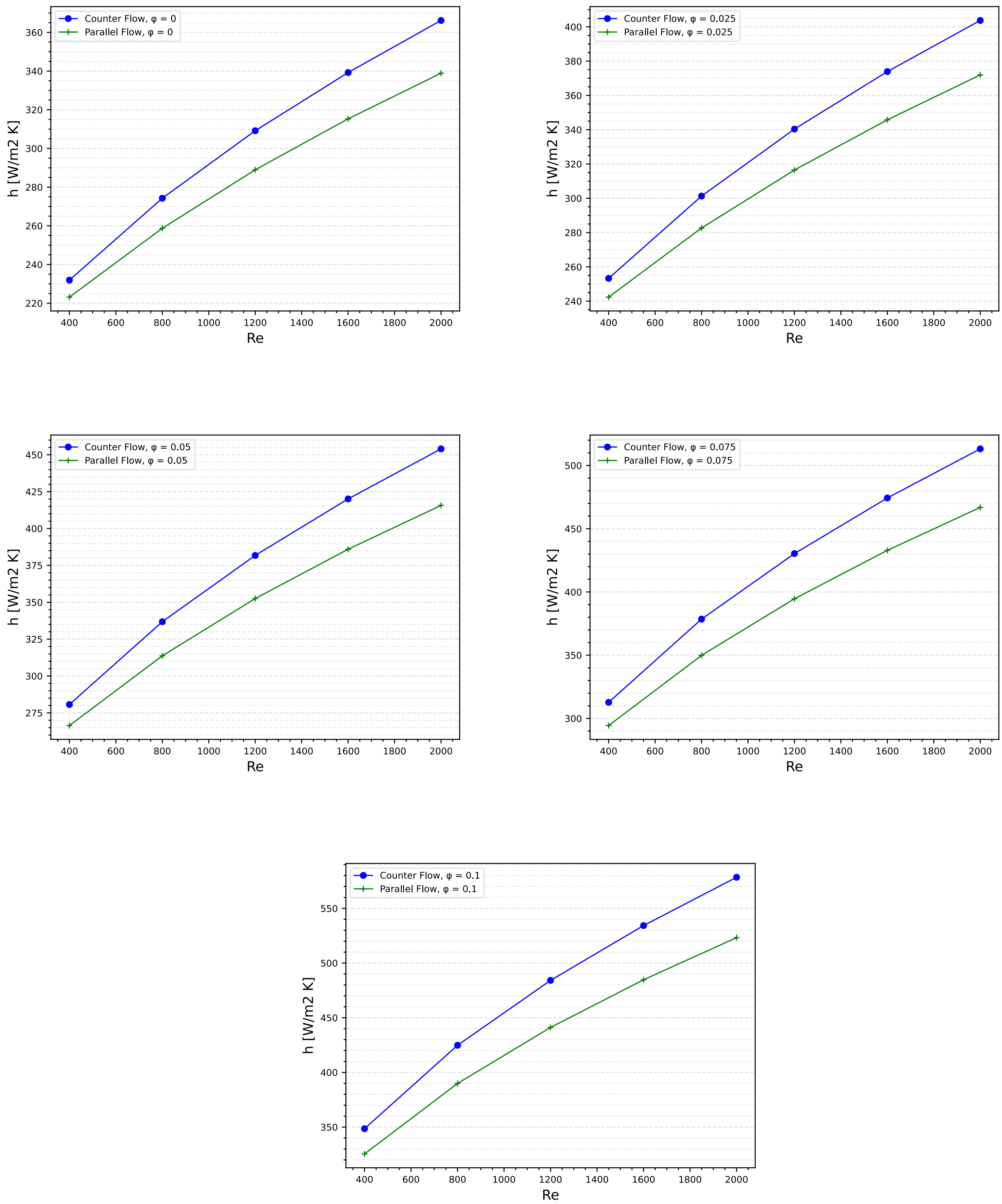

Figure 5.8: Comparison heat transfer coefficient vs Reynolds number in counter and parallel flow.

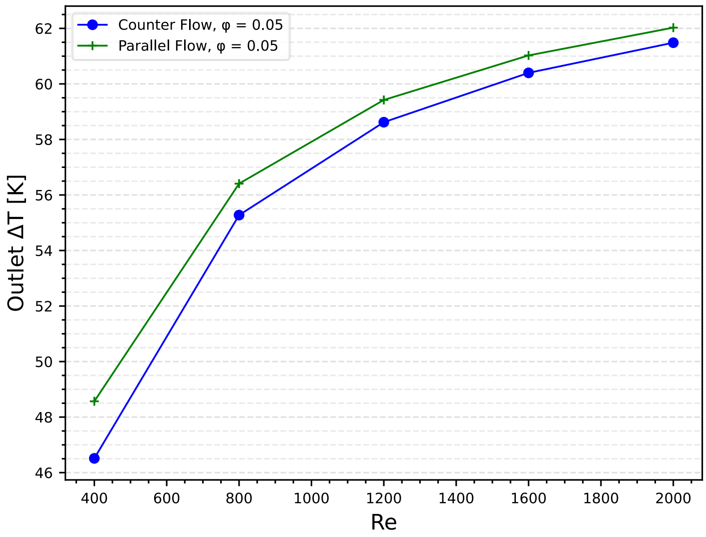

Figure 5.9: Comparison outlet temperature difference of counter and parallel flow vs Reynolds number.

5.3.2 Effect of different nanofluid volume fraction

Figure 5.10 illustrates the effect of different Reynolds numbers against the average Nusselt numbers for various volume fractions of nanoparticles in the counter flow configuration. It is observed that the average Nusselt number enhances with increasing nanoparticle volume fractions and Reynolds number. The boundary layer decreases by increasing the nanoparticles volume fraction and Reynolds number [26]. This effect makes the velocity and temperature gradient increase near the wall. The maximum average Nusselt number enhancement occurs at 0.1 volume fraction and Reynolds number 2000. The correlation 28 was derived by curve fitting the results shown in Figure 5.10 to predict the value of the Nusselt number in counter flow.

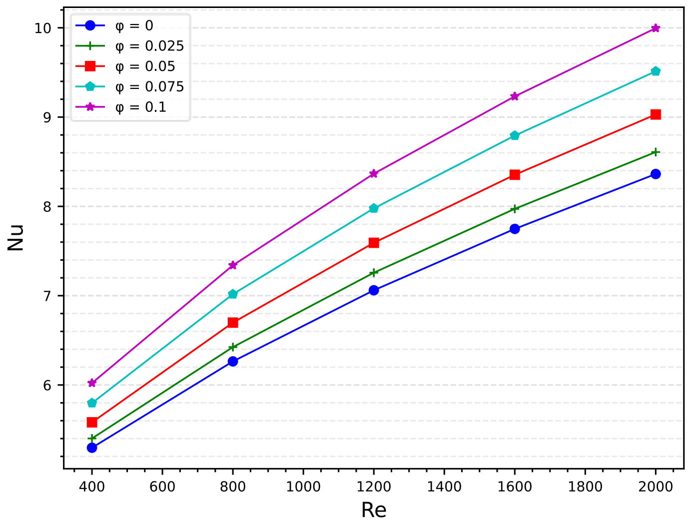

Figure 5.10: Variation of Nusselt number vs Reynolds number for different volume fractions in counter flow.

$$Nu = 0.08837 \times Re^{0.553} + 25.37 \times \varphi^{1.304} + 2.622 \qquad \text{RMSE} = 0.1305 \quad R^2 = 0.9921 \qquad (28)$$

Figure 5.11 shows the effect of different Reynolds numbers against average Nusselt numbers for different volume fractions of nanoparticles in parallel flow configuration. The same as counter flow, it can be seen that the Nusselt number increases by increasing nanoparticles volume fraction and Reynolds number. The maximum average Nusselt number enhancement occurs at 0.1 volume fraction and Reynolds number 2000. Correlation 29 was derived by curve fitting the results shown in Figure 5.11 to predict the value of the Nusselt number in parallel flow.

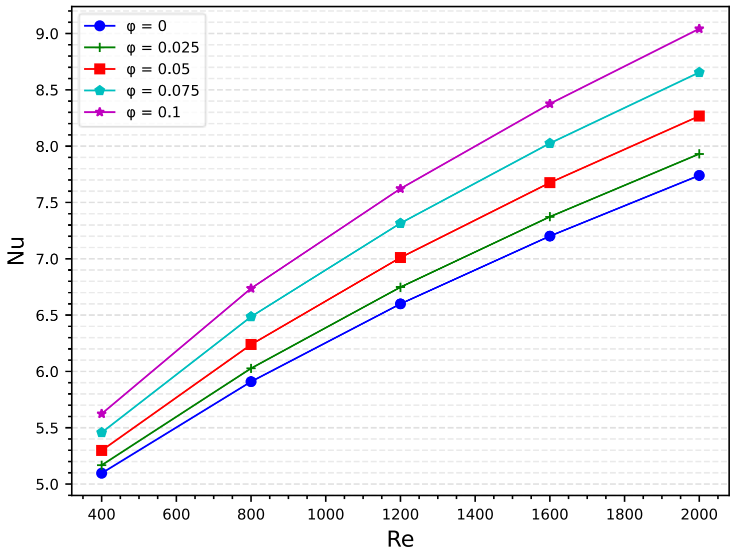

Figure 5.11: Variation of Nusselt number vs Reynolds number for different volume fractions in parallel flow.

$$Nu = 0.3178 \times Re^{0.3952} + 24.24 \times \varphi^{1.392} + 1.44 \qquad \text{RMSE} = 0.1183 \qquad R^2 = 0.9902 \qquad (29)$$

Figure 5.12 shows the effect of various nanoparticle volume fractions and Reynolds number for the pressure drop of the inlet and outlet of the inner tube in the DTHE. It can be concluded that increasing nanoparticle volume fractions and Reynolds number increases pressure drop. The gradient of pressure drop is higher for bigger Reynolds numbers than lower Reynolds numbers. As the friction factor in laminar flow is primarily dependent on the Reynolds number and surface roughness, the friction factor remains unchanged. However, the pressure drop increases due to the higher viscosity of the nanofluid compared to water.

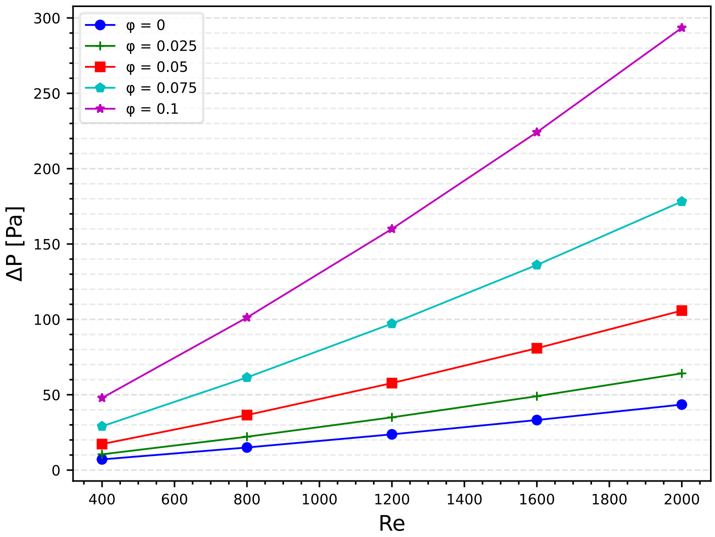

Figure 5.12: The effect of different nanoparticles volume fractions on pressure drop for different Reynolds number.

Figure 5.13 shows the contours of static pressure, static temperature, and velocity magnitude of inner and outer tubes in the DTHE. Reynolds number and nanofluid volume fraction for this counter flow configuration are 400 and 0.1, respectively. Figure 5.13 b illustrates changes in temperature near the copper wall and the heat transfer between the cold and hot flow. The analysis reveals that the maximum temperature change occurs near the wall, where the cold nanofluid and hot water exchange heat across the copper tube's thickness. The heat transfer from the hot water to the cold nanofluid intensifies along the inner tube's length. Near the outlet of the inner tube, a pronounced temperature gradient extends towards the tube's center.

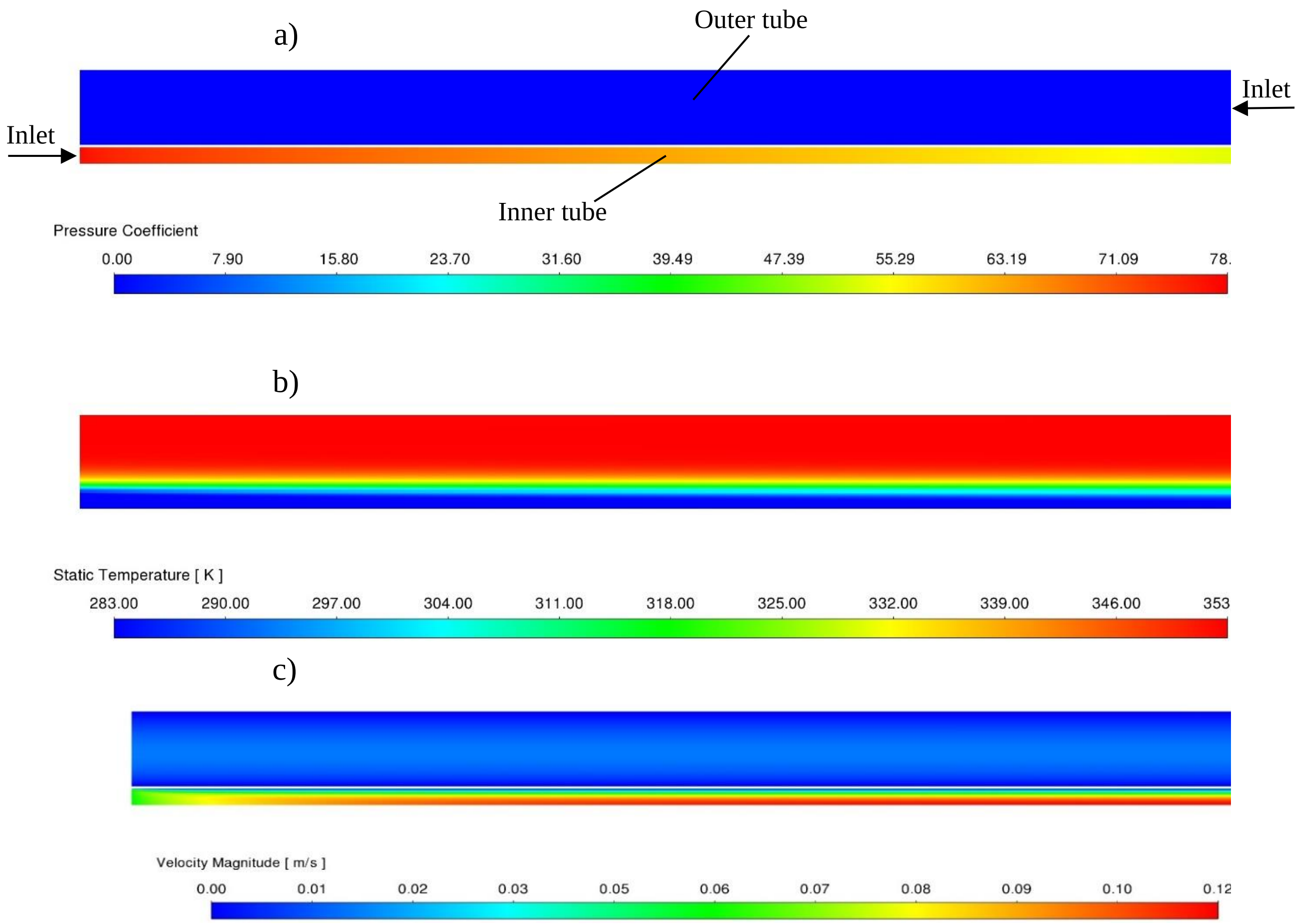

Figure 5.13: Colour plots of a) Pressure coefficient, b) Temperature, c) Velocity for Re=400 and 0.1 volume fraction.

Figure 5.14 represents the maximum enhancement of the average Nusselt number compared to pure water for counter and parallel flow configurations. This figure shows that increasing nanoparticle volume fractions increases the average Nusselt number enhancement. The maximum average Nusselt number enhancement occurs in the highest Reynolds number, which shows that the effect of nanoparticles is noticeable at higher Reynolds numbers. For all cases, the enhancement of the average Nusselt number for counter flow is bigger than the parallel flow.

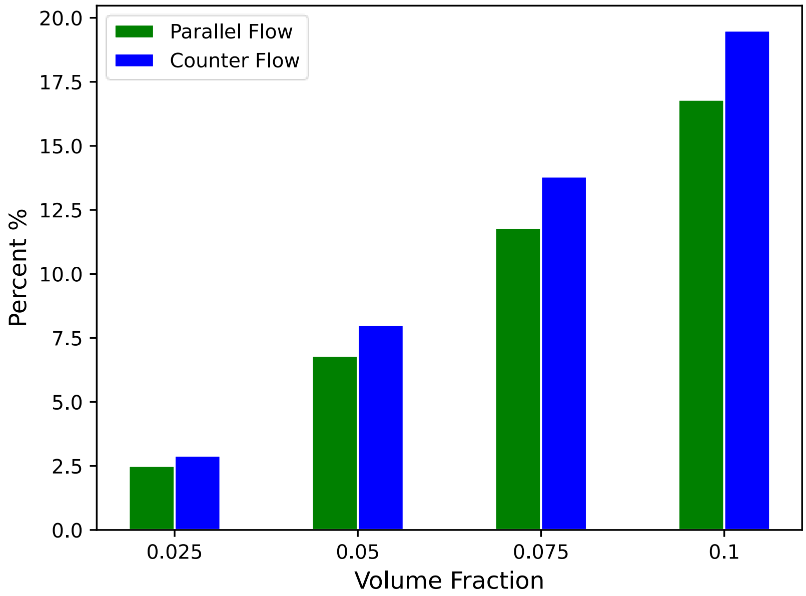

Figure 5.14: Maximum enhancement of Nusselt number compared to pure water in counter and parallel flow for different nanoparticle volume fractions at Re=2000.

Figure 5.15 and Figure 5.16 show the performance evaluation criteria (thermal efficiency) of DTHE for both counter and parallel flow configurations. In both configurations, the PEC increases by increasing the nanoparticle volume fractions and Reynolds number. The gradient of PEC decreases by increasing the Reynolds number, and for lower nanoparticle volume fractions, this gradient is lower. Using nanoparticles in the high Reynolds numbers is more efficient than using them in the lower Reynolds numbers. For all cases, the PEC of counter flow is higher than parallel flow. The correlations 30 and 31 were derived by curve fitting the results shown in Figure 5.15 and Figure 5.16 to predict the value of the PEC in counter and parallel flow, respectively.

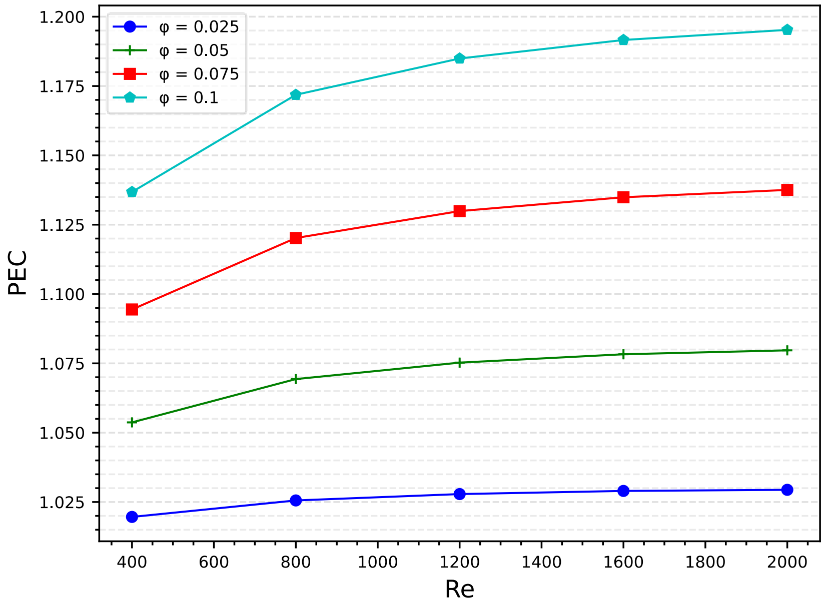

Figure 5.15: Variation of thermal efficiency vs Reynolds number for different volume fractions in counter flow.

$$PEC = 0.5709 \times Re^{0.03049} + 2.438 \times \varphi^{1.137} + 0.2875 \qquad \text{RMSE} = 0.009129 \qquad R^2 = 0.9813 \qquad (30)$$

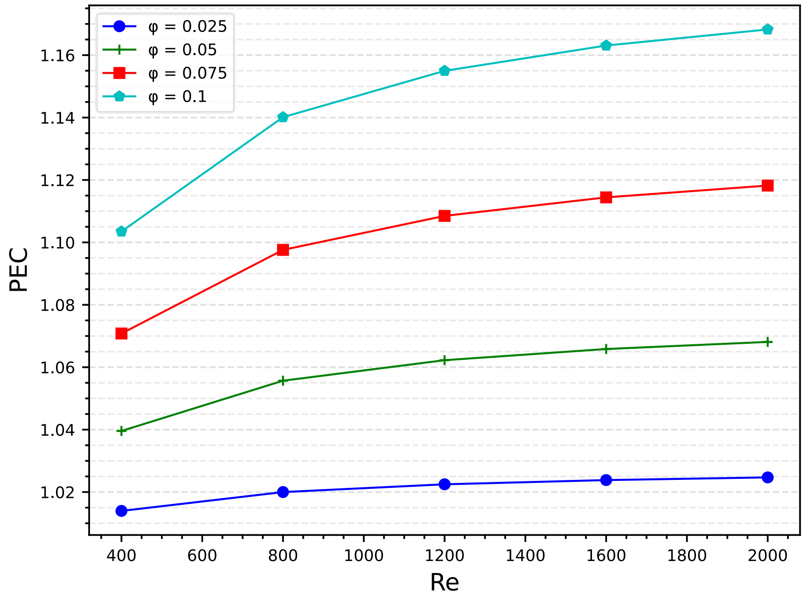

Figure 5.16: Variation of thermal efficiency vs Reynolds number for different volume fractions in parallel flow.

$$PEC = 0.03076 \times Re^{0.1972} + 2.471 \times \varphi^{1.204} + 0.87 \qquad \text{RMSE} = 0.008704 \quad R^2 = 0.9751 \qquad (31)$$

The present study validates the accuracy of Equation 28, extracted from Figure 5.10 by curve fitting, by comparing it with available data in the literature, as shown in Figure 5.17. Specifically, the average Nusselt number ratio from the experimental study by Heyhat, et al. [254] and the numerical two-phase model by Shirvan, et al. [253], for nanoparticle volume fractions of 0.001 and 0.01, was compared with Equation 28 for Reynolds numbers ranging from 400 to 2000. The results indicated that equation 28 provided a better fit to the experimental data in comparison to the numerical two-phase model. The maximum deviation of equation 28 from the experimental results was found to be less than 6.5%.

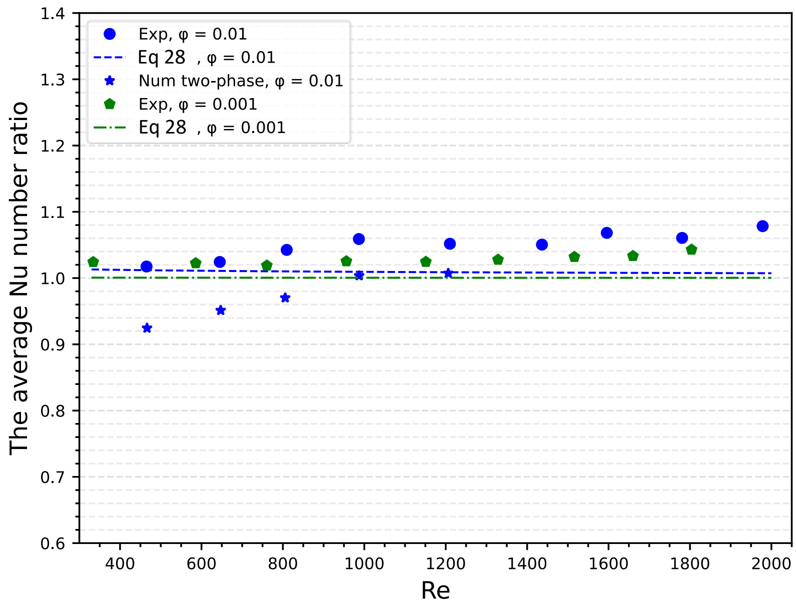

Figure 5.17: Validation of Equation 28 with the experimental results from Heyhat, et al. [254] and the numerical two-phase model from Shirvan, et al. [253].

Figure 5.18 depicts the dimensionless exergy destruction against Reynolds number for various volume fractions. The exergy destruction serves as a clear indicator of the amount of available work lost during a process, thereby indicating the level of energy degradation in the DTHE. The results show that the exergy destruction in the DTHE decreases with increasing Reynolds number and volume fractions. This indicates that the utilisation of nanofluids in DTHEs leads to improved energy loss and enhanced efficiency. Furthermore, a comparison of exergy destruction between counter flow and parallel flow reveals that energy loss is lower in the counter flow configuration as compared to the parallel flow configuration.

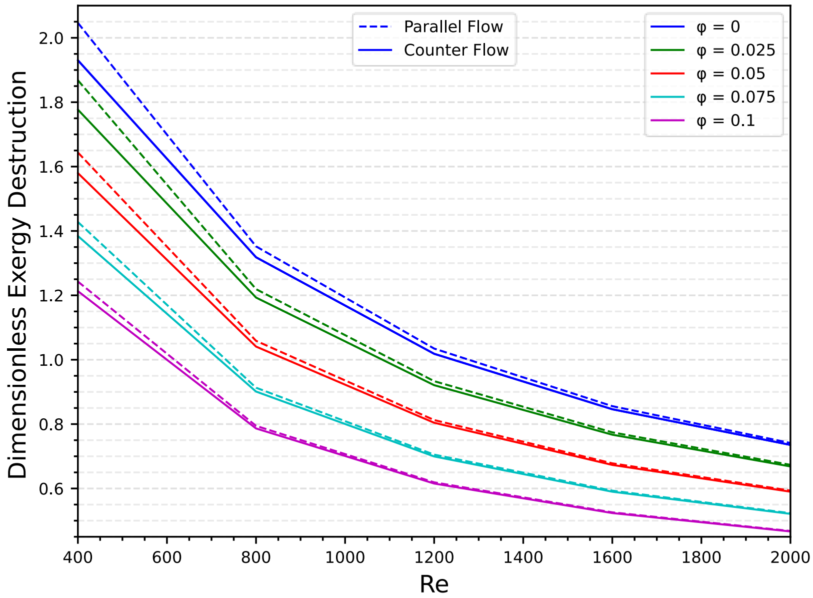

Figure 5.18: Dimensionless exergy destruction vs Reynolds number for counter and parallel flow configurations.

5.3.3 Effect of different nanofluids

Nine different nanofluids, namely CuO, ZnO, Fe_3O_4, Diamond, Ag, TiO_2, Al_2O_3, SiC, and SiO_2, were selected to evaluate their impact on the performance of the DTHE without turbulator insertion. Figure 5.19 and Figure 5.20 depict the percentage enhancement in the average Nusselt number and pressure drop for these nanofluids at a Reynolds number of 1200 and a volume fraction of 0.05, in comparison to water. The findings indicated that the SiO_2 nanofluid exhibits the highest Nusselt number and pressure drop rise when compared to other nanofluids. This difference can be attributed to SiO_2's lower thermal conductivity and density compared to the other nanoparticles. As a result, at the same Reynolds number, SiO_2 achieves a higher average velocity. This increased fluid velocity significantly impacts the heat transfer coefficient and forced convection [280]. Similarly, it was observed that CuO nanofluid demonstrated the smallest increase in Nusselt number and pressure drop when compared to water. For comparison with existing literature, the results by Yogaraj, et al. [281], who used ZnO and TiO_2 nanofluids, reported heat transfer enhancements of 18.5% and 15.5%, respectively.

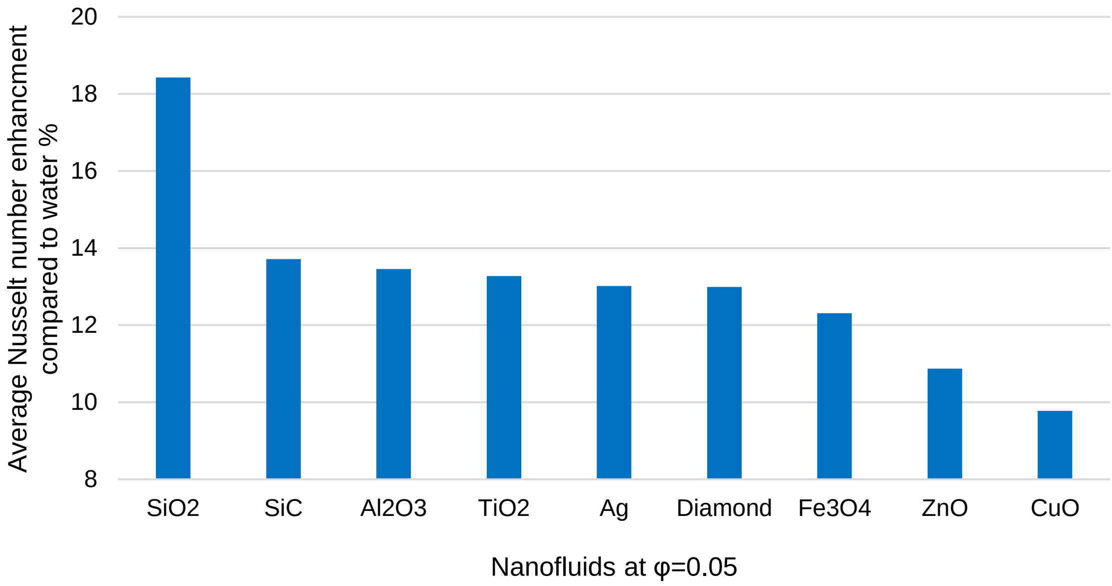

Figure 5.19: Percentage enhancement in the average Nusselt number of different nanofluids compared to water, without turbulator insertion, at a Reynolds number of 1200 and a volume fraction of 0.05.

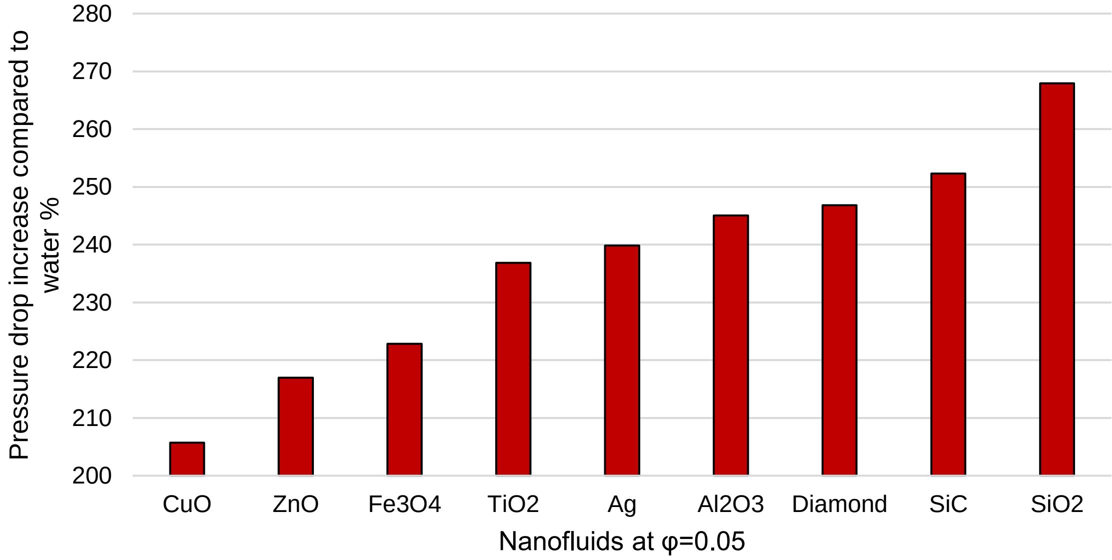

Figure 5.20: Percentage enhancement in pressure drop of different nanofluids compared to water, without turbulator insertion, at a Reynolds number of 1200 and a volume fraction of 0.05.

Figure 5.21 depicts the PEC for different nanofluids at a Reynolds number of 1200 and a volume fraction of 0.05 without turbulator insertion. All nanofluids exhibited a PEC greater than 1, indicating that despite an increase in pressure drop, the use of nanofluids is justified by the enhancement of the DTHE performance. Furthermore, the results demonstrated that the heat transfer rate increase for SiO_2 nanofluid is more significant compared to the pressure drop increase, with this nanofluid achieving the highest PEC of 1.18. Conversely, CuO, having a minimal increase in heat transfer rate, recorded the lowest PEC, suggesting it is not recommended for use as a nanofluid in heat exchangers.

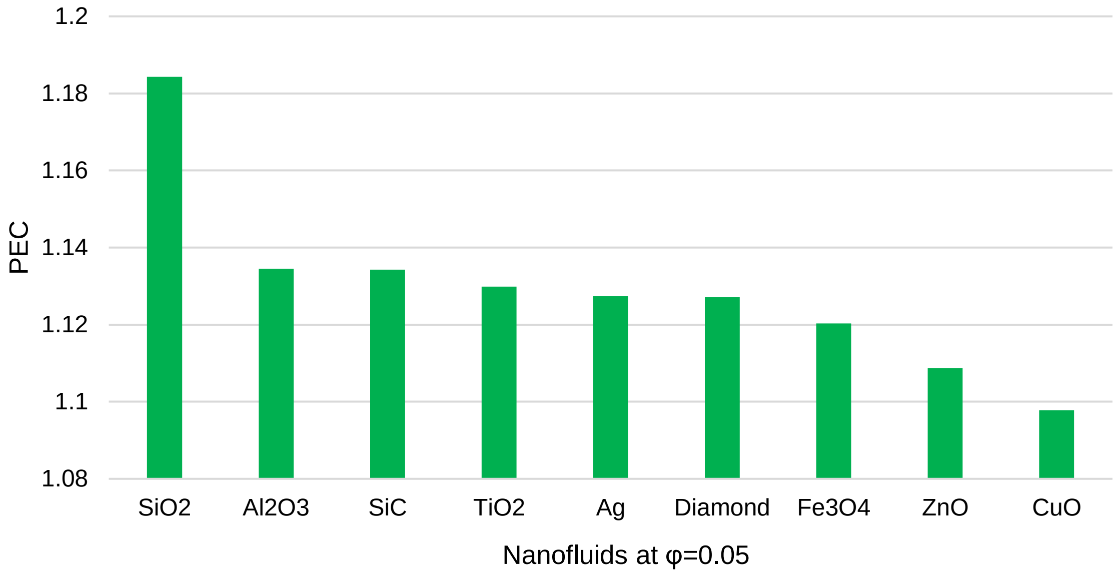

Figure 5.21: PEC for different nanofluids, without turbulator insertion, at a Reynolds number of 1200 and a volume fraction of 0.05.

5.4 Performance of DTHE with transvers turbulator insertion

5.4.1 Effect of different shape of turbulator

Figure 5.22 illustrates the average Nusselt number of the inner tube against Reynolds numbers for various rib shapes and CuO nanofluid. The data indicates that the utilisation of nanofluid leads to a notable increase in the Nusselt number compared to using pure water, and this effect is further enhanced when turbulator insertion is employed. Specifically, the trapezoidal and triangular turbulators exhibit the higher Nusselt numbers, with trapezoidal ribs yielding the superior results compared to other rib shapes. On the other hand, the rectangular ribs showed the least increase in Nusselt number among all the different rib shapes. The observed rise in the Nusselt number can be attributed to two main factors. Firstly, the incorporation of nanoparticles enhances the thermal properties of the working fluid. Secondly, the insertion of turbulator induces additional mixing and secondary flow, which reduces the thermal boundary layer close to the wall [26]. The Nusselt number increases with the increase of the Reynolds number due to an increase in momentum and mixing flow. These combined effects of nanoparticles and turbulator insertion led to improved heat transfer performance of the DTHE.

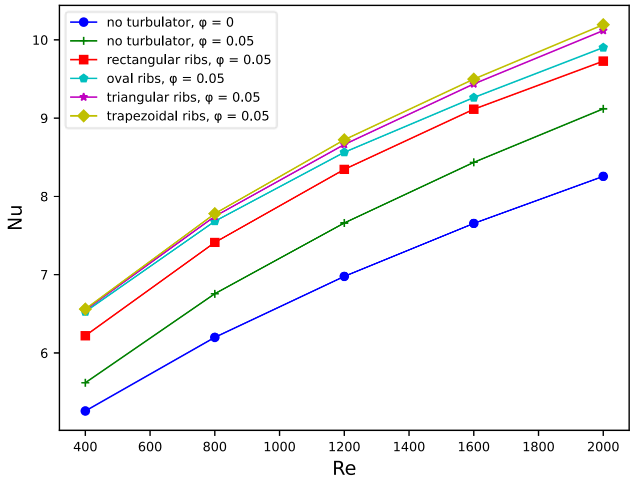

Figure 5.22: The average Nusselt number against Reynolds numbers for various rib shapes, CuO nanofluid φ=0.05, S=5.71, W=0.29, and H=0.29.

Figure 5.23 depicts the inner tube's pressure drop and friction factor against Reynolds numbers for various rib shapes and CuO nanofluid. The addition of nanoparticles to the working fluid increases the pressure drop compared to pure water, and this increase becomes more pronounced when a turbulator is inserted into the DTHE. The pressure drop and friction factor are critical parameters that affect the performance of DTHEs. The figures reveal that the triangular rib shape exhibits the highest pressure drop and friction factor, whereas the oval turbulator demonstrates the lowest values. The triangular rib shape, by virtue of its shape, is likely to present a more abrupt obstruction to the flow, leading to increased flow separation and consequently higher energy losses. This phenomenon is further compounded by the formation of a more pronounced recirculation zone behind the rib, which contributes to an increase in the system's overall resistance to flow, reflected in the heightened pressure drop [282]. Comparatively, the trapezoidal rib, while still inducing a significant pressure drop, might offer a slightly less aggressive interruption to the flow due to their sloped faces. The gradient provided by the trapezoidal shape potentially allows for a more gradual deviation of the flow, which in turn might result in a somewhat reduced pressure drop relative to triangular ribs. Due to its longer length at the top of the shape, the rectangular rib induces a lower pressure drop. Conversely, the oval rib, characterized by a smoother surface, diminishes the friction between the flow and the turbulator. This results in a reduced pressure drop and friction factor compared to other shapes.

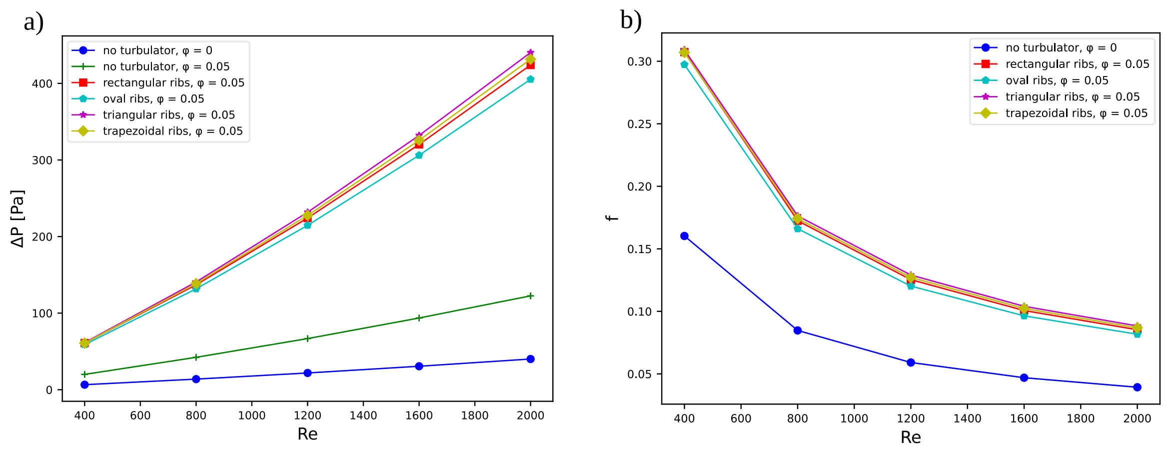

Figure 5.23: a) the pressure drop and b) friction factor against Reynolds numbers for various rib shapes, CuO nanofluid φ=0.05, S=5.71, W=0.29, and H=0.29.

Figure 5.24 presents colour plots illustrating the a) normalized temperature, b) normalized velocity magnitude, c) normalized radial velocity, and d) pressure coefficient for various shapes, including triangular, trapezoidal, rectangular, and oval, using the CuO nanofluid with a φ=0.05. The normalized parameters for temperature, velocity magnitude, and radial velocity are obtained by dividing each local parameter by the inlet temperature and velocity, respectively. The results show that the trapezoidal, triangular, and oval shapes exhibit a more uniform normalized temperature distribution than the rectangular shape. This suggests that the mixing and secondary flow contribute to a more evenly distributed temperature in the flow. Furthermore, the triangular shape experiences the highest intensity of pressure coefficient, while the oval shape exhibits the lowest. This phenomenon is attributed to the creation of smoother obstacles in the path of the flow, leading to variations in pressure distribution. The normalized velocity magnitude and normalized radial velocity plots provide insights into the flow patterns around the different shapes and describe the formation of vortices behind each rib. It can be seen that the change in normalized magnitude velocity and normalized radial velocity is more pronounced in triangular and trapezoidal shapes when compared to rectangular and oval shapes.

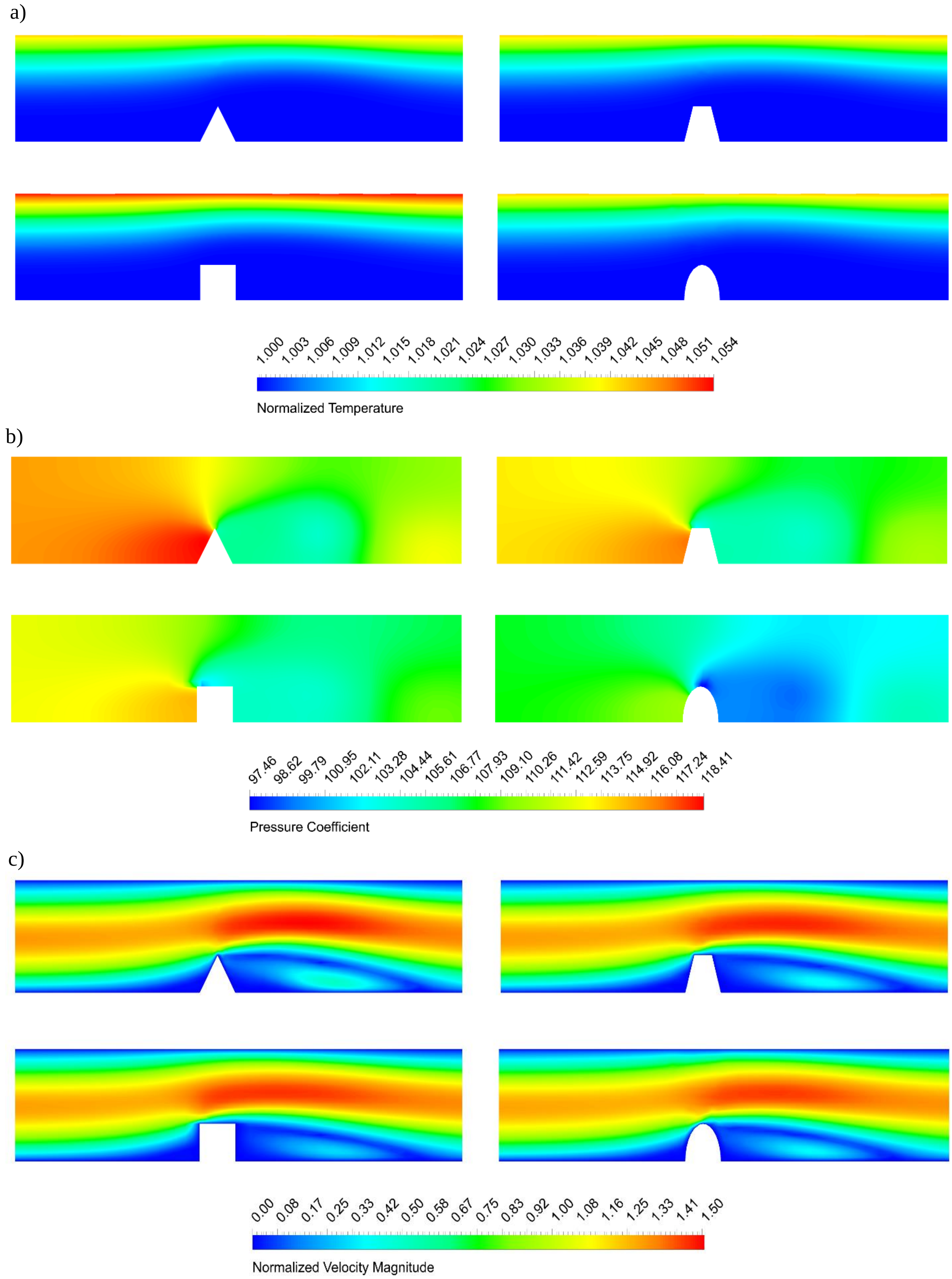
a)
1.000 1.003 1.006 1.009 1.012 1.015 1.018 1.021 1.024 1.027 1.030 1.033 1.036 1.039 1.042 1.045 1.048 1.051 1.054
Normalized Temperature
b)
97.46 98.62 99.79 100.95 102.11 103.28 104.44 105.61 106.77 107.93 109.10 110.26 111.42 112.59 113.75 114.92 116.08 117.24 118.41
Pressure Coefficient
c)
0.00 0.08 0.17 0.25 0.33 0.42 0.50 0.58 0.67 0.75 0.83 0.92 1.00 1.08 1.16 1.25 1.33 1.41 1.50
Normalized Velocity Magnitude

d)

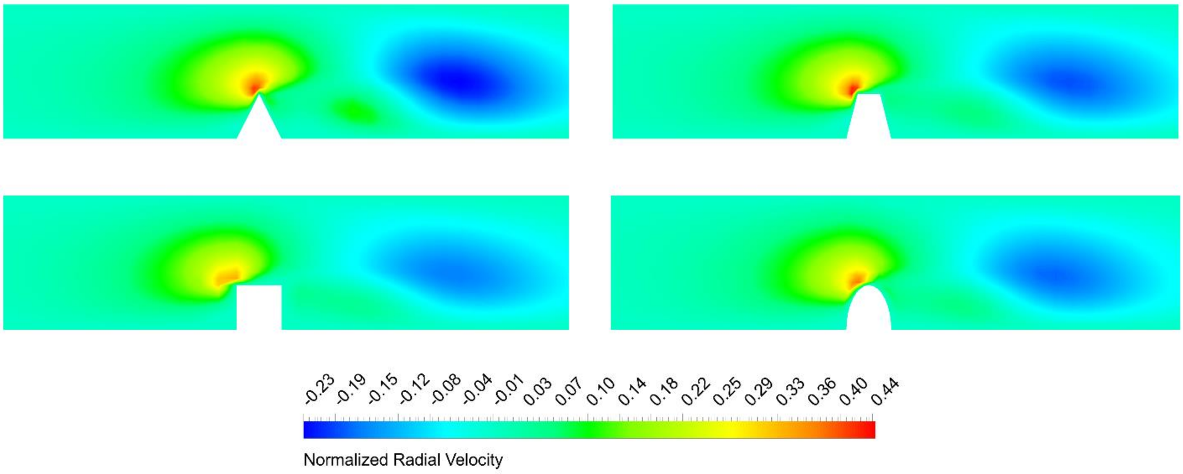

Figure 5.24: Colour plots of a) normalized temperature, b) pressure coefficient, c) normalized velocity magnitude, and d) normalized radial velocity for different geometries, utilising CuO nanofluid at Re=800, φ=0.05, S=5.71, W=0.29, and H=0.29.

Figure 5.25 illustrates the recirculation lengths associated with different rib geometries in a flow with a Reynolds number of 1200, using CuO nanofluid at a volume fraction φ=0.05. The recirculation zones, a key factor in the enhancement of heat transfer, are initiated at the flow separation points, locations proximate to the top of the ribs, and extend downstream to the points of flow reattachment on the turbulator wall. In a descending order of length, the trapezoidal rib induces the longest recirculation zone, followed by the triangular rib, then the oval, and finally the rectangular rib, which generates the shortest length. The length of the recirculation zone is crucial, as it directly influences the intensity of fluid mixing and the generation of secondary flow patterns within the flow field. The secondary flow is instrumental in disrupting thermal boundary layers and augmenting convective heat transfer, as quantified by the Nusselt number [26]. Hence, the data imply that the ribs with trapezoidal and triangular shapes are more effective in enhancing the heat transfer rate compared to those with oval and rectangular shapes. This phenomenon is attributable to the more pronounced fluid dynamic activities within the recirculation zones created by the trapezoidal and triangular rib configurations [282]. Table 5.1 shows the recirculation length in millimeters for each rib type, listed from longest to shortest: trapezoidal rib, triangular rib, oval rib, and rectangular rib.

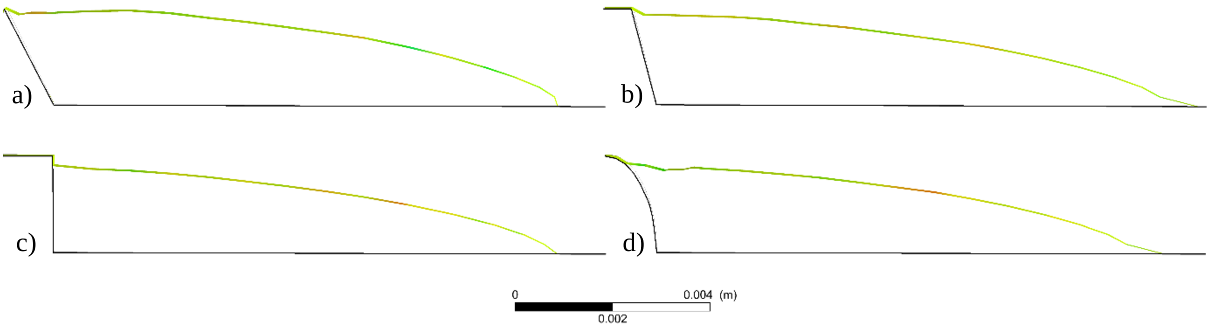

Figure 5.25: Recirculation length of a) triangular, b) trapezoidal, c) rectangular, and d) oval ribs for Reynolds number of 1200, CuO nanofluid φ=0.05, S=5.71, W=0.29, and H=0.29.

Table 5.1: Recirculation length of different ribs (trapezoidal, triangular, oval, rectangular).

Turbulator	**Recirculation length [mm]**
Trapezoidal	11.55
Triangular	10.41
Oval	10.40
Rectangular	10.32

5.4.2 Effect of different height of the ribs

Figure 5.26 presents the average Nusselt number of the inner tube plotted against Reynolds numbers for different ratios of the height of the trapezoidal rib to the radius of the inner tube (H) in the presence of SiO_2 nanofluid. The graph demonstrates that as the H increases, the Nusselt number shows an upward trend. This phenomenon can be attributed to the enhanced mixing and secondary flow resulting from the increased obstruction in the flow caused by the trapezoidal rib. As a result, the thermal boundary layer decreases [26], leading to an overall increase in heat transfer. Furthermore, a noticeable enhancement occurs at H=0.57, where the average Nusselt number of the DTHE exceeds 40. These results indicate a significant improvement in the average Nusselt number at this specific H value compared to the other H values. The Nusselt number of all cases shows an increasing trend with the rise in the Reynolds number.

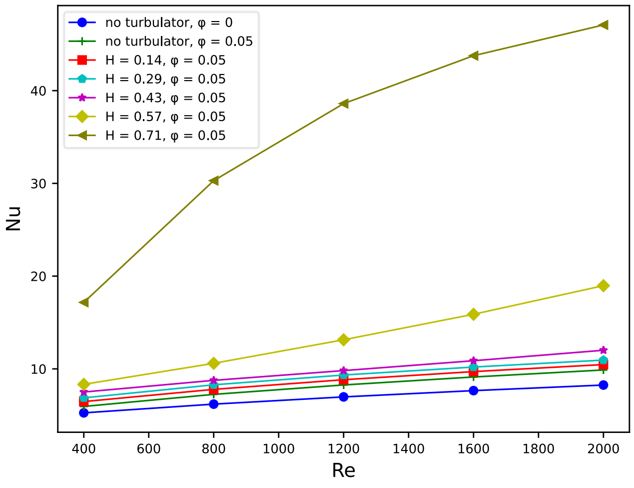

Figure 5.26: The average Nusselt number and heat transfer coefficient of inner tube against Reynolds numbers for different H, SiO_2 nanofluid φ=0.05, S=5.71, and W=0.29.

Figure 5.27 the inner tube's pressure drop and friction factor are depicted against Reynolds numbers for different ratios of the height of the trapezoidal rib to the radius of the inner tube (H) in the presence of SiO_2 nanofluid. The graph clearly illustrates that both the pressure drop and friction factor increase as the value of H increases. This is attributed to the greater obstruction in the flow resulting from the increased rib height. Notably, the impact of this increase is significant for H=0.71, where the flow experiences maximum obstruction.

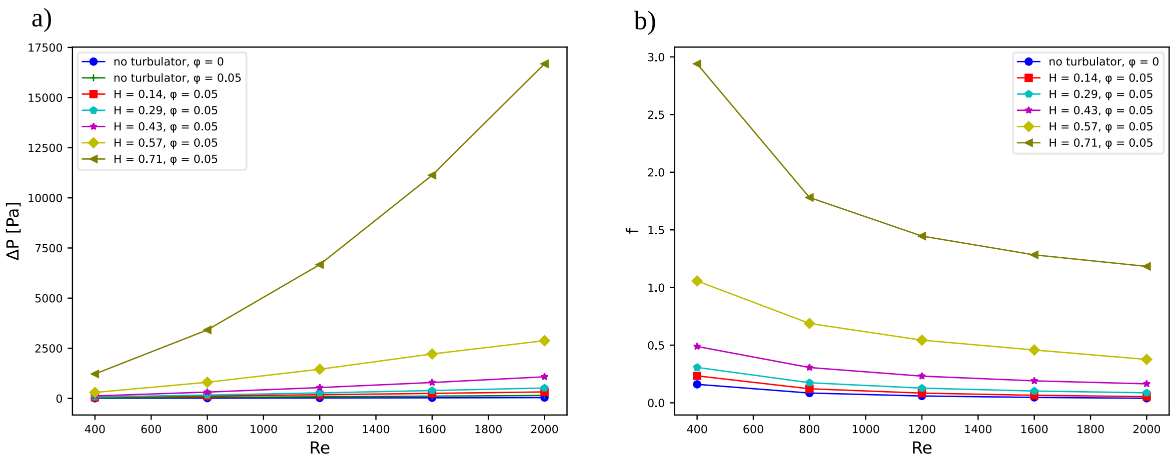

Figure 5.27: a) pressure drop and b) friction factor of inner tube against Reynolds numbers for different H, SiO_2 nanofluid φ=0.05, S=5.71, and W=0.29.

Figure 5.28 presents color plots that visually represent the a) normalized temperature and b) normalized velocity magnitude at various heights of trapezoidal ribs using a SiO_2 nanofluid with φ = 0.05. The findings indicate that when the height of the ribs is increased, the temperature distribution within the flow becomes more uniform. This uniformity is attributed to enhanced mixing and the development of secondary flow patterns caused by the presence of taller obstacles in the flow path. As a result of these effects, the thermal boundary layer is disrupted after passing each rib, reducing its thickness [26]. This reduction contributes to an improved heat transfer rate within the system. However, as the height of the ribs increases, the velocity magnitude reveals the formation of vortices and a corresponding decrease in flow velocity. This phenomenon results in an increase in pressure drop across the system.

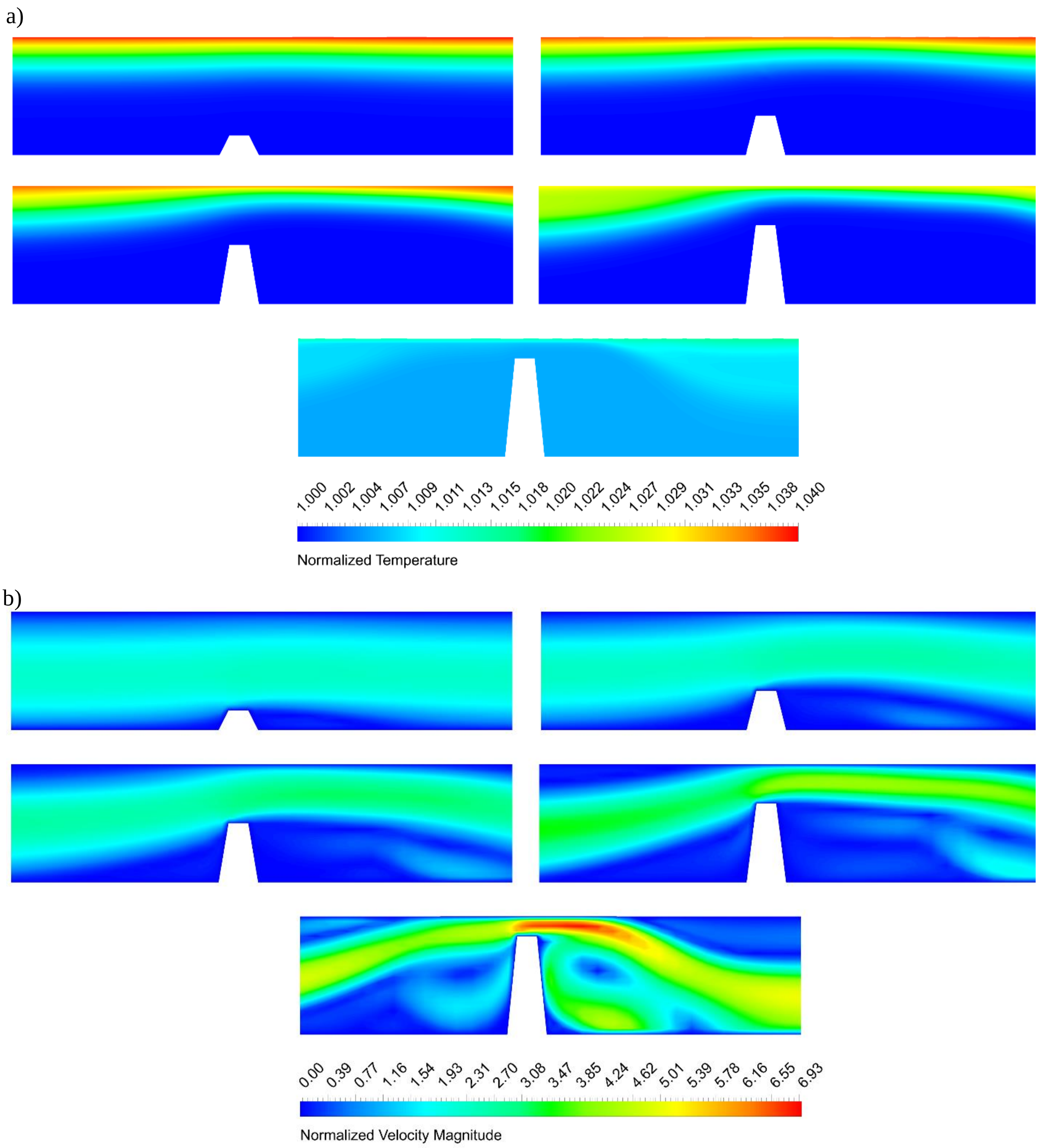

Figure 5.28: Colour plots of a) normalized temperature and b) normalized velocity magnitude for different height, utilising SiO_2 nanofluid at Re=1200, φ=0.05, S=5.71, and W=0.29.

5.4.3 Effect of different distances between the ribs

Figure 5.29 and Figure 5.30 present the inner tube's average Nusselt number, pressure drop, and friction factor against Reynolds numbers. These figures illustrate the impact of rectangular ribs and varying ratios of the distances between the ribs to the inner tube radius (S) when Al_2O_3 nanofluid is used. The findings indicate a significant improvement in the average Nusselt number, pressure drop, and friction factor when a turbulator is utilised, compared to where no turbulator is employed or when nanofluid is used alone. When the distances between ribs exceed a value of S=5.71, there is only a minor influence on the average Nusselt number, pressure drop, and friction factor. However, as the distances between the ribs decrease, the number of ribs increases, leading to interactions between the flow and the rib obstacles at closer distances. Consequently, this generates enhanced secondary flow and increased mixing within the fluid stream. Furthermore, it can be deduced that the parameter S exerts a greater effect on the heat transfer and fluid flow characteristics than the parameter W. However, its effect is less significant than parameter H.

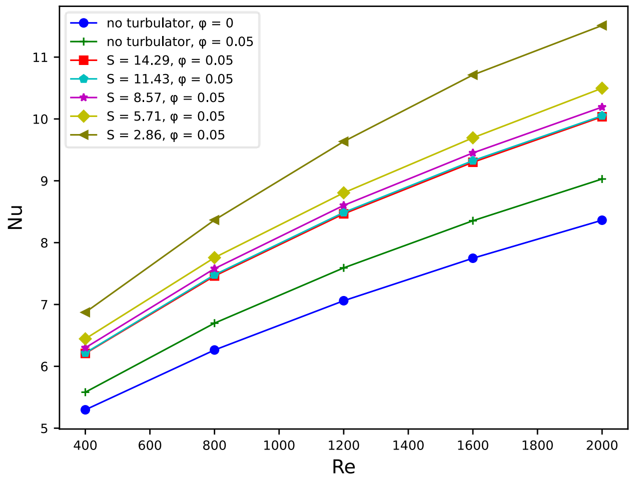

Figure 5.29: The average Nusselt number of inner tube against Reynolds numbers for different S, Al_2O_3 nanofluid φ=0.05, W=0.29, and H=0.29.

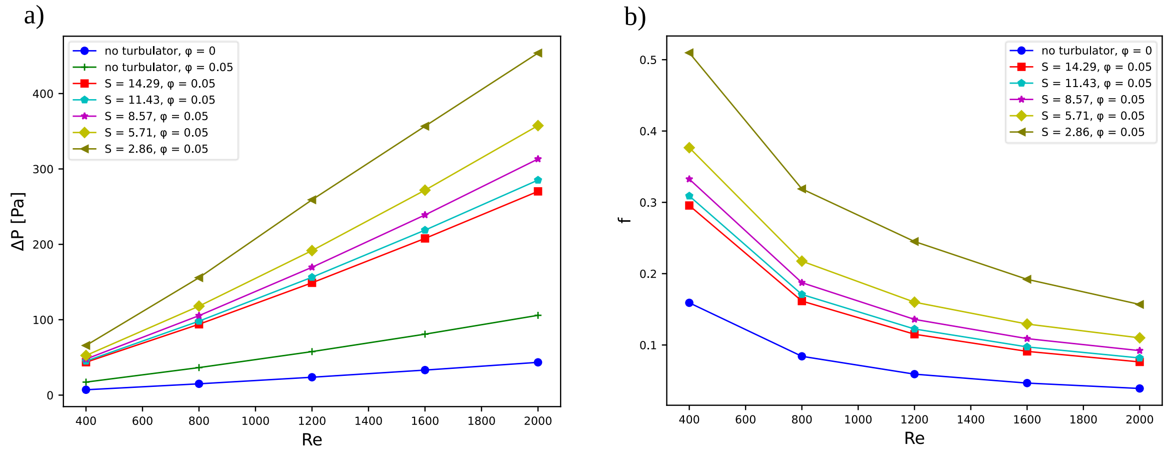

Figure 5.30: a) pressure drop and b) friction factor of inner tube against Reynolds numbers for different S, Al_2O_3 nanofluid φ=0.05, W=0.29, and H=0.29.

5.4.4 Effect of different width of the ribs

Figure 5.31 and Figure 5.32 represent the average Nusselt number, pressure drop, and friction factor of the inner tube against Reynolds numbers for different ratios of the rectangular rib width to the inner tube radius (W) in the presence of SiO_2 nanofluid. The findings reveal a substantial enhancement in the average Nusselt number, pressure drop, and friction factor when employing a turbulator and nanofluid compared to cases with no turbulator and nanofluid alone. These figures demonstrate that changes in the parameter W have a limited impact on the average Nusselt number, pressure drop, and friction factor. For example, the change in the average Nusselt number for Re=1200 between values of W=0.43 and 0.57 is 0.26%. However, the corresponding percentage changes for Re=1200 for S=8.57 and 5.71 and H=0.43 and 0.57 are observed to be 2.36% and 33.85%, respectively. So, variations in W exhibit a minimal influence on generating secondary flow and mixing within the fluid stream. For all cases, it is observed that the average Nusselt number and pressure drop increased with an increase in Reynolds number, while the friction factor decreases with increasing Reynolds number.

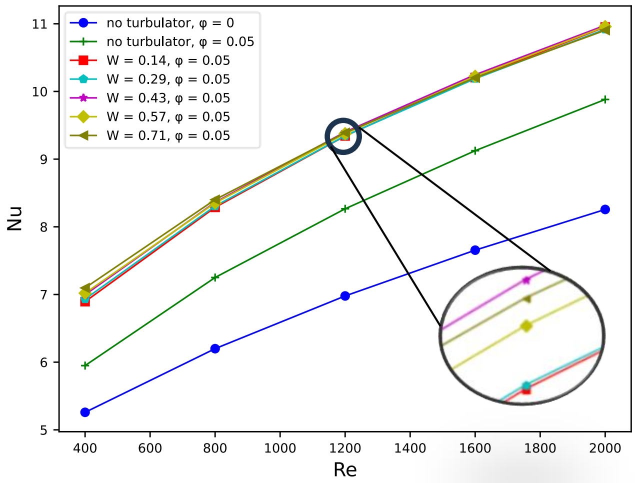

Figure 5.31: The average Nusselt number of inner tubes against Reynolds numbers for different W, SiO_2 nanofluid φ=0.05, S=5.71, and H=0.29.

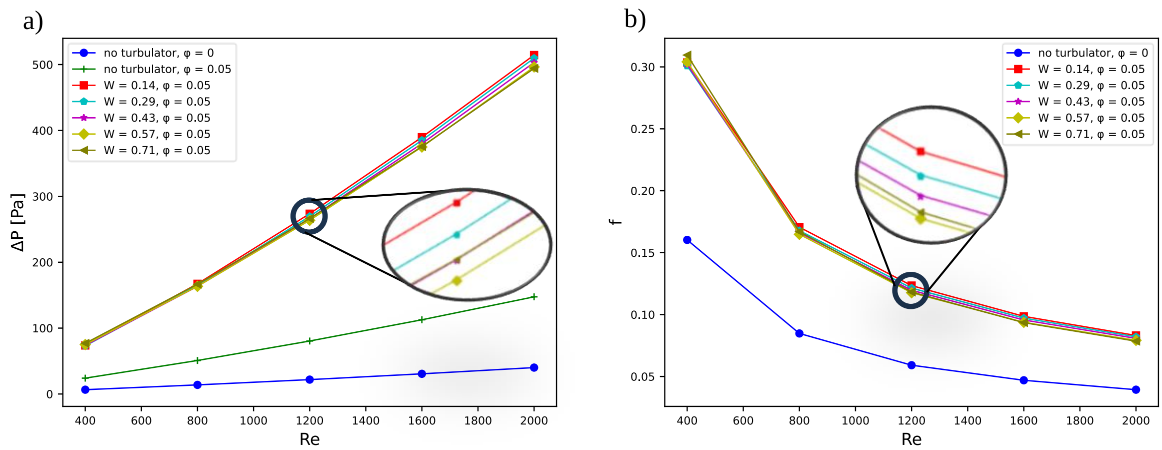

Figure 5.32: a) pressure drop and b) friction factor of inner tube against Reynolds numbers for different W, SiO_2 nanofluid φ=0.05, S=5.71, and H=0.29.

Figure 5.33 illustrates the ratio of the average Nusselt number and friction factor for SiO_2 and various dimensionless parameters, W, S, and H, to the average Nusselt number and friction factor of water without turbulator insertion. This figure indicates that the height of the ribs exerts the most significant influence on enhancing the heat transfer rate while also resulting in the highest friction factor. Conversely, the width of the ribs has the least impact on both heat transfer rate and friction factor. This occurs because taller ribs induce more mixing and secondary flow, which reduces the thermal boundary layer [26]. The spacing between the ribs ranks as the second most influential parameter. Decreasing the distance between the ribs increases the number of ribs, leading to higher heat transfer rates and friction factors. The comparative analysis of the results, emphasizing the increased heat transfer, alongside the statistical investigation by Tavousi, et al. [3] regarding enhanced heat transfer through the combination turbulator insertion and nanofluid techniques, indicates that the improvement in heat transfer rate observed in the current study exceeds the average outcomes previously reported. In their study, the average heat transfer rate enhancement was approximately 131%, while the maximum enhancement of the average Nusselt number was approximately 470%. For comparison, the results by Dhumal and Havaldar [283], who employed twisted and helical tapes, reported a maximum heat transfer enhancement of 315%.

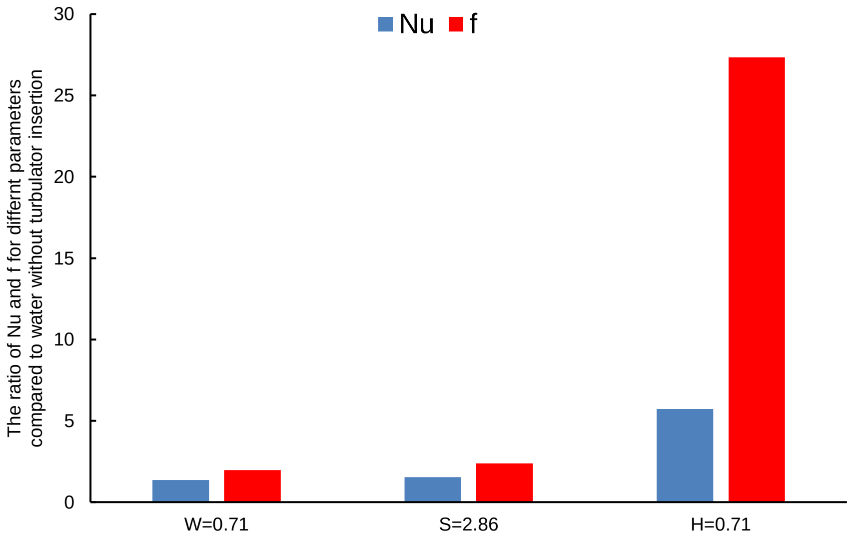

Figure 5.33: The ratio of average Nusselt number and friction factor for SiO_2 and various dimensionless parameters, W, S, and H, to the average Nusselt number and friction factor of water without turbulator insertion.

Figure 5.34 shows the PEC for different shapes of ribs and Figure 5.35 shows the maximum PEC for all cases studied including using nanofluid alone with no turbulator and using turbulator insertion and SiO_2 nanofluid. PEC is a significant parameter that relates the useful criteria (Nusselt number) to the penalty criteria (friction factor) and provides valuable insights into the performance of heat exchangers. It can be observed that the trapezoidal turbulator exhibits the highest Nusselt number and heat transfer coefficient. However, the oval turbulator shows the highest PEC due to its lower friction factor when compared to the other turbulator shapes. The rectangular turbulator had the worst PEC, as it exhibited the lowest improvement in Nusselt number and heat transfer coefficient while having a high friction factor. The triangular ribs had the highest friction factor among the four turbulators, resulting in a low PEC. It was concluded that all the turbulators, the PEC was more than 1. The highest PEC was 1.91 for H=0.71, and the lowest PEC was 1.08 for W=0.71, as shown in Figure 5.35. The results demonstrated that the change in the width of the ribs produced the lowest PEC. The change in rib width decreased the PEC of DTHE compared to using nanofluids without turbulator insertion. This decrease is attributed to the increase in the friction factor, which outweighs the increase in the Nusselt number. For comparison, the results by Dhumal and Havaldar [283], who employed twisted and helical tapes, reported a maximum PEC of 3.06.

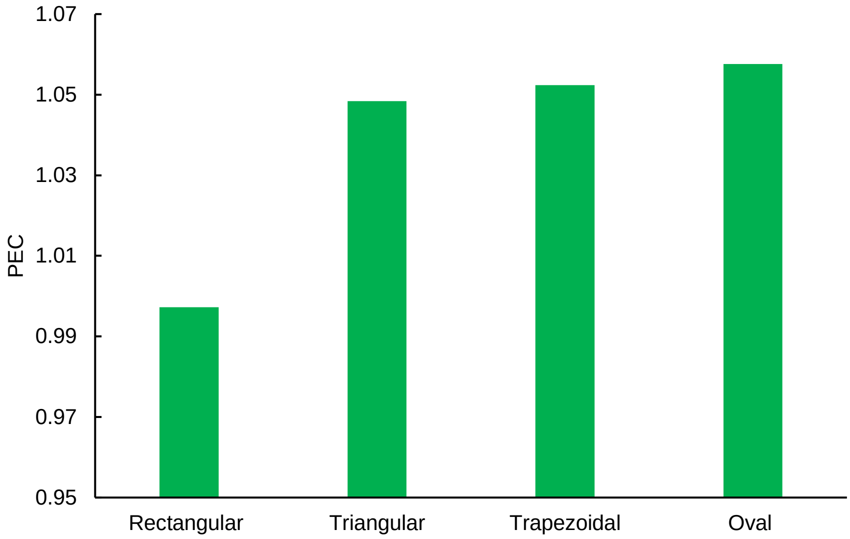

Figure 5.34: PEC for the different shapes of ribs.

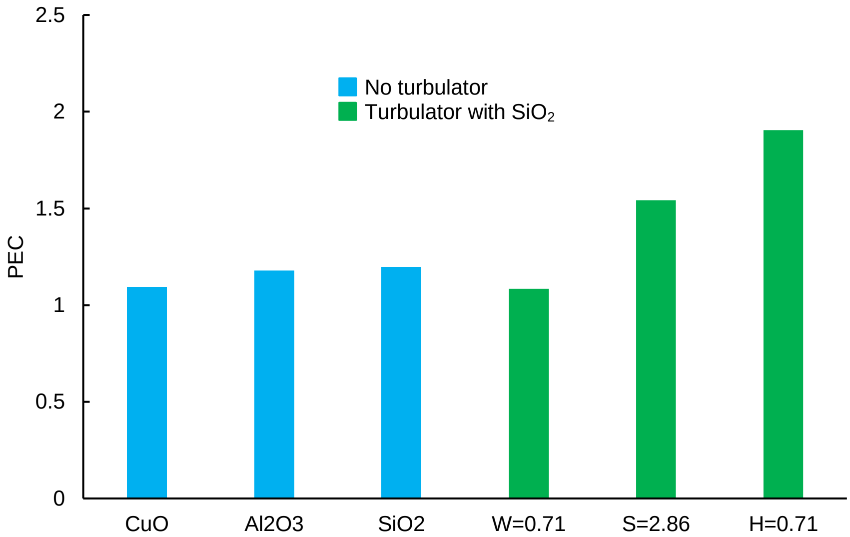

Figure 5.35: Maximum PEC achieved for all cases.

5.5 Performance of DTHE with helical turbulator insertion

5.5.1 Effect of different shape of helical turbulator

Figure 5.36 illustrates the average Nusselt number of the inner tube against Reynolds numbers for various helical turbulator shapes with SiO_2 nanofluid and a volume fraction 0.05 as the working fluid. In all cases, the twist ratio, height, and width of the turbulators were 1 to 0.04 m, and 0.002 m, and 0.001 m, respectively. The results indicate that the use of nanofluids significantly increases the Nusselt number compared to pure water. This increase is further enhanced by the insertion of turbulators. Specifically, the helical triangular turbulator shows considerably higher Nusselt numbers than other shapes. Conversely, the oval, rectangular, and trapezoidal helical turbulators exhibit similar average Nusselt numbers, with the trapezoidal shape demonstrating the lowest value.

The rise in the Nusselt number can be attributed to two primary factors. First, the nanoparticles enhance the thermal properties of the fluid. Second, the turbulators induce additional mixing and secondary flows, reducing the thermal boundary layer near the wall. The distinct geometry of helical triangular turbulators generates more intense secondary flows and turbulence within the fluid [55]. This effect arises because the sharp angles of the triangular turbulators disrupt the flow more effectively than smoother shapes, such as ovals, rectangles, or trapezoids. This disruption diminishes the thickness of the thermal boundary layer, thereby enhancing the rate of heat transfer. Also, the Nusselt number increases with the increase of the Reynolds number due to an increase in momentum and mixing flow. These combined effects of nanoparticles and turbulator insertion led to improved heat transfer performance of the DTHE.

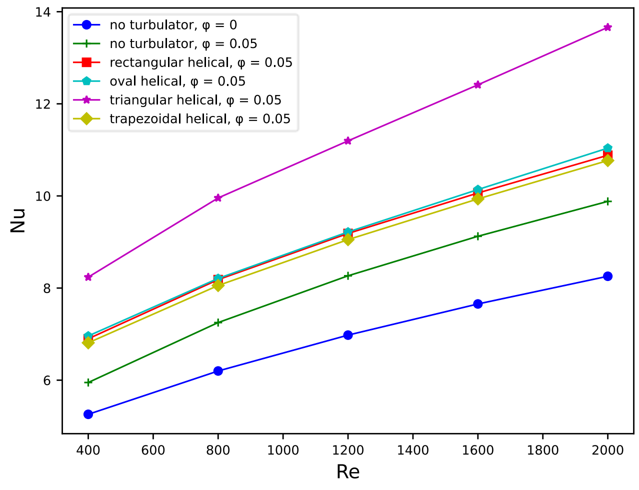

Figure 5.36: The average Nusselt number against Reynolds numbers for various helical turbulators, SiO_2 nanofluid φ=0.05, twisted ratio 1 to 0.04 m, w=0.001 m, and H=0.29.

Figure 5.37 depicts the pressure drop across the inner tube against Reynolds numbers for various helical turbulator shapes using SiO_2 nanofluid with a volume fraction of 0.05 as the working fluid. For all cases, the twist ratio, height, and width of the turbulators were 1, 0.04 m, 0.002 m, and 0.001 m, respectively. As it can be seen, the addition of nanoparticles to the working fluid results in an increased pressure drop compared to pure water, an effect that is accentuated by the insertion of a helical turbulator into the DTHE. The figure reveals that the pressure drops for all helical turbulator shapes are approximately same; however, the helical triangular and rectangular turbulators exhibit the highest pressure drop, while the helical oval and trapezoidal turbulators demonstrate the lowest values. This discrepancy can be attributed to the varying surface areas of each turbulator shape, indicating that the oval and trapezoidal turbulators create less friction compared to the rectangular and triangular turbulators.

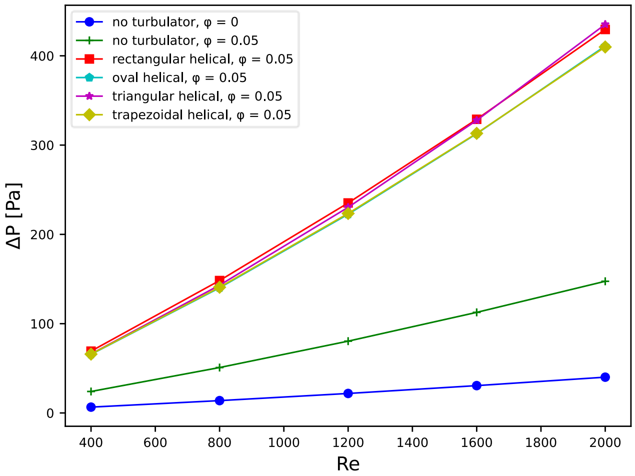

Figure 5.37: The pressure drop against Reynolds numbers for various shapes of helical turbulators, SiO_2 nanofluid φ=0.05, twisted ratio 1 to 0.04 m, w=0.001 m, and H=0.29.

Figure 5.38 displays color plots that show the velocity magnitude and temperature contour for various helical shapes, triangular, trapezoidal, rectangular, and oval, utilising SiO_2 nanofluid at a Reynolds number of 1200 and a volume fraction φ=0.05. The results indicate that changes in velocity magnitude are more significant in the triangular and oval helical shapes compared to the rectangular and trapezoidal shapes. Furthermore, the rectangular and trapezoidal shapes maintain a more uniform temperature distribution than the triangular and oval shapes. This discrepancy can be attributed to the more intense secondary and swirl flows observed in the triangular and oval shapes, which disrupt the thermal boundary layer after passing the helical ribs [26], leading to sharper temperature gradients, especially noted in the triangular configurations.

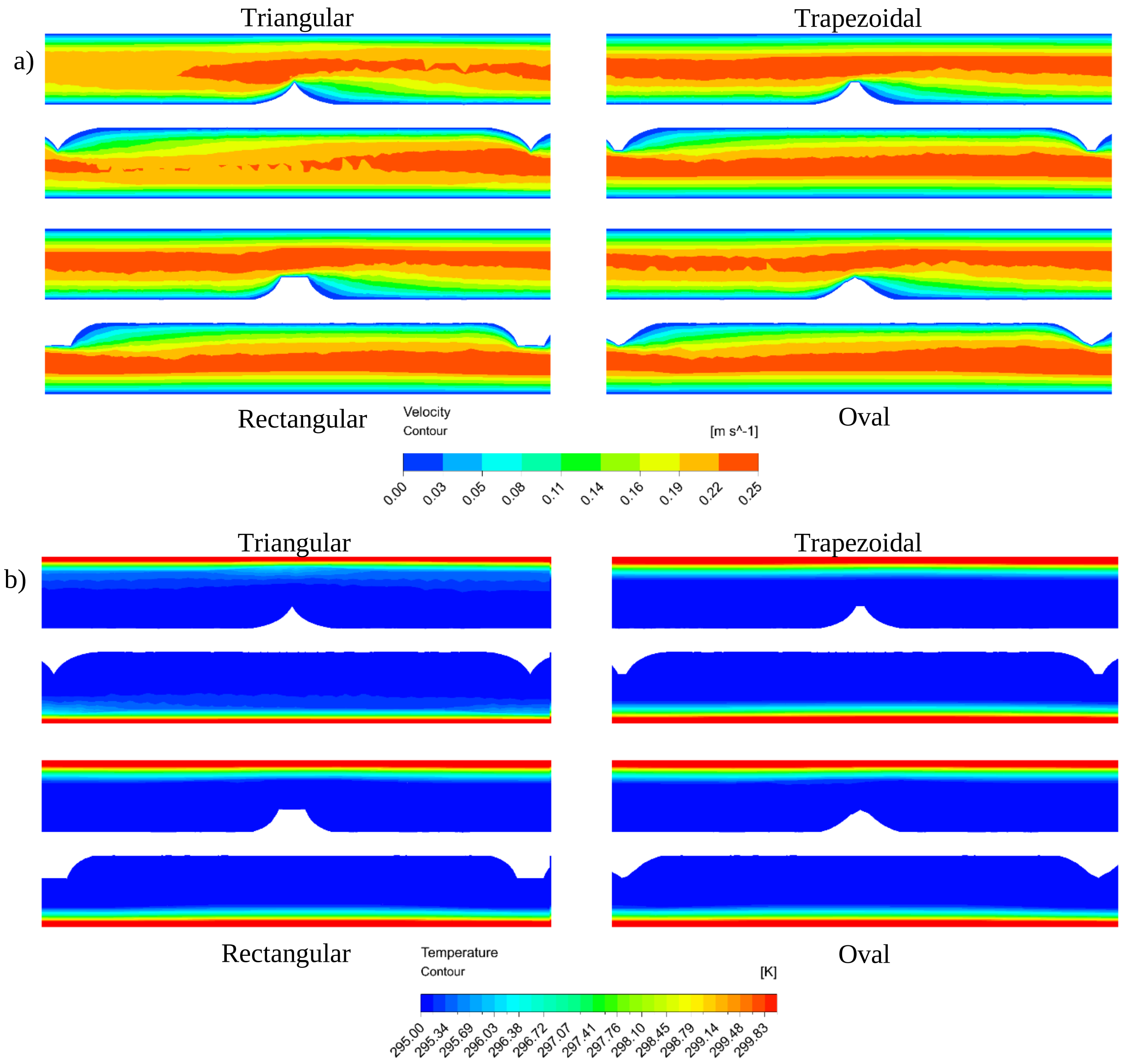

Figure 5.38: Colour plots of a) velocity magnitude and b) static temperature for different shapes of helical turbulators , utilising SiO_2 nanofluid at Re=1200, φ=0.05, twisted ratio 1 to 0.04 m, w=0.001 m, and H=0.29.

Figure 5.39 depicts the PEC of DTHE for various helical shapes, triangular, trapezoidal, rectangular, and oval, using SiO_2 nanofluid at a Reynolds number of 1200 and a volume fraction φ=0.05. The results indicate that the triangular helical shapes exhibit the highest PEC, reaching up to 1.2, surpassing the other helical shapes. All other configurations, including oval, trapezoidal, and rectangular shapes, show a PEC of less than 1, which is also lower than the DTHE without turbulator insertion, only utilising nanofluid. This suggests that under these conditions, the helical shapes are not optimized for design, making them ineffective. This ineffectiveness is primarily due to the increased friction factor outweighing the enhanced heat transfer.

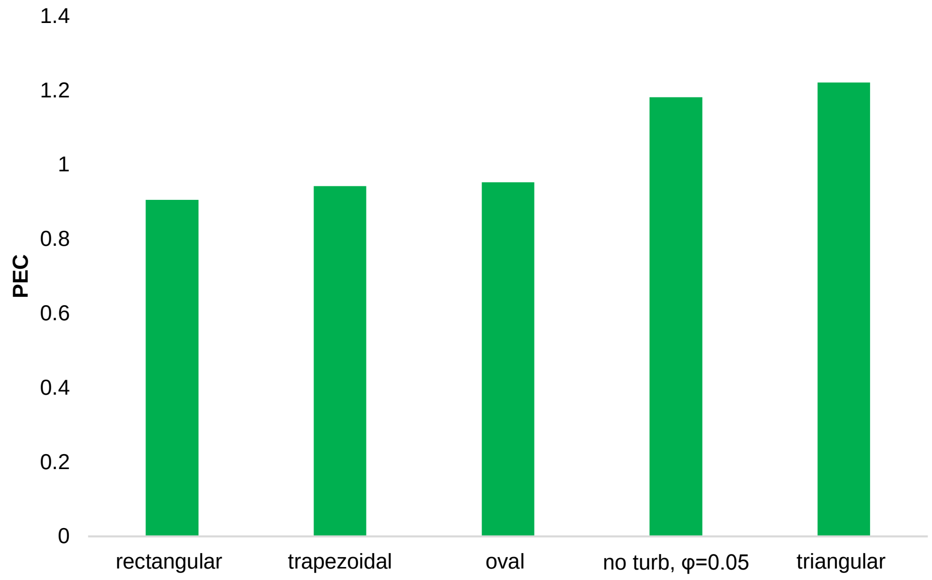

Figure 5.39: PEC of different shapes of helical turbulators utilising SiO2 nanofluid at Re=1200, φ=0.05, twisted ratio 1 to 0.04 m, w=0.001 m, and H=0.29.

5.5.2 Effect of different height of helical turbulator

Figure 5.40 illustrates the variation in the average Nusselt number within the inner tube for different ratios of the height of the triangular helical turbulator to the radius of the inner tube (H), using SiO_2 nanofluid at a Reynolds number of 1200 and a volume fraction φ=0.05. It is observed that the Nusselt number increases with H. This increase can be attributed to enhanced secondary and swirl flows due to greater flow obstruction from the triangular helical shape, which reduces the thermal boundary layer thickness and enhances heat transfer [26]. A notable increase is observed at H=0.71, where the average Nusselt number exceeds 44, indicating a substantial improvement at this specific H value compared to others. For comparison with recent literature, Maleki, et al. [284]'s study, which employed a combination of passive and active methods, reported a heat transfer enhancement of up to 277.5%. However, in the present study, the maximum enhancement achieved through the combination of helical turbulators and SiO_2 nanofluid reached 567.38%.

Figure 5.41 presents the pressure drop in the inner tube for different ratios of the height of the triangular helical turbulator to the radius of the inner tube (H), using SiO_2 nanofluid at a Reynolds number of 1200 and a volume fraction φ=0.05. The pressure drop escalates with increasing H, correlating with the increased obstruction caused by the taller helical turbulators. The most significant impact is noted at H=0.71, where the flow encounters maximum obstruction, leading to the highest pressure drop up 648 Pa.

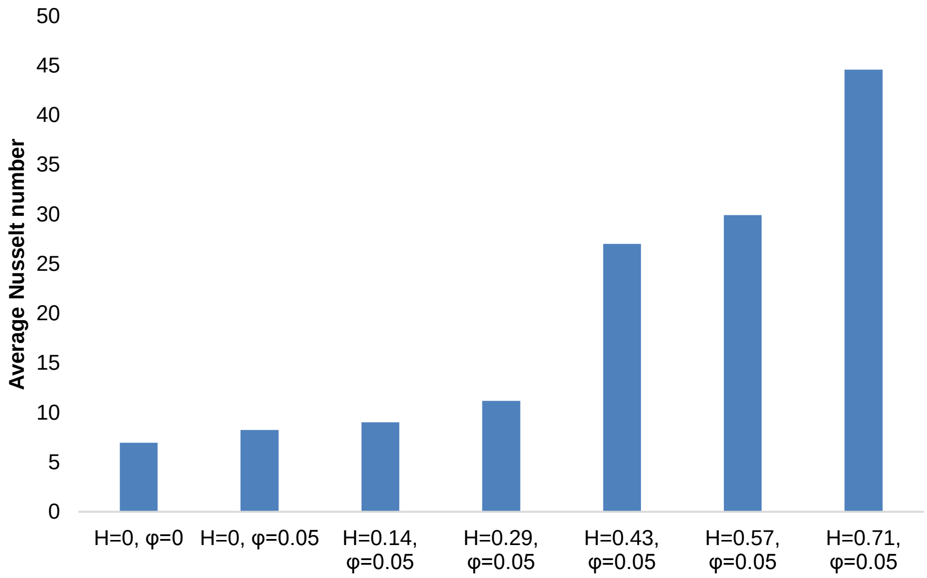

Figure 5.40: Average Nusselt number of the inner tube for different ratios of the height of the triangular helical turbulator to the radius of the inner tube (H), using SiO_2 nanofluid at a Reynolds number of 1200 and a volume fraction φ=0.05.

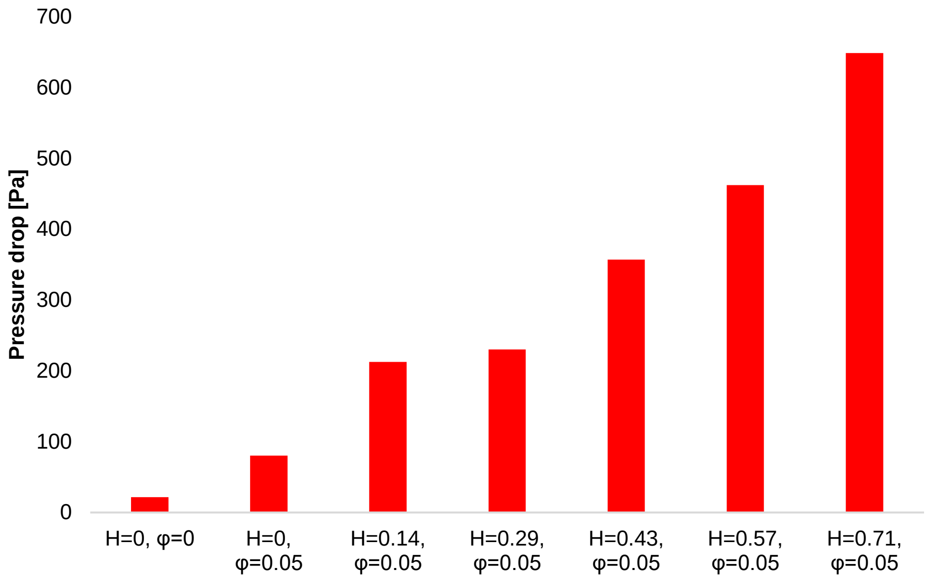

Figure 5.41: Pressure drop of the inner tube for different ratios of the height of the triangular helical turbulator to the radius of the inner tube (H), using SiO_2 nanofluid at a Reynolds number of 1200 and a volume fraction φ=0.05.

Figure 5.42 shows the maximum PEC for different ratios of the height of the triangular helical turbulator to the radius of the inner tube (H), using SiO_2 nanofluid at a Reynolds number of 1200 and a volume fraction φ=0.05. It is evident that the PEC values exceed 1 in all scenarios, indicating that enhancement in heat transfer predominates over the increase in friction factor. Furthermore, an increase in the height of the helical turbulator results in higher PEC values, reaching up to 3.17 when H=0.71. This suggests that the swirl flow significantly boosts the heat transfer rate with only a minimal rise in friction factor, thus optimizing the performance of the DTHE. For comparison with recent literature, Maleki, et al. [284]'s study, reported a PEC enhancement of 3.92 using a combination of passive and active methods, including the application of an external magnetic field.

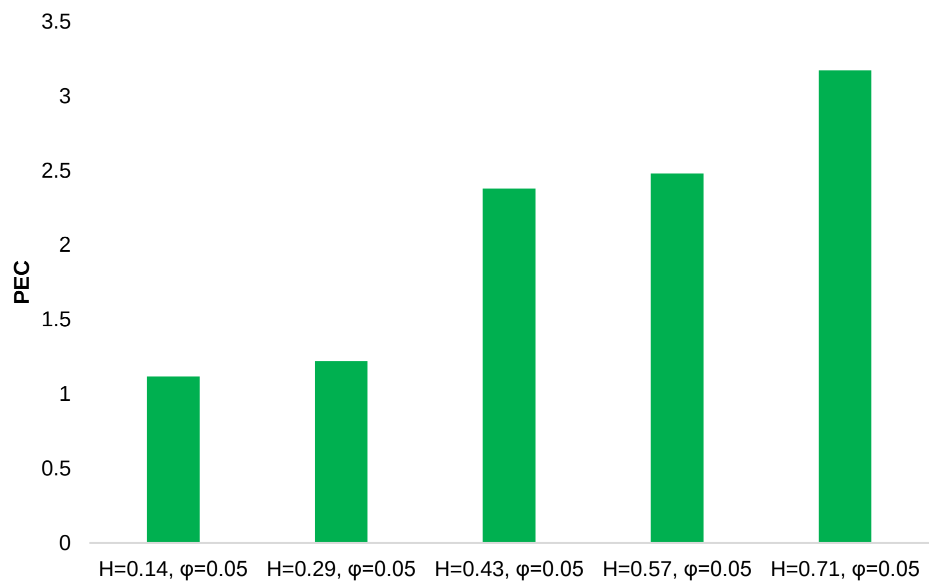

Figure 5.42: Maximum PEC for different ratios of the height of the triangular helical turbulator to the radius of the inner tube (H), using SiO_2 nanofluid at a Reynolds number of 1200 and a volume fraction φ=0.05.

Figure 5.43 illustrates the bulk temperature within the inner tube for different ratios of the height of the triangular helical turbulator to the radius of the inner tube (H), using SiO_2 nanofluid at a Reynolds number of 1200 and a volume fraction φ=0.05. The graph shows that as the height of the helical turbulators increases, the bulk temperature of the inner tube also increases. This is because higher helical turbulators enhance secondary and swirl flows within the inner fluid. These flows improve the distribution of heat transferred from the outer tube to the inner fluid. Consequently, the bulk temperature for H=0.71 is closer to the temperature of the outer fluid, while for H=0.14, there is a maximum difference between the outer fluid temperature and the inner fluid bulk temperature.

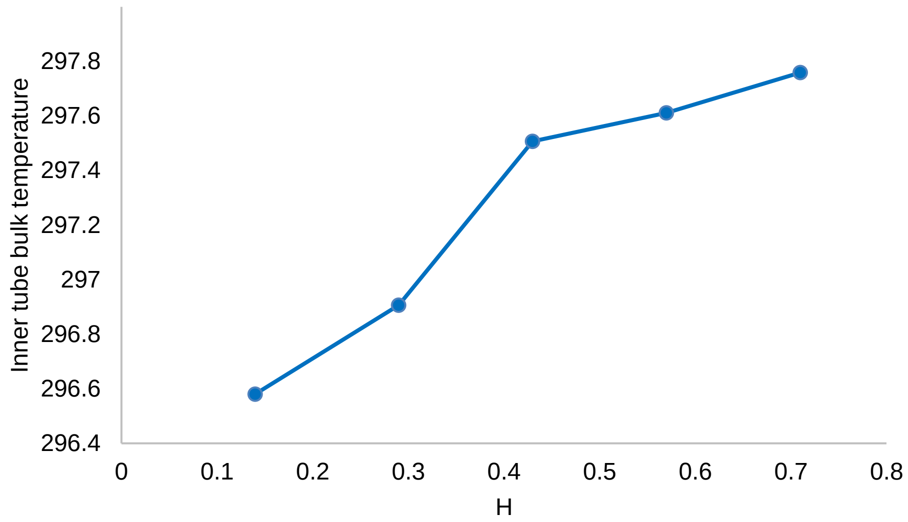

Figure 5.43: Bulk temperature within the inner tube for different H, using SiO_2 nanofluid at a Reynolds number of 1200 and a volume fraction φ=0.05.

Figure 5.44 displays color plots representing a) the velocity in the x-direction, b) the velocity in the z-direction, and c) the static temperature at different heights of a triangular helical turbulator using a SiO_2 nanofluid with a volume fraction φ=0.05. The data suggest that increasing the height of the helical turbulator leads to a more uniform temperature distribution across the flow. This uniformity is primarily due to enhanced secondary and swirling flow patterns, which are promoted by taller obstacles in the flow path. These obstacles disrupt the thermal boundary layer at each pitch [26], thinning it and thereby enhancing heat transfer rates within the system. However, increasing the height of the helical turbulator also intensifies the velocity in the z-direction, induces vortices, and slows the flow velocity, which results in a higher pressure drop across the system.

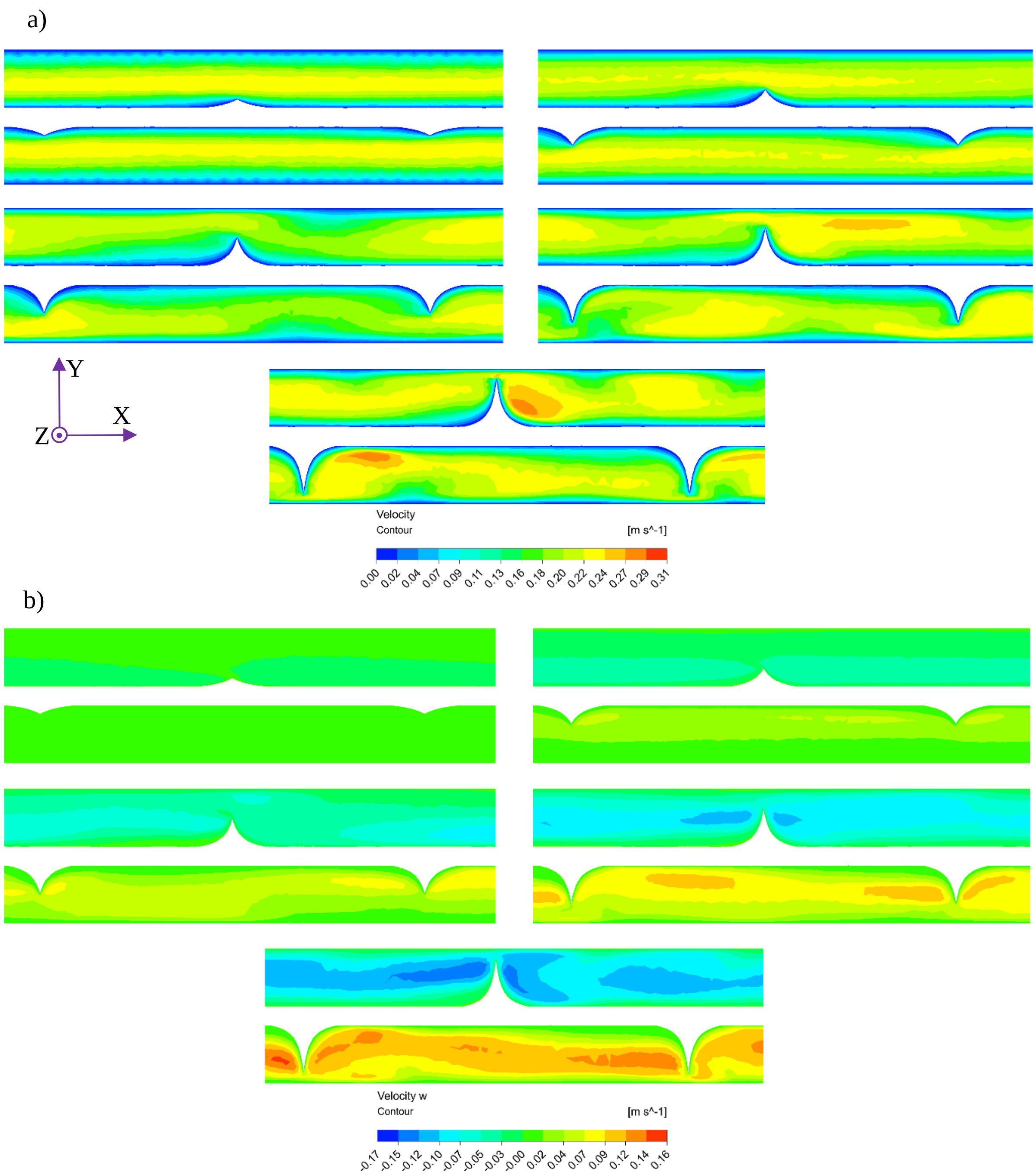
a)
Y
X
Z
Velocity
Contour
[m s^-1]
0.00 0.02 0.04 0.07 0.09 0.11 0.13 0.16 0.18 0.20 0.22 0.24 0.27 0.29 0.31
b)
Velocity w
Contour
[m s^-1]
-0.17 -0.15 -0.12 -0.10 -0.07 -0.05 -0.03 -0.00 0.02 0.04 0.07 0.09 0.12 0.14 0.16

c)

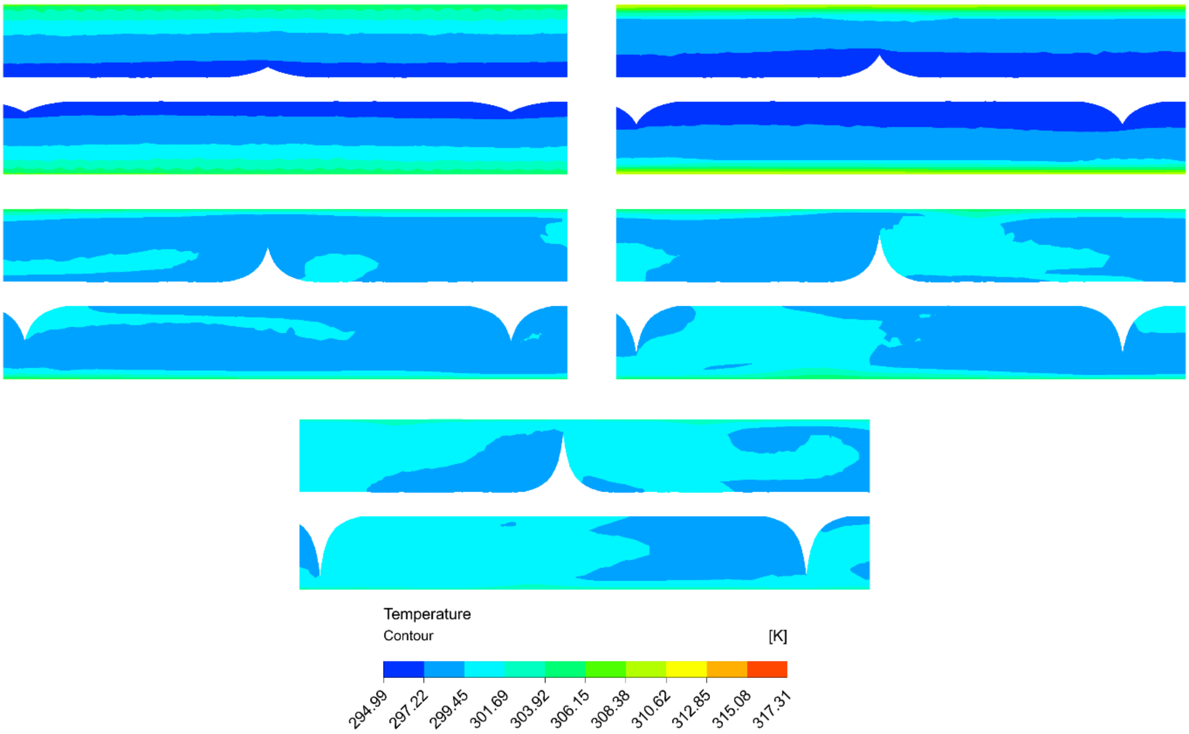

Figure 5.44: Colour plots of a) the velocity in the x-direction, b) the velocity in the z-direction, and c) the static temperature at different heights of a triangular helical turbulator using a SiO_2 nanofluid at a Reynolds number of 1200 with a volume fraction φ=0.05.

5.6 Comparison between transverse and helical turbulator

This section compares the effects of two types of turbulators, transverse and helical, on the performance of the DTHE. Figure 5.45 illustrates the enhancement in the average Nusselt number when a combination of SiO_2 nanofluid (φ=0.05) and both types of turbulators (in triangular shapes) is used, relative to pure water and the same nanofluid without any turbulators. The results show that the helical turbulator offers a greater enhancement in the Nusselt number than the transverse turbulator, both against pure water and the nanofluid without turbulator insertion. This enhancement is attributed to the helical turbulators not only disrupting the flow direction along the tube but also inducing a swirling motion. This swirling motion increases mixing and secondary flow and extends the contact time between the fluid and the tube's inner wall, compared to the transverse turbulator. Thus, helical turbulators demonstrate a more effective heat transfer rate than transverse turbulators.

Furthermore, Figure 5.46 presents the pressure drop ratios for the DTHE employing both turbulator types, compared to configurations using only pure water and the nanofluid without turbulators. The findings indicate that the helical turbulator results in a smaller increase in pressure drop than the transverse turbulator. This difference is likely due to the helical design creating fewer flow obstructions and the swirling motion reducing pressure drops, unlike the direct flow disruption caused by the transverse turbulator. Consequently, it is concluded that helical turbulators enhance the heat transfer rate more effectively by producing a lower pressure drop compared to transverse turbulators.

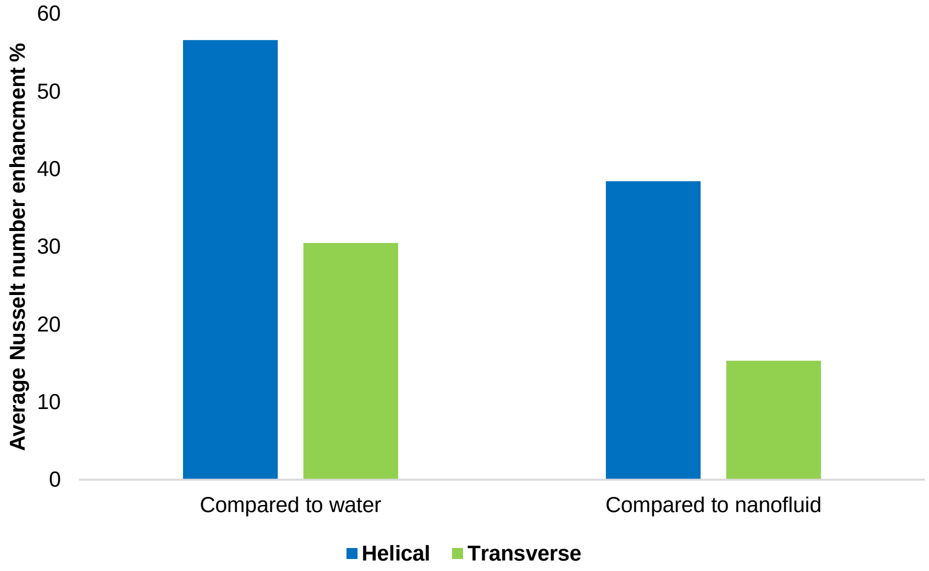

Figure 5.45: Enhancement in the average Nusselt number when a combination of SiO_2 nanofluid ($\varphi=0.05$) and both types of turbulators (in triangular shape) is used, relative to pure water and the same nanofluid without any turbulators at a Reynolds number of 400.

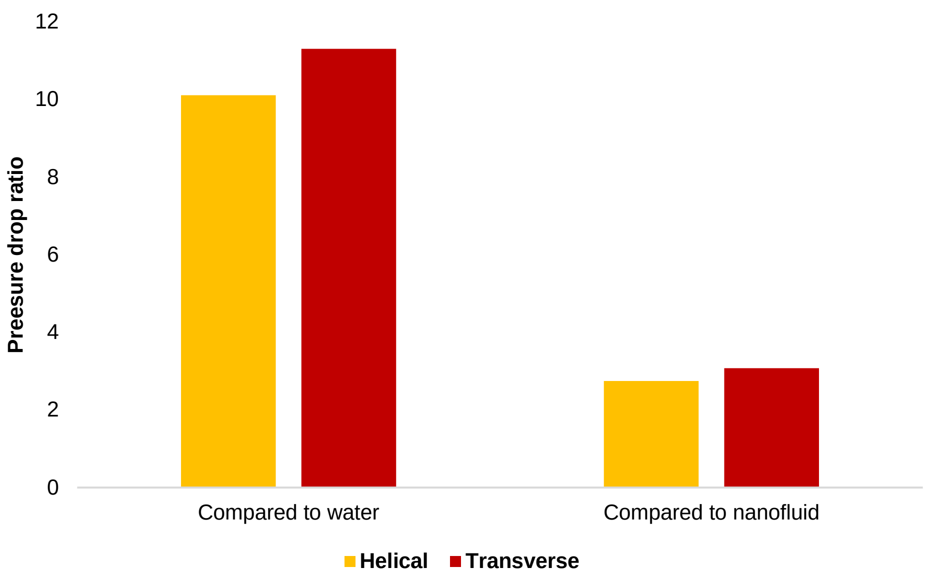

Figure 5.46: Increase in the pressure drop when a combination of SiO_2 nanofluid (φ=0.05) and both types of turbulators (in triangular shapes) is used, relative to pure water and the same nanofluid without any turbulators at a Reynolds number of 400.

Figure 5.47 illustrates the maximum PEC achieved with both transverse and helical turbulators. As previously mentioned, the Nusselt number enhancement is greater for the helical turbulator, while the increase in pressure drop is more significant for the transverse turbulator. Thus, it can be inferred that the helical turbulator provides a better PEC. Specifically, the highest PEC value for the helical turbulator, at 3.17, is observed with a triangular shape using SiO_2 nanofluid and an H value of 0.71. Conversely, the maximum PEC of 1.9 for the transverse turbulator is achieved with a trapezoidal shape using the same height and nanofluid.

Figure 5.48 presents the streamlines in both transverse and helical turbulators for a rectangular shape case. It is apparent that the streamlines in the helical turbulator navigate around the turbulators more smoothly compared to the direct disruption caused by the transverse turbulators, which results in vortices forming behind the ribs. Additionally, it demonstrates that the flow path line in the helical turbulator is longer over the same distance compared to the transverse turbulator. This results in the fluid being in contact with the inner tube wall for a longer period, thereby enhancing heat exchange with the hot fluid in the outer tube.

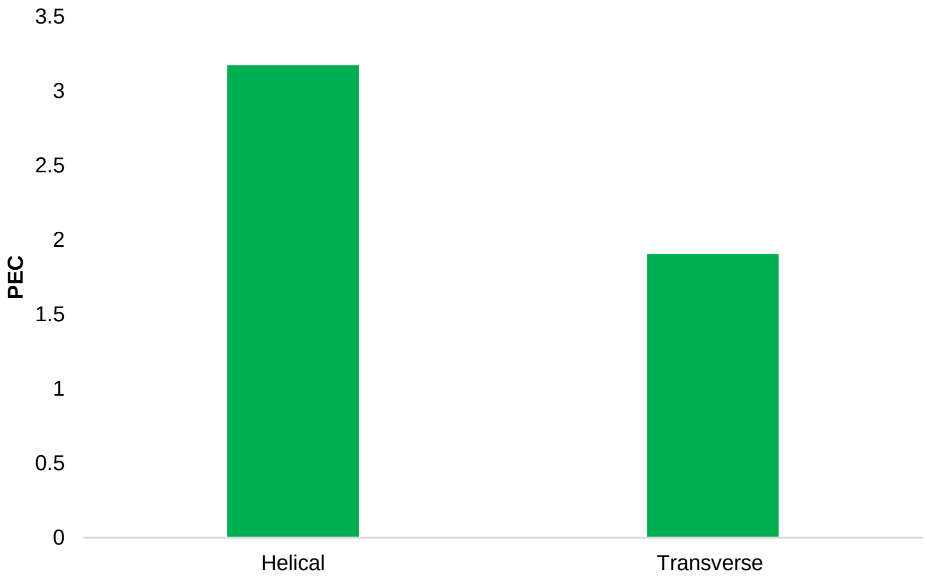

Figure 5.47: Maximum PEC achieved with both transverse and helical turbulators.

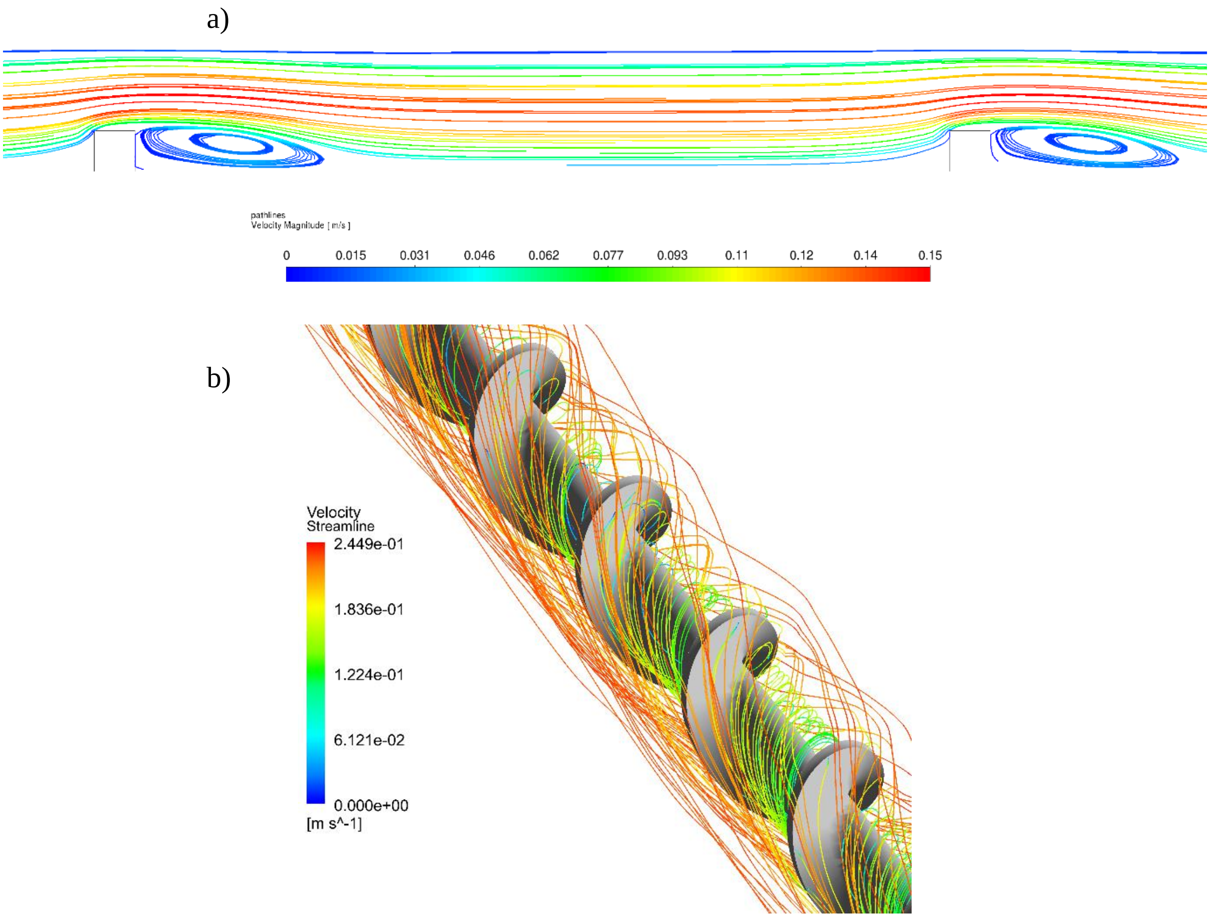

Figure 5.48: Streamlines in both a) transverse and b) helical turbulators for a rectangular shape case.

5.7 Comparative analysis of results

In this section, the results and outcomes of the current research are compared with other published works, focusing on the most recent studies. As previously discussed, enhancing heat transfer in heat exchangers can be categorized into three main methods: passive, active, and combined. Generally, active methods yield a greater increase in heat transfer compared to passive methods due to the utilising of external forces and power. Conversely, passive methods, which do not rely on external forces, offer advantages such as lower costs and easier maintenance.

This section aims to quantify the increment in heat transfer for passive, active, and combined methods and compare these increments with the results obtained in this study. This comparative analysis provides a clearer understanding of how the findings of this research align with real-world applications and the extent to which they are practical and effective. By systematically comparing the heat transfer enhancement achieved through different methods, this analysis underscores the practical relevance and applicability of the study's results. The findings from this research are evaluated against the backdrop of existing literature to highlight their significance and potential impact on the field of heat transfer enhancement in heat exchangers. This approach ensures a comprehensive assessment of the study's contributions and situates its results within the broader context of ongoing research and technological advancements.

- **Passive method**

The passive method of enhancing heat transfer can be categorized into four main techniques: using nanofluids, turbulator insertion, geometry modifications, and extended surface areas (fins). In this study, we employed turbulator insertion and nanofluids to investigate the enhancement of the heat transfer rate in a DTHE. Recent studies from each technique were reviewed to compare the percentage increase in heat transfer with the enhancements observed in this study.

Yogaraj, et al. [281] used zinc oxide and titanium oxide nanofluids with ethylene glycol as the base fluid in a counterflow DTHE, achieving a maximum heat transfer enhancement of 18.5% for zinc oxide. Marzouk, et al. [285] designed a turbulator using a one-meter steel nail rod in a DTHE, focusing on the pitch length of the nail rods, and achieved a maximum heat transfer enhancement of 90%. Chaurasiya, et al. [286] used corrugated tubes for the inner and outer tubes of a DTHE, implementing different helix angles, and achieved a maximum PEC of

1.17 and a 33% improvement in the Nusselt number. Firoozeh, et al. [287] employed the geometry change technique on the inner tube of a DTHE by varying the groove angles to improve the heat transfer rate. This investigation explored different groove angles and achieved a maximum enhancement of 32% in the heat transfer rate. Ashraf, et al. [288] utilised the extended surface area technique with arrow fins to enhance the performance of a DTHE. The study investigated varying numbers and heights of arrow fins and achieved a maximum improvement of 113.2% in the heat transfer rate. Sharaf, et al. [289] used a combination of techniques, including turbulator insertion, geometry change, and nanofluid, to enhance the heat transfer rate of a helical DTHE. A spring wire was inserted, and silicon dioxide nanofluid with water as the base fluid was used, resulting in a maximum heat transfer rate increase of 174%.

- **Active method**

Jawarneh, et al. [290] conducted an experimental study using the active method to enhance heat transfer in a DTHE by utilising jet vortex flow. By employing a vortex generator to create swirl flow with inclined holes and different inlet angles, a maximum heat transfer enhancement of 82% was achieved. Li, et al. [291] applied an audible acoustic field to enhance heat transfer in a DTHE. Investigating various parameters including sound pressure level and acoustic frequency, a maximum efficiency of 76.22% was achieved.

- **Combined method**

Maleki, et al. [284] combined passive and active methods to enhance heat transfer in a DTHE. Using a wire oscillator inside the inner tube as an electromagnetic vibration source and copper oxide nanofluid, a maximum heat transfer enhancement of 277.5% and a maximum PEC of 3.92 were achieved. Hedeshi, et al. [292] used ultrasonic vibration combined with a nanofluid in a DTHE. Employing ultrasonic waves at a frequency of 40 kHz and a power of 60 watts, along with aluminum oxide nanofluid, the thermal system efficiency of the DTHE was improved by up to 42.3%.

Table 5.2 provides a summary of recent studies employing various methods, including passive, active, and combined approaches, to enhance the heat transfer rate in DTHEs.

Table 5.2: Recent studies on heat transfer enhancement methods.

Author	**Method**	**Heat transfer enhancement [%] or PEC**
Yogaraj, et al. [281]	Passive: Nanofluid	18.5

Author	Method	Heat transfer enhancement [%] or PEC
Sharaf, et al. [293]	Passive: Turbulator insertion	112
Dhumal and Havaldar [283]	Passive: Turbulator insertion	315 PEC: 3.06
Marzouk, et al. [285]	Passive: Turbulator insertion	90
Chaurasia and Sarviya [294]	Passive: Turbulator insertion	100 PEC: 1.5
Dandoutiya and Kumar [295]	Passive: Turbulator insertion	105.47 PEC: 1.35
Ali and Shehab [296]	Passive: Geometry change	50 PEC: 9.07
Zhang, et al. [297]	Passive: Geometry change	PEC: 3.2
Firoozeh, et al. [287]	Passive: Geometry change	32
Chaurasiya, et al. [286]	Passive: Geometry change	33 PEC: 1.17
Hasan, et al. [298]	Passive: Extended surface area (fin)	210
Ashraf, et al. [288]	Passive: Extended surface area (fin)	113.2
Sharaf, et al. [289]	Passive: Combined techniques	174
Izadi, et al. [299]	Passive: Combined techniques	11.91
Jawarneh, et al. [290]	Active	82
Li, et al. [291]	Active	76.22
Maleki, et al. [284]	Combined	277.5 PEC: 3.92
Hedeshi, et al. [292]	Combined	42.3 PEC: 1.42

Author	Method	Heat transfer enhancement [%] or PEC
Azizi, et al. [300]	Combined	15

From the table, it is evident that different methods offer varying levels of heat transfer enhancement in DTHEs. This study focused on a combination of turbulator insertion and nanofluids as passive method to enhance heat transfer rates. Specifically, the increase in heat transfer due to the use of nanofluids alone in this study was 18.43%. When combined with helical turbulator insertion, the heat transfer enhancement reached up to 567.38% compared to using pure water without any turbulator insertion. Additionally, the maximum PEC achieved in this study was 3.17.

Comparing these results with those in Table 5.2 shows that the technique employed in this study provides a substantial enhancement. However, the PEC for the combined methods in other studies is higher, likely due to the advantages of using external forces and power. Furthermore, comparing the results of this study with those from the literature review for passive methods (as shown in Figure 2.17) indicates that the enhancement achieved in this study surpasses the average increase in heat transfer from various passive techniques. This demonstrates the effectiveness of the current turbulator designs and justifies their use. In conclusion, the combination of turbulator insertion and nanofluids used in this study significantly improves heat transfer rates in DTHEs, providing a competitive alternative to other enhancement methods. The results underscore the potential of these techniques to enhance thermal performance in practical applications.

Chapter 6: Conclusions and Future Work

In this study, an advanced study of heat transfer and fluid flow characteristics in a double tube heat exchanger was conducted through the investigation of various nanofluids and turbulator designs, utilising computational fluid dynamics tools provided by ANSYS Fluent versions 2020 to 2023. The research rigorously explored the hydrothermal interactions within DTHE systems configured with both helical and transverse turbulators, examining the performance of different nanofluids such as CuO, ZnO, Fe_3O_4, Diamond, Ag, TiO_2, Al_2O_3, SiC, and SiO_2. The study also investigated the impact of various turbulator designs, focusing on the roles of shape, height, width, and different distances between ribs in influencing fluid flow and enhancing convective heat transfer. A single-phase model was considered for the nanofluids, and a coupled approach for velocity-pressure simulations, along with a second-order upwind scheme for momentum and energy equations based on the finite volume method, was employed for simulations of the DTHE.

The detailed analysis highlights the differential impacts of turbulator configurations, revealing that helical turbulators, which induce a more effective swirl flow, generally outperform transverse turbulators in terms of improving heat transfer while minimizing pressure drops. These findings underscore the potential for tailored design considerations in thermal management systems, particularly in optimizing heat exchanger performance for industrial applications in HVAC systems, power generation, and beyond, making the results highly relevant for real-world engineering challenges. Some findings emerged from this study; however, the following represent some of the most significant and pivotal results.

- SiO_2 nanofluid achieved the highest increase in heat transfer, with an 18.4% improvement and a performance evaluation criterion (PEC) of 1.18. In contrast, CuO nanofluid showed the least improvement, with a 9.8% increase in heat transfer and a PEC of 1.1, compared to a DTHE utilising pure water without turbulator insertion.
- In transverse turbulator insertions, the trapezoidal shape exhibited the maximum increase in Nusselt number, the triangular shape caused the greatest pressure drop, and the oval shape provided a more favourable PEC.

- Changes in the height of the turbulators had a more pronounced effect on the Nusselt number and friction factor than changes in the width, pitch ratio, and distance between the ribs.
- Triangular helical turbulator showed the highest increases in Nusselt number, pressure drop, and PEC among the helical designs.
- Helical turbulators demonstrated superior performance over transverse ones by creating more effective swirl flows and lower pressure drops.
- The helical turbulator designs achieved a maximum PEC of 3.17, whereas transverse turbulators reached a maximum of 1.9, suggesting that helical turbulators are more advantageous for use in DTHEs than their transverse counterparts.

In this study, an attempt was made to employ novel turbulator designs and less studied nanofluids within double tube heat exchangers to enhance their performance for real-world applications. The exploration focused on leveraging these innovative approaches to push the boundaries of what's possible in heat exchanger efficiency and effectiveness. This extensive body of research has significantly advanced the understanding of how these enhancements can improve efficiency and performance in heat exchange systems. Despite these efforts, several areas remain unexplored and could serve as fertile ground for future research. The potential for further innovation and optimization in DTHE design and operation presents an exciting opportunity for upcoming studies. These unexplored areas not only promise to refine existing heat transfer models but also aim to integrate novel materials and geometries that could revolutionize the efficiency standards of current systems. As the demand for more efficient thermal management solutions increases in industrial applications, the exploration of these new frontiers becomes increasingly critical. The areas that can be explored are:

1. **Comparative analysis of techniques**: Investigate different enhancement techniques, such as turbulator insertion, extended surfaces, geometry modifications, and the use of nanofluids, separately. This involves precisely comparing the results to determine which technique offers the best heat transfer rate and friction factor.
2. **Combination of techniques**: Explore the synergistic effects of combining various techniques such as turbulator insertion with geometry changes, extended surfaces with turbulator insertions, and the integration of nanofluids with geometry modifications or extended surfaces.

3. **Exploration of alternative working fluids**: Investigate the enhancement techniques using different working fluids besides water, across a broad range of fluid temperatures. This could uncover new insights into the adaptability and efficiency of double tube heat exchangers with various fluids.
4. **Perforated turbulator insertions**: Investigate the performance impact of perforated helical and transverse turbulator insertions. This study could reveal potential improvements in heat transfer and fluid dynamics within the double tube heat exchanger.
5. **Transient regime studies**: Explore the effects of turbulator insertion, extended surfaces, geometry modifications, and nanofluid techniques under transient operating conditions to understand the dynamic responses of double tube heat exchangers.
6. **Integration of multiple techniques**: Investigate the effects of integrating three or four different enhancement techniques simultaneously. This comprehensive approach could lead to significant breakthroughs in maximizing the performance of double tube heat exchangers.
7. **Investigation of combined enhancement methods:** Study the combination of turbulator insertion and nanofluid use with active methods of heat transfer enhancement. This approach would delve into the effectiveness of integrating passive techniques with active ones to achieve superior thermal performance improvements in double tube heat exchangers.
8. **Experimental analysis:** While this study made efforts in design and experimental setup (details provided in Appendix A), it is worth exploring new turbulator insertions and nanofluids in experimental work.

References

[1] A. E. Bergles, "Techniques to augment heat transfer," *Handbook of heat transfer.(A 74-17085 05-33) New York, McGraw-Hill Book Co., 1973,* pp. 10-1, 1973.

[2] R. Webb and E. Eckert, "Application of rough surfaces to heat exchanger design," *international journal of heat and mass transfer,* vol. 15, no. 9, pp. 1647-1658, 1972.

[3] E. Tavousi, N. Perera, D. Flynn, and R. Hasan, "Heat transfer and fluid flow characteristics of the passive method in double tube heat exchangers: a critical review," *International Journal of Thermofluids,* p. 100282, 2023.

[4] C. Sus, "Enhancing thermal conductivity of fluids with nanoparticles, developments and applications of non-Newtonian flows," *ASME, FED, MD, 1995,* vol. 231, pp. 99-I05, 1995.

[5] S. K. Das, S. U. Choi, W. Yu, and T. Pradeep, *Nanofluids: science and technology*. John Wiley & Sons, 2007.

[6] Y. Ding, H. Alias, D. Wen, and R. A. Williams, "Heat transfer of aqueous suspensions of carbon nanotubes (CNT nanofluids)," *International Journal of Heat and Mass Transfer,* vol. 49, no. 1-2, pp. 240-250, 2006.

[7] S. Z. Heris, M. N. Esfahany, and S. G. Etemad, "Experimental investigation of convective heat transfer of Al2O3/water nanofluid in circular tube," *International journal of heat and fluid flow,* vol. 28, no. 2, pp. 203-210, 2007.

[8] B. C. Pak and Y. I. Cho, "Hydrodynamic and heat transfer study of dispersed fluids with submicron metallic oxide particles," *Experimental Heat Transfer an International Journal,* vol. 11, no. 2, pp. 151-170, 1998.

[9] S. Kakac, H. Liu, and A. Pramuanjaroenkij, *Heat exchangers: selection, rating, and thermal design*. CRC press, 2002.

[10] R. K. Shah and D. P. Sekulic, *Fundamentals of heat exchanger design*. John Wiley & Sons, 2003.

[11] H. Mohammed, H. A. Hasan, and M. Wahid, "Heat transfer enhancement of nanofluids in a double pipe heat exchanger with louvered strip inserts," *International Communications in Heat and Mass Transfer,* vol. 40, pp. 36-46, 2013.

[12] R. Andrzejczyk, T. Muszynski, and P. Kozak, "Experimental and computational fluid dynamics studies on straight and U-bend double tube heat exchangers with active and passive enhancement methods," *Heat Transfer Engineering,* vol. 42, no. 3-4, pp. 167-180, 2021.

[13] F. Morris and W. G. Whitman, "Heat Transfer for Oils and Water in Pipes1," *Industrial & Engineering Chemistry,* vol. 20, no. 3, pp. 234-240, 1928.

[14] P. Naphon, "Heat transfer and pressure drop in the horizontal double pipes with and without twisted tape insert," *International Communications in Heat and Mass Transfer,* vol. 33, no. 2, pp. 166-175, 2006/02/01/ 2006, doi: https://doi.org/10.1016/j.icheatmasstransfer.2005.09.007.

[15] J. Córcoles, J. Moya-Rico, A. Molina, and J. Almendros-Ibáñez, "Numerical and experimental study of the heat transfer process in a double pipe heat exchanger with inner corrugated tubes," *International Journal of Thermal Sciences,* vol. 158, p. 106526, 2020.

[16] C. V. M. Braga and F. E. M. Saboya, "Turbulent heat transfer, pressure drop and fin efficiency in annular regions with continuous longitudinal rectangular fins," *Experimental Thermal and Fluid Science,* vol. 20, no. 2, pp. 55-65, 1999/10/01/ 1999, doi: https://doi.org/10.1016/S0894-1777(99)00026-6.

[17] B.-H. Chun, H. U. Kang, and S. H. Kim, "Effect of alumina nanoparticles in the fluid on heat transfer in double-pipe heat exchanger system," *Korean Journal of Chemical Engineering,* vol. 25, no. 5, pp. 966-971, 2008.

[18] C. Yildiz, Y. Biçer, and D. Pehlivan, "Heat transfers and pressure drops in rotating helical pipes," *Applied energy,* vol. 50, no. 1, pp. 85-94, 1995.

[19] M. Legay, B. Simony, P. Boldo, N. Gondrexon, S. Le Person, and A. Bontemps, "Improvement of heat transfer by means of ultrasound: Application to a double-tube heat exchanger," *Ultrasonics Sonochemistry,* vol. 19, no. 6, pp. 1194-1200, 2012/11/01/ 2012, doi: https://doi.org/10.1016/j.ultsonch.2012.04.001.

[20] H. H. Habeeb, R. A. Khalefa, and S. Kaska, "Performance Enhancement of the Vertical Double Pipe Heat Exchanger by Applying of Bubbling Generation on the Shell Side," *Kirkuk University Journal/Scientific Studies (KUJSS),* vol. 13, no. 1, pp. 156-171, 2018.

[21] M. Omidi, M. Farhadi, and M. Jafari, "A comprehensive review on double pipe heat exchangers," *Applied Thermal Engineering,* vol. 110, pp. 1075-1090, 2017/01/05/ 2017, doi: https://doi.org/10.1016/j.applthermaleng.2016.09.027.

[22] W. El-Maghlany, E. Eid, M. Teamah, and I. Shahrour, "Experimental study for double pipe heat exchanger with rotating inner pipe," *Int J Adv Sci Tech Res,* vol. 4, no. 2, pp. 507-524, 2012.

[23] Z. Zhang, Y. Ding, C. Guan, H. Yan, and W. Yang, "Heat transfer enhancement in double-pipe heat exchanger by means of rotor-assembled strands," *Chemical Engineering and Processing: Process Intensification,* vol. 60, pp. 26-33, 2012/10/01/ 2012, doi: https://doi.org/10.1016/j.cep.2012.06.003.

[24] S. Anitha, K. Loganathan, and M. Pichumani, "Approaches for modelling of industrial energy systems: correlation of heat transfer characteristics between magnetohydrodynamics hybrid nanofluids and performance analysis of industrial length-scale heat exchanger," *Journal of Thermal Analysis and Calorimetry,* pp. 1-16, 2020.

[25] S. Liu and M. Sakr, "A comprehensive review on passive heat transfer enhancements in pipe exchangers," *Renewable and Sustainable Energy Reviews,* vol. 19, pp. 64-81, 2013/03/01/ 2013, doi: https://doi.org/10.1016/j.rser.2012.11.021.

[26] M. Sheikholeslami, M. Gorji-Bandpy, and D. D. Ganji, "Review of heat transfer enhancement methods: Focus on passive methods using swirl flow devices," *Renewable and Sustainable Energy Reviews,* vol. 49, pp. 444-469, 2015/09/01/ 2015, doi: https://doi.org/10.1016/j.rser.2015.04.113.

[27] P. Bharadwaj, A. D. Khondge, and A. W. Date, "Heat transfer and pressure drop in a spirally grooved tube with twisted tape insert," *International Journal of Heat and Mass Transfer,* vol. 52, no. 7, pp. 1938-1944, 2009/03/01/ 2009, doi: https://doi.org/10.1016/j.ijheatmasstransfer.2008.08.038.

[28] T. Alam and M.-H. Kim, "A comprehensive review on single phase heat transfer enhancement techniques in heat exchanger applications," *Renewable and Sustainable Energy Reviews,* vol. 81, pp. 813-839, 2018.

[29] N. Targui and H. Kahalerras, "Analysis of a double pipe heat exchanger performance by use of porous baffles and pulsating flow," *Energy conversion and management,* vol. 76, pp. 43-54, 2013.

[30] W. Duangthongsuk and S. Wongwises, "An experimental investigation of the heat transfer and pressure drop characteristics of a circular tube fitted with rotating turbine-type swirl generators," *Experimental Thermal and Fluid Science,* vol. 45, pp. 8-15, 2013/02/01/ 2013, doi: https://doi.org/10.1016/j.expthermflusci.2012.09.009.

[31] O. Shewale, P. Mane, S. Gazge, and P. Hameed, "Experimental investigation of double pipe heat exchanger with helical fins on the inner rotating tube," *International Journal of Research in Engineering and Technology*, vol. 3, no. 7, pp. 98-102, 2014.
[32] O. Keklikcioglu and V. Ozceyhan, "A review of heat transfer enhancement methods using coiled wire and twisted tape inserts," *Heat Transfer: Models, Methods And Applications*, pp. 199-217, 2018.
[33] H. H. Hamed, A. E. Mohammed, R. A. Khalefa, O. A. Habeeb, and M. A. Abdulqader, "The Effect of using Compound Techniques (Passive and Active) on the Double Pipe Heat Exchanger Performance," *Egyptian Journal of Chemistry*, vol. 64, no. 6, pp. 2797-2802, 2021.
[34] V. D. Zimparov and V. M. Petkov, "Compound heat transfer enhancement by a combination of spirally corrugated tubes with a twisted tape," in *International Heat Transfer Conference Digital Library*, 2002: Begel House Inc.
[35] M. Bahiraei, N. Mazaheri, and M. Hanooni, "Performance enhancement of a triple-tube heat exchanger through heat transfer intensification using novel crimped-spiral ribs and nanofluid: A two-phase analysis," *Chemical Engineering and Processing-Process Intensification*, vol. 160, p. 108289, 2021.
[36] C. Yildiz, Y. Bíçer, and D. Pehlívan, "Influence of fluid rotation on the heat transfer and pressure drop in double-pipe heat exchangers," *Applied Energy*, vol. 54, no. 1, pp. 49-56, 1996/05/01/ 1996, doi: https://doi.org/10.1016/0306-2619(95)00070-4.
[37] E. F. Akyürek, K. Geliş, B. Şahin, and E. Manay, "Experimental analysis for heat transfer of nanofluid with wire coil turbulators in a concentric tube heat exchanger," *Results in Physics*, vol. 9, pp. 376-389, 2018.
[38] S. M. HM and R. N. Hegde, "Investigations on the effect of disturbed flow using differently configured turbulators and Alumina nanofluid as a coolant in a double tube heat exchanger," *Experimental Heat Transfer*, vol. 35, no. 3, pp. 282-307, 2022.
[39] R. Andrzejczyk, T. Muszynski, and P. Kozak, "Experimental investigation of heat transfer enhancement in straight and U-bend double-pipe heat exchanger with wire insert," *Chemical Engineering and Processing-Process Intensification*, vol. 136, pp. 177-190, 2019.
[40] A. Ponshanmugakumar and R. Rajavel, "Enhancement of heat transfer in double pipe heat exchanger," *Materials Today: Proceedings*, vol. 16, pp. 706-713, 2019.
[41] H. Karakaya and A. Durmuş, "Heat transfer and exergy loss in conical spring turbulators," *International Journal of Heat and Mass Transfer*, vol. 60, pp. 756-762, 2013.
[42] P. Durga Prasad and A. Gupta, "Augmentation of heat transfer and pressure drop characteristics inside a double pipe U-Tube heat exchanger by using twisted tape inserts," in *Emerging Trends in Science, Engineering and Technology*: Springer, 2012, pp. 33-45.
[43] C. Yildiz, Y. Biçer, and D. Pehlivan, "Effect of twisted strips on heat transfer and pressure drop in heat exchangers," *Energy Conversion and Management*, vol. 39, no. 3-4, pp. 331-336, 1998.
[44] E. K. Akpinar, Y. Bicer, C. Yildiz, and D. Pehlivan, "Heat transfer enhancements in a concentric double pipe exchanger equipped with swirl elements," *International communications in heat and mass transfer*, vol. 31, no. 6, pp. 857-868, 2004.
[45] C. Gnanavel, R. Saravanan, and M. Chandrasekaran, "Heat transfer enhancement through nano-fluids and twisted tape insert with rectangular cut on its rib in a double pipe heat exchanger," *Materials Today: Proceedings*, vol. 21, pp. 865-869, 2020. [Online]. Available: 0.97.

[46] N. Mashoofi, S. M. Pesteei, A. Moosavi, and H. Sadighi Dizaji, "Fabrication method and thermal-frictional behavior of a tube-in-tube helically coiled heat exchanger which contains turbulator," *Applied Thermal Engineering,* vol. 111, pp. 1008-1015, 2017/01/25/ 2017, doi: https://doi.org/10.1016/j.applthermaleng.2016.09.163.
[47] M. M. K. Bhuiya, A. S. M. Sayem, M. Islam, M. S. U. Chowdhury, and M. Shahabuddin, "Performance assessment in a heat exchanger tube fitted with double counter twisted tape inserts," *International Communications in Heat and Mass Transfer,* vol. 50, pp. 25-33, 2014/01/01/ 2014, doi: https://doi.org/10.1016/j.icheatmasstransfer.2013.11.005.
[48] S. Eiamsa-ard, C. Thianpong, and P. Promvonge, "Experimental investigation of heat transfer and flow friction in a circular tube fitted with regularly spaced twisted tape elements," *International Communications in Heat and Mass Transfer,* vol. 33, no. 10, pp. 1225-1233, 2006.
[49] P. Promvonge, "Thermal performance in circular tube fitted with coiled square wires," *Energy Conversion and Management,* vol. 49, no. 5, pp. 980-987, 2008.
[50] S. W. Chang, Y. J. Jan, and J. S. Liou, "Turbulent heat transfer and pressure drop in tube fitted with serrated twisted tape," *International Journal of Thermal Sciences,* vol. 46, no. 5, pp. 506-518, 2007.
[51] M. Nakhchi, J. Esfahani, and K. Kim, "Numerical study of turbulent flow inside heat exchangers using perforated louvered strip inserts," *International Journal of Heat and Mass Transfer,* vol. 148, p. 119143, 2020.
[52] E. Z. Ibrahim, "Augmentation of laminar flow and heat transfer in flat tubes by means of helical screw-tape inserts," *Energy Conversion and Management,* vol. 52, no. 1, pp. 250-257, 2011/01/01/ 2011, doi: https://doi.org/10.1016/j.enconman.2010.06.065.
[53] P. Naphon, "Effect of coil-wire insert on heat transfer enhancement and pressure drop of the horizontal concentric tubes," *International Communications in Heat and Mass Transfer,* vol. 33, no. 6, pp. 753-763, 2006/07/01/ 2006, doi: https://doi.org/10.1016/j.icheatmasstransfer.2006.01.020.
[54] S. Eiamsa-ard, S. Pethkool, C. Thianpong, and P. Promvonge, "Turbulent flow heat transfer and pressure loss in a double pipe heat exchanger with louvered strip inserts," *International Communications in Heat and Mass Transfer,* vol. 35, no. 2, pp. 120-129, 2008/02/01/ 2008, doi: https://doi.org/10.1016/j.icheatmasstransfer.2007.07.003.
[55] S. Zhang, L. Lu, C. Dong, and S. H. Cha, "Performance evaluation of a double-pipe heat exchanger fitted with self-rotating twisted tapes," *Applied Thermal Engineering,* vol. 158, p. 113770, 2019.
[56] E. K. Akpinar and Y. Bicer, "Investigation of heat transfer and exergy loss in a concentric double pipe exchanger equipped with swirl generators," *International journal of thermal sciences,* vol. 44, no. 6, pp. 598-607, 2005.
[57] R. Aridi, S. Ali, T. Lemenand, J. Faraj, and M. Khaled, "CFD analysis on the spatial effect of vortex generators in concentric tube heat exchangers–A comparative study," *International Journal of Thermofluids,* vol. 16, p. 100247, 2022.
[58] E. K. Akpinar, "Evaluation of heat transfer and exergy loss in a concentric double pipe exchanger equipped with helical wires," *Energy Conversion and Management,* vol. 47, no. 18, pp. 3473-3486, 2006/11/01/ 2006, doi: https://doi.org/10.1016/j.enconman.2005.12.014.
[59] A. S. Yadav, "Effect of half length twisted-tape turbulators on heat transfer and pressure drop characteristics inside a double pipe u-bend heat exchanger," *JJMIE,* vol. 3, no. 1, pp. 17-22, 2009.

[60] S. Eiamsa-ard, K. Wongcharee, P. Eiamsa-Ard, and C. Thianpong, "Heat transfer enhancement in a tube using delta-winglet twisted tape inserts," *Applied Thermal Engineering*, vol. 30, no. 4, pp. 310-318, 2010.

[61] S. C. Shashank and S. Taji, "Experimental studies on effect of coil wire insert on heat transfer enhancement and friction factor of double pipe heat exchanger," *International Journal of Computational Engineering Research*, vol. 3, no. 5, 2013.

[62] M. Sheikholeslami, M. Hatami, M. Jafaryar, F. Farkhadnia, D. D. Ganji, and M. Gorji-Bandpy, "Thermal management of double-pipe air to water heat exchanger," *Energy and Buildings*, vol. 88, pp. 361-366, 2015/02/01/ 2015, doi: https://doi.org/10.1016/j.enbuild.2014.11.076.

[63] J. Moya-Rico, A. Molina, J. Belmonte, J. C. Tendero, and J. Almendros-Ibáñez, "Experimental characterization of a double tube heat exchanger with inserted twisted tape elements," *Applied Thermal Engineering*, vol. 174, p. 115234, 2020.

[64] Q. J. Slaiman and A. N. Znad, "Enhancement of Heat Transfer in The Tube-Sid of A Double Pipe Heat Exchanger by Wire Coils," *Al-Nahrain Journal for Engineering Sciences*, vol. 16, no. 1, pp. 51-57, 2013.

[65] A. García, P. G. Vicente, and A. Viedma, "Experimental study of heat transfer enhancement with wire coil inserts in laminar-transition-turbulent regimes at different Prandtl numbers," *International Journal of Heat and Mass Transfer*, vol. 48, no. 21, pp. 4640-4651, 2005/10/01/ 2005, doi: https://doi.org/10.1016/j.ijheatmasstransfer.2005.04.024.

[66] S. Padmanabhan, O. Y. Reddy, K. V. A. K. Yadav, V. B. Raja, and K. Palanikumar, "Heat transfer analysis of double tube heat exchanger with helical inserts," *Materials Today: Proceedings*, 2021.

[67] S. Pourahmad and S. M. Pesteei, "Effectiveness-NTU analyses in a double tube heat exchanger equipped with wavy strip considering various angles," *Energy Conversion and Management*, vol. 123, pp. 462-469, 2016/09/01/ 2016, doi: https://doi.org/10.1016/j.enconman.2016.06.063.

[68] P. Murugesan, K. Mayilsamy, S. Suresh, and P. S. S. Srinivasan, "Heat transfer and pressure drop characteristics in a circular tube fitted with and without V-cut twisted tape insert," *International Communications in Heat and Mass Transfer*, vol. 38, no. 3, pp. 329-334, 2011/03/01/ 2011, doi: https://doi.org/10.1016/j.icheatmasstransfer.2010.11.010.

[69] A. T. Wijayanta, B. Kristiawan, and M. Aziz, "Internal flow in an enhanced tube having square-cut twisted tape insert," *Energies*, vol. 12, no. 2, p. 306, 2019.

[70] Z. Iqbal, K. Syed, and M. Ishaq, "Fin design for conjugate heat transfer optimization in double pipe," *International Journal of Thermal Sciences*, vol. 94, pp. 242-258, 2015.

[71] Z. Iqbal, K. Syed, and M. Ishaq, "Optimal fin shape in finned double pipe with fully developed laminar flow," *Applied thermal engineering*, vol. 51, no. 1-2, pp. 1202-1223, 2013.

[72] K. S. Syed, M. Ishaq, and M. Bakhsh, "Laminar convection in the annulus of a double-pipe with triangular fins," *Computers & fluids*, vol. 44, no. 1, pp. 43-55, 2011.

[73] H. Kahalerras and N. Targui, "Numerical analysis of heat transfer enhancement in a double pipe heat exchanger with porous fins," *International Journal of Numerical Methods for Heat & Fluid Flow*, 2008.

[74] R. L. Mohanty, S. Bashyam, and D. Das, "Numerical analysis of double pipe heat exchanger using heat transfer augmentation techniques," *International Journal of Plastics Technology*, vol. 18, no. 3, pp. 337-348, 2014.

[75] L. Zhang *et al.*, "Effects of the arrangement of triangle-winglet-pair vortex generators on heat transfer performance of the shell side of a double-pipe heat exchanger enhanced by helical fins," *Heat and Mass Transfer*, vol. 53, no. 1, pp. 127-139, 2017.

[76] M. A. Hussein and V. M. Hameed, "Experimental Investigation on the Effect of Semi-circular Perforated Baffles with Semi-circular Fins on Air–Water Double Pipe Heat Exchanger," *Arabian Journal for Science and Engineering,* vol. 47, no. 5, pp. 6115-6124, 2022.

[77] N. S. Reddy, K. Rajagopal, and P. Veena, "Experimental investigation of heat transfer enhancement of a double pipe heat exchanger with helical fins in the annulus side," *International Journal of Dynamics of Fluids,* vol. 13, no. 2, pp. 285-293, 2017.

[78] V. Mathanraj, V. L. Krishna, J. L. V. Babu, and S. A. Kumar, "Experimental investigation on heat transfer in double pipe heat exchanger employing triangular fins," in *IOP Conference Series: Materials Science and Engineering,* 2018, vol. 402, no. 1: IOP Publishing, p. 012137.

[79] V. M. Hameed and B. M. Essa, "Turbulent flow heat transfer and pressure loss in a double pipe heat exchanger with triangular fins," *International journal of energy and environment,* vol. 7, no. 2, p. 149, 2016.

[80] A. B. Colaço, V. C. Mariani, M. R. Salem, and L. dos Santos Coelho, "Maximizing the thermal performance index applying evolutionary multi-objective optimization approaches for double pipe heat exchanger," *Applied Thermal Engineering,* vol. 211, p. 118504, 2022.

[81] Z. Iqbal, K. Syed, and M. Ishaq, "Optimal convective heat transfer in double pipe with parabolic fins," *International Journal of Heat and Mass Transfer,* vol. 54, no. 25-26, pp. 5415-5426, 2011.

[82] R. Raj, N. S. Lakshman, and Y. Mukkamala, "Single phase flow heat transfer and pressure drop measurements in doubly enhanced tubes," *International Journal of Thermal Sciences,* vol. 88, pp. 215-227, 2015.

[83] B. Jalili, N. Aghaee, P. Jalili, and D. D. Ganji, "Novel usage of the curved rectangular fin on the heat transfer of a double-pipe heat exchanger with a nanofluid," *Case Studies in Thermal Engineering,* p. 102086, 2022.

[84] M. Iqbal and K. Syed, "Thermally developing flow in finned double-pipe heat exchanger," *International journal for numerical methods in fluids,* vol. 65, no. 10, pp. 1145-1159, 2011.

[85] L. Wang, Y. Lei, and S. Jing, "Performance of a Double-Tube Heat Exchanger with Staggered Helical Fins," *Chemical Engineering & Technology,* vol. 45, no. 5, pp. 953-961, 2022.

[86] K. Syed, Z. Iqbal, and M. Ishaq, "Optimal configuration of finned annulus in a double pipe with fully developed laminar flow," *Applied Thermal Engineering,* vol. 31, no. 8-9, pp. 1435-1446, 2011.

[87] W. Ahmad, K. S. Syed, M. Ishaq, A. Hassan, and Z. Iqbal, "Numerical study of conjugate heat transfer in a double-pipe with exponential fins using DGFEM," *Applied Thermal Engineering,* vol. 111, pp. 1184-1201, 2017.

[88] J. Taborek, "Double-Pipe and Multitube Heat Exchangers with Plain and Longitudinal Finned Tubes," *Heat Transfer Engineering,* vol. 18, no. 2, pp. 34-45, 1997/01/01 1997, doi: 10.1080/01457639708939894.

[89] E. Cao, *Heat transfer in process engineering*. McGraw-Hill Education, 2010.

[90] L. Zhang, H. Guo, J. Wu, and W. Du, "Compound heat transfer enhancement for shell side of double-pipe heat exchanger by helical fins and vortex generators," *Heat and Mass Transfer,* vol. 48, no. 7, pp. 1113-1124, 2012.

[91] L. Zhang, W. Du, J. Wu, Y. Li, and Y. Xing, "Fluid flow characteristics for shell side of double-pipe heat exchanger with helical fins and pin fins," *Experimental Thermal and Fluid Science*, vol. 36, pp. 30-43, 2012/01/01/ 2012, doi: https://doi.org/10.1016/j.expthermflusci.2011.08.001.

[92] M. Kind, H. Martin, P. Stephan, W. Roetzel, B. Spang, and H. Müller-Steinhagen, "VDI Heat Atlas," ed: Springer, 2010.

[93] R. Eason, Y. Bayazitoglu, and A. Meade, "Enhancement of heat transfer in square helical ducts," *International journal of heat and mass transfer*, vol. 37, no. 14, pp. 2077-2087, 1994.

[94] L. Zhang *et al.*, "Heat transfer enhancement by streamlined winglet pair vortex generators for helical channel with rectangular cross section," *Chemical Engineering and Processing-Process Intensification*, vol. 147, p. 107788, 2020.

[95] A. El Maakoul, M. El Metoui, A. Ben Abdellah, S. Saadeddine, and M. Meziane, "Numerical investigation of thermohydraulic performance of air to water double-pipe heat exchanger with helical fins," *Applied Thermal Engineering*, vol. 127, pp. 127-139, 2017/12/25/ 2017, doi: https://doi.org/10.1016/j.applthermaleng.2017.08.024.

[96] A. El Maakoul, K. Feddi, S. Saadeddine, A. Ben Abdellah, and M. El Metoui, "Performance enhancement of finned annulus using surface interruptions in double-pipe heat exchangers," *Energy Conversion and Management*, vol. 210, p. 112710, 2020/04/15/ 2020, doi: https://doi.org/10.1016/j.enconman.2020.112710.

[97] D. Majidi, H. Alighardashi, and F. Farhadi, "Experimental studies of heat transfer of air in a double-pipe helical heat exchanger," *Applied Thermal Engineering*, vol. 133, pp. 276-282, 2018/03/25/ 2018, doi: https://doi.org/10.1016/j.applthermaleng.2018.01.057.

[98] K. S. Syed, M. Ishaq, Z. Iqbal, and A. Hassan, "Numerical study of an innovative design of a finned double-pipe heat exchanger with variable fin-tip thickness," *Energy Conversion and Management*, vol. 98, pp. 69-80, 2015/07/01/ 2015, doi: https://doi.org/10.1016/j.enconman.2015.03.038.

[99] A. Zohir, M. Habib, and M. Nemitallah, "Heat transfer characteristics in a double-pipe heat exchanger equipped with coiled circular wires," *Experimental heat transfer*, vol. 28, no. 6, pp. 531-545, 2015.

[100] N. Mashoofi, S. M. Pesteei, A. Moosavi, and H. S. Dizaji, "Fabrication method and thermal-frictional behavior of a tube-in-tube helically coiled heat exchanger which contains turbulator," *Applied Thermal Engineering*, vol. 111, pp. 1008-1015, 2017.

[101] M. Sheikholeslami, M. Gorji-Bandpy, and D. D. Ganji, "Experimental study on turbulent flow and heat transfer in an air to water heat exchanger using perforated circular-ring," *Experimental Thermal and Fluid Science*, vol. 70, pp. 185-195, 2016/01/01/ 2016, doi: https://doi.org/10.1016/j.expthermflusci.2015.09.002.

[102] M. Sheikholeslami, M. Gorji-Bandpy, and D. D. Ganji, "Effect of discontinuous helical turbulators on heat transfer characteristics of double pipe water to air heat exchanger," *Energy Conversion and Management*, vol. 118, pp. 75-87, 2016/06/15/ 2016, doi: https://doi.org/10.1016/j.enconman.2016.03.080.

[103] V. K. Karanth and K. Murthy, "Numerical study of heat transfer in a finned double pipe heat exchanger," *World Journal of Modelling and Simulation*, vol. 11, no. 1, pp. 43-54, 2015.

[104] A. El Maakoul, A. Laknizi, S. Saadeddine, A. Ben Abdellah, M. Meziane, and M. El Metoui, "Numerical design and investigation of heat transfer enhancement and performance for an annulus with continuous helical baffles in a double-pipe heat exchanger," *Energy Conversion and Management*, vol. 133, pp. 76-86, 2017/02/01/ 2017, doi: https://doi.org/10.1016/j.enconman.2016.12.002.

[105] N. Sreedhard and G. Varghese, "Analysis of Longitudinal Fin Patterns in a Concentric Double Tube Heat Exchanger using LMTD and CFD Techniques”," *International Journal of Applied Engineering Research*, vol. 12, no. 17, pp. 6471-6479, 2017.
[106] Z. Zhang, Z. Yu, and X. Fang, "An experimental heat transfer study for helically flowing outside petal-shaped finned tubes with different geometrical parameters," *Applied Thermal Engineering*, vol. 27, no. 1, pp. 268-272, 2007/01/01/ 2007, doi: https://doi.org/10.1016/j.applthermaleng.2006.07.008.
[107] M. R. Salem, M. B. Eltoukhey, R. K. Ali, and K. M. Elshazly, "Experimental investigation on the hydrothermal performance of a double-pipe heat exchanger using helical tape insert," *International Journal of Thermal Sciences*, vol. 124, pp. 496-507, 2018/02/01/ 2018, doi: https://doi.org/10.1016/j.ijthermalsci.2017.10.040.
[108] S. Yadav and S. K. Sahu, "Heat transfer augmentation in double pipe water to air counter flow heat exchanger with helical surface disc turbulators," *Chemical Engineering and Processing-Process Intensification*, vol. 135, pp. 120-132, 2019.
[109] M. Sheikholeslami and D. Ganji, "Heat transfer improvement in a double pipe heat exchanger by means of perforated turbulators," *Energy Conversion and management*, vol. 127, pp. 112-123, 2016.
[110] K. Shaji, "Numerical analysis on a double pipe heat exchanger with twisted tape induced swirl flow on both sides," *Procedia Technology*, vol. 24, pp. 436-443, 2016.
[111] M. Yassin, M. Shedid, H. Abd El-Hameed, and A. Basheer, "Heat transfer augmentation for annular flow due to rotation of inner finned pipe," *International Journal of Thermal Sciences*, vol. 134, pp. 653-660, 2018.
[112] M. Ravikumar and Y. A. Raj, "Investigation of fin profile on the performance of the shell and tube heat exchanger," *Materials Today: Proceedings*, vol. 45, pp. 7910-7916, 2021.
[113] S. Sivalakshmi, M. Raja, and G. Gowtham, "Effect of helical fins on the performance of a double pipe heat exchanger," *Materials Today: Proceedings*, vol. 43, pp. 1128-1131, 2021.
[114] A. A. R. Darzi, M. Farhadi, and K. Sedighi, "Experimental investigation of convective heat transfer and friction factor of Al2O3/water nanofluid in helically corrugated tube," *Experimental thermal and fluid science*, vol. 57, pp. 188-199, 2014.
[115] S. Vaezi, S. Karbalaee, and P. Hanafizadeh, "Effect of aspect ratio on heat transfer enhancement in alternating oval double pipe heat exchangers," *Applied Thermal Engineering*, vol. 125, pp. 1164-1172, 2017.
[116] S. Yang, L. Zhang, and H. Xu, "Experimental study on convective heat transfer and flow resistance characteristics of water flow in twisted elliptical tubes," *Applied Thermal Engineering*, vol. 31, no. 14-15, pp. 2981-2991, 2011.
[117] X.-h. Tan, D.-s. Zhu, G.-y. Zhou, and L.-d. Zeng, "Heat transfer and pressure drop performance of twisted oval tube heat exchanger," *Applied thermal engineering*, vol. 50, no. 1, pp. 374-383, 2013.
[118] J.-A. Meng, X.-G. Liang, Z.-J. Chen, and Z.-X. Li, "Experimental study on convective heat transfer in alternating elliptical axis tubes," *Experimental Thermal and Fluid Science*, vol. 29, no. 4, pp. 457-465, 2005.
[119] V. Kumar, S. Saini, M. Sharma, and K. Nigam, "Pressure drop and heat transfer study in tube-in-tube helical heat exchanger," *Chemical Engineering Science*, vol. 61, no. 13, pp. 4403-4416, 2006.
[120] X. Tang, X. Dai, and D. Zhu, "Experimental and numerical investigation of convective heat transfer and fluid flow in twisted spiral tube," *International Journal of Heat and Mass Transfer*, vol. 90, pp. 523-541, 2015.

[121] J. M. Gorman, K. R. Krautbauer, and E. M. Sparrow, "Thermal and fluid flow first-principles numerical design of an enhanced double pipe heat exchanger," *Applied Thermal Engineering*, vol. 107, pp. 194-206, 2016.
[122] A. Asadi, M. Zaboli, A. Mogharrebi, S. Saedodin, and D. Ganji, "Numerical analysis of turbulence-inducing elements with various geometries and utilization of hybrid nanoparticles in a double pipe heat exchanger," *Alexandria Engineering Journal*, vol. 61, no. 5, pp. 3633-3644, 2022.
[123] T. J. Rennie and V. G. Raghavan, "Numerical studies of a double-pipe helical heat exchanger," *Applied Thermal Engineering*, vol. 26, no. 11-12, pp. 1266-1273, 2006.
[124] D. Huu-Quan, A. M. Rostami, M. S. Rad, M. Izadi, A. Hajjar, and Q. Xiong, "3D numerical investigation of turbulent forced convection in a double-pipe heat exchanger with flat inner pipe," *Applied Thermal Engineering*, vol. 182, p. 116106, 2021.
[125] D. Brough, J. Ramos, B. Delpech, and H. Jouhara, "Development and validation of a TRNSYS type to simulate heat pipe heat exchangers in transient applications of waste heat recovery," *International Journal of Thermofluids*, vol. 9, p. 100056, 2021.
[126] S. Pesteei, N. Mashoofi, S. Pourahmad, and A. Roshan, "Numerical investigation on the effect of a modified corrugated double tube heat exchanger on heat transfer enhancement and exergy losses," *International Journal of Heat and Technology*, vol. 35, no. 2, pp. 243-248, 2017.
[127] H. S. Dizaji, S. Jafarmadar, and F. Mobadersani, "Experimental studies on heat transfer and pressure drop characteristics for new arrangements of corrugated tubes in a double pipe heat exchanger," *International Journal of Thermal Sciences*, vol. 96, pp. 211-220, 2015.
[128] H.-Z. Han, B.-X. Li, H. Wu, and W. Shao, "Multi-objective shape optimization of double pipe heat exchanger with inner corrugated tube using RSM method," *International Journal of Thermal Sciences*, vol. 90, pp. 173-186, 2015.
[129] R. Yang and F. P. Chiang, "An experimental heat transfer study for periodically varying-curvature curved-pipe," *International Journal of Heat and Mass Transfer*, vol. 45, no. 15, pp. 3199-3204, 2002/07/01/ 2002, doi: https://doi.org/10.1016/S0017-9310(02)00023-6.
[130] W.-L. Chen and W.-C. Dung, "Numerical study on heat transfer characteristics of double tube heat exchangers with alternating horizontal or vertical oval cross section pipes as inner tubes," *Energy Conversion and Management*, vol. 49, no. 6, pp. 1574-1583, 2008/06/01/ 2008, doi: https://doi.org/10.1016/j.enconman.2007.12.007.
[131] C. Luo, K. Song, T. Tagawa, and T. Liu, "Heat Transfer Enhancement in a Novel Annular Tube with Outer Straight and Inner Twisted Oval Tubes," *Symmetry*, vol. 12, no. 8, p. 1213, 2020. [Online]. Available: https://www.mdpi.com/2073-8994/12/8/1213.
[132] J.-A. Zambaux, J.-L. Harion, S. Russeil, and P. Bouvier, "The effect of successive alternating wall deformation on the performance of an annular heat exchanger," *Applied Thermal Engineering*, vol. 90, pp. 286-295, 2015/11/05/ 2015, doi: https://doi.org/10.1016/j.applthermaleng.2015.06.091.
[133] M. Hashemian, S. Jafarmadar, J. Nasiri, and H. Sadighi Dizaji, "Enhancement of heat transfer rate with structural modification of double pipe heat exchanger by changing cylindrical form of tubes into conical form," *Applied Thermal Engineering*, vol. 118, pp. 408-417, 2017/05/25/ 2017, doi: https://doi.org/10.1016/j.applthermaleng.2017.02.095.
[134] M. A. Moawed, E. Ibrahim, and A. Gomaa, "Thermal performance of a pipe in pipe heat exchanger with sinusoidal inner pipe," *Energy Conversion and Management*, vol.

49, no. 4, pp. 678-686, 2008/04/01/ 2008, doi: https://doi.org/10.1016/j.enconman.2007.07.036.
[135] R. Webb, "Principles of Enhanced Heat Transfer. John Wiely & Sons," *Inc., New York*, pp. 293-294, 1994.
[136] R. Bhadouriya, A. Agrawal, and S. V. Prabhu, "Experimental and numerical study of fluid flow and heat transfer in an annulus of inner twisted square duct and outer circular pipe," *International Journal of Thermal Sciences*, vol. 94, pp. 96-109, 2015/08/01/ 2015, doi: https://doi.org/10.1016/j.ijthermalsci.2015.02.019.
[137] C. Luo and K. Song, "Thermal performance enhancement of a double-tube heat exchanger with novel twisted annulus formed by counter-twisted oval tubes," *International Journal of Thermal Sciences*, vol. 164, p. 106892, 2021. [Online]. Available: JADID PERCENTAGE.
[138] H. S. Dizaji, S. Jafarmadar, and S. Asaadi, "Experimental exergy analysis for shell and tube heat exchanger made of corrugated shell and corrugated tube," *Experimental Thermal and Fluid Science*, vol. 81, pp. 475-481, 2017.
[139] W. Wang, Y. Zhang, K.-S. Lee, and B. Li, "Optimal design of a double pipe heat exchanger based on the outward helically corrugated tube," *International Journal of Heat and Mass Transfer*, vol. 135, pp. 706-716, 2019.
[140] S. Pethkool, S. Eiamsa-ard, S. Kwankaomeng, and P. Promvonge, "Turbulent heat transfer enhancement in a heat exchanger using helically corrugated tube," *International Communications in Heat and Mass Transfer*, vol. 38, no. 3, pp. 340-347, 2011/03/01/ 2011, doi: https://doi.org/10.1016/j.icheatmasstransfer.2010.11.014.
[141] S. Laohalertdecha and S. Wongwises, "The effects of corrugation pitch on the condensation heat transfer coefficient and pressure drop of R-134a inside horizontal corrugated tube," *International Journal of Heat and Mass Transfer*, vol. 53, no. 13, pp. 2924-2931, 2010/06/01/ 2010, doi: https://doi.org/10.1016/j.ijheatmasstransfer.2010.01.037.
[142] R. Webb, R. Narayanamurthy, and P. Thors, "Heat transfer and friction characteristics of internal helical-rib roughness," *J. Heat Transfer*, vol. 122, no. 1, pp. 134-142, 2000.
[143] Z. Li, Y. Yao, Q. Wang, J. Cai, Y. Wu, and H. Wang, "Effect of internal helical-rib roughness on mixed convection flow and heat transfer in heated horizontal pipe flow of supercritical water," *International Journal of Heat and Mass Transfer*, vol. 130, pp. 1272-1287, 2019.
[144] H. Han, B. Li, and W. Shao, "Multi-objective optimization of outward convex corrugated tubes using response surface methodology," *Applied Thermal Engineering*, vol. 70, no. 1, pp. 250-262, 2014/09/05/ 2014, doi: https://doi.org/10.1016/j.applthermaleng.2014.05.016.
[145] S. Wongwises and M. Polsongkram, "Condensation heat transfer and pressure drop of HFC-134a in a helically coiled concentric tube-in-tube heat exchanger," *International Journal of Heat and Mass Transfer*, vol. 49, no. 23, pp. 4386-4398, 2006/11/01/ 2006, doi: https://doi.org/10.1016/j.ijheatmasstransfer.2006.05.010.
[146] V. Kumar, B. Faizee, M. Mridha, and K. Nigam, "Numerical studies of a tube-in-tube helically coiled heat exchanger," *Chemical Engineering and Processing: Process Intensification*, vol. 47, no. 12, pp. 2287-2295, 2008.
[147] L. Shao, J.-t. Han, G.-p. Su, and J.-h. Pan, "Condensation heat transfer of R-134A in horizontal straight and helically coiled tube-in-tube heat exchangers," *Journal of hydrodynamics*, vol. 19, no. 6, pp. 677-682, 2007.
[148] S. U. Choi and J. A. Eastman, "Enhancing thermal conductivity of fluids with nanoparticles," Argonne National Lab., IL (United States), 1995.

[149] S. Lee, S.-S. Choi, S. Li, and, and J. Eastman, "Measuring thermal conductivity of fluids containing oxide nanoparticles," 1999.

[150] W. Yu, D. M. France, J. L. Routbort, and S. U. Choi, "Review and comparison of nanofluid thermal conductivity and heat transfer enhancements," *Heat transfer engineering,* vol. 29, no. 5, pp. 432-460, 2008.

[151] R. Saidur, K. Y. Leong, and H. A. Mohammed, "A review on applications and challenges of nanofluids," *Renewable and Sustainable Energy Reviews,* vol. 15, no. 3, pp. 1646-1668, 2011/04/01/ 2011, doi: https://doi.org/10.1016/j.rser.2010.11.035.

[152] N. Ali, J. A. Teixeira, and A. Addali, "A Review on Nanofluids: Fabrication, Stability, and Thermophysical Properties," *Journal of Nanomaterials,* vol. 2018, p. 6978130, 2018/06/04 2018, doi: 10.1155/2018/6978130.

[153] L. Yang, W. Ji, M. Mao, and J.-n. Huang, "An updated review on the properties, fabrication and application of hybrid-nanofluids along with their environmental effects," *Journal of Cleaner Production,* vol. 257, p. 120408, 2020/06/01/ 2020, doi: https://doi.org/10.1016/j.jclepro.2020.120408.

[154] K.-F. V. Wong and T. Kurma, "Transport properties of alumina nanofluids," *Nanotechnology,* vol. 19, no. 34, p. 345702, 2008/07/16 2008, doi: 10.1088/0957-4484/19/34/345702.

[155] N. Kumar and S. S. Sonawane, "Experimental study of Fe2O3/water and Fe2O3/ethylene glycol nanofluid heat transfer enhancement in a shell and tube heat exchanger," *International Communications in Heat and Mass Transfer,* vol. 78, pp. 277-284, 2016/11/01/ 2016, doi: https://doi.org/10.1016/j.icheatmasstransfer.2016.09.009.

[156] J. G. Monroe, S. Kumari, J. D. Fairley, K. B. Walters, M. J. Berg, and S. M. Thompson, "On the energy harvesting and heat transfer ability of a ferro-nanofluid oscillating heat pipe," *International Journal of Heat and Mass Transfer,* vol. 132, pp. 162-171, 2019/04/01/ 2019, doi: https://doi.org/10.1016/j.ijheatmasstransfer.2018.11.096.

[157] V. Nageswara Rao and B. Ravi Sankar, "Heat transfer and friction factor investigations of CuO nanofluid flow in a double pipe U-bend heat exchanger," *Materials Today: Proceedings,* vol. 18, pp. 207-218, 2019/01/01/ 2019, doi: https://doi.org/10.1016/j.matpr.2019.06.294.

[158] M. E. Nakhchi and J. A. Esfahani, "CFD approach for two-phase CuO nanofluid flow through heat exchangers enhanced by double perforated louvered strip insert," *Powder Technology,* vol. 367, pp. 877-888, 2020/05/01/ 2020, doi: https://doi.org/10.1016/j.powtec.2020.04.043.

[159] S. S. J. Aravind and S. Ramaprabhu, "Graphene–multiwalled carbon nanotube-based nanofluids for improved heat dissipation," *RSC Advances,* 10.1039/C3RA22653K vol. 3, no. 13, pp. 4199-4206, 2013, doi: 10.1039/C3RA22653K.

[160] A. D. Manasrah, Ismail W. Almanassra, N. N. Marei, U. A. Al-Mubaiyedh, T. Laoui, and M. A. Atieh, "Surface modification of carbon nanotubes with copper oxide nanoparticles for heat transfer enhancement of nanofluids," *RSC Advances,* 10.1039/C7RA10406E vol. 8, no. 4, pp. 1791-1802, 2018, doi: 10.1039/C7RA10406E.

[161] A. O. Borode, N. A. Ahmed, and P. A. Olubambi, "A review of heat transfer application of carbon-based nanofluid in heat exchangers," *Nano-Structures & Nano-Objects,* vol. 20, p. 100394, 2019/10/01/ 2019, doi: https://doi.org/10.1016/j.nanoso.2019.100394.

[162] D. R. Karana and R. R. Sahoo, "Performance effect on the TEG system for waste heat recovery in automobiles using ZnO and SiO2 nanofluid coolants," *Heat Transfer—Asian Research,* vol. 48, no. 1, pp. 216-232, 2019, doi: https://doi.org/10.1002/htj.21379.

[163] A. F. Niwalkar, J. M. Kshirsagar, and K. Kulkarni, "Experimental investigation of heat transfer enhancement in shell and helically coiled tube heat exchanger using SiO2/ water nanofluids," *Materials Today: Proceedings*, vol. 18, pp. 947-962, 2019/01/01/ 2019, doi: https://doi.org/10.1016/j.matpr.2019.06.532.

[164] D. Huang, Z. Wu, and B. Sunden, "Effects of hybrid nanofluid mixture in plate heat exchangers," *Experimental Thermal and Fluid Science*, vol. 72, pp. 190-196, 2016/04/01/ 2016, doi: https://doi.org/10.1016/j.expthermflusci.2015.11.009.

[165] S. Anitha, T. Thomas, V. Parthiban, and M. Pichumani, "What dominates heat transfer performance of hybrid nanofluid in single pass shell and tube heat exchanger?," *Advanced Powder Technology*, vol. 30, no. 12, pp. 3107-3117, 2019/12/01/ 2019, doi: https://doi.org/10.1016/j.apt.2019.09.018.

[166] S. K. Singh and J. Sarkar, "Improving hydrothermal performance of hybrid nanofluid in double tube heat exchanger using tapered wire coil turbulator," *Advanced Powder Technology*, vol. 31, no. 5, pp. 2092-2100, 2020.

[167] S. A. Angayarkanni and J. Philip, "Review on thermal properties of nanofluids: Recent developments," *Advances in Colloid and Interface Science*, vol. 225, pp. 146-176, 2015/11/01/ 2015, doi: https://doi.org/10.1016/j.cis.2015.08.014.

[168] R. B. Ganvir, P. V. Walke, and V. M. Kriplani, "Heat transfer characteristics in nanofluid—A review," *Renewable and Sustainable Energy Reviews*, vol. 75, pp. 451-460, 2017/08/01/ 2017, doi: https://doi.org/10.1016/j.rser.2016.11.010.

[169] P. C. Mukesh Kumar and M. Chandrasekar, "A review on helically coiled tube heat exchanger using nanofluids," *Materials Today: Proceedings*, vol. 21, pp. 137-141, 2020/01/01/ 2020, doi: https://doi.org/10.1016/j.matpr.2019.04.199.

[170] M. Awais *et al.*, "Heat transfer and pressure drop performance of Nanofluid: A state-of- the-art review," *International Journal of Thermofluids*, vol. 9, p. 100065, 2021/02/01/ 2021, doi: https://doi.org/10.1016/j.ijft.2021.100065.

[171] Y. Xuan and Q. Li, "Heat transfer enhancement of nanofluids," *International Journal of heat and fluid flow*, vol. 21, no. 1, pp. 58-64, 2000.

[172] R. R. Riehl and S. Mancin, "Estimation of Thermophysical Properties for Accurate Numerical Simulation of Nanofluid Heat Transfer Applied to a Loop Heat Pipe," *International Journal of Thermofluids*, p. 100158, 2022.

[173] L. S. Sundar, P. Bhramara, N. R. Kumar, M. K. Singh, and A. C. Sousa, "Experimental heat transfer, friction factor and effectiveness analysis of Fe3O4 nanofluid flow in a horizontal plain tube with return bend and wire coil inserts," *International Journal of Heat and Mass Transfer*, vol. 109, pp. 440-453, 2017.

[174] W. Duangthongsuk and S. Wongwises, "Heat transfer enhancement and pressure drop characteristics of TiO2–water nanofluid in a double-tube counter flow heat exchanger," *International Journal of Heat and Mass Transfer*, vol. 52, no. 7-8, pp. 2059-2067, 2009.

[175] A. M. Hussein, "Thermal performance and thermal properties of hybrid nanofluid laminar flow in a double pipe heat exchanger," *Experimental Thermal and Fluid Science*, vol. 88, pp. 37-45, 2017.

[176] N. R. Kumar, P. Bhramara, B. M. Addis, L. S. Sundar, M. K. Singh, and A. C. Sousa, "Heat transfer, friction factor and effectiveness analysis of Fe3O4/water nanofluid flow in a double pipe heat exchanger with return bend," *International Communications in Heat and Mass Transfer*, vol. 81, pp. 155-163, 2017.

[177] N. R. Kumar, P. Bhramara, L. S. Sundar, M. K. Singh, and A. C. Sousa, "Heat transfer, friction factor and effectiveness of Fe3O4 nanofluid flow in an inner tube of double pipe U-bend heat exchanger with and without longitudinal strip inserts," *Experimental Thermal and Fluid Science*, vol. 85, pp. 331-343, 2017.

[178] M. H. Esfe, S. Saedodin, O. Mahian, and S. Wongwises, "Heat transfer characteristics and pressure drop of COOH-functionalized DWCNTs/water nanofluid in turbulent flow at low concentrations," *International Journal of Heat and Mass Transfer,* vol. 73, pp. 186-194, 2014.
[179] A. A. Arani and J. Amani, "Experimental study on the effect of TiO2–water nanofluid on heat transfer and pressure drop," *Experimental Thermal and Fluid Science,* vol. 42, pp. 107-115, 2012.
[180] M. H. Esfe, S. Saedodin, and M. Mahmoodi, "Experimental studies on the convective heat transfer performance and thermophysical properties of MgO–water nanofluid under turbulent flow," *Experimental thermal and fluid science,* vol. 52, pp. 68-78, 2014.
[181] A. J. N. Khalifa and M. A. Banwan, "Effect of volume fraction of γ-Al2O3 nanofluid on heat transfer enhancement in a concentric tube heat exchanger," *Heat Transfer Engineering,* vol. 36, no. 16, pp. 1387-1396, 2015.
[182] R. S. Khedkar, S. S. Sonawane, and K. L. Wasewar, "Heat transfer study on concentric tube heat exchanger using TiO2–water based nanofluid," *International communications in Heat and Mass transfer,* vol. 57, pp. 163-169, 2014.
[183] M. Goodarzi *et al.*, "Investigation of heat transfer performance and friction factor of a counter-flow double-pipe heat exchanger using nitrogen-doped, graphene-based nanofluids," *International Communications in Heat and Mass Transfer,* vol. 76, pp. 16-23, 2016.
[184] H. M. Maghrabie *et al.*, "Intensification of heat exchanger performance utilizing nanofluids," *International Journal of Thermofluids,* vol. 10, p. 100071, 2021.
[185] W. M. El-Maghlany, A. A. Hanafy, A. A. Hassan, and M. A. El-Magid, "Experimental study of Cu–water nanofluid heat transfer and pressure drop in a horizontal double-tube heat exchanger," *Experimental Thermal and Fluid Science,* vol. 78, pp. 100-111, 2016.
[186] D. Han, W. He, and F. Asif, "Experimental study of heat transfer enhancement using nanofluid in double tube heat exchanger," *Energy Procedia,* vol. 142, pp. 2547-2553, 2017.
[187] C. Qi, T. Luo, M. Liu, F. Fan, and Y. Yan, "Experimental study on the flow and heat transfer characteristics of nanofluids in double-tube heat exchangers based on thermal efficiency assessment," *Energy Conversion and Management,* vol. 197, p. 111877, 2019.
[188] A. Zamzamian, S. N. Oskouie, A. Doosthoseini, A. Joneidi, and M. Pazouki, "Experimental investigation of forced convective heat transfer coefficient in nanofluids of Al2O3/EG and CuO/EG in a double pipe and plate heat exchangers under turbulent flow," *Experimental Thermal and Fluid Science,* vol. 35, no. 3, pp. 495-502, 2011.
[189] A. R. Darzi, M. Farhadi, and K. Sedighi, "Heat transfer and flow characteristics of Al2O3–water nanofluid in a double tube heat exchanger," *International Communications in Heat and Mass Transfer,* vol. 47, pp. 105-112, 2013.
[190] R. Aghayari, H. Maddah, F. Ashori, A. Hakiminejad, and M. Aghili, "Effect of nanoparticles on heat transfer in mini double-pipe heat exchangers in turbulent flow," *Heat and Mass Transfer,* vol. 51, no. 3, pp. 301-306, 2015/03/01 2015, doi: 10.1007/s00231-014-1415-0.
[191] M. Sarafraz and F. Hormozi, "Intensification of forced convection heat transfer using biological nanofluid in a double-pipe heat exchanger," *Experimental Thermal and Fluid Science,* vol. 66, pp. 279-289, 2015.
[192] M. A. E.-M. Mohamed, A. J. Gutiérrez-Trashorras, and E. B. Marigorta, "Numerical Investigation of Heat Transfer with Nanofluids in Concentric Tube Heat Exchanger under Transitional Flow," *Energy,* vol. 1, no. 1, 2020.

[193] D. Zheng, J. Wang, Y. Pang, Z. Chen, and B. Sundén, "Heat transfer performance and friction factor of various nanofluids in a double-tube counter flow heat exchanger," *Thermal Science*, no. 00, pp. 280-280, 2020.
[194] W. Duangthongsuk and S. Wongwises, "An experimental study on the heat transfer performance and pressure drop of TiO2-water nanofluids flowing under a turbulent flow regime," *International Journal of Heat and Mass Transfer*, vol. 53, no. 1-3, pp. 334-344, 2010.
[195] D. Madhesh and S. Kalaiselvam, "Experimental study on the heat transfer and flow properties of Ag–ethylene glycol nanofluid as a coolant," *Heat and Mass Transfer*, vol. 50, no. 11, pp. 1597-1607, 2014.
[196] D. Nagaraju and A. R. Mohammad, "Effect of graphene-based nanofluid on heat transfer performance of alternate elliptical axis oval tube heat exchanger," *Applied Nanoscience*, vol. 12, no. 6, pp. 1839-1858, 2022.
[197] S. H. Hashemi Karouei, S. S. M. Ajarostaghi, M. Gorji-Bandpy, and S. R. Hosseini Fard, "Laminar heat transfer and fluid flow of two various hybrid nanofluids in a helical double-pipe heat exchanger equipped with an innovative curved conical turbulator," *Journal of Thermal Analysis and Calorimetry*, vol. 143, no. 2, pp. 1455-1466, 2021.
[198] V. Mokkapati and C.-S. Lin, "Numerical study of an exhaust heat recovery system using corrugated tube heat exchanger with twisted tape inserts," *International Communications in Heat and Mass Transfer*, vol. 57, pp. 53-64, 2014/10/01/ 2014, doi: https://doi.org/10.1016/j.icheatmasstransfer.2014.07.002.
[199] H. Maddah, M. Alizadeh, N. Ghasemi, and S. R. Wan Alwi, "Experimental study of Al2O3/water nanofluid turbulent heat transfer enhancement in the horizontal double pipes fitted with modified twisted tapes," *International Journal of Heat and Mass Transfer*, vol. 78, pp. 1042-1054, 2014/11/01/ 2014, doi: https://doi.org/10.1016/j.ijheatmasstransfer.2014.07.059.
[200] M. Nakhchi and J. Esfahani, "Numerical investigation of turbulent Cu-water nanofluid in heat exchanger tube equipped with perforated conical rings," *Advanced Powder Technology*, vol. 30, no. 7, pp. 1338-1347, 2019.
[201] O. Sadeghi, H. Mohammed, M. Bakhtiari-Nejad, and M. Wahid, "Heat transfer and nanofluid flow characteristics through a circular tube fitted with helical tape inserts," *International Communications in Heat and Mass Transfer*, vol. 71, pp. 234-244, 2016.
[202] S. Suresh, K. Venkitaraj, and P. Selvakumar, "Comparative study on thermal performance of helical screw tape inserts in laminar flow using Al2O3/water and CuO/water nanofluids," *Superlattices and Microstructures*, vol. 49, no. 6, pp. 608-622, 2011.
[203] K. Sharma, L. S. Sundar, and P. Sarma, "Estimation of heat transfer coefficient and friction factor in the transition flow with low volume concentration of Al2O3 nanofluid flowing in a circular tube and with twisted tape insert," *International Communications in Heat and Mass Transfer*, vol. 36, no. 5, pp. 503-507, 2009.
[204] K. Wongcharee and S. Eiamsa-Ard, "Enhancement of heat transfer using CuO/water nanofluid and twisted tape with alternate axis," *International Communications in Heat and Mass Transfer*, vol. 38, no. 6, pp. 742-748, 2011.
[205] M. Naik, G. R. Janardana, and L. S. Sundar, "Experimental investigation of heat transfer and friction factor with water–propylene glycol based CuO nanofluid in a tube with twisted tape inserts," *International Communications in Heat and Mass Transfer*, vol. 46, pp. 13-21, 2013.
[206] W. Azmi, K. Sharma, P. Sarma, R. Mamat, S. Anuar, and L. S. Sundar, "Numerical validation of experimental heat transfer coefficient with SiO2 nanofluid flowing in a

tube with twisted tape inserts," *Applied Thermal Engineering,* vol. 73, no. 1, pp. 296-306, 2014.

[207] S. Eiamsa-ard and K. Kiatkittipong, "Heat transfer enhancement by multiple twisted tape inserts and TiO2/water nanofluid," *Applied Thermal Engineering,* vol. 70, no. 1, pp. 896-924, 2014.

[208] M. Naik, S. S. Fahad, L. S. Sundar, and M. K. Singh, "Comparative study on thermal performance of twisted tape and wire coil inserts in turbulent flow using CuO/water nanofluid," *Experimental Thermal and Fluid Science,* vol. 57, pp. 65-76, 2014.

[209] W. Azmi, K. Sharma, P. Sarma, R. Mamat, and S. Anuar, "Comparison of convective heat transfer coefficient and friction factor of TiO2 nanofluid flow in a tube with twisted tape inserts," *International Journal of Thermal Sciences,* vol. 81, pp. 84-93, 2014.

[210] A. Azari and M. Derakhshandeh, "An experimental comparison of convective heat transfer and friction factor of Al2O3 nanofluids in a tube with and without butterfly tube inserts," *Journal of the Taiwan Institute of Chemical Engineers,* vol. 52, pp. 31-39, 2015.

[211] M. Akhavan-Behabadi, M. Shahidi, and M. Aligoodarz, "An experimental study on heat transfer and pressure drop of MWCNT–water nano-fluid inside horizontal coiled wire inserted tube," *International Communications in Heat and Mass Transfer,* vol. 63, pp. 62-72, 2015.

[212] S. S. Chougule and S. Sahu, "Heat transfer and friction characteristics of Al2O3/water and CNT/water nanofluids in transition flow using helical screw tape inserts–a comparative study," *Chemical Engineering and Processing: Process Intensification,* vol. 88, pp. 78-88, 2015.

[213] M. Khoshvaght-Aliabadi and M. Eskandari, "Influence of twist length variations on thermal–hydraulic specifications of twisted-tape inserts in presence of Cu–water nanofluid," *Experimental Thermal and Fluid Science,* vol. 61, pp. 230-240, 2015.

[214] L. S. Sundar, G. Otero-Irurueta, M. K. Singh, and A. C. Sousa, "Heat transfer and friction factor of multi-walled carbon nanotubes–Fe3O4 nanocomposite nanofluids flow in a tube with/without longitudinal strip inserts," *International Journal of Heat and Mass Transfer,* vol. 100, pp. 691-703, 2016.

[215] S. Chougule, V. V. Nirgude, P. D. Gharge, M. Mayank, and S. Sahu, "Heat transfer enhancements of low volume concentration CNT/water nanofluid and wire coil inserts in a circular tube," *Energy Procedia,* vol. 90, pp. 552-558, 2016.

[216] R. Mashayekhi, E. Khodabandeh, M. Bahiraei, L. Bahrami, D. Toghraie, and O. A. Akbari, "Application of a novel conical strip insert to improve the efficacy of water–Ag nanofluid for utilization in thermal systems: a two-phase simulation," *Energy Conversion and Management,* vol. 151, pp. 573-586, 2017.

[217] W. Bai, W. Chen, C. Zeng, G. Wu, and X. Chai, "Thermo-hydraulic performance investigation of heat pipe used annular heat exchanger with densely longitudinal fins," *Applied Thermal Engineering,* vol. 211, p. 118451, 2022.

[218] M. Chandra Sekhara Reddy and V. Vasudeva Rao, "Experimental investigation of heat transfer coefficient and friction factor of ethylene glycol water based TiO2 nanofluid in double pipe heat exchanger with and without helical coil inserts," *International Communications in Heat and Mass Transfer,* vol. 50, pp. 68-76, 2014/01/01/ 2014, doi: https://doi.org/10.1016/j.icheatmasstransfer.2013.11.002.

[219] P. V. D. Prasad, A. V. S. S. K. S. Gupta, and K. Deepak, "Investigation of Trapezoidal-Cut Twisted Tape Insert in a Double Pipe U-Tube Heat Exchanger using Al2O3/Water Nanofluid," *Procedia Materials Science,* vol. 10, pp. 50-63, 2015/01/01/ 2015, doi: https://doi.org/10.1016/j.mspro.2015.06.025.

[220] A. Karimi, A. A. Al-Rashed, M. Afrand, O. Mahian, S. Wongwises, and A. Shahsavar, "The effects of tape insert material on the flow and heat transfer in a nanofluid-based double tube heat exchanger: two-phase mixture model," *International Journal of Mechanical Sciences*, vol. 156, pp. 397-409, 2019.
[221] C. Gnanavel, R. Saravanan, and M. Chandrasekaran, "Heat transfer augmentation by nano-fluids and Spiral Spring insert in Double Tube Heat Exchanger–A numerical exploration," *Materials Today: Proceedings*, vol. 21, pp. 857-861, 2020.
[222] M. Karuppasamy, R. Saravanan, M. Chandrasekaran, and V. Muthuraman, "Numerical exploration of heat transfer in a heat exchanger tube with cone shape inserts and Al2O3 and CuO nanofluids," *Materials Today: Proceedings*, vol. 21, pp. 940-947, 2020.
[223] S. K. Singh and J. Sarkar, "Experimental hydrothermal characteristics of concentric tube heat exchanger with V-cut twisted tape turbulator using PCM dispersed mono/hybrid nanofluids," *Experimental Heat Transfer*, pp. 1-22, 2020.
[224] S. K. Singh and J. Sarkar, "Thermohydraulic behavior of concentric tube heat exchanger inserted with conical wire coil using mono/hybrid nanofluids," *International Communications in Heat and Mass Transfer*, vol. 122, p. 105134, 2021.
[225] M. Khoshvaght-Aliabadi, H. Shabanpour, A. Alizadeh, and O. Sartipzadeh, "Experimental assessment of different inserts inside straight tubes: Nanofluid as working media," *Chemical Engineering and Processing: Process Intensification*, vol. 97, pp. 1-11, 2015.
[226] P. D. Prasad, A. Gupta, M. Sreeramulu, L. S. Sundar, M. Singh, and A. C. Sousa, "Experimental study of heat transfer and friction factor of Al2O3 nanofluid in U-tube heat exchanger with helical tape inserts," *Experimental thermal and fluid science*, vol. 62, pp. 141-150, 2015.
[227] M. Khoshvaght-Aliabadi, M. Akbari, and F. Hormozi, "An empirical study on vortex-generator insert fitted in tubular heat exchangers with dilute Cu–water nanofluid flow," *Chinese journal of chemical engineering*, vol. 24, no. 6, pp. 728-736, 2016.
[228] P. D. Prasad and A. Gupta, "Experimental investigation on enhancement of heat transfer using Al2O3/water nanofluid in a u-tube with twisted tape inserts," *International Communications in Heat and Mass Transfer*, vol. 75, pp. 154-161, 2016.
[229] S. Khanmohammadi, Z. Rahimi, S. Khanmohammadi, and M. Afrand, "Triple-objective optimization of a double-tube heat exchanger with elliptic cross section in the presence TiO 2 nanofluid," *Journal of Thermal Analysis and Calorimetry*, vol. 140, no. 1, pp. 477-488, 2020.
[230] P. M. Kumar and M. Chandrasekar, "Heat transfer and friction factor analysis of MWCNT nanofluids in double helically coiled tube heat exchanger," *Journal of Thermal Analysis and Calorimetry*, pp. 1-13, 2020.
[231] G. Huminic and A. Huminic, "Heat transfer characteristics in double tube helical heat exchangers using nanofluids," *International Journal of Heat and Mass Transfer*, vol. 54, no. 19-20, pp. 4280-4287, 2011.
[232] Z. Wu, L. Wang, and B. Sundén, "Pressure drop and convective heat transfer of water and nanofluids in a double-pipe helical heat exchanger," *Applied Thermal Engineering*, vol. 60, no. 1, pp. 266-274, 2013/10/02/ 2013, doi: https://doi.org/10.1016/j.applthermaleng.2013.06.051.
[233] W. I. A. Aly, "Numerical study on turbulent heat transfer and pressure drop of nanofluid in coiled tube-in-tube heat exchangers," *Energy Conversion and Management*, vol. 79, pp. 304-316, 2014/03/01/ 2014, doi: https://doi.org/10.1016/j.enconman.2013.12.031.
[234] A. A. Lakew and O. Bolland, "Working fluids for low-temperature heat source," *Applied Thermal Engineering*, vol. 30, no. 10, pp. 1262-1268, 2010.

[235] S. Padmanabhan, O. Y. Reddy, K. V. A. K. Yadav, V. B. Raja, and K. Palanikumar, "Heat transfer analysis of double tube heat exchanger with helical inserts," *Materials Today: Proceedings*, vol. 46, pp. 3588-3595, 2021.
[236] H. Eshgarf, A. A. Nadooshan, and A. Raisi, "A review of multi-phase and single-phase models in the numerical simulation of nanofluid flow in heat exchangers," *Engineering Analysis with Boundary Elements*, vol. 146, pp. 910-927, 2023.
[237] A. Albojamal and K. Vafai, "Analysis of single phase, discrete and mixture models, in predicting nanofluid transport," *International Journal of Heat and Mass Transfer,* vol. 114, pp. 225-237, 2017.
[238] F. P. Incropera, D. P. DeWitt, T. L. Bergman, and A. S. Lavine, *Fundamentals of heat and mass transfer*. Wiley New York, 1996.
[239] L.-L. Tian, X. Liu, S. Chen, and Z.-G. Shen, "Effect of fin material on PCM melting in a rectangular enclosure," *Applied Thermal Engineering,* vol. 167, p. 114764, 2020.
[240] C. Raju, N. A. Ahammad, K. Sajjan, N. A. Shah, S.-J. Yook, and M. D. Kumar, "Nonlinear movements of axisymmetric ternary hybrid nanofluids in a thermally radiated expanding or contracting permeable Darcy Walls with different shapes and densities: Simple linear regression," *International Communications in Heat and Mass Transfer,* vol. 135, p. 106110, 2022.
[241] R. K. Ajeel, K. Sopian, and R. Zulkifli, "A novel curved-corrugated channel model: thermal-hydraulic performance and design parameters with nanofluid," *International Communications in Heat and Mass Transfer*, vol. 120, p. 105037, 2021.
[242] K. Sharma, P. Sarma, W. Azmi, R. Mamat, and K. Kadirgama, "Correlations to predict friction and forced convection heat transfer coefficients of water based nanofluids for turbulent flow in a tube," *International Journal of Microscale and Nanoscale Thermal and Fluid Transport Phenomena,* vol. 3, no. 4, pp. 1-25, 2012.
[243] X. Zhou, Y. Jiang, Y. Wang, Y. Jiang, and H. Huang, "Comprehensive heat transfer performance analysis of liquid metal based nanofluid laminar flow in circular tube," *International Journal of Mechanical Sciences,* vol. 175, p. 105530, 2020.
[244] T. Hayat, M. Imtiaz, A. Alsaedi, and M. A. Kutbi, "MHD three-dimensional flow of nanofluid with velocity slip and nonlinear thermal radiation," *Journal of Magnetism and Magnetic Materials,* vol. 396, pp. 31-37, 2015.
[245] H. Kaneez *et al.*, "Thermal analysis of magnetohydrodynamics (MHD) Casson fluid with suspended iron (II, III) oxide-aluminum oxide-titanium dioxide ternary-hybrid nanostructures," *Journal of Magnetism and Magnetic Materials,* vol. 586, p. 171223, 2023.
[246] A. Ijam and R. Saidur, "Nanofluid as a coolant for electronic devices (cooling of electronic devices)," *Applied Thermal Engineering,* vol. 32, pp. 76-82, 2012.
[247] T. Anwar, P. Kumam, and S. Muhammad, "New fractional model to analyze impacts of Newtonian heating, shape factor and ramped flow function on MgO–SiO2–Kerosene oil hybrid nanofluid," *Case Studies in Thermal Engineering,* vol. 38, p. 102361, 2022.
[248] E. N. Sieder and G. E. Tate, "Heat transfer and pressure drop of liquids in tubes," *Industrial & Engineering Chemistry,* vol. 28, no. 12, pp. 1429-1435, 1936.
[249] R. K. Shah and A. L. London, *Laminar flow forced convection in ducts: a source book for compact heat exchanger analytical data*. Academic press, 2014.
[250] V. Gnielinski, "New equations for heat and mass transfer in turbulent pipe and channel flow," *International chemical engineering,* vol. 16, no. 2, pp. 359-367, 1976.
[251] H. Hausen, "Neue Gleichungen fur die Warmeubertragung bei freier oder erzwungener Stromung," *Allg. Waermetech,* vol. 9, pp. 75-79, 1959.
[252] M. H. Bahmani, O. A. Akbari, M. Zarringhalam, G. Ahmadi Sheikh Shabani, and M. Goodarzi, "Forced convection in a double tube heat exchanger using nanofluids with

constant and variable thermophysical properties," *International Journal of Numerical Methods for Heat & Fluid Flow,* vol. 30, no. 6, pp. 3247-3265, 2020.
[253] K. M. Shirvan, M. Mamourian, S. Mirzakhanlari, and R. Ellahi, "Numerical investigation of heat exchanger effectiveness in a double pipe heat exchanger filled with nanofluid: a sensitivity analysis by response surface methodology," *Powder Technology,* vol. 313, pp. 99-111, 2017.
[254] M. Heyhat, F. Kowsary, A. Rashidi, M. Momenpour, and A. Amrollahi, "Experimental investigation of laminar convective heat transfer and pressure drop of water-based Al2O3 nanofluids in fully developed flow regime," *Experimental Thermal and Fluid Science,* vol. 44, pp. 483-489, 2013.
[255] S. Hong and A. Bergles, "Augmentation of laminar flow heat transfer in tubes by means of twisted-tape inserts," 1976.
[256] M. Iwaniszyn *et al.*, "Entrance effects on forced convective heat transfer in laminar flow through short hexagonal channels: Experimental and CFD study," *Chemical Engineering Journal,* vol. 405, p. 126635, 2021.
[257] M. Gupta, V. Singh, R. Kumar, and Z. Said, "A review on thermophysical properties of nanofluids and heat transfer applications," *Renewable and Sustainable Energy Reviews,* vol. 74, pp. 638-670, 2017.
[258] A. Sofiah, M. Samykano, A. Pandey, K. Kadirgama, K. Sharma, and R. Saidur, "Immense impact from small particles: Review on stability and thermophysical properties of nanofluids," *Sustainable Energy Technologies and Assessments,* vol. 48, p. 101635, 2021.
[259] M. Awais, A. A. Bhuiyan, S. Salehin, M. M. Ehsan, B. Khan, and M. H. Rahman, "Synthesis, heat transport mechanisms and thermophysical properties of nanofluids: A critical overview," *International Journal of Thermofluids,* vol. 10, p. 100086, 2021.
[260] O. A. Akbari, D. Toghraie, A. Karimipour, A. Marzban, and G. R. Ahmadi, "The effect of velocity and dimension of solid nanoparticles on heat transfer in non-Newtonian nanofluid," *Physica E: Low-Dimensional Systems and Nanostructures,* vol. 86, pp. 68-75, 2017.
[261] A. Kamyar, R. Saidur, and M. Hasanuzzaman, "Application of computational fluid dynamics (CFD) for nanofluids," *International Journal of Heat and Mass Transfer,* vol. 55, no. 15-16, pp. 4104-4115, 2012.
[262] T. Bergman, "Effect of reduced specific heats of nanofluids on single phase, laminar internal forced convection," *International Journal of heat and mass Transfer,* vol. 52, no. 5-6, pp. 1240-1244, 2009.
[263] D. Dey, P. Kumar, and S. Samantaray, "A review of nanofluid preparation, stability, and thermo-physical properties," *Heat Transfer—Asian Research,* vol. 46, no. 8, pp. 1413-1442, 2017.
[264] S. E. B. Maïga, C. T. Nguyen, N. Galanis, and G. Roy, "Heat transfer behaviours of nanofluids in a uniformly heated tube," *Superlattices and Microstructures,* vol. 35, no. 3-6, pp. 543-557, 2004.
[265] P. Keblinski, J. A. Eastman, and D. G. Cahill, "Nanofluids for thermal transport," *Materials today,* vol. 8, no. 6, pp. 36-44, 2005.
[266] S. El Bécaye Maïga, C. Tam Nguyen, N. Galanis, G. Roy, T. Maré, and M. Coqueux, "Heat transfer enhancement in turbulent tube flow using Al2O3 nanoparticle suspension," *International Journal of Numerical Methods for Heat & Fluid Flow,* vol. 16, no. 3, pp. 275-292, 2006.
[267] R. S. Vajjha and D. K. Das, "Experimental determination of thermal conductivity of three nanofluids and development of new correlations," *International journal of heat and mass transfer,* vol. 52, no. 21-22, pp. 4675-4682, 2009.

[268] M. M. Heyhat, A. Abdi, and A. Jafarzad, "Performance evaluation and exergy analysis of a double pipe heat exchanger under air bubble injection," *Applied Thermal Engineering,* vol. 143, pp. 582-593, 2018.
[269] A. Bejan, G. Tsatsaronis, and M. Moran, "Thermal Design and Optimization John Wiley and Sons," *Inc. New York,* 1996.
[270] H. S. Dizaji, S. Jafarmadar, M. Abbasalizadeh, and S. Khorasani, "Experiments on air bubbles injection into a vertical shell and coiled tube heat exchanger; exergy and NTU analysis," *Energy Conversion and Management,* vol. 103, pp. 973-980, 2015.
[271] J. Lin, Y. Hong, and J. Lu, "New method for the determination of convective heat transfer coefficient in fully-developed laminar pipe flow," *Acta Mechanica Sinica,* vol. 38, no. 1, pp. 1-10, 2022.
[272] H. E. Ahmed, M. Ahmed, I. M. Seder, and B. Salman, "Experimental investigation for sequential triangular double-layered microchannel heat sink with nanofluids," *International Communications in Heat and Mass Transfer,* vol. 77, pp. 104-115, 2016.
[273] F. M. White, *Fluid mechanics*. Tata McGraw-Hill Education, 1979.
[274] M. Noorbakhsh, S. S. M. Ajarostaghi, M. Zaboli, and B. Kiani, "Thermal analysis of nanofluids flow in a double pipe heat exchanger with twisted tapes insert in both sides," *Journal of Thermal Analysis and Calorimetry,* vol. 147, no. 5, pp. 3965-3976, 2022.
[275] N. Mashoofi, S. Pourahmad, and S. Pesteei, "Study the effect of axially perforated twisted tapes on the thermal performance enhancement factor of a double tube heat exchanger," *Case studies in thermal engineering,* vol. 10, pp. 161-168, 2017.
[276] M. Hemmat Esfe, A. A. Abbasian Arani, R. Shafiei Badi, and M. Rejvani, "ANN modeling, cost performance and sensitivity analyzing of thermal conductivity of DWCNT–SiO2/EG hybrid nanofluid for higher heat transfer," *Journal of Thermal Analysis and Calorimetry,* vol. 131, no. 3, pp. 2381-2393, 2018.
[277] M. H. Bahmani, O. A. Akbari, M. Zarringhalam, G. A. S. Shabani, and M. Goodarzi, "Forced convection in a double tube heat exchanger using nanofluids with constant and variable thermophysical properties," *International Journal of Numerical Methods for Heat & Fluid Flow,* 2019.
[278] A. Salimi, M. Khoshvaght-Aliabadi, and S. Rashidi, "On thermal management of pouch type lithium-ion batteries by novel designs of wavy minichannel cold plates: Comparison of co-flow with counter-flow," *Journal of Energy Storage,* vol. 52, p. 104819, 2022.
[279] M. Khoshvaght-Aliabadi, A. Feizabadi, A. Salimi, and M. M. Rashidi, "Temperature nonuniformity management in heat sinks through applying counter-flow design complex minichannels," *Korean Journal of Chemical Engineering,* vol. 39, no. 6, pp. 1436-1449, 2022.
[280] A. K. Tiwari, P. Ghosh, and J. Sarkar, "Performance comparison of the plate heat exchanger using different nanofluids," *Experimental Thermal and Fluid Science,* vol. 49, pp. 141-151, 2013.
[281] D. Yogaraj *et al.*, "Thermal performance analysis of a counter-flow double-pipe heat exchanger using titanium oxide and zinc oxide nanofluids," *Materials Today: Proceedings,* 2023.
[282] J. C. Tyacke, Y. Dai, and P. G. Tucker, "Impact of rib shape on heat transfer using LES," *Applied Mathematical Modelling,* vol. 97, pp. 244-267, 2021.
[283] G. S. Dhumal and S. N. Havaldar, "Enhancing heat transfer performance in a double tube heat exchanger: Experimental study with twisted and helical tapes," *Case Studies in Thermal Engineering,* vol. 51, p. 103613, 2023.
[284] N. M. Maleki, S. Pourahmad, R. H. Khoshkhoo, and M. Ameri, "Performance improvement of a double tube heat exchanger using novel electromagnetic vibration

(EMV) method in the presence of Al2O3-water and CuO-water nanofluid; An experimental study," *Energy,* vol. 281, p. 128193, 2023.
[285] S. Marzouk, F. A. Almehmadi, A. Aljabr, and M. A. Sharaf, "Numerical and experimental investigation of heat transfer enhancement in double tube heat exchanger using nail rod inserts," *Scientific Reports,* vol. 14, no. 1, p. 9637, 2024.
[286] P. K. Chaurasiya *et al.*, "Heat transfer and friction factor correlations for double pipe heat exchanger with inner and outer corrugation," *Energy Sources, Part A: Recovery, Utilization, and Environmental Effects,* vol. 45, no. 1, pp. 18-45, 2023.
[287] S. T. Firoozeh, N. Pourmahmoud, and M. Khalilian, "Two-tube heat exchanger with variable groove angle on the inner pipe surface: Experimental study," *Applied Thermal Engineering,* vol. 234, p. 121274, 2023.
[288] G. Ashraf, S. Bilal, M. Ishaq, S. K. Saifullah, A. Alqahtani, and M. Malik, "Thermodynamic optimization in laminar and fully developed flow in double pipe heat exchanger with arrow-shaped extended surfaces: a novel design," *Case Studies in Thermal Engineering,* vol. 54, p. 103947, 2024.
[289] M. A. Sharaf, S. Marzouk, A. Aljabr, F. A. Almehmadi, A. Kaood, and S. Alqaed, "Heat transfer enhancement in a double-pipe helical heat exchanger using spring wire insert and nanofluid," *Journal of Thermal Analysis and Calorimetry,* pp. 1-17, 2024.
[290] A. M. Jawarneh, M. Al-Widyan, and Z. Al-Mashhadani, "Experimental study on heat transfer augmentation in a double pipe heat exchanger utilizing jet vortex flow," *Heat Transfer,* vol. 52, no. 1, pp. 317-332, 2023.
[291] J. Li, S. Hou, D. Teng, and G. Shen, "Experimental research on enhanced heat transfer of double-pipe exchanger with audible acoustic field," *International Journal of Heat and Mass Transfer,* vol. 201, p. 123565, 2023.
[292] M. Hedeshi, A. Jalali, A. Arabkoohsar, and A. Amiri Delouei, "Nanofluid as the working fluid of an ultrasonic-assisted double-pipe counter-flow heat exchanger," *Journal of Thermal Analysis and Calorimetry,* vol. 148, no. 16, pp. 8579-8591, 2023.
[293] M. A. Sharaf, S. Marzouk, A. Aljabr, F. A. Almehmadi, T. Alam, and D. A. Teklemariyem, "Effects of multi-spring wires on hydrothermal performance of double tube heat exchanger," *Case Studies in Thermal Engineering,* vol. 60, p. 104689, 2024.
[294] S. R. Chaurasia and R. Sarviya, "Experimental thermal performance analysis of fluid flow in a heat exchanger pipe with novel double strip helical screw tape inserts for utilization of energy resources," *Energy Sources, Part A: Recovery, Utilization, and Environmental Effects,* vol. 45, no. 2, pp. 4268-4281, 2023.
[295] B. K. Dandoutiya and A. Kumar, "Study of thermal performance of double pipe heat exchanger using W-cut twisted tape," *Energy Sources, Part A: Recovery, Utilization, and Environmental Effects,* vol. 45, no. 2, pp. 5221-5238, 2023.
[296] M. A. Ali and S. N. Shehab, "Numerical analysis of heat convection through a double-pipe heat exchanger: dimpled influence," *Journal of Engineering Research,* vol. 11, no. 1, p. 100016, 2023.
[297] Y. Zhang, M. Hangi, X. Wang, and A. Rahbari, "A comparative evaluation of double-pipe heat exchangers with enhanced mixing," *Applied Thermal Engineering,* vol. 230, p. 120793, 2023.
[298] M. F. Hasan, M. Danışmaz, and B. M. Majel, "Thermal performance investigation of double pipe heat exchanger embedded with extended surfaces using nanofluid technique as enhancement," *Case Studies in Thermal Engineering,* vol. 43, p. 102774, 2023.
[299] M. Izadi, H. M. Alshehri, F. Hosseinzadeh, M. S. Rad, and M. B. B. Hamida, "Numerical study on forced convection heat transfer of TiO2/water nanofluid flow

inside a double-pipe heat exchanger with spindle-shaped turbulators," *Engineering Analysis with Boundary Elements,* vol. 150, pp. 612-623, 2023.

[300] Y. Azizi, M. Bahramkhoo, and A. Kazemi, "Influence of non-uniform magnetic field on the thermal efficiency hydrodynamic characteristics of nanofluid in double pipe heat exchanger," *Scientific Reports,* vol. 13, no. 1, p. 407, 2023.

Appendices

Appendix A

Experimental setup and design overview of a double tube heat exchanger

This research encompasses the development of an experimental framework aimed at designing a novel double tube heat exchanger. Initially, quotations are obtained from various suppliers for standard double tube heat exchangers, which are summarised in Table 6.1. These models are typically solid and non-modular, lacking the flexibility required for our experimental purposes, especially the frequent cleaning necessitated by the use of nanofluids and the associated sedimentation. The double tube heat exchager's size, dimensions, and material were obtained from the literature review and previously published work.

To overcome these challenges, a new design is proposed that allows for easy disassembly and modification of the inner tube dimensions. This design not only meets the specific experimental requirements but also reduces overall costs compared to the previously available options. Figure 6.1 illustrates this design, highlighting the different parts of the DTHE. A key feature of this design includes the integration of a Poly Tetra Fluoro Ethylene (PTFE) gland mechanism, which adjusts to provide a tight seal around the inner tube. This adjustment is achieved by applying pressure through gland by two screws that expand the PTFE to seal the interface. The main parts of double tube heat exchanger are depicted in Figure 6.2 to Figure 6.6.

Furthermore, the experimental setup includes a comprehensive arrangement of the necessary apparatus configured on a test rig. This rig comprises the newly designed DTHE, storage tanks for hot and cold fluids, pumps for circulation, flow control valves, and various measurement devices such as flow meter, thermometer and pressure gauges, a chiller and a heater, which are used to maintain the required temperatures of the working fluids. The schematic of this setup is detailed in Figure 6.7. Materials selected for the outer and inner pipes are mild steel and copper (high thermal conductivity), respectively, in compliance with British and International Standards (ASTM).

Regarding Figure 6.7 the test rig includes a chiller and heater to regulate the temperature conditions within the DTHE. Fluid circulation is facilitated by two pumps, while flow rates are controlled using valves strategically positioned throughout the system. Prior to testing, all measurement devices, including a datalogger, flow meter, thermometer, pressure gauge, and viscometer, are calibrated to ensure the accuracy of the data collected. The laboratory setup also incorporates a magnetic stirrer and an ultrasonic bath, crucial for preparing homogeneous and stable nanofluid mixtures.

In addition, a comprehensive investigation was conducted to identify the materials and equipment necessary for the experimental work. By reviewing relevant literature and previous experimental studies, a list of required materials was compiled. Various suppliers were researched online to source each item. The finalized list of required materials, along with suggested suppliers, was then prepared for purchasing. Table 6.2 presents all the items and materials needed to conduct the experimental work for future studies.

Table 6.1: Prices of DTHEs obtained from various UK suppliers.

Company Name	Price of DTHE [£]
Specialist Heat Exchangers Ltd	2950
HRS	1475
UK Exchangers Ltd	2500

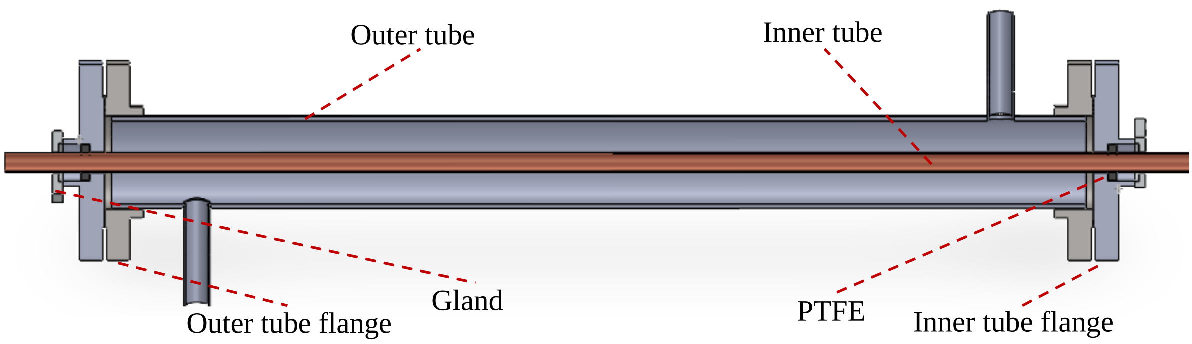

Figure 6.1: Schematic overview of the double tube heat exchanger showcasing various parts.

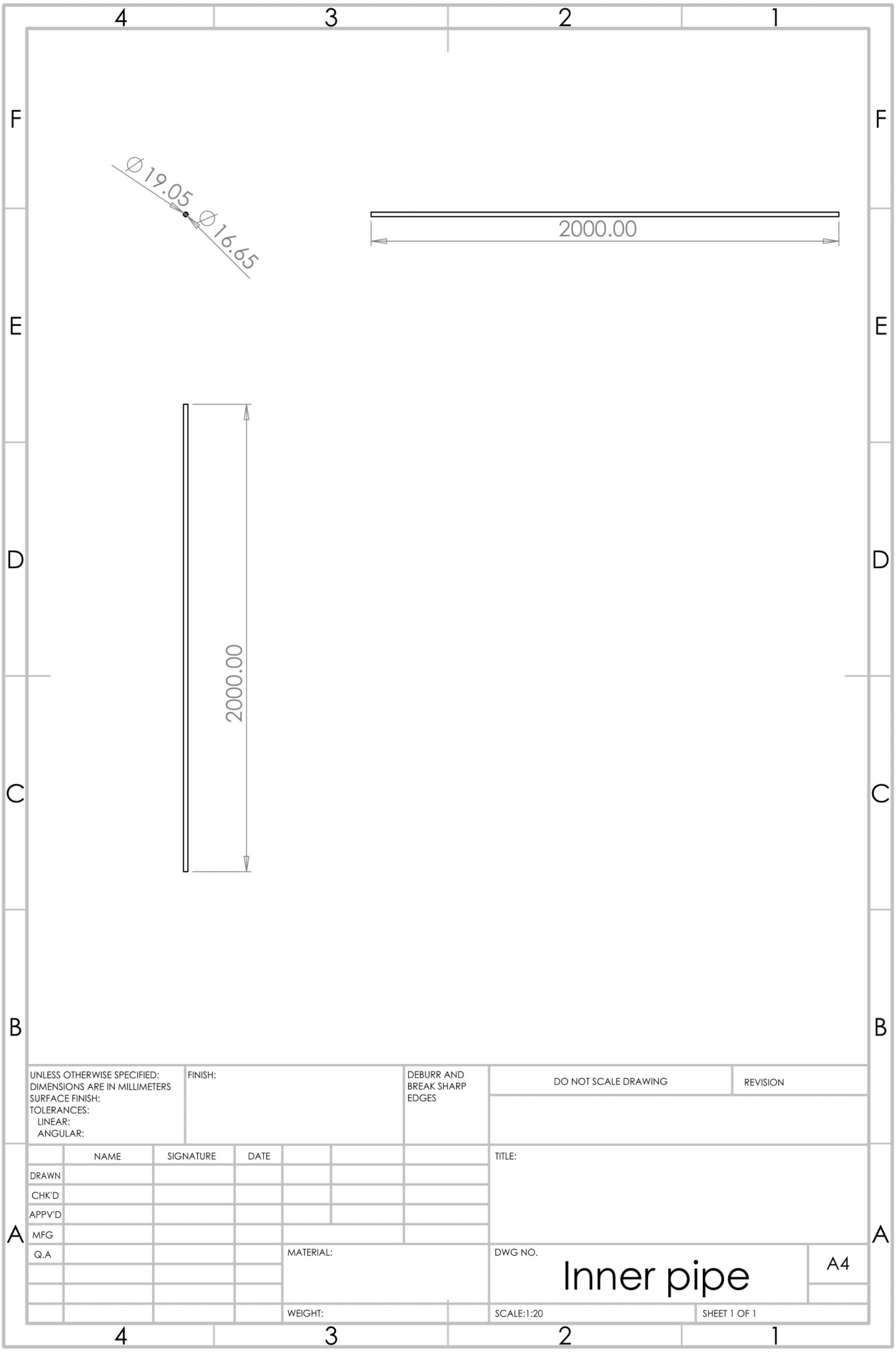

Figure 6.2: Detailed drawing of the inner tube design for the double tube heat exchanger.

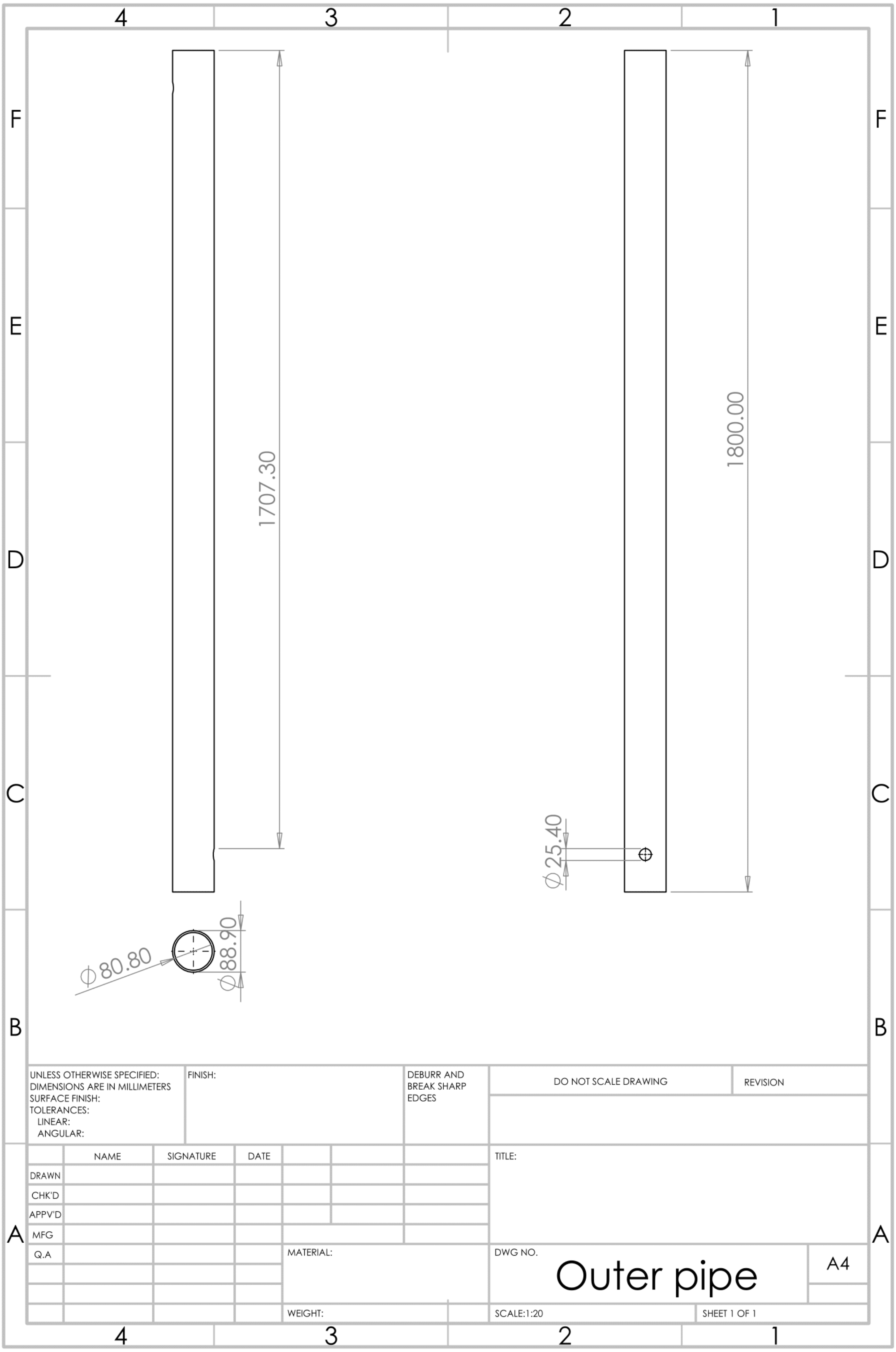

Figure 6.3: Detailed drawing of the outer tube design for the double tube heat exchanger.

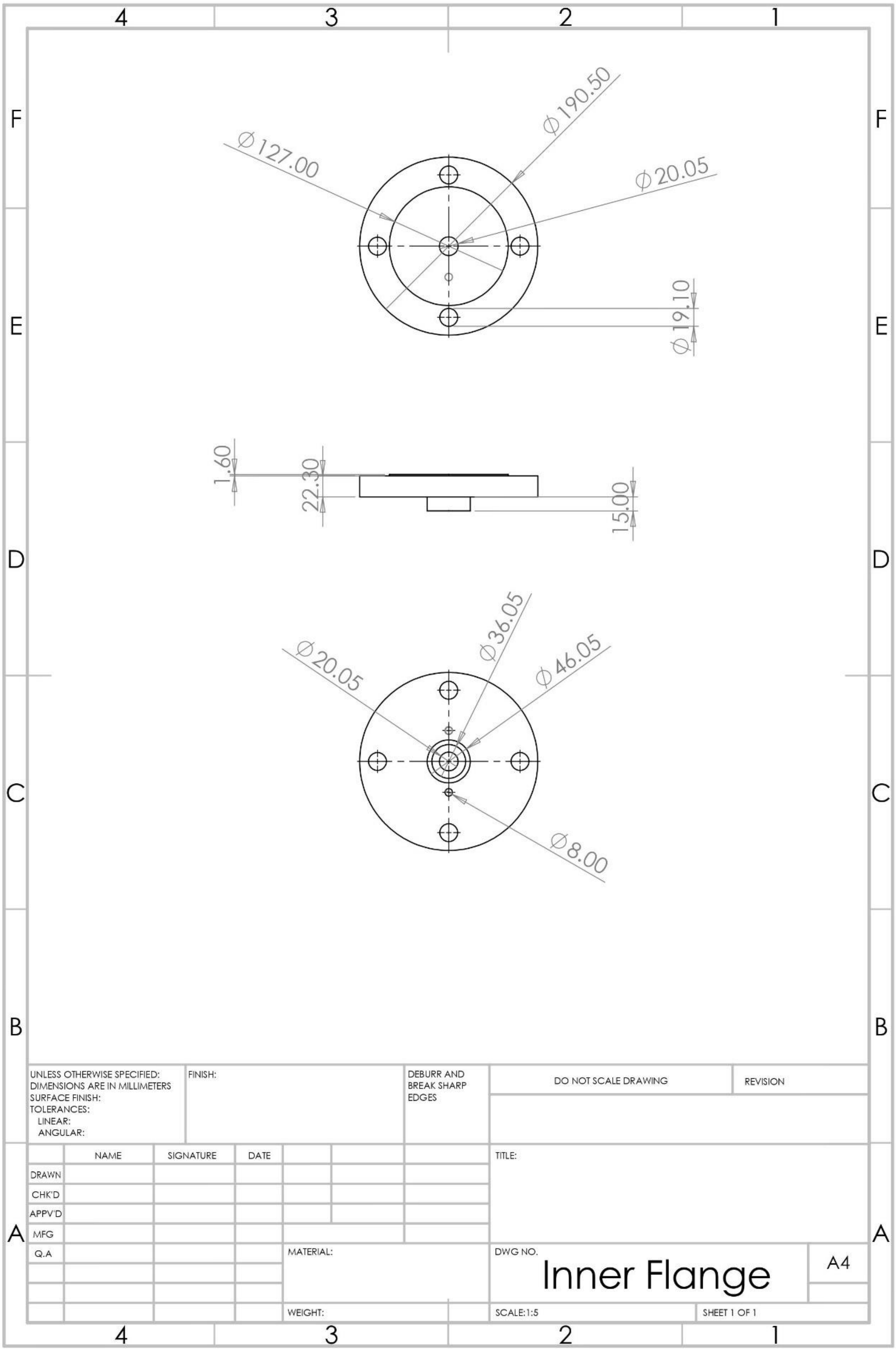

Figure 6.4: Detailed drawing of the inner tube flange design for the double tube heat exchanger.

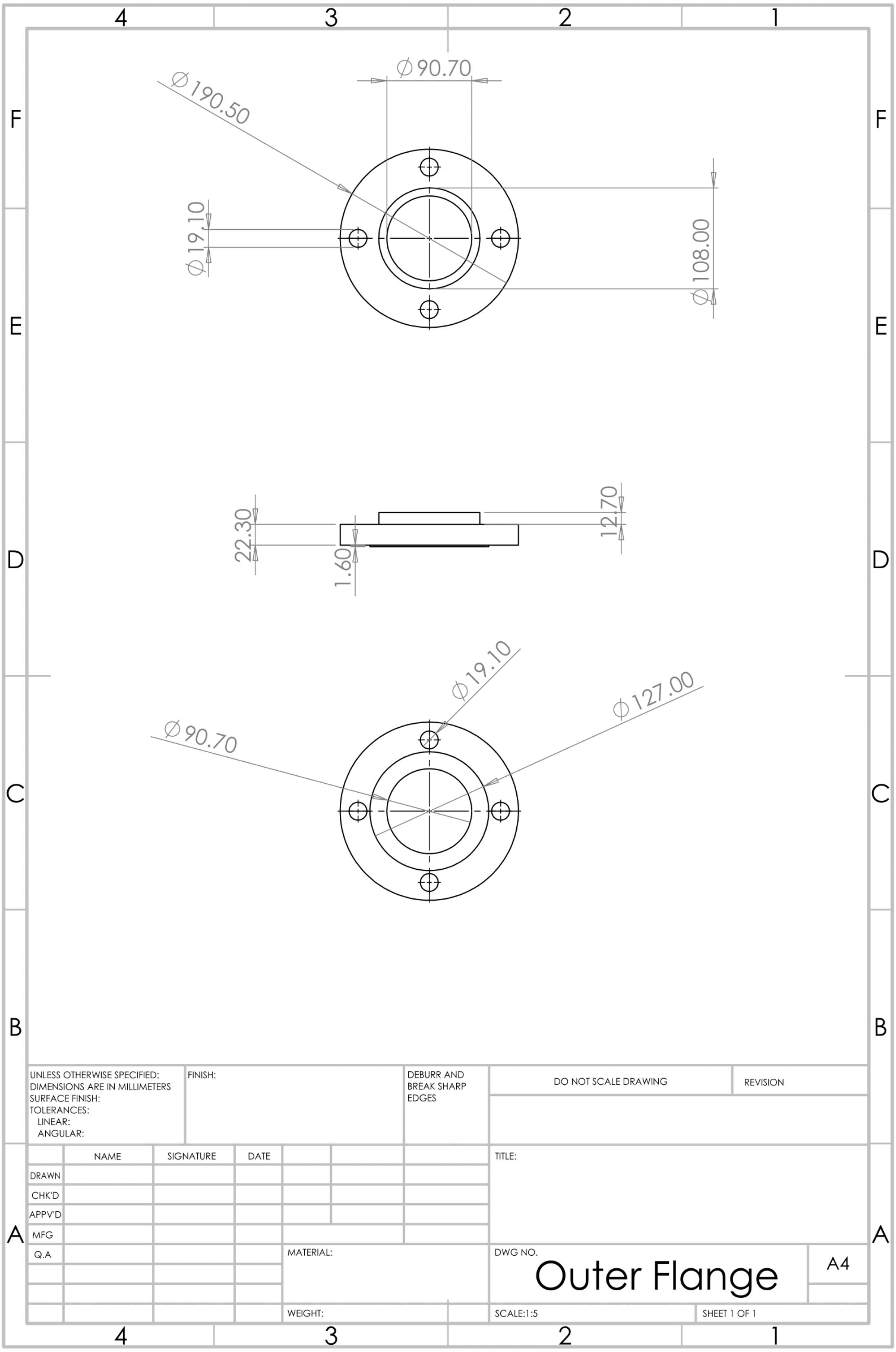

Figure 6.5: Detailed drawing of the outer tube flange design for the double tube heat exchanger.

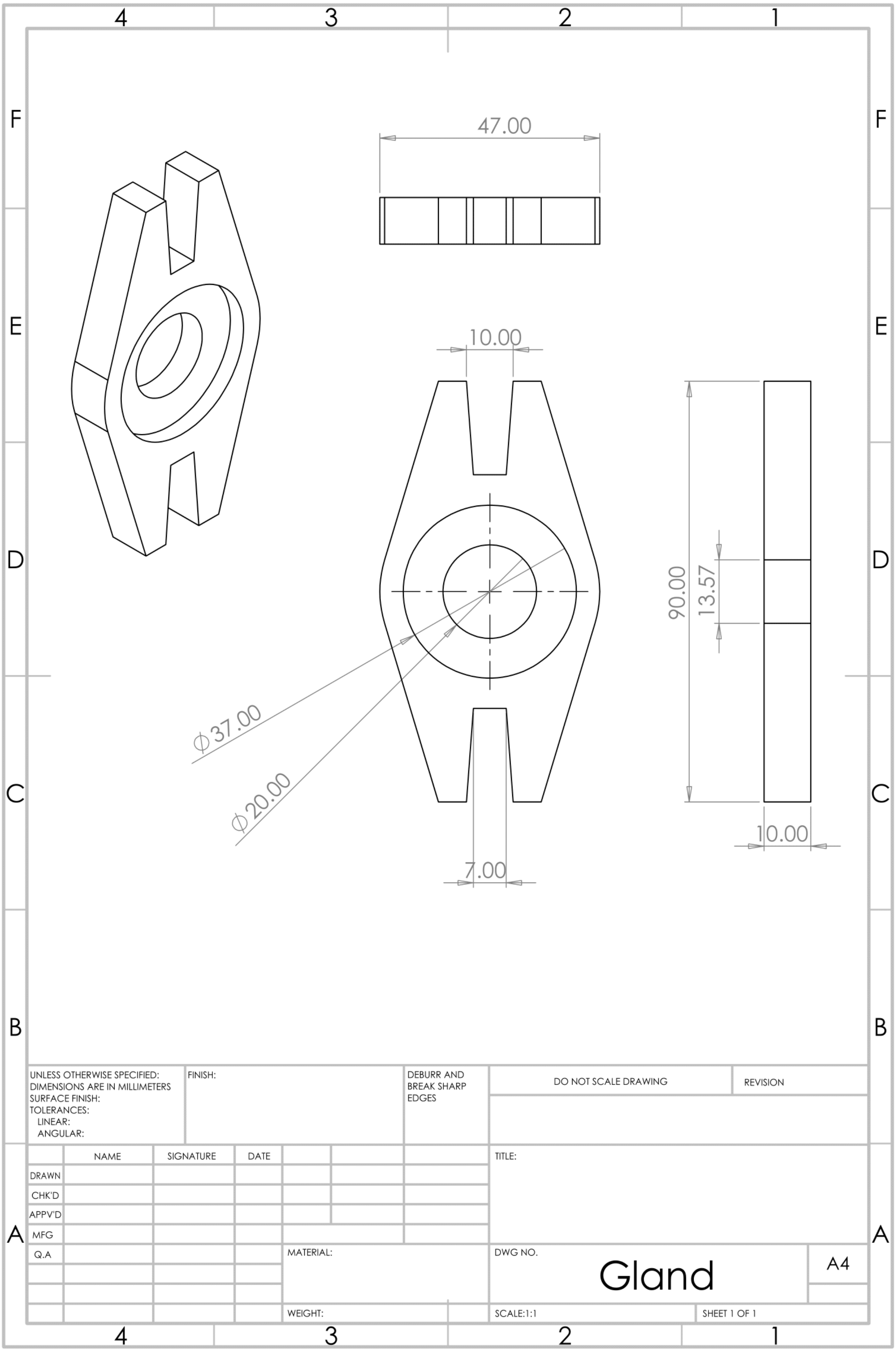

Figure 6.6: Detailed drawing of the gland design for the double tube heat exchanger.

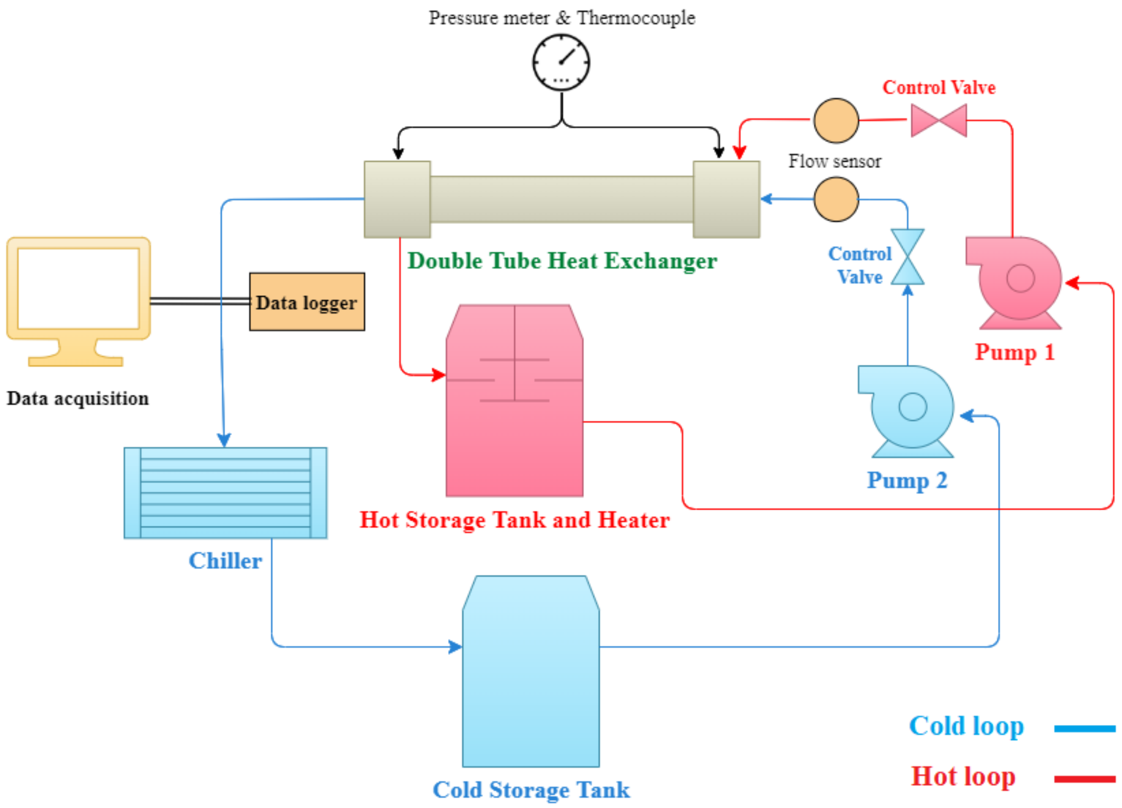

Figure 6.7: Schematic diagram of the proposed experimental test rig setup.

Table 6.2: List of required items for the experimental setup of DTHE.

No.	Required items	Supplier	Application
1	Mild Steel Pipe Nominal (Standard): 3 inches Outer Diameter: 88.9 mm Wall Thickness: 4.05 Length 1.8 meters	Edwards Metals Ltd	Outer tube
2	Mild Steel Pipe Nominal (standard): 1 inch Length: 0.2 meters	Edwards Metals Ltd	Inlet and outlet flow connection
3	Copper pipe Nominal (standard): 1/2 inches Outside diameter: 15.875 mm Wall Thickness: 1.2 mm Length: 2 meters	Edwards Metals Ltd	Inner tube
4	Copper pipe Nominal (standard): 5/8 inches Outside diameter: 19.05 mm Wall Thickness: 1.2 mm Length: 2 meters	Edwards Metals Ltd	Inner tube
5	Copper pipe Nominal (standard): 3/4 inches Outside diameter: 22.225 mm Wall Thickness: 1.6 mm Length: 2 meters	Edwards Metals Ltd	Inner tube

No.	Required items	Supplier	Application
6	Mild Steel Round Bar Diameter: 180 mm Thickness: 35 mm	Edwards Metals Ltd	Using for flange
7	Mild Steel Round Bar Diameter: 180 mm Thickness: 40 mm	Edwards Metals Ltd	Using for flange
8	Gland Packing Seal (PTFE) Size: thickness × width = 10mm × 10mm	RS Components Ltd	To seal between inner tube and flange
9	Gland Packing Seal (Graphite) Size: thickness × width = 8mm × 8mm	RS Components Ltd	To seal between inner tube and flange
10	Natural Rubber Gasket Nominal (standard): 3 inches Outside diameter: 136.5 mm Inside diameter: 88.9 mm Thickness: 3 mm	RS Components Ltd	Gasket between two faces of flanges
11	Flexible Tube (PVC) Inside diameter: 16 mm Outside diameter: 22 mm	RS Components Ltd	Used as a connector in the system
12	Flexible Tube (PVC) Inside diameter: 20 mm Outside diameter: 26.5 mm	RS Components Ltd	Used as a connector in the system
13	Flexible Tube (PVC) Inside diameter: 32 mm Outside diameter: 39.2 mm	RS Components Ltd	Used as a connector in the system
14	Flexible Tube (PVC) Inside diameter: 13 mm Outside diameter: 20 mm	RS Components Ltd	Used as a connector in the system
15	PTFE Tape Size: 12m × 12mm	RS Components Ltd	To seal threads in connectors
16	Flow Meter ifm electronic, 0.1-25 L/min Flow Controller, PNP Output, 19-30 V dc, LED, 1/2 in Pipe Diameter, M12	RS Components Ltd	To measure flow rates of inner and outer flow
17	Electric Cable (flow meter) ifm electronic Female M12 to Free End Sensor Actuator Cable, 4 Core, 5m	RS Components Ltd	Flow meter connector
18	AC/DC Adapters XP Power 24W Plug-In AC/DC Adapter 24V dc Output, 1A Output	RS Components Ltd	Flow meter connector
19	Thermocouple Wire PTFE Sheath Twin Twisted, Type K, 1/0.2mm, Unscreened, 25m	RS Components Ltd	Thermocouple system
20	AA Battery 1.5V	RS Components Ltd	To supply power for pressure manometer devices
21	Extension Lead 5m 4 Socket Type G - British Power strip	RS Components Ltd	To access electricity
22	Gate Valve Sferaco Tap Operculum 102004, 1/2in	RS Components Ltd	Open and close flow

No.	Required items	Supplier	Application
23	Pipe Fitting Stainless Steel, Straight Hexagon Hose Nipple, Male R 1/2in x Male	RS Components Ltd	Used as a connector in the system
24	Pipe Fitting Stainless Steel Pipe Fitting Hexagon Hexagon Nipple, Male R 1/2in x Male R 1/2in	RS Components Ltd	Used as a connector in the system
25	Pipe Fitting Copper Pipe Fitting, Push Fit 90° Equal Tee for 15mm pipe	RS Components Ltd	Used as a connector in the system
26	Pipe Fitting Georg Fischer Galvanised Malleable Iron Fitting Tee, Female BSPP 1/2in to Female BSPP 1/2in to Female BSPP 1/2in	RS Components Ltd	Used as a connector in the system
27	Pipe Fitting Copper Pipe Fitting, Solder Equal Tee for 15 x 15 x 15mm pipe	RS Components Ltd	Used as a connector in the system
28	Flow Meter Connector Stainless Steel Pipe Fitting, Straight Octagon Union, Female G 1/2in x Female G 1/2in	RS Components Ltd	Used as a connector in the flow meter
29	Thermal Insulation RS PRO Flame Retardant Calcium-Magnesium Silicate Thermal Insulating Sheet, 5m x 610mm x 6mm	RS Components Ltd	Insulation for outside of outer tube
30	Pump Connection Georg Fischer Black Malleable Iron Fitting Reducer Socket, Female BSPP 1-1/2in to Female BSPP 1in	RS Components Ltd	Used as a connector in the water pump
31	Pump Connection Georg Fischer Galvanised Malleable Iron Fitting, Straight Reducer Bush, Male BSPT 1in to Female BSPP 1/2in	RS Components Ltd	Used as a connector in the water pump
32	Thermocouple Connector 4mm Probe, IEC, RoHS Compliant Standard	RS Components Ltd	Used as a connector in the thermocouple system
33	Fitting Reducer Size: 15mm × 22mm	Screwfix Direct Ltd	Used as a connector in the piping system
34	Fitting Reducer Size: 28mm × 22mm	Screwfix Direct Ltd	Used as a connector in the piping system
35	Fitting Reducer Tee Size: 15mm × 15mm × 22mm	Screwfix Direct Ltd	Used as a connector in the piping system
36	Water Pump Salamander Pumps CT50+ Xtra Regenerative Twin Shower Pump 1.5bar	Screwfix Direct Ltd	Water pump for inner flow
37	Water Pump Grundfos UPS 15-50N Traditional Secondary Hot Water Circulator 230V	Screwfix Direct Ltd	Water pump for outer flow
38	Pressure Manometer Model: 2023P 0mbar to 7bar, 0.15	Farnell	To measure pressure drop

No.	Required items	Supplier	Application
39	Data Logger Bundle Temperature, 8 Channels, 10, TC-08	Farnell	To collect temperature data

Appendix B

Python code for validating Nusselt numbers from various empirical correlations

```
import numpy as np
import iapws
from iapws import IAPWS95

Ti1 = 283
To1 = 353
# TI = IAPWS95 (T= Ti1 + 273.15, x=0)
# TO = IAPWS95 (T= To1 + 273.15, x=0)
# known values
    # Inner tube
D1 = 0.014
D2 = 0.016
th = (D2-D1)/2

mi = 0.003918823       # mass flow rate inner tube

cpi = 4179
d1 = 997.1
k1 = 0.613
mu1 = 0.000891
Pr1 = (mu1*cpi)/k1
Ci = mi*cpi

print (cpi,Pr1,d1,k1,mu1,Ci,'\n\n\n')

    # Outer tube
D3 = 0.08

mo = 0.053743854         # mass flow rate outer tube

cpo = 4179
d2 = 997.1
k2 = 0.613
mu2 = 0.000891
Pr2 = (mu2*cpo)/k2
Co = mo*cpo

L = 1.8
pi = 3.141592653
k3 = 387.6

#Unknown values
Pw = pi*(D2+D3)                          # The wetted perimeter for
pressure drop calculation in the annulus
Ph = pi*D2                                # the heat transfer perimeter of
the annulus
Ac = (pi*((D3**2)-(D2**2)))/4             # The net free-flow area of the
annulus
Dh = (4*Ac)/Pw                           # The hydraulic diameter based on
the total wetted perimeter for pressure drop calculation
De = (4*Ac)/Ph                           # the hydraulic diameter based on
the heat transfer perimeter "equivalent diameter"
Ai = 0.25*pi*(D1**2)
Ao = 0.25*pi*((D3**2)-(D2**2))
Pw_i = pi*(D1+0.002)
```

```
Ph_i = pi*0.002
Ac_i = 0.25*pi*((D1**2)-(0.002**2))
Dh_i = (4*Ac_i)/Pw_i
De_i = (4*Ac_i)/Ph_i

print (' th=',th,'\n Pw=',Pw,'\n Ph=',Ph,'\n Ac=',Ac,'\n Dh=',Dh,'\n
De=',De, '\n Ai=',Ai,'\n Ao=',Ao,'\n Ac_i=',Ac_i,'\n Dh_i=',Dh_i,'\n
De_i=',De_i)

ui = mi/(d1*Ai)
uo = mo/(d2*Ao)
ui_i = mi/(d1*Ac_i)

Rei = (d1*ui*D1)/mu1
Reo = (d2*uo*Dh)/mu2
Rei_i = (d1*ui_i*Dh_i)/mu1

print (' ui=',ui,'\n uo=',uo,'\n Rei=',Rei,'\n Reo=',Reo,'\n
ui_i=',ui_i,'\n Rei_i=',Rei_i)

Y1i = (Rei*Pr1*D1)/L
Y1o = (Reo*Pr2*De)/L

NuL1i = 3.66 +   ( (0.19*(Y1i**0.8)) / (1+ (0.117*(Y1i**0.467)) ))   #
Hausen4 for laminar flow (3.9) KAKAC
NuL1o = 3.66 +   ( (0.19*(Y1o**0.8)) / (1+ (0.117*(Y1o**0.467)) ))   #
Hausen4 for laminar flow T constant (3.9) KAKAC
NuL2i = 1.953 * (Y1i**(1/3))                                           # q
constant(3.11) KAKAC
NuL2o = 1.953 * (Y1o**(1/3))                                           # q
constant(3.11) KAKAC
NuL3i = 4.05 * (Rei**0.17) * (Pr1**(1/3))
NuL3o = 4.05 * (Reo**0.17) * (Pr2**(1/3))
NuL4i = 1.86 * (Y1i**(0.33))
NuL4o = 1.86 * (Y1o**(0.33))
Nu = ( (3.66**3) +  ((1.61**3) * Y1i))**(1/3)
Nu5 = 0.644 * (1/(Pr1**(1/6))) * (Y1i**(1/2))
print (' Y1i=',Y1i,'\n Y1o=',Y1o,'\n NuL1i=',NuL1i,'\n NuL1o=',NuL1o,'\n
NuL2i=',NuL2i,'\n NuL2o=',NuL2o,'\n NuL3i=',NuL3i,'\n NuL3o=',NuL3o,'\n
NuL4i=',NuL4i,'\n NuL4o=',NuL4o,'\n Nu=',Nu,'\n Nu5=',Nu5)

hi = (NuL2i*k1)/D1
ho = (NuL2o*k2)/Dh
# hi = (*k1)/D1
# ho = (151.4438825*k2)/De

Y2 = (1/(hi*pi*D1*L)) + ((np.log( (D2/2)/(D1/2))) / (2*pi*k3*L)) +
(1/(ho*pi*D2*L))
# Y2 = ( (D2/2) / (hi*(D1/2)) ) + (((D2/2) * np.log( (D2/2)/(D1/2))) /
(k3)) + (1/(ho))
UA = 1/Y2
# UA = U * pi * D1 * L
#UA = 17
# UI = 1/hi + (D1 * np.log(D2/D1))/(2*k3) + (D2/(D1 * ho))
# ui = 1/UI

print (' hi=',hi,'\n ho=',ho,'\n Y2=',Y2,'\n UA=',UA)

if Ci<Co :
    Cm = Ci
    Cs = Ci/Co
```

```
else:
        Cm= Co
        Cs = Co/Ci

NTU = UA/Cm

e = (1 - (np.exp( -(1-Cs)*NTU)))/ (1 - (Cs * (np.exp(-(1-Cs)*NTU))))

print (' Ci=',Ci,'\n Co=',Co,'\n Cm=',Cm,'\n Cs=',Cs,'\n NTU=',NTU,'\n
e=',e)

Q = Cm*(-Ti1+To1)
q = e*Q
Ti2 = (q/Ci) + Ti1
To2 = (q/Co) - To1

print (' Q=',Q,'\n q=',q,'\n Ti2=',Ti2,'\n To2=',To2)
```

Appendix C

Full text of publications

1. Heat transfer and fluid flow characteristics of the passive method in double tube heat exchangers: a critical review.

17 (2023) 100282

Contents lists available at ScienceDirect

International Journal of Thermofluids

journal homepage: www.sciencedirect.com/journal/international-journal-of-thermofluids

Heat transfer and fluid flow characteristics of the passive method in double tube heat exchangers: A critical review

Ebrahim Tavousi [a], Noel Perera [a,*], Dominic Flynn [b], Reaz Hasan [c]

[a] School of Engineering and the Built Environment, Faculty of Computing, Engineering and the Built Environment, Birmingham City University, Birmingham, B4 7XG, UK
[b] Vehicle Efficiency, Jaguar Land Rover, Gaydon, CV35 0BJ
[c] Department of Mechanical Engineering, Military Institute of Science and Technology, Dhaka, 1216, Bangladesh

A R T I C L E I N F O

Keywords:
Double tube heat exchanger
Concentric tube heat exchanger
Nanofluid
Heat transfer rate
Nusselt number
Friction factor
Pressure drop

A B S T R A C T

With the growing need for more energy, it is imperative to design efficient heat exchangers that are simpler, cheaper to manufacture, have higher heat transfer rates, and low in pressure drop. One of these heat exchangers is the double tube heat exchanger that is used in many industries. From past to present, double tube heat exchangers have caught the attention of researchers because of their simplicity and wide range of applications. This review paper contains a critical analysis of the impact of different passive methods on the heat transfer and fluid flow characteristics of the fluid in double tube heat exchangers. There are different techniques to increase the heat transfer rate in double tube heat exchangers, such as turbulator insertion, extended surface (fin), in tube geometry change, nanofluids and a combination of these techniques. All these techniques are reviewed in detail to determine the heat transfer rate and friction factor enhancement in the double tube heat exchangers. Statistical analysis was provided to compare the impacts of these different techniques on the heat transfer and fluid flow characteristics of the double tube heat exchanger performance. It was concluded that a combination of turbulator inserts and nanofluids is the best technique to increase the heat transfer rate. Also, this technique provides the highest potential for heat transfer enhancement based on the standard deviation. On the other hand, extended surface (fin) is the worst-performing technique because of the high friction factor. This review article provides new ideas and gaps in the present knowledge for further investigations.

1. Introduction

A heat exchanger is a device used to transfer thermal energy between two or more fluids, separated by solid material. The applications of heat exchangers are extensive in industries where it is used to crystallize, concentrate, distil, fractionate, pasteurize, sterilize and control a process fluid. Some common heat exchangers are cooling towers, air preheaters, evaporators, condensers, automobile radiators, and shell and tube exchangers. Heat exchangers are classified in many ways, for example, according to the transfer process, the number of fluids, surface compactness, construction, flow arrangements, and heat transfer mechanisms. One of the standard classifications is based on the construction of heat exchangers (Fig. 1). These classifications are divided into four subcategories: tubular, plate-type, extended surface, and regenerative. The tubular section is divided into four subcategories: double-pipe, shell and tube, spiral tube, and pipe coil [1, 2].

One of the common heat exchangers is the double tube heat exchanger (DTHE). These are used widely in industries and engineering applications such as refrigeration, air-conditioning, power plant, solar water heater and the process industry [3]. The main advantages of DTHEs are working with high pressure and temperature of working fluids, simple maintenance, modular construction, cost-effectiveness, and its simplicity (consisting of two concentric tubes) [4]. The purpose of using DTHEs is to transfer heat between the cold and hot regions (Fig. 2). The flow directions of hot and cold fluids in DTHEs can either be parallel or counter. It is crucial and challenging for researchers to find ways and solutions to increase the DTHE's heat transfer rate and efficiency. In this regard, extensive research carried out experimentally and numerically related to DTHEs to enhance heat transfer and improve fluid characteristics.

One of the earliest publications related to DTHEs dates back to 1928 [5]. The research into DTHEs expanded rapidly after 1928 and was divided into different categories. Some scholars focused on geometry change and the insertion of elements in inner and outer tubes [6, 7].

* Corresponding author.
E-mail address: Noel.Perera@bcu.ac.uk (N. Perera).

https://doi.org/10.1016/j.ijft.2023.100282

Available online 22 January 2023

2. Numerical investigation of laminar heat transfer and fluid flow characteristics of Al_2O_3 nanofluid in a double tube heat exchanger.

The current issue and full text archive of this journal is available on Emerald Insight at:
https://www.emerald.com/insight/0961-5539.htm

Numerical investigation of laminar heat transfer and fluid flow characteristics of Al_2O_3 nanofluid in a double tube heat exchanger

Ebrahim Tavousi and Noel Perera
School of Engineering and the Built Environment, Faculty of Computing, Engineering and the Built Environment, Birmingham City University, Birmingham, UK

Dominic Flynn
Department of Vehicle Efficiency, Jaguar Land Rover, Gaydon, UK, and

Reaz Hasan
Department of Mechanical Engineering, Faculty of Mechanical Engineering, Military Institute of Science and Technology, Dhaka, Bangladesh

Received 8 March 2023
Revised 22 May 2023
2 August 2023
Accepted 9 August 2023

Abstract

Purpose – The purpose of the study is to numerically investigate the characteristics of laminar heat transfer and fluid flow in a double tube heat exchanger (DTHE) using water-aluminum oxide (Al_2O_3) nanofluid. The study examines the effects of nanofluid in both counter and parallel flow configurations. Furthermore, an exergy analysis is conducted to assess the impact of nanofluid on exergy destruction.

Design/methodology/approach – The single-phase method has been used for Al_2O_3 nanoparticles in water as base fluid in a laminar regime for Reynolds numbers from 400 to 2,000. The effects of nanoparticle volume fractions (0 to 0.1), Nusselt number, Reynolds number, heat transfer coefficient, pressure drop, performance evaluation criteria (PEC) and the impact of counter and parallel flow direction have been studied.

Findings – The findings indicate that the incorporation of nanoparticles into the water enhances the heat transfer rate of DTHE. This enhancement is attributed to the improved thermal properties of the working fluid and its impact on the thermal boundary layer. Nusselt number, heat transfer coefficient, and PEC increase by approximately 19.5%, 58% and 1.2, respectively, in comparison to pure water. Conversely, the pressure drop experiences a 5.3 times increase relative to pure water. Exergy analysis reveals that nanofluids exhibit lower exergy destruction compared to pure water. The single-phase method showed better agreement with the experimental results compared to the two-phase method.

Originality/value – Dimensionless correlations were derived and validated with experimental and numerical results for the Nusselt number and PEC for both counter and parallel flow configurations based on the Reynolds number and nanoparticles volume fraction with high accuracy to predict the performance of DTHE without performing time-consuming simulations. Also, an exergy analysis was performed to compare the exergy destruction between nanofluid and pure water.

Keywords Double tube heat exchanger, Concentric tube heat exchanger, Nanofluid, Heat transfer rate, Nusselt number, Heat transfer coefficient, Pressure drop, Thermal efficiency

Paper type Research paper

International Journal of Numerical Methods for Heat & Fluid Flow

0961-5539
DOI 10.1108/HFF-03-2023-0114

Conflict of interest: The authors declare that they have no conflict of interest.

3. Numerical Investigation of Heat Transfer and Fluid Flow Characteristics of Al_2O_3 Nanofluid In A Double Tube Heat Exchanger With Turbulator Insertion.

Proceedings of the 9th World Congress on Mechanical, Chemical, and Material Engineering (MCM'23)
Brunel University, London, United Kingdom –August 06-08, 2023
Paper No. HTFF 218
DOI: 10.11159/htff23.218

Numerical Investigation of Heat Transfer and Fluid Flow Characteristics of Al_2O_3 Nanofluid In A Double Tube Heat Exchanger With Turbulator Insertion

Ebrahim Tavousi[1], Noel Perera[1], Dominic Flynn[2], Reaz Hasan[3]
[1]School of Engineering and the Built Environment, Faculty of Computing, Engineering and the Built Environment, Birmingham City University, Birmingham, B4 7XG, UK
Ebrahim.Tavousi@mail.bcu.ac.uk
[2]Vehicle Efficiency, Jaguar Land Rover, Gaydon, CV35 0BJ
[3]Department of Mechanical Engineering, Military Institute of Science and Technology, Dhaka, 1216, Bangladesh

Abstract - One of the primary objectives associated with the double tube heat exchanger is to enhance the heat transfer rate and improve the overall system performance. A promising approach to achieve these improvements involves combining turbulator insertion and nanofluid techniques. This study presents a numerical investigation that examines the impact of Al_2O_3-water nanofluid within the inner tube, along with turbulator insertion in the form of square-shaped ribs, on the heat transfer and fluid flow characteristics of the double tube heat exchanger. The findings indicate that an increase in the volume fraction of nanofluid leads to an enhanced heat transfer rate. Additionally, reducing the spacing between the turbulator ribs in the double tube heat exchanger results in an increase of up to 50% in the Nusselt number compared to a heat exchanger without turbulator insertion. The maximum performance evaluation criterion achieved in this study is 1.05.

Keywords: Double pipe heat exchanger, Heat transfer, Nanofluid, Nusselt number, Turbulator, Friction factor, Thermal efficiency

1. Introduction

A heat exchanger is a device used to transfer thermal energy between two or more fluids separated by solid material. One of the common heat exchangers is the double tube heat exchanger (DTHE). DTHEs are used to transfer heat between the cold and hot regions. These are used widely in industries and engineering applications such as refrigeration, air-conditioning, power plant, solar water heater, and the process industry [1-3]. One of the important challenges with heat exchangers is improving heat transfer capability [4-7].

Karimi [8] evaluated numerically the effect of twisted tape insertion and Al_2O_3-water nanofluid for the Reynolds number 250 to 2250 and 3000 to 9000 in a counter flow DTHE. The nanoparticle volume fractions were 1, 2, and 3%, and the cold nanofluid and superheat steam flowed in the inner and outer tubes, respectively. The results of the study demonstrated that the Nusselt number experienced a 22% increase as a result of twisted tape insertion alone and a 30% increase when a combination of twisted tape and nanofluid were employed, in comparison to the plain tube (without turbulator) and pure water conditions. Also, they concluded that using twisted tapes at high Reynolds numbers is more economical than low Reynolds numbers. Gnanavel [9] numerically studied the effect of heat transfer and fluid flow characteristics of spiral spring insertion and different nanofluids, including TiO_2, BeO, ZnO, and CuO, in a DTHE. In the conducted study, the Reynolds number range employed was from 1000 to 10000. The working fluids utilized were hot nanofluid and cold water, which were directed through the inner and outer tubes, respectively. The Nusselt number enhancements were obtained up to 117.39, 63.09, 56.63, and 47.62% for TiO_2, BeO, ZnO, and CuO, respectively. The maximum fiction factor increment was obtained for CuO with a value of 312%. The thermal performance factor decreased with the rise of the Reynolds number for all cases. Karuppasamy [10] investigated numerically the effect of cone shape insertion and Al_2O_3-water and CuO-water nanofluid on the performance of a DTHE. The volume fraction and range of Reynolds number were 1% and 2000 to 10000, respectively. The results showed that Al_2O_3-water gives a higher heat transfer rate than CuO-water, with the amount of 65% and 56%, respectively. The friction factor augmentation for Al_2O_3-water and CuO-water nanofluid were 50% and 47%.

4. Effect of novel turbulators on the hydrothermal performance of counterflow double tube heat exchanger using nanofluids.

International Journal of Heat and Fluid Flow 107 (2024) 109427

Contents lists available at ScienceDirect

International Journal of Heat and Fluid Flow

journal homepage: www.elsevier.com/locate/ijhff

Effect of novel turbulators on the hydrothermal performance of counterflow double tube heat exchanger using nanofluids

Ebrahim Tavousi [a], Noel Perera [a,*], Dominic Flynn [b], Reaz Hasan [a], Mostafizur Rahman [a]

[a] *College of Engineering, Faculty of Computing, Engineering and the Built Environment, Birmingham City University, Birmingham, B4 7XG, UK*
[b] *Vehicle Efficiency, Jaguar Land Rover, Gaydon, CV35 0BJ, UK*

A R T I C L E I N F O

Keywords:
Double tube heat exchanger
Turbulator insertion
Nanofluid
Nusselt number
Heat transfer coefficient
Pressure drop
Thermal efficiency
Rib

A B S T R A C T

Double pipe heat exchangers are widely used across various industries. Enhancing their performance not only benefits these industries but also contributes to reduced fossil fuel consumption and pollution. This study employs the passive method with a combination turbulator insertion and nanofluid technique to enhance the heat transfer rate and improve the double tube heat exchanger performance. The novelty of this study lies in the use of new turbulator insertions and various nanofluids to investigate the heat transfer and fluid flow characteristics under laminar and counter flow configuration. The study examined four types of turbulator insertions, including triangular, rectangular, trapezoidal, and oval, in conjunction with CuO, SiO_2, Al_2O_3 water-based nanofluids in a single-phase model. The findings revealed that the trapezoidal ribs exhibited higher Nusselt number and friction factor than the other rib shapes. Conversely, the oval ribs demonstrated a better performance evaluation criteria than the other rib shapes. Furthermore, the study explored different geometrical parameters such as rib width, height, and spacing, determining that rib height has the most significant impact on enhancing the heat transfer. The study achieved maximum performance evaluation criteria of 1.2 and 1.9 for SiO_2 nanofluid without turbulator insertion and with turbulator insertion, respectively.

1. Introduction

The demand for energy has been on the rise due to urbanization and the expanding global population. The use of gas, oil, coal, and other fossil fuels has adverse effects on the environment, contributing to the escalation of global warming. Therefore, adopting energy-saving measures and harnessing renewable energy sources represent effective solutions to mitigate this issue (Hosseinzadeh et al., 2020). One of the most commonly employed and crucial devices in both industrial and commercial settings is the double tube heat exchangers (DTHE). Therefore, creating an efficient thermal system within DTHEs can lead to cost reduction and substantial energy savings (Hussain and Sheremet, 2023; Venkatesh, 2023). DTHE represents the simplest form of a heat exchanger, wherein hot and cold fluids circulate in either parallel or counterflow configurations (Rao and Sankar, 2019). The utilization of DTHEs finds extensive application across various industries, including but not limited to chemical, food, oil, gas, pharmaceutical, solar energy, waste heat recovery, geothermal, combustion, latent heat energy storage, and air conditioning (Omidi et al., 2017; Li, 2022; Louis et al., 2022). Improving the heat transfer efficiency of heat exchangers presents a notable challenge (Liu and Sakr, 2013; Rohsenow et al., 1998). Improving heat exchanger's performance can be categorized into three broad approaches: active, passive, and combined methods (Cancan et al., 2014). Active methods involve the application of external power to augment heat transfer through means such as vibration, electric fields, mechanical aids, or magnetic fields (Jadhav et al., 2016; Maleki et al., 2023). On the other hand, passive methods rely on extended surfaces and elements instead of external power (Hangi et al., 2022; Lalegani et al., 2018). Combined methods encompass the synergistic utilization of active and passive methods (Alam and Kim, 2018).

Tavousi, et al. (Tavousi et al., 2023) systematically classified passive methods into five main categories: turbulator insertion (Pourahmad and Pesteei, 2016), extended surface area (fins) (El Maakoul et al., 2020), geometry changes (Luo and Song, 2021), using nanofluids (Tavousi et al., 2023), and combinations of these techniques (Singh and Sarkar, 2021). A statistical investigation of more than 100 studies was conducted on the passive methods. The statistical investigation showed that the combined techniques of turbulator insertion and nanofluid have the maximum increase in heat transfer rate. A diverse range of turbulator insertions and nanofluids can be employed to enhance the performance

* Corresponding author.
E-mail address: noel.perera@bcu.ac.uk (N. Perera).

https://doi.org/10.1016/j.ijheatfluidflow.2024.109427
Received 1 March 2024; Received in revised form 6 May 2024; Accepted 11 May 2024
Available online 17 May 2024